Conrad Mook

OFFICE OF ADVANCED RESEARCH AND TECHNOLOGY
SPACE VEHICLES DIVISION

[redacted]

(NASA-TM-82259) PROCEEDINGS OF MEETING ON CHARGED PARTICLE RADIATION EFFECTS (National Aeronautics and Space Administration) 235 p

N81-72957

Unclas
00/72 15766

PROCEEDINGS OF MEETING ON

CHARGED PARTICLE RADIATION EFFECTS

MARCH 19-20, 1964
NASA HEADQUARTERS
WASHINGTON, D. C.

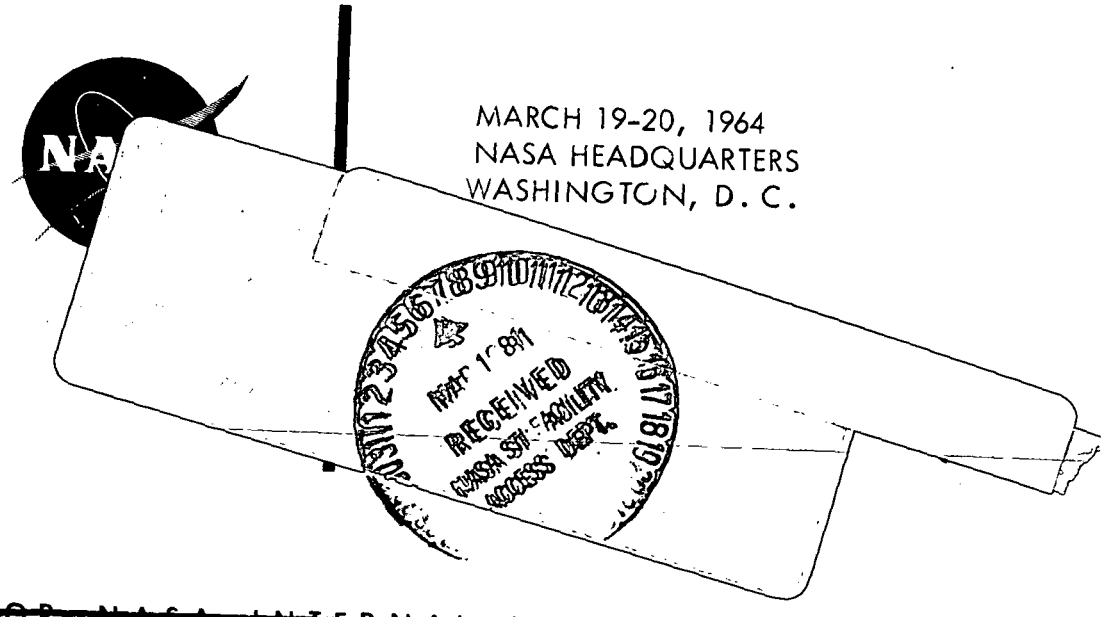

MAR 1 '81
RECEIVED
NASA STI FACILITY
ACCESS DEPT.

[redacted]

NATIONAL AERONAUTICS AND SPACE ADMINISTRATION
WASHINGTON 25, D.C.

IN REPLY REFER TO: RV-1

January 29, 1964

TO: Director, Marshall Space Flight Center
Director, Ames Research Center
Director, Goddard Space Flight Center
Director, Jet Propulsion Laboratory
Director, Langley Research Center
Director, Lewis Research Center
Director, Manned Spacecraft Center

FROM: Associate Administrator for Advanced Research and Technology

SUBJECT: Meeting to discuss Charged Particle Radiation Effects

A meeting on Charged Particle Radiation Effects will be held at NASA Headquarters at 9:00 a.m. on March 19-20, 1964 in the OART Conference Room 5018 of Federal Office Building 10B, 600 Independence Avenue S.W., Washington, D.C. The Centers are asked to participate in this meeting in accordance with their activities, interest and requirements in the subject area.

Objectives of the meeting will be:

1) An exchange of current information regarding progress in understanding and predicting radiation damage and its effects;

2) an exchange of information regarding present and proposed radiation damage research, with special attention being devoted to use of in-house capabilities; and

3) the identification of research tasks where additional effort is required.

In order to insure adequate time for presentations and discussions, it is requested that brief abstracts along with time estimates for proposed presentations be submitted in advance of the meeting. This information, together with a list of those persons planning to attend should be forwarded to Mr. Arthur Reetz (Code RV-1) Office of Advanced Research and Technology, NASA Headquarters, Washington, D.C. 20546.

R J Bisplinghoff

Raymond L. Bisplinghoff

TABLE OF CONTENTS

	Page
Meeting Announcement	1
Outline of JPL Dynamitron Research Program, FY 1965	3
Charged Particle Radiation Damage Studies at the Ames Research Center - B. E. Cunningham - Ames Research Center	5
Marshall Space Flight Center Radiation Damage Program - Raymond L. Gause - Marshall Space Flight Center	9
Radiation Damage and Effect Studies - J. W. Blue - Lewis Research Center	11
Electron Radiation Effects with the Lewis 3 MeV Dynamitron Accelerator - H. H. Grimes - Lewis Research Center	21
Effects of Impurities on Radiation Damage of Silicon Solar Cells - TM X-52007 Joseph Mandelkorn, Lawrence Schwartz, Jacob Broder, Harold Kautz, and Robert Ulman - Lewis Research Center	29
A Note on the Talk by Joe Mandelkorn and NASA Technical Memorandum TM X-52007 - F. G. Cunningham and M. M. Sokoloski - Goddard Space Flight Center	39
Outline of the Program Concerning Radiation Effects in Solar Cells and Semiconductor Materials - M. Schach and P. H. Fang - Goddard Space Flight Center	43
Satellite Experiments with Solar Cells - Ramond C. Waddel - Goddard Space Flight Center	51
Effect of Electron Radiation on TV Lens Components - Lawrence Kobren - Goddard Space Flight Center	67
Preliminary Study on the Effect of Electron Radiation on Echo II Balloon Material - Lawrence Kobren - Goddard Space Flight Center	77

TABLE OF CONTENTS

(Cont'd)

	Page
Radiation Effects Experiment on Micropower Microelectronics - Marjorie Townsend - Goddard Space Flight Center	83
Status Report and Description of the NASA Space Radiation Effects Laboratory - Emanuel Rind - Langley Research Center	85
Radiation Effects on Aromatic Main Chain Polymers - George F. Pezdirtz, Howard L. Price, and Vernon L. Bell - Langley Research Center	103
Effects of Gamma Radiation on Polyesters - George D. Sands, Howard L. Price, and George F. Pezdirtz - Langley Research Center	127
The Effects of Electron Radiation on the Optical Transmission of Several Transparent Materials - Gilbert A. Haynes - Langley Research Center	145
Review of Langley's Solar Cell Degradation Effort - J. L. Patterson and W. E. Ellis - Langley Research Center	159
Radiation Effects on Semiconductor Electronics - F. R. Bryant and W. C. Hulten - Langley Research Center	175
Damage to Germanium Produced by 22 and 40 MeV Protons - Roger A. Breckenridge and Chris Gross - Langley Research Center	189
A Method for Measuring the Diffusion Length in Solar Cells and Preliminary Results - Marvin E. Beatty and Gerald F. Hill - Langley Research Center	209
Location of Energy Defect Levels in Proton and Electron Irradiated Silicon by Means of Infrared Absorption - Gerald F. Hill and Marvin E. Beatty - Langley Research Center	219
Remarks on Doses Outside the Magnetosphere, and on Effects Especially on Surfaces and Photographic Films - Trutz Foelsche - Langley Research Center	235
List of Attendees	249

OUTLINE OF JPL DYNAMITRON RESEARCH PROGRAM, FY 1965

1. Physics Section: Studies of fission fragment interaction with matter: rate and mode of energy loss; fragment energy-charge relationship; number and energy distribution secondary electron ejected from surfaces; and response of solid-state detectors to fission fragments. The future experimental program will include: nuclear physics experiments designed to exploit the large current capability of the machine; fission electric cell irradiations; and, possibly, subcritical assembly experiments.

As sideline efforts, the machine will be used by:

2. Advanced Propulsion Engineering Section: Provide various types of radiation environment for study of radiation effects. One purpose: to establish realistic shielding criteria for advanced nuclear-electric spacecraft systems.

(3 MeV Dynamitron expected to go into operation about June 1964)

PAGE 2 INTENTIONALLY BLANK

CHARGED PARTICLE RADIATION DAMAGE STUDIES AT THE AMES RESEARCH CENTER

B. E. Cunningham
Ames Research Center
Moffett Field, California

I. Charged particle radiation damage studies underway at Ames since 1959. Studies have been done with positive ions of hydrogen and heavier gases. Two general types of studies, both concerned with erosion, or sputtering, of metallic surfaces.

A. Investigation of the mechanism of sputtering

1. Early work of Bader and Snouse with 3 Kev N^+ and N_2^+, reported in NASA TR and presented to AVS in 1961. Work concerned with sputtering yield of copper under normal-incident N_2^+ ion bombardment. (Yield in atoms per ion as function of 3 Kev ion flux, effect of copper temperature).

2. Later work of Snouse, with 1 to 8 Kev N_2^+ ion beam in vacuum, on sputtering yields and angular distributions of sputtered polycrystalline copper, soon to be released as NASA TN D-2235. (Yield in atoms per ion as function of energy and angle of incidence of incidence of ions).

3. Present work of Snouse to be concerned with effects of crystal structure on sputtering yield.

   a. Experiments to be conducted with single crystals of copper and nickel in 1 to 200 Kev noble gas ion beams.

   b. Yield as function of crystal orientation, ion energy and angle of incidence to be measured.

4. Recent work of Moorhead on stopping cross sections of various materials for protons and single-charged helium ions at 70 to 190 Kev.

PAGE 4 INTENTIONALLY BLANK

a. Technique for determining mass per unit area of the stopping material developed for this experimental program. (Thin layer of stopping material on gold-plated piezoelectric quartz crystal and measurement of resultant change in crystal frequency).

b. Stopping cross sections measured for combinations of ions and carbon or aluminum, present experiments to include proton and silicon monoxide combination.

B. Parallel effort, in same time period, to investigate effects of sputtering on optical properties of metallic surfaces.

1. Early work by Anderson and Nothwang with 1 Kev plasma of H^+, H_2^+, and H_3^+ reported in NASA TN and presented to AVS in 1963. (Evaluate change in total hemispherical emittance and solar absorptance of titanium alloy, pure aluminum, and electrolytic copper as function of flux (or time)).

2. Present work of Anderson to evaluate changes in optical properties of various coatings and substrate materials, 1 Kev ion plasma as in earlier experiments.

II. Proposed charged particle radiation damage research programs. Effect of proton radiation on polymeric materials to be studied. Combined effects of charged particle radiation and other constituents of space environment on polymeric, metallic and electronic materials.

A. First work to be done with 400 kv proton accelerator.

1. Studies by Moorhead will include effect of proton radiation, in vacuum, on the molecular structure and surface erosion of polymeric materials and establish correlation parameters for absorbed radiation doses.

2. Effects of proton radiation on mechanical and optical properties of polymers will be studied to characterize the effects of the solar wind on materials likely to be used for long-time space missions.

B. Work on effects of combined environment to be done with 3 Mev proton accelerator.

1. Studies of the effect of charged particle radiation on materials to be done in 5-foot diameter chamber in 10^{-8} torr or lower pressure range in combination with solar radiation and microparticle bombardment.

2. Effect of the combined environment on various material properties will be studied. Facility will be designed to enable materials to be tested within the vacuum chamber.

MARSHALL SPACE FLIGHT CENTER
RADIATION DAMAGE PROGRAM

BY
RAYMOND L. GAUSE
MATERIALS DIVISION
PROPULSION AND VEHICLE ENGINEERING LABORATORY
MARSHALL SPACE FLIGHT CENTER

I. INTRODUCTION

The Marshall Space Flight Center (MSFC) Radiation Damage Program is directed primarily toward the study of the combined effects of radiation, vacuum, and temperature on the fundamental and engineering properties of non-metallic materials. It was initiated in November, 1961 with the awarding of contract NAS8-2450 to the General Dynamics Corporation for the investigation of the effects of high energy neutron and gamma radiation, cryogenic temperatures, and vacuum on the engineering properties of non-metallic materials. Since that time, the program has been expanded to include fundamental studies to determine the effects of gamma radiation and vacuum on the structure of polymers. Additionally, experiments are planned for the investigation of the effects of ultraviolet and charged particle radiation, vacuum, and temperature on the functional properties of non-metallic spacecraft materials. The program is being directed by the Materials Division of the MSFC Propulsion and Vehicle Engineering Laboratory.

II. PROGRAM OUTLINE

To date, contractual, inter-governmental, and MSFC in-house investigations are underway or planned. A brief outline of each of these is given below:

TYPE OF INVESTIGATION	PURPOSE	ORGANIZATION/CONTRACT TITLE
Contractual	Generation of engineering data on the effects of combined environments on the properties of non-metals.	General Dynamics/Fort Worth, NAS8-2450, "Investigation of the Combined Effects of Nuclear Radiation, Cryo-temperatures, and Vacuum on Engineering Materials."
	Generation of engineering data on the effects of space indigenous radiation, temperature, and vacuum on space vehicle materials.	Contract in process of negotiation.
	Validation of computer programs for predicting the activation of space vehicle materials by on-board nuclear power sources.	Contract in process of negotiation.

PAGE 6 INTENTIONALLY BLANK

TYPE OF INVESTIGATION	PURPOSE	ORGANIZATION/CONTRACT TITLE
Inter-Governmental	Fundamental study of the effects of vacuum and gamma radiation on polymer structure.	Oak Ridge National Laboratory/ MSFC Working Agreement-ORNL to perform the irradiation using MSFC vacuum equipment.
MSFC In-House	"In situ" evaluation of the effects of charged particle and ultraviolet radiation, vacuum and temperature on the properties of spacecraft materials.	Materials Division

III. PROGRAM STATUS

As indicated, the primary objective of the contractual effort is to provide immediate, practical, engineering-type data which can be used by vehicle designers for the judicious selection of environmentally stable materials for spacecraft fabrication and control. To date, extensive radiation, cryogenic temperature, and vacuum environmental data have been obtained for approximately sixty-five materials.

An agreement was formulated between the MSFC and the Atomic Energy Commission's Oak Ridge National Laboratory (ORNL) for a cooperative study to determine the changes in polymer structure produced by exposure to vacuum and gamma radiation simultaneously. The ORNL will make the irradiations in vacuum using MSFC furnished vacuum equipment and the new ORNL Cobalt 60 Facility presently being constructed. The vacuum system has been shipped to ORNL by MSFC and the program will be initiated as soon as the Cobalt 60 Facility is completed.

A two-mev Van de Graaff accelerator and a solar irradiator will be used by MSFC in an in-house investigation of the combined effects of charged particle and ultraviolet radiation on materials exposed to vacuum and extreme temperatures. Equipment is being fabricated which will permit measurement of material properties both during (in situ) and after exposure. Presently, a building to house the accelerator and solar irradiator is being constructed. Initial experiments are scheduled to commence in mid-August.

RADIATION DAMAGE AND EFFECT STUDIES

J. W. Blue
NASA-Lewis Research Center
Cleveland, Ohio

INTRODUCTION

The work I will describe is current projects in the Radiation Physics Branch of the Nuclear Reactor Division. Since this is current work, the results presented are preliminary. For some experiments there are no results as yet, so that only a discussion of approach and purpose is given.

ALPHA PARTICLE DAMAGE TO SOLAR CELLS

Investigator: A. B. Smith

Interplanetary space probes which rely on solar cell panels for electrical power will have to contend with the radiation damage due to alpha particles as well as protons. About 10% of the particles emitted in a solar flare consist of alpha particles. Essentially no work has been done in evaluating the effect of alpha particle radiation on solar cells; consequently, a program is in progress to determine their effect on solar cells.

Solar cells of 1 and 10 ohm-cm of both n/p and p/n types have been irradiated with 42 MeV alpha particles from the cyclotron. The cells were irradiated unilluminated at 25°C and in vacuum. Preliminary results are presented in Figure 1, where the change in short-circuit current with particle flux is shown. The smooth curves are averages drawn through experimental points which in most cases are the results from several cells of the same type. Proton bombardments were included to facilitate a comparison between the two types of particles. The result for protons on 1 ohm-cm p/n cells is nearly coincident with curve for alpha particles on 1 ohm-cm n/p cells and is not shown to avoid confusion.

Figure 2 shows the data plotted as in $\left[(I_{SO}/I_S)^2 - 1\right]$ vs. ln Φ. Theory predicts these plots to be straight lines with a unit slope which indicates a linear change in minority carrier trapping probability with integrated flux. The plots are straight lines and the slopes are nearly the same.

The results obtained so far indicate the ratio of the critical integrated flux (CIF) for the two types of particles to be about 5 for 1 ohm-cm p/n cells and n/p cells, that is $(CIF)_p/(CIF)_\alpha \approx 5$. This result is statistical in nature, since the same cell has not been used for both proton and alpha bombardment. Continued tests will improve the confidence level in the ratio of critical fluxes. This ratio will also be obtained for higher resistivity cells.

A STUDY OF HIGH ENERGY NEUTRON INTERACTIONS IN SILICON

Investigator: W. K. Roberts

This experiment has been included in a conference on charged particle effects, not because we believe the neutron to be charged, but rather that some of the secondary interactions produced by a neutron and by a proton are the same.

Consider a high energy proton traversing a slice of silicon. It makes either Coulomb interactions or nuclear interactions. Distant Coulomb collisions result in excitation and ionization of the silicon atom and the close collisions result in silicon nuclei recoiling through the lattice. A few protons will make close enough collisions to come within the range of nuclear forces, then the silicon atom will recoil and may carry some of the incident energy as an excited nucleus.

It is presumed that the radiation damage to silicon arises from the effect of the recoiling silicon atoms. The energy spectrum of recoiling silicon atoms is greatly different for the case of 10 MeV protons than for 10 MeV neutrons. The Coulomb cross section

$$\frac{d\sigma}{dQ} = \frac{2\pi Z^2 e^4}{MV^2 Q^2}$$

clearly favors the small recoil silicon energy, Q, whereas the silicon recoils from a neutron nuclear interaction have much higher energy. The few protons that do come within the range of nuclear forces will have silicon recoil atoms of comparable energy to those from neutron interactions. It is this connection that makes this neutron experiment of interest to the person considering proton damage to silicon.

The experiment (See Figure 3) will utilize the cyclotron beam to produce neutrons. The time-of-flight of these to a silicon fully depleted solid state detector will be measured, if the neutron interacts with a silicon nucleus. In other words the solid state detector

serves as the neutron target. The pulse from the solid state detector starts the time-of-flight clock and also is integrated to give a pulse, the size of which is propertional to the energy deposited in silicon. A two dimensional pulse height analyzer will be used to give spectra of energy deposition as a function of the incident neutron energy.

RADIATION DAMAGE TO PIEZOELECTRIC QUARTZ

Investigator: R. W. H. Webeler

Biological systems are the most sensitive systems to energetic particle irradiation. Among the inorganic materials the electrical properties of semiconductors are the most sensitive to irradiation. Much is learned by studying sensitive systems, since the reactions are generally less complex at low damage levels. It would be of interest to examine a very sensitive system to radiation damage in which the property being examined is mechanical rather than electrical. Dislocations undoubtedly play a role in some radiation induced electrical properties, however some purely mechanical property, e.g., an elastic constant, is expected to depend much more directly on dislocation mobility.

In an effort to find a material, radiation sensitive to mechanical property changes, we are examining the change in internal friction and resonant frequency of a single crystal cylinder of piezoelectric quartz cut so that the Z axis coincides with the long axis of the cylinder. The arrangement of the electrodes, used to induce oscillation of the cylinder about a nodal point in the center of the rod, is shown in Figure 4. A second set of electrodes, not shown but identical to the upper set and phased 180° from that set, is positioned about the lower half of the cylinder. The application of a small voltage at the proper frequency will excite the quartz rod to oscillate in a torsional mode. A bridge arrangement permits a measurement of the resistance, which arises as a result of the power that goes as internal friction. A crystal has been irradiated to about 10^{13} nvt at liquid nitrogen temperature and the internal friction was then measured as the crystal warmed. A representative curve of the results is shown in Figure 4. A peak was observed at about 90°K. When the crystal was cooled and warmed a second time, the peak is less pronounced, indicating annealing has occurred.

The experiment will be repeated with a longer crystal so that excitation with the third harmonic is possible. From the temperatures of the annealing peaks, the activation energy of the defect responsible for the internal friction peak can be obtained.

THERMOLUMINESCENCE

Investigator: J. A. Partridge

Studies of particle irradiated alkali halides are in progress, for the purpose of understanding the mechanisms of radiation damage. By heating irradiated single crystals, light is observed at certain temperatures, called thermoluminescence peaks. The temperature at which the light occurs and the wave length of the emission has been the object of earlier studies.

Present work is a study of the kinetics of the processes. One scheme is that of isothermal annealing wherein the temperature of an irradiated crystal is raised to a temperature just below a peak and the distribution in time of the emitted light then indicates the order of the processes.

Typical results are shown in Figure 5. The curve is interpreted as being a mixture of zero and first order. A model which would fit the observed results is also shown in the figure. From these data rate constants are obtained.

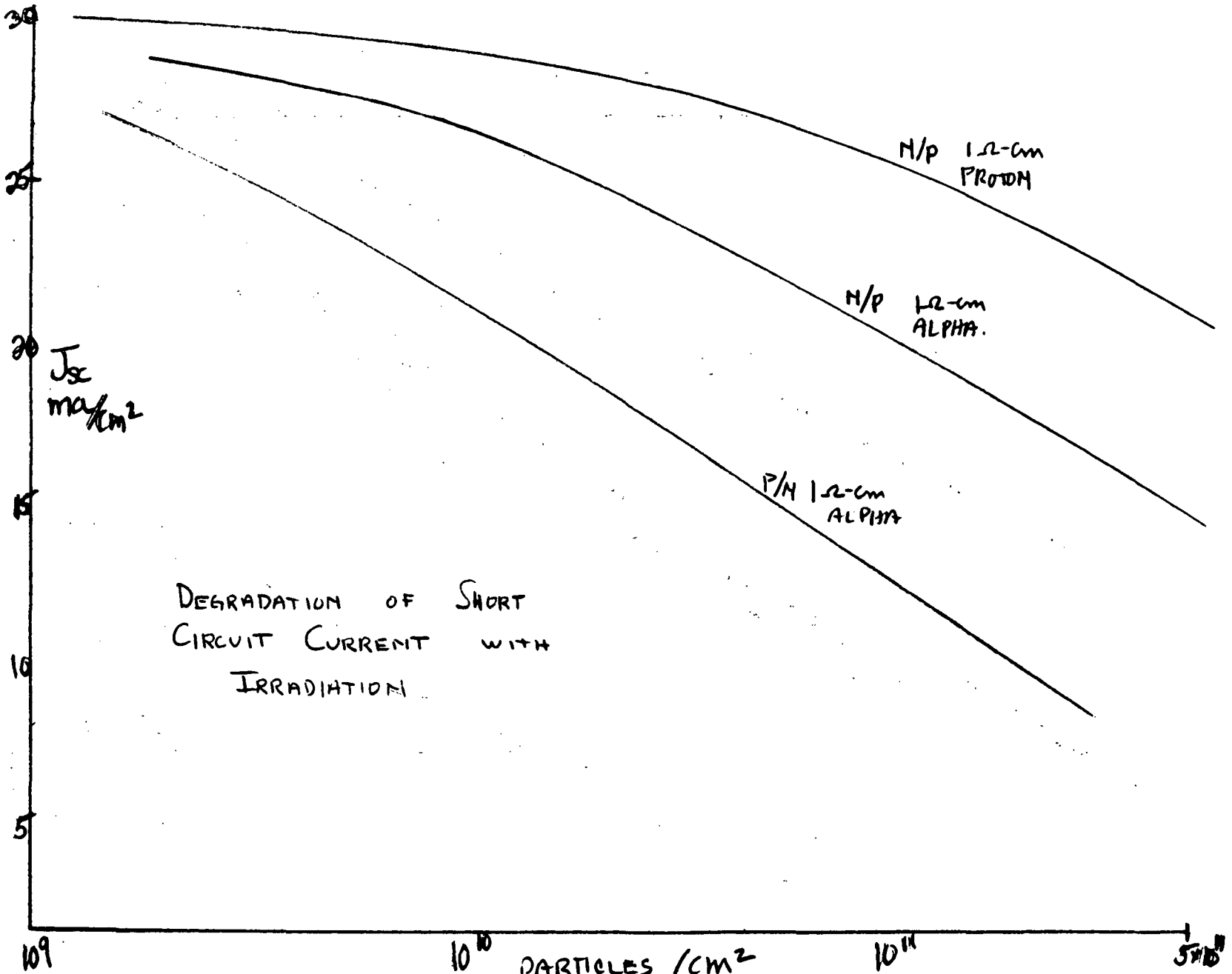
30
25
20
15
10
5
J_{sc} ma/cm²
N/p 1Ω-cm PROTON
N/p 1Ω-cm ALPHA.
P/N 1Ω-cm ALPHA
DEGRADATION OF SHORT CIRCUIT CURRENT WITH IRRADIATION
10^9
10^{10}
PARTICLES /CM²
10^{11}
5×10^{11}

Fig. 1

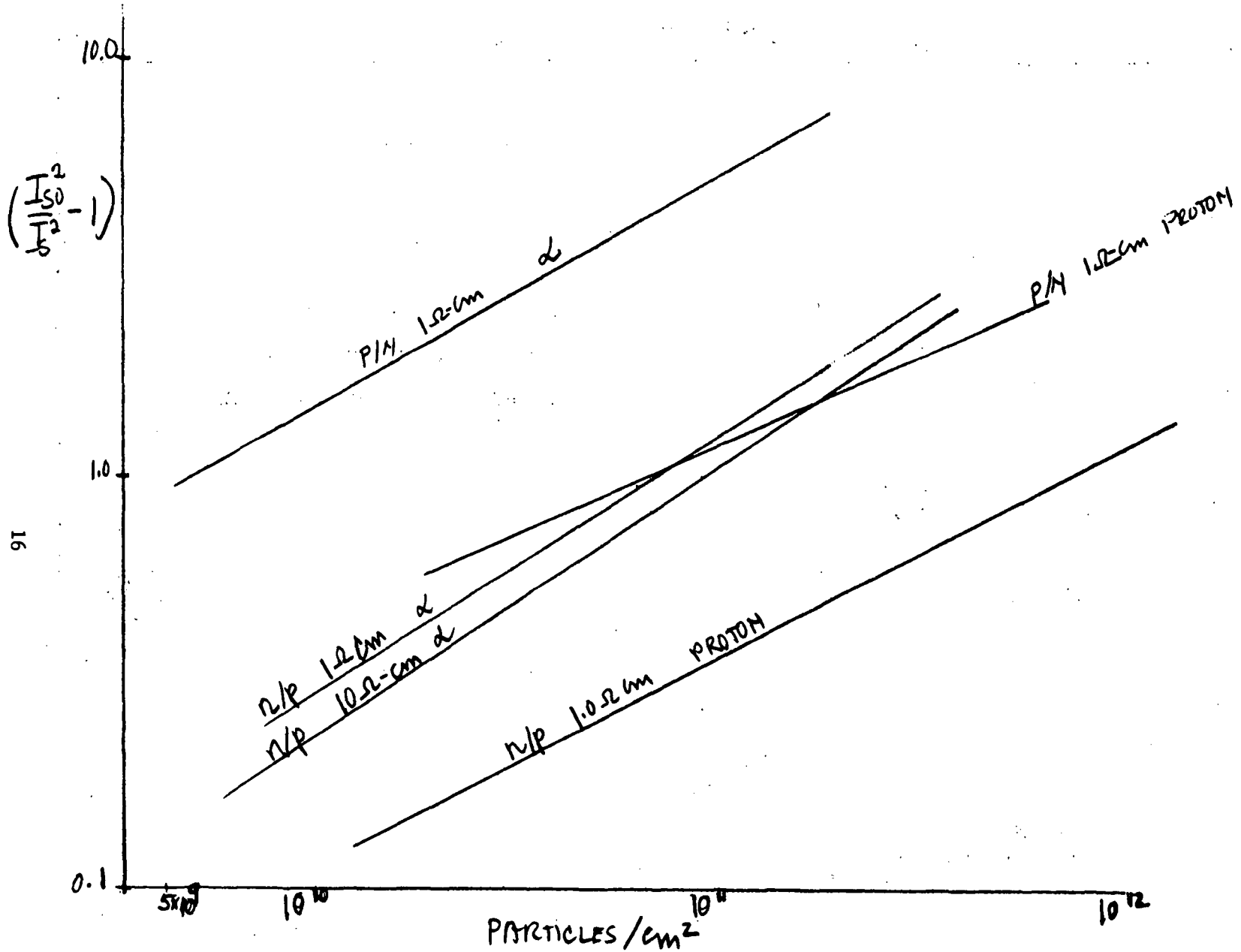
10.0
1.0
0.1
$\left(\frac{I_{SO}^2}{I_S^2} - 1\right)$
P/N 1Ω-cm α
P/N 1Ω-cm PROTON
n/p 1Ω-cm α
n/p 10Ω-cm α
n/p 1.0Ω-cm PROTON
5×10^{9}
10^{10}
10^{11}
10^{12}
PARTICLES/cm²

Fig. 2

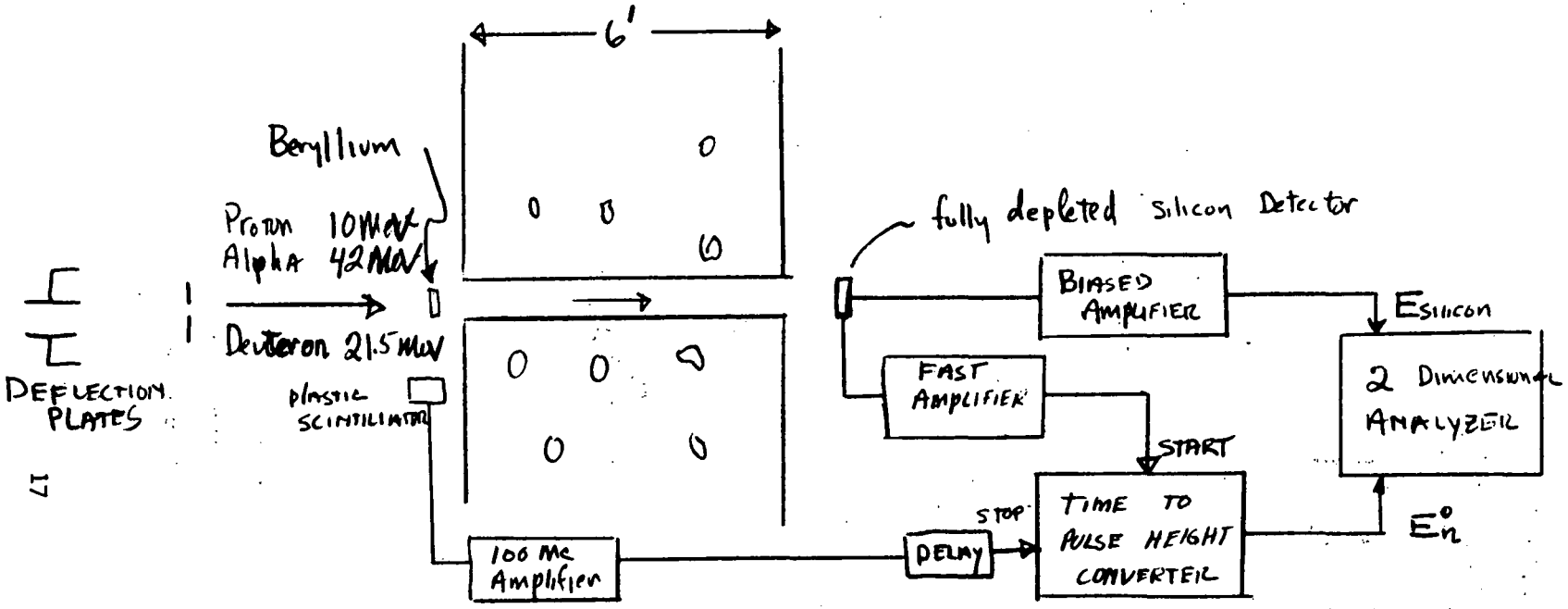

Experiment to study of Energy loss in Silicon.

Fig. 3

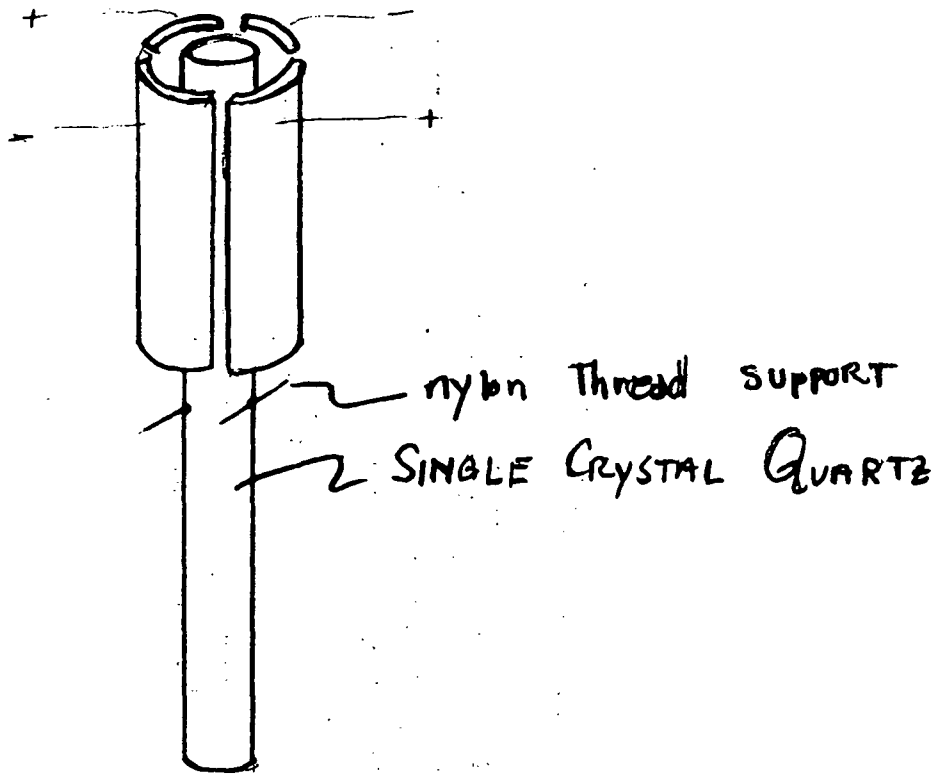
+
−
−
+
nylon Thread SUPPORT
SINGLE CRYSTAL QUARTZ

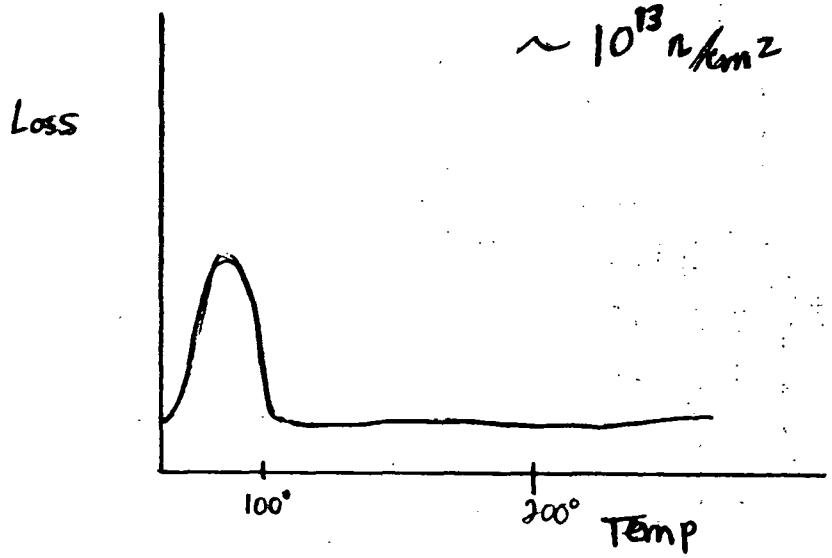
~ 10^13 n/cm^2
Loss
100°
200°
Temp

Fig. 4

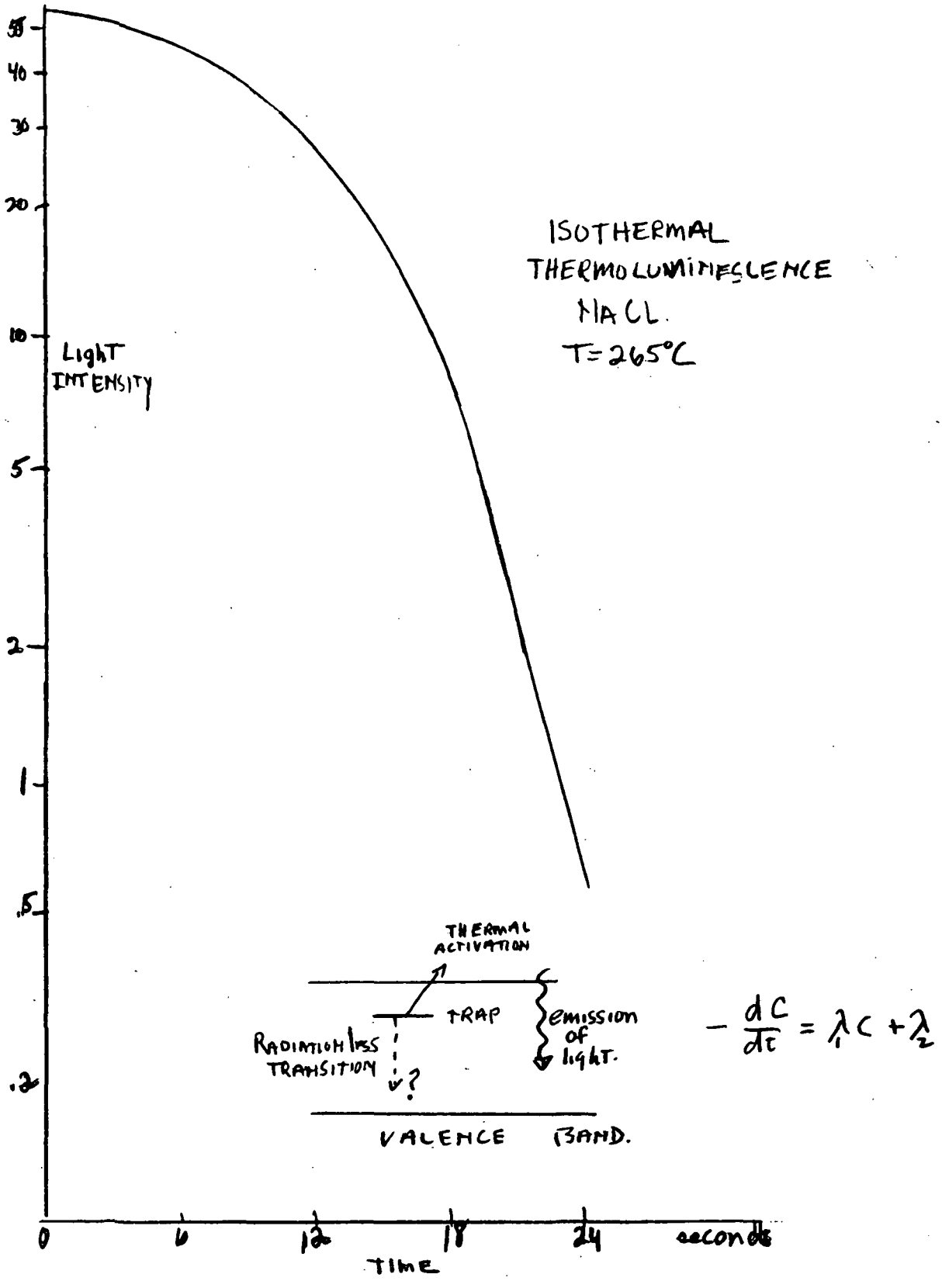

$$-\frac{dC}{dt} = \lambda_1 C + \lambda_2$$

Fig. 5

Electron Radiation Effects with the Lewis 3 MEV Dynamitron Accelerator

by

H. H. Grimes
Lewis Research Center

Generally speaking, mention of the words "radiation effects" in engineering circles usually means "radiation damage". That is, "What particular parameter changes will occur in a device or material used near a nuclear reactor or in the Van Allen belts?" To be sure, deleterious parameter changes are indeed important radiation effects, and at Lewis we both sponsor research designed to study the "damage" to specific devices and also participate in other such programs in cooperation with research and development divisions from both Lewis and other NASA Centers.

However, our primary interest is in a broad area of radiation effects study which is not directed toward the acquisition of special design parameters for devices or materials but which rather attempts to investigate the effects of radiation from a more fundamental standpoint. Charged particle radiation is particularly valuable for this type of research because of the simplicity of the damage produced. I now want to talk briefly about several of these studies in our present program. Then I will say a few more words about the more device oriented work that we are doing.

In the first category falls (1) the study of charged particle effects - primarily electron - in pure metal crystals to provide a better theoretical understanding of the damage process, (2) a study of the type and behavior of point defects produced by bombardment of certain ionic and refractory compounds and how they relate to the deformation character of these materials and (3) study of the effect of radiation induced defects on the superconducting behavior of metals and alloys.

Other research which is more device oriented includes the modification of doped crystal and semiconductor lasers which are operated in a radiation environment, and the degradation of solar cells subjected to electron irradiation.

Let us now consider these programs in more detail.

The displacement of atoms from their normal lattice sites by energetic particles is an aspect of radiation damage which has received much attention

PAGE 20 INTENTIONALLY BLANK

in recent years. Considerable research effort has been expended in trying to determine the number and types of defects introduced by various radiations and the relation between defects and physical property changes. Several theories have been proposed which attempt to provide a quantitative measure of the damage expected.

In its present state, radiation damage theory permits only an approximate calculation of the number of atoms displaced. This is due not only to a lack of quantitative information about the parameters in the theory but also because the effects of simplifying assumptions in the theory have not been fully evaluated. The current status of defect solid state theory is such that it is not possible to calculate the relation between physical property changes and concentration of radiation induced defects with a high degree of accuracy. Theoretical calculations of radiation damage concentrations exceed experimental determinations by a factor of some three to ten even in the best understood materials. This relationship is important not only to a basic understanding of the defect solid state but also as a quantitative measure of defect concentration in evaluating proposed theoretical models of radiation damage.

In the Solid State Physics Section of the Materials and Structures Division we have initiated a program of experiments utilizing the Dynamitron Accelerator aimed at obtaining a better understanding of the detailed mechanisms of displacement effects and the defect solid state in general. These experiments are concerned with determining the parameters required for radiation damage calculations, evaluating the various assumptions used in the models for radiation damage calculations and studying the relationship between defects and structure sensitive properties. The program is limited to the study of electron damage in metallic single crystals, and the measurement of electrical resistivity as the defect sensitive property.

Electron bombardment in the 0.1 to 3.0 Mev range offers several advantages over fission fragments, neutrons, and ions for this program.

1. Electrons in this energy range can be used for studying the displacement threshold since the energy can be adjusted so that the damage consists only of simple interstitial - vacancy pairs (Frenkel Defects).

2. These Frenkel defects produced are randomly distributed in the crystal rather than in the localized regions of complex damage obtained with more massive particles.

3. The environmental conditions are relatively easy to control and the samples do not acquire radioactivity during electron irradiations.

4. The greater range of electrons compared to ions (typically, an order of magnitude larger) permit greater flexibility in the design of experiments.

and finally,

5. With the Dynamitron Accelerator, appreciable damage to a sample can be accumulated in convenient times. A 50 $\mu a/cm^2$ beam density for one hour corresponds to a total dose of 10^{18} electrons/cm^2. If each electron produced one Frenkel pair, this dose would produce adequate damage for experimental study. However, we have to use thin targets to minimize beam energy degradation and target heating and as a result less than one percent of the impinging electrons would be involved in displacement collisions. The Dynamitron, with a maximum rating of about 3000 $\mu a/cm^2$, is able to produce the damage required.

The specific goals in this program are several. First, to determine the displacement threshold as a function of crystallographic direction in a variety of metal crystals. The irradiations are performed at liquid helium temperatures in order to "freeze-in" the damage. An attempt will be made to correlate this information with crystal parameters in order to obtain relationships of general validity. Particular emphasis is placed on the determination of the "probability of displacement" function. This function appears in the expression for the number of displacements per primary knock-on, i.e.,

$$N_d = n_o \phi \sigma_d = n_o \phi \int_{E_d}^{E_m} P(E)\, d\sigma(E) \quad , \text{ where}$$

n_o = density of atoms

ϕ = flux

$P(E)$= prob. of displacement

$\sigma(E)$=relativistic scattering cross section

It is usually assumed that P(E) is simple step function or a multiple step function or a ramp formation; that is,

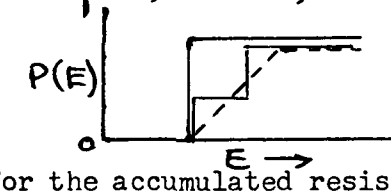

Using actual data for the accumulated resistivity vs. energy, we will work backwards to obtain P(E) function from this data and the Frenkel defect resistivity which is the second aspect of this research. The Frenkel defect resistivity is determined from the energy dependence of resistivity vs. dose experiments. A third aspect of this program is to study the recovery distribution spectrum of radiation induced defects. The defects produced will, of course, be simply interstitials and vacancies with various separations, and by bombarding single crystals in various directions the relative abundance of

stable Frenkel pairs will be varied. Since the recovery kinetics for each separation is different, it is expected that the characteristics of the various stable Frenkel defect configurations can be determined in this way. A fourth point of this study is to determine the transition to multiple defect production. In low mass metals, 3 mev electrons are capable of producing clusters of defects similar to those produced by neutron and ion bombardment. The transition from simple to multiple defect production will give important information on the model used to calculate multiple defect production and would, therefore, be useful to understanding all types of radiation damage.

And finally, we will determine the effect of focusing collisions. Where focusing collisions are possible, large amounts of energy are transferred via a series of focused atomic collisions for great distances through a crystal lattice without producing the permanent damage expected on the basis of the energy involved. At low temperatures where the defocusing effect of atomic vibrations is eliminated, it has been proposed, and observed in ion sputtering experiments, that focusing collisions occur predominantly in certain close-packed crystal directions. It is important to test the effectiveness of focusing collisions in radiation damage because the present calculations, which do not include focusing, exceed the number of defects produced by experiment. Study of the temperature dependence of defect production should help towards an understanding of the effectiveness of focusing collisions.

The second research program listed deals with the nature and motions of certain point defects produced by irradiation of one of a class of very high melting materials known as the refractory metal carbides. Representative of this group is TaC which has a melting point of over 3800°C. It is extremely brittle, and tends to be non-stoichiometric. (Usually about 1% carbon deficient).

Despite its attractiveness as a high temperature material, relatively little is known about its chemical, physical, and mechanical properties. For example, it is not really clear what type of bonding exists in the material, i.e., whether it is primarily metallic, covalent, or ionic. It has certain properties characteristic of each, and these vary with C content. As simple a property as electrical conductivity is not well understood in this material either in terms of mechanism or in actual value. And while it is well accepted that this material is very brittle, the reason for low ductility is not really understood. However, it is fairly safe to say that this brittle behavior is associated with the defect structure of the material; whether due to the carbon deficiency or impurities is not known. It is clear though that an improvement of the mechanical behavior of these materials will evolve from a detailed knowledge of the type, concentrations and properties of the point defects present in them.

A simple way to introduce defects into these materials for study is by particle irradiation -- preferably charged particles for reasons stated before. Information of the nature of defects produced will come from radiation damage annealing, Hall effect measurements and threshold determinations. The effect of irradiation induced defects on mechanical behavior involves conventional testing procedures.

Specifically, in this program thin wires of tantalum carbide will be irradiated with electrons of energies up to 3 Mev at cryogenic temperatures. The defect-sensitive property measured is again electrical resistivity. Displacement threshold energies will be determined as an important part of the experiment, but will be complicated because of the large mass difference between the tantalum and carbon atoms (181 and 12, respectively). Samples with differing percentages of carbon will be irradiated to determine what role the carbon atoms play in the rate of damage production. Also, if reliable values for the cross sections of displacements at various electron energies can be determined theoretically, we will learn the resistivity of Frenkel defects in TaC and consequently determine the defect concentrations.

The more informative phase of this program will, undoubtedly, be the damage annealing experiments. Differentiation of defect types, and mobilities can be obtained this way. In order to determine the mechanism involved in an annealing process, both isochronal and isothermal anneals will be used.

The interpretation of these data for TaC will be a very difficult one at best and will undoubtedly involve the use of considerable other data and theory. The application of this information to the improvement or understanding of mechanical properties is a long step but nevertheless an important one.

The third program is one in which charged particle radiation is used to produce certain changes in the crystal lattice resulting in modification of the superconducting behavior of the material. As you probably know, for a practical superconducting device (say, a magnet in a space electric power system) the weight penalty of the required refrigeration system and magnet windings can be reduced by raising the transition temperature of the superconductor or by improving the current carrying capacity. In the past, certain techniques have been somewhat successful in doing this. Cold working of Nb_3Sn alloy into a filamentary structure has been used to significantly increase the transition temperature and current carrying capacity of the superconductor. At G.E. other work involving neutron irradiation of this alloy has also resulted in an increased current carrying capacity. And finally, the addition of certain impurities (generally interstitial) to certain transition metals has resulted in changes in the superconducting behavior of them, both lowering and raising the transition temperature. It is the purpose of our program to study the bases for these changes by performing and interpreting controlled experiments on pure metals and alloys using well characterized charged particle radiation, simple deformation and various dissolved interstitial impurities.

The effects observed seem to be volume effects, that is, related to a more homogeneous distortion of the electron distribution rather than localized perturbations of defects.

To date, most of the work in this area has involved study of the impurity and deformation effects. The use of charged particle irradiation

here, however, seems promising since the damage produced is more uniformly distributed throughout the crystal than with neutrons where displacement spikes are common. The information obtained here will be utilized to improve understanding and performance in certain promising alloys and compounds.

A fourth program which is more device oriented, but which nevertheless retains a fundamental character is the effect of defects introduced by charged particle radiation on the laser properties of materials.

Particle damage to both ionic materials and semiconducting materials is known to affect certain properties of the crystal which also are essential for laser action. For example, in doped crystals the laser action depends on the population inversion of certain activated states, that is, the disporportionate population of a metastable energy level of the impurities in the crystal. Particle irradiation can further ionize these atoms, thereby changing both the number and nature of transitions that can occur. It can enhance pumping efficiency and possibly the probability of spontaneous emission. In general, it can either improve or damage the laser.

The same general arguments apply to semiconductor lasers which depend on the number of electrons and holes that can recombine at the p-n junction. The effect of particle irradiation on these materials in reducing the minority carrier lifetime is well known.

To date, due to the usual procurement delays, the work until now has mainly involved looking at absorption spectra of doped ruby crystals in the range 2000 - 12,000 Å. Irradiation with both X-rays and electrons caused spectral changes at frequencies characteristic of ruby laser operation. Some 17% increase in absorption has been observed which could only be annealed out by heating to 1000°C for 30 minutes.

Other work at the University of Michigan has shown that γ - irradiation of ruby lasers could improve the output, apparently by enhancing the pumping efficiency.

This laser work is rather new at Lewis, and in fact, with the exception of the Michigan work, is almost unique in the field of laser research. Our laser equipment finally arrived this week and the laser operation aspect of our work has just started. Both doped crystal lasers, like ruby, $CaWO_4$, CaF_2, and semiconductor lasers will be studied in this program.

Another device oriented program, which perhaps comes closest to being a radiation "damage" study, is one involving the effect of charged particle damage to thin film solar cells. This program is being done as a cooperation effort between Chemistry and Energy Conversion Division, Nuclear

Reactor Division, and Materials and Structures Division and has the purpose of evaluating plastic laminated thin film CdS solar cells in simulated Van Allen radiation. Dr. Blue from the Nuclear Reactor Division has mentioned the aspects of this work which have to do with high energy proton effects. I will talk only about electron effects. The solar cell performance is, in either case, evaluated by C&EC Division.

The solar cells are being evaluated from the standpoint of several parameters. First, the effect of radiation on junction characteristics and power output are being studied. Secondly, the effect of ionizing radiation on the plastic encapsulant is also of great interest. Quantities being measured are shunt resistance, series resistance, a fudge factor, α, in the voltage-current characteristic curve, the reverse saturation current; and under a solar simulator, the spectral response and output; that is, the open circuit voltage, short circuit current and maximum power. Samples of various plastics are also being studied. Preliminary electron and UV damage studies on various plastics showed three promising encapsulants -- Tedlar, weather-durable Mylar and "H" film. Groups of 10 cells encapsulated in these plastics were then irradiated at 2.5, 1.0, and 0.6 Mev. After an initial dose of $10^{15} e/cm^2$, no degradation was observed. Tedlar had a tendency to darken then anneal. The other plastics were undamaged.

A second irradiation was at $10^{16} e/cm^2$. The Tedlar definitely darkened and did not anneal. Mylar got quite brittle, but "H" film was undamaged. Forty percent of the Tedlar cells had failed due to delamination. Of the remaining Tedlar cells, the output short-circuit current and maximum power had dropped to 75% of their original values. This was due entirely to darkening of the Tedlar. Both Mylar and "H" film encapsulated cells showed no deterioration of their electrical properties.

At $4 \times 10^{16} e/cm^2$, Tedlar covered cells had completely failed due to complete degradation of the plastic. At $10^{17} e/cm^2$ Mylar is extremely brittle and very difficult to handle. All cells appeared to be badly damaged immediately after irradiation. Short circuit currents at this time were down 50-80%.

A few days ago, however, further testing has shown that considerable annealing has taken place and now the short-circuit current degradation is only down 0-20%. These data are preliminary and are still being followed.

In conclusion, I have attempted to give you a feeling for the direction our overall program of accelerator connected research is taking. Because of the brief time we have actually been operating, our programs are few in number and for the most part are in the early stages. In the near future we will undoubtedly be in a better position to discuss more details.

TECHNICAL MEMORANDUM

TM X-52007

EFFECTS OF IMPURITIES ON RADIATION DAMAGE OF SILICON SOLAR CELLS

by Joseph Mandelkorn, Lawrence Schwartz, Jacob Broder,
Harold Kautz, and Robert Ulman
Lewis Research Center
Cleveland, Ohio

NATIONAL AERONAUTICS AND SPACE ADMINISTRATION

PAGE 28 INTENTIONALLY BLANK

EFFECTS OF IMPURITIES ON RADIATION

DAMAGE OF SILICON SOLAR CELLS

by Joseph Mandelkorn, Lawrence Schwartz, Jacob Broder,
Harold Kautz, and Robert Ulman

Lewis Research Center
National Aeronautics and Space Administration
Cleveland, Ohio

Some effects of impurities in the base material of silicon solar cells on junction characteristics and radiation damage were determined in previous work comparing n-on-p and p-on-n solar cells.[1,2,3] This work had established the fact that the substitution of boron for phosphorus in the base material of solar cells increased the minority-carrier diffusion length preserved in the base material after bombardment. It was also determined in the same work that the optimum concentration of boron in the base material of cells for achievement of good junction characteristics and maximum power output after bombardment corresponds to that of 10-ohm-cm material.

Later experiments indicated that the diffusion-length degradation in the base region of the n-on-p cell, caused by high-energy-particle bombardment, was related to interaction of boron atoms with bombardment-produced lattice defects.

A theory was formulated to explain the effects of impurities on the basis of the following hypothesis: The probability of a donor or acceptor atom associating with a lattice defect in silicon to create a recombination center is determined by the properties and concentration of donor or acceptor atoms and the density of lattice defects.

The density of lattice defects in a single-crystal silicon ingot varies with position in the ingot and is a function of single-crystal growth conditions. The defect density in silicon is further increased by processing the material to make a device or by high-energy-particle bombardment. If the hypothesis holds true, then no matter what the density of lattice defects or their cause (growth, processing, bombardment), there should be an observable dependence of minority-carrier diffusion length on the specific acceptor or donor element as well as on its concentration in the material or device.

To test the hypothesis, solar cells were made from silicon ingots containing either boron, aluminum, indium, gallium, or gadolinium as acceptors. Gadolinium and other rare earth elements exhibit valence behavior similar to that of the elements in Group 3 of the periodic table, and gadolinium was found to act as an acceptor in silicon.

The concentrations of the various acceptor elements in the silicon ingots grown for the experiment were controlled to yield silicon in the 10- to 20-ohm-cm resistivity range, in accordance with previous findings.[2,3] Some difficulty was encountered in growing a large-diameter 20-ohm-cm silicon ingot doped with gadolinium. Apparently, only a small percentage of gadolinium atoms added to silicon undergo room-temperature ionization. At first, a good-quality 50-ohm-cm gadolinium-doped ingot was grown. Subsequently, by addition of large quantities of gadolinium to a silicon melt, a 20-ohm-cm ingot was grown; however, the strains produced by the high concentration of gadolinium in the ingot reduced minority-carrier diffusion lengths in most regions to values below 100 microns. The best sections of the ingot were selected, and cells were made from wafers cut from these sections. These cells had initial base-region diffusion lengths exceeding 120 microns.

Additional groups of cells were made from several boron-doped ingots having boron concentrations corresponding to a range of resistivities from 1 to 1000-ohm-cm.

Finally, since oxygen has been identified as an impurity affecting radiation damage in silicon,[4] groups of cells were also made from various grades of 10-ohm-cm float-zone silicon. Typical float-zone silicon differs from conventional Czochralski silicon in that it contains approximately one-hundredth the oxygen concentration that Czochralski silicon contains.[5]

All cells were made by a fabrication process previously described.[3] The cells had good junction characteristics and diffusion lengths exceeding 120 microns. Many of the cells made from aluminum-doped silicon had unusually good junction characteristics and diffusion lengths exceeding 150 microns.

Selected groups of cells were first subjected to a series of 1-Mev electron bombardments. The junction characteristic,[3] diffusion length, and power output under a solar simulator were measured for each cell after each bombardment.

Table 1 presents average characteristics of the selected groups of cells after bombardment. Because the cells within each group had uniform characteristics after bombardment, valid differentiation in terms of average diffusion length preserved was possible.

Comparison of the 1-, 10-, and 100-ohm-cm C-B cell group data clearly shows that decreasing the boron concentration in the base material increased the magnitude of diffusion length preserved after any specific bombardment dose.

Fig. 1 shows the diffusion length plotted as a function of the bombardment dose. The slopes of the plots do not conform with the

half-power dependence predicted from simple recombination theory.[6] The magnitudes of the slopes for the various boron-doped groups increases with increasing boron concentration in the base region of the cells. The 50-ohm-cm Gd group plot has the smallest magnitude of slope despite the fact that the acceptor concentration in the base region of the cells in the Gd group is much higher than that of the 100-ohm-cm C-B group.

Equivalent results were obtained in a series of 10-Mev proton bombardments of the various boron-doped Czochralski cell groups. Several of the 10- to 20-ohm-cm groups containing acceptor elements other than boron were also subjected to the series of 10-Mev proton bombardments.[7] A relative-long-wavelength collection efficiency method[7] was used to measure diffusion lengths of proton-bombarded cells. The aluminum-doped cells preserved [redacted] longer base-region diffusion lengths after each bombardment than cells doped with an equal concentration of boron.

The Table 1 data do not show any significant difference between the 10-ohm-cm FZ-B group and the 10-ohm-cm C-B group in degradation of diffusion length and thus indicate no large effects on radiation damage were produced by oxygen in this case. The 10-ohm-cm FZ-B-Cl_2 group does, however, undergo less diffusion-length degradation than the other 10-ohm-cm groups. The superior behavior of the FZ-B-Cl_2 group did not manifest itself in a series of 10-Mev proton bombardments.

Subsequently, sample wafers of the materials used to create the different groups were analyzed for impurity content by mass spectrography. The samples included wafers from completely processed solar cells that were treated to remove contacts and the diffused region. The FZ-B and the Czochralski materials were found to contain less than 0.2 part per million of chlorine, whereas the FZ-B-Cl_2 samples contained approximately 1 part per million of chlorine. Further evidence that chlorine affects radiation damage of float-zone material was obtained from an experiment in which cells were fabricated from wafers of a float-zone ingot by using two different diffusion processes to form the p-n junction. In one case the standard process was used,[3] and, in the second case, phosphorus trichloride was carried in a stream of reducing gas over the heated wafers. Under electron bombardment, the phosphorus trichloride cells had superior behavior comparable to that of the FZ-B-Cl_2 group, whereas they showed no superiority under proton bombardment.

Table 1 also presents data on curve-power-factor degradation of bombarded solar cells. The curve power factor (CPF) is defined as the ratio, expressed in percent, of the maximum power output of a cell to the product of its open-circuit voltage and short-circuit current. The decreases in curve power factor listed in the table occur because of increases in base-region series parasitic resistance as a result of

majority-carrier removal under bombardment. The 100-ohm-cm C-B group is very adversely affected after the first bombardment, while the 10-ohm-cm cells are seriously affected only after the final dose. Of the 10-ohm-cm cell groups, the C-B group is most affected, while the FZ-B group is least affected. The latter result indicates that oxygen in silicon acts to increase carrier removal rate.

After final bombardment measurements were made, two of the FZ-B-Cl_2 cells were reduced to a thickness of 0.006 inch from the original thickness of approximately 0.015 inch. Measurement of the CPF of these cells showed that the cells regained the CPF values they had after the third bombardment. Cells 0.006-inch thick have been fabricated without difficulty and may find use in lightweight collapsible module solar cell arrays having small surface area when collapsed.

Degradation of the 10-ohm-cm cell due to carrier removal is not of practical concern because of the extremely heavy bombardment dose required to affect the CPF of 10-ohm-cm cells. Carrier removal, however, does affect the validity of diffusion-length measurements made on high-resistivity cells. The diffusion lengths listed in Table 1 were obtained by the method described by Rosenzweig,[8] which relates the short-circuit current measured under electron beam irradiation to diffusion length. The extremely high base series parasitic resistance that existed in the 100-ohm-cm cells after the fourth bombardment prevented the measurement of short-circuit current of the cells. The 10-micron diffusion length listed for the 100-ohm-cm C-B cells is, therefore, the apparent rather than the actual diffusion length. Similarly, data obtained on 1000-ohm-cm cells after small bombardment doses were not valid and therefore are not listed in Table 1.

In conclusion, a relation between the element used as an acceptor or donor in the base region of solar cells and the diffusion length preserved in the base region after bombardment has been shown to exist. Since simple recombination theory does not take into account the role of acceptors or donors as participants in the formation of recombination centers, it cannot be expected that the results of the experiments conform with the aforementioned theory.

The effects of impurities on the original characteristics of silicon material and devices is often obscured by uncontrolled variables in growth and processing. High-dose particle bombardment was used to inject sufficient lattice defects to make the effects of original defect density variation in the materials investigated negligible. Bombardment thus permitted the clear discernment of the effects of impurities. The aluminum-doped cells were found to be highly superior in terms of diffusion length retained after bombardment. This result correlates with the fact that many of the aluminum-doped cells had superior diffusion lengths prior to bombardment. A similar correlation occurred in that the high chlorine content float-zone material, from which cells

with superior bombardment behavior were made, had a higher minority-carrier lifetime than other samples of float-zone material grown by identical processes. These correlations are in agreement with predictions based upon the hypothesis stated at the beginning of the paper.

Analysis of junction characteristics of the various groups of cells made in this study and in a previous study[3] revealed a dependence of the junction characteristic on the specific acceptor element and on its concentration in the base material of the cells. It was found that, the lower the concentration of various acceptors in the base material, the more "ideal" were the junction characteristics of cells.[3] Aluminum appears to be the most desirable acceptor element in silicon for the creation of fine quality junctions. Impurities in silicon affect junction characteristics by creating strains in the material due to misfit in the lattice, by associating with lattice defects to create recombination centers in the junction region, and by migrating to and precipitating in the junction region during high-temperature fabrication processing. The aluminum atom apparently creates minimum disturbance in the silicon lattice, and, as the bombardment results show, has [redacted] LESS [redacted] tendency to combine with lattice defects to form recombination centers. Aluminum is, therefore, a most attractive acceptor for use in silicon.

The activity of acceptor or donor atoms in the creation of recombination centers in silicon is attributed to association of vacancies with these atoms to produce a recombination-center configuration. Spin resonance measurements have permitted determination of configurations of vacancies in silicon with oxygen or phosphorus that act as trapping centers.[9,10] It is, therefore, reasonable to assume that certain configurations of vacancies in silicon with impurities result in recombination centers.

The authors wish to thank Calvin Davidson of the Lewis Research Center for growing the Czochralski materials used in the investigation and the Dow Corning Company for supplying the float-zone materials. We thank R. Statler of the Naval Research Laboratory for electron-bombardment and diffusion-length measurements, W. Rosenzweig of the Bell Telephone Laboratories for diffusion-length measurements and helpful discussions, and W. R. Willardson and A. J. Socha of the Bell and Howell Research Center for mass spectrograph analyses of samples.

REFERENCES

1. Mandelkorn, J., Kesperis, J., McAfee, C., Pharo, W., and Schwartz, L.: Proceedings of the Fourteenth Annual Power Sources Conference, May 1960, p. 42.

2. Mandelkorn, J., McAfee, C., Kesperis, J., Schwartz, L., and Pharo, W.: Proceedings of the Fifteenth Annual Power Sources Conference, May 1961, p. 102.

3. Mandelkorn, J., McAfee, C., Kesperis, J., Schwartz, L., and Pharo, W.: J. Electrochem. Soc., 109, 313, 1962.

4. Wertheim, G. K., and Buchanan, D. D. E.: J. Appl. Phys., 30, 1232, 1959.

5. Kaiser, W., Keck, P. H., and Lange, C. F.: Phys. Rev. 101, 1264, 1956.

6. Rosenzweig, W., Gummel, H. K., and Smits, F. M.: Bell System Tech. J., 42, 399, 1963.

7. Mandelkorn, J., et al.: To be published.

8. Rosenzweig, W.: Bell System Tech. J., 41, 1573, 1962.

9. Bemski, G.: J. Appl. Phys. 30, 1195, 1959.

10. Watkins, G. D., and Corbett, J. W.: Discussions Faraday Soc., 31, 86, 1961.

Lewis Research Center
National Aeronautics and Space Administration
Cleveland, Ohio, February 10, 1964

TABLE 1. - EFFECTS OF 1-MEV ELECTRON BOMBARDMENT ON DIFFUSION LENGTH, L, AND CURVE POWER FACTOR, CPF, OF SOLAR CELLS

Cell group (a)	Number of samples	Dose, e/sq cm							
		1.2×10^{15}		4.8×10^{15}		1.5×10^{16}		4.1×10^{16}	
		L	CPF	L	CPF	L	CPF	L	CPF
1-ohm-cm C-B	5	17	70	9	70	4.5	68	2.5	68
10-ohm-cm C-B	8	30	70	18	70	11.5	66	8.5	60
10-ohm-cm FZ-B	5	32	70	19	70	12.5	68	8.5	66
10-ohm-cm FZ-B-Cl_2	4	43	70	26	70	16	68	10	63
50-ohm-cm C-Gd	4	37	60	26	54	----	--	15.5	--
100-ohm-cm C-B	6	65	30	44	--[1]	31	--	10	--

[a]C, Czochralski; B, boron doped; FZ, float zone; Cl_2, high chlorine content; Gd, gadolinium doped.

E-2412

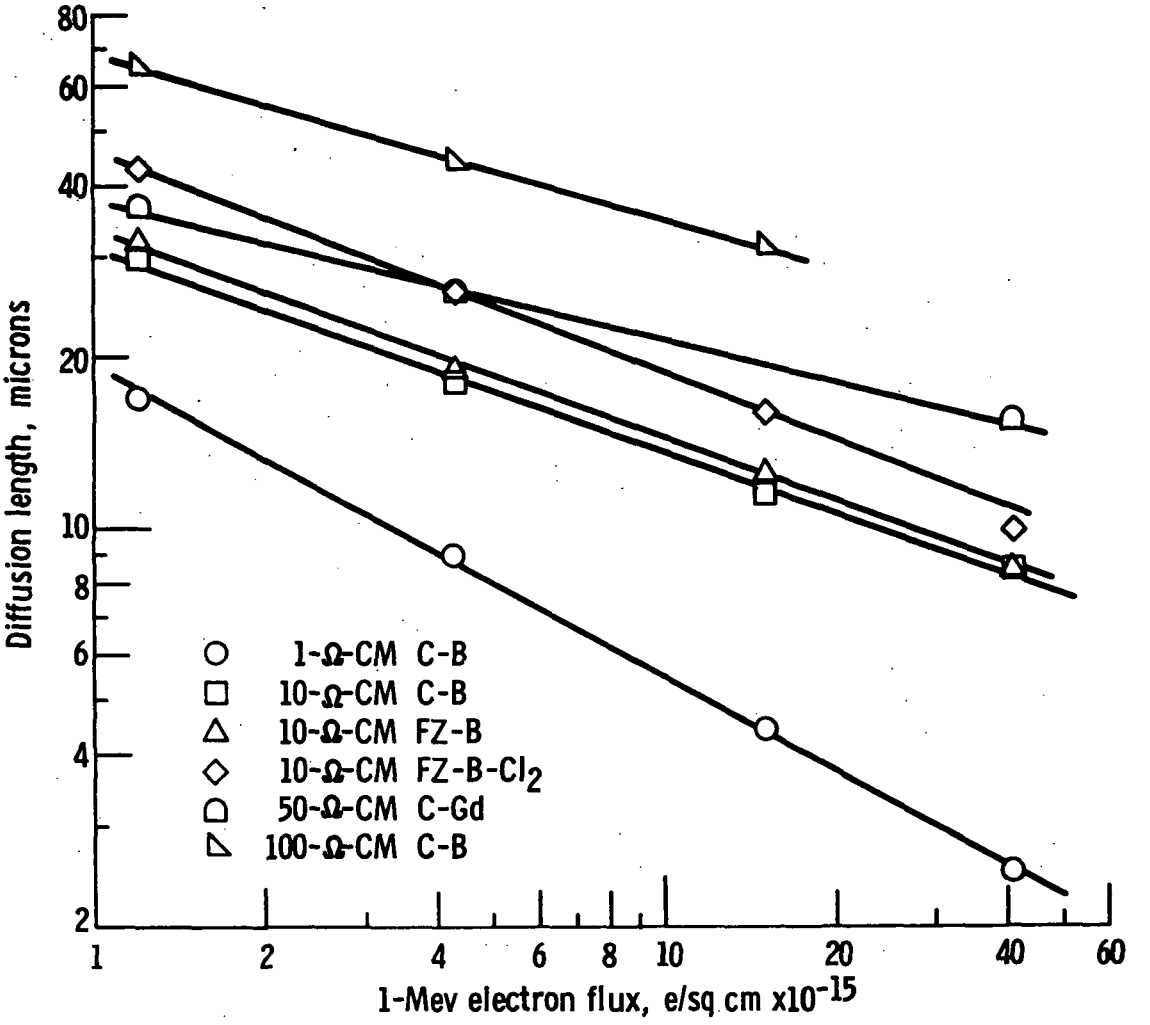

Figure 1. - Diffusion-length degradation versus 1-Mev electron flux.

A NOTE ON THE TALK AND NASA TECHNICAL MEMORANDUM TMX-52007 PRESENTED AT THE NASA HQ CHARGED PARTICLE RADIATION EFFECTS MEETING, MARCH 19-20, 1964 by J. Mandelkorn

---

by

F. G. Cunningham and M. M. Sokoloski
Goddard Space Flight Center
Greenbelt, Maryland

In the following note we shall attempt to include some remarks on various questions that arose during the talk of Mr. J. Mandelkorn which we feel are pertinent to the overall NASA Radiation Effects Program.

It should be noted that the authors feel that the experimental results of Mr. Mandelkorn's work are interesting and encouraging. However, theoretical questions were raised at the time by the author and it is to these questions that the present discussion is directed.

The ability of the p-n junction to collect the minority carriers can be described by a diffusion length. It is an average quantity calculable from a mobility and an "average lifetime". However, it must be recalled that it is not strictly correct to imply that the reciprocal lifetimes are additive. It is well known that the carrier mobility depends upon the type of impurities and the lattice scattering mechanism, and is based upon an effective mass tensor approximation which depends on the crystallographic structure. Optical phonons have been shown to play an important part in silicon[2], even though it is a non-polar crystal, and impurities in the lattice will only magnify this effect. This consideration must be undertaken before any theory is put forward concerning the apparent increase of the radiation resistance of silicon solar cells.

The interpretation of the radiation damage phenomenon is still an open and difficult question. The so-called half power law dependence of the diffusion length upon radiation flux is a very rough first approximation and has little theoretical justification, being based upon a "damage" coefficient whose evaluation is theory dependent. Attempts to validate this half power law with diffusion length measurements based upon an idealized diffusion function; i.e., the error function, is unjustified[3].

PAGE 38 INTENTIONALLY BLANK

The same error was made in an attempt by Simon, Denney and Downing[4] to utilize this approximation to determine the energy dependence of proton damage in silicon. Therefore, we should be well advised to consider this problem more carefully.

The distinction between recombination centers and carrier removal centers is only relative. A tremendous amount of information concerning these centers needs to be determined: The energy level with respect to the band edges, the charge state as a function of Fermi-level, the structure, the mobilities, the cross-sections for carrier capture, etc. In addition, other recombination mechanisms, e.g., direct band-band transitions via multi-phonon (acoustical) and optical phonon emission are known to exist. Since optical phonons have been shown to be not negligible in silicon[2], recombination by this mechanism, especially in highly doped silicon, cannot be overlooked. To our knowledge the relative importance of these possible recombination mechanisms and recombination via levels in the band gap has not been determined.

A great deal of experimental work has been done on determining the capture cross sections in silicon and germanium and it has been found that cross sections range all the way from 10^{-12} cm^2 to 10^{-24} cm^2[5]. The centers with cross-sections in the range 10^{-21} to 10^{-24} cm^2 are associated with Coulomb repulsive centers, those in the range from 10^{-15} to 10^{-12} are associated with Coulomb attractive centers while those in the intermediate range of 10^{-15} to 10^{-17} cm^2 are known or presumed to be neutral.

It is known that centers exist which act almost exclusively as traps; e.g., the probability for an electron captured by a trap and to be re-emitted to the conduction band is much greater than the probability for recombining with a hole in the valence band. In other words, the lifetime of the electron in the trap is short compared with the recombination lifetime; this we call multiple trapping because the electron can be captured and re-emitted to the conduction band many times before recombination finally occurs. In other traps, the subsequent recombination directly from the trap can compete with re-emission to the conduction band: Here we have some multiple trapping. Recombination centers exist which upon capturing an electron immediately captures a hole. Hence, it follows that recombination centers are not merely polarized centers capable of capturing carriers, nor are they associated with chemical impurities in all cases. All these processes go on simultaneously and yield a rather complicated picture. This complication renders the experimental determination of lifetimes very difficult. However, even though the results so obtained are in some cases dubious, it is felt that this method gives more consistent results than a direct diffusion

measurement. In addition, even though we are interested here only in bulk effects, surface effects can play an important role in recombination processes[6], and can interfere with meaningful interpretations of lifetime measurements.

Once we have determined some of the parameters discussed above we must still construct a theory for the lifetime since the measurements will, at best, give only crude averages. It is important to recognize that the current phenomenological theory of Shockley and Read[7] does not provide the required formalism to do this.

The above enumeration of the physical problems can be summarized into a single statement: The TMX paper and the talk of Mr. Mandelkorn did not verify the crucial questions.

In conclusion, without some answers to the problems discussed here we will not be able to go very far in our attempts to understand the phenomenon of radiation damage or to improve the radiation resistance of our semiconductor devices. It is pertinent to observe that the questions are not trivial nor are they answered at this time.

Acknowledgement

We would like to thank Dr. P. Fang for many interesting and illuminating comments rendered to us during the preparation of this note.

References

1. G. K. Wertheim, J. Appl. Phys. 30, 1166 (1959).
2. W. G. Spitzer & H. Y. Fan, Phys. Rev. 109, 1011 (1958); H. Y. Fan & A. K. Ramdas, J. Appl. Phys. 30, 1127 (1959); M. Lax, Phys. Rev. 119, 1502 (1960).
3. G. M. Goureau, Soviet Phys. JETP 6, 123 (1958).
4. J. M. Denney, R. G. Downing & G. W. Simon, Phys. Rev. 129, 2454 (1963).
5. See, for example, review articles by A. Rowe, Phys. Rev. 97. 322 (1955); G. Bemski, Proc. IRE 46, 990 (1958).
6. O. L. Curtis, Jr., J. Appl. Phys. 30, 1175 (1959).
7. W. Shockley & W. T. Read, Jr., Phys. Rev. 87, 835 (1952).

OUTLINE OF THE PROGRAM CONCERNING RADIATION EFFECTS IN SOLAR CELLS AND SEMICONDUCTOR MATERIALS

by

M. Schach and P. H. Fang
Goddard Space Flight Center
Greenbelt, Maryland

The existence of trapped charged particle radiation and the wide applicability of semiconductor devices in spacecraft systems provides the basis for a continuing interest in radiation effects. The work described in this paper will outline the effort in-house and under contract which is directed toward an understanding of the nature of damage in photovoltaic materials.

Under the in-house effort are five areas of experimental research: (1) Electron-spin resonance (ESR) studies of the defect structure, (2) optical observation of the structure of solar cells and crystal perfection, (3) measurement of electrical properties, (4) study of the lifetime of minority carriers, (5) measurement of the effects of radiation on solar cells and two areas of theoretical study: (a) recombination statistics and dynamics in impurity semiconductors and (b) general analysis of relaxation dispersion phenomenon.

Currently, ESR seems to be the only microscopic or direct method of studying radiation damage in solids. This technique has been successful in establishing the A center and E center in n-type irradiated silicon. The radiation produces defect centers some of which seem to be paramagnetic and may therefore be detected by observing the magnetic dipole transitions in a magnetic field of the "paramagnetic" electrons. The observation and study of these transitions or "lines" may give all or part of the following information: (1) Number of damage centers; (2) rate of damage formation; (3) annealing of damage centers; (4) structure of the center as obtained from (a) the g-tensor (spectroscopic splitting factor, a tensor of rank two), whose principal axis reflect the symmetry properties of the center; (b) the magnetic interaction with nuclei of the host lattice (hyperfine structure), which would give an indication of the location of the center within the host lattice; (5) effect of impurities (controlled or uncontrolled) on damage rate and damage centers; (6) effect of energy of radiation on type and rate of damage; (7) motion of the vacancy created by radiation determined by relaxation and line width measurements, change in the environment of the damage centers as a function of temperature.

PAGE 42 INTENTIONALLY BLANK

At the present time, work is in an exploratory stage and preparations for experimentation are being made. Methods and calculations for investigating radiation damage by ESR are being studied and are proceeding along the following three lines: (1) Study of wave guide theory, magnetic field distribution in rectangular and cylindrical cavities, matching of microwave components to lines, methods of matching, and methods for determining cavity "Q's "; (2) study and evaluation of spin resonance detection schemes; (3) study of the fundamental principles of magnetic resonance, and conditions under which electron resonance is observed in semiconductors, metals, diamagnetic and paramagnetic crystals.

The radiation resistance of a solar cell depends upon its detailed physical structure and the changes in structure which occur during the charged particle bombardment. Some of the relevant physical properties are the depth of the p-n junction, the location of the drift field, the concentration gradient and the degree of crystal perfection. Some techniques exist for obtaining adequate measurements of these quantities. Others must be developed. Currently, an indentation technique proposed by Shockley for measuring junction depth is being tried and an infrared transmission microscopy for impurity concentration measurements is being explored.

In order to understand the changes in solar cell current and voltage which occur as a result of particle irradiation, the changes in the antecedent electrical properties must be studied. Cell current depends, for example, on carrier concentration, mobility, number, and location of recombination and trapping centers. These and related quantities may be determined by measurements of the Hall coefficient and electrical conductivity (as a function of temperature) of the magnetoresistivity, of the Seebeck coefficient, and the dielectric constant. A description of the Hall and electrical conductivity apparatus being prepared is given in NASA Technical Note D-1695. Measurements of the dielectric constant of silicon before and after irradiation are in progress and the design of an experiment to measure the electrical conductivity dispersion employing a modulated light source suitable for a range of carrier lifetimes down to the microsecond range corresponding to pre- and post-irradiated silicon and possibly gallium arsenide is being developed.

The description of the radiation effects work into "experimental" and "theoretical" is, of course, artificial and the distinction is made to indicate the degree of emphasis. One study currently underway which depends on both aspects is an attempt to describe the damage as a function of depth, specifically, the change in cell current as a function of distance from the cell surface. This work may provide a means of assessing the contribution of a drift field to solar cell stability under charged particle radiation.

Both the in-house and the Catholic University (Grant) theoretical investigation of the recombination of electrons and holes will be concerned with band to band transitions and recombination through intermediate states in the band gap. The effort is being directed toward non-equilibrium conditions as occur under solar cell illumination. Under steady-state conditions the electron-hole removal occurs at a constant rate and the characteristic lifetime may be different than for transient conditions. In the usual treatment of the statistics of the recombinations of holes and electrons in semiconductors, various traps are assumed which have several energy levels in the energy gap. Under the present conditions of semiconductor technology, it is still very difficult to control the species of impurities and lattice defects in semiconductors so that it is not very well understood which trapping center gives rise to which transition mechanism. Since transport properties are so sensitive to the species and concentration of impurities, it is desirable to provide materials experimentally which have a specified kind of impurity and a specified amount of impurity on the one hand, and to calculate transition probabilities theoretically based on a specified model of impurity on the other hand. The theoretical investigation will be concentrated on: (1) The determination of the energy levels of impurities, vacancies, and interstitials; (2) the calculation of transition probabilities of various elementary processes; and (3) the determination of the relations between the transport properties and the atomic properties of impurities, vacancies and interstitials by the correlation function method.

The work to be carried on under contract consists of: (1) The development of solar cells which incorporate a drift field in order to reduce their susceptibility to radiation damage (Texas Instrument Corp., Electro-Optical Systems Corp., and Heliotek Corp.), (2) an investigation of electron and

X-ray damage in CdS and related materials (Univ. of Delaware Grant, Professor K. Boer), (3) radiation damage studies (RCA Princeton and Mountaintop, STL, and General Atomics), (4) theoretical analysis of radiation damage (Catholic University Grant, outlined above), and (5) experimental investigation of radiation effects in semiconductors (University of Illinois)

The objective of the drift field cell contracts is to produce an impurity concentration gradient adjacent to and below the n/p junction. Five methods are being investigated as follows: (1) Outward diffusion of silicon with a very high impurity concentration. (2) Alloyed (AlSi, with a eutectic temperature at 560°C) diffusion of two silicon slices with very different impurity concentrations. (3) Epitaxial deposition of Si on a Si substrate with a very different impurity concentration, after that, thermal diffusion cycling (about 1250°C for 24 hours). (4) Deposition of Si with variable increasing or decreasing concentration during the epitaxial growth on the Si substrate. In the simplest case, two "reactors" which contain the liquid $SiCl_4$ + impurities are used. One reactor contains a different impurity concentration from the other. (5) Double inward diffusion on a very thin slice of silicon, either n or p type

The changes in the electrical properties of CdS following charged particle and X-ray irradiation may be due to the introduction of bulk defects, surface defects, or to changes in the barrier layer. The work at the University of Delaware will attempt the following: (1) An initial study will be made to establish the vacuum conditions for reproducible results, presumably in the range of 10^{-8} torr. (2) The radiation damage of electrons and photons will be investigated as a function of radiation energy. A stepwise increase of maximum radiation energy between the damage-annealing cycles will enable us to determine critical energies for certain types of damage processes and to distinguish between them. (3) The influence of temperature during the damage will be investigated in order to obtain information on necessary diffusion processes. (4) The temperature dependence of annealing will be investigated in order to distinguish between different types of defects and to compare these temperatures with critical temperatures for well-known diffusion processes in CdS. (5) The influence

on doping for CdS single crystals and for evaporated layers with different stoichiometric composition will be investigated, and (6) The spectral distribution of photoconductivity near the band edge, the method of glow curves (conductivity) and spectral distribution of photo emf will be used in order to obtain information about the defect structure.

The program at RCA, Princeton, will be concerned with an investigation of the properties of Si and GaAs. The specific areas to be studied are the following: (1) A comparison of the irradiated and unirradiated recombination centers using electron paramagnetic resonance (ESR) techniques. Correlations with studies of lifetime under identical annealing conditions will be carried out to see if the centers which are responsible for the anomalous lifetime behavior are identical to or different from the paramagnetic centers produced at 5 mev. The resonance behavior of proton irradiated silicon will also be studied. (2) Recombination and trapping studies will be extended to multivalent centers and, possibly, to the compound semiconductors, such as GaAs. Both theoretical and experimental work is required to clarify this situation. (3) Study of impurity effect on the electrical properties and radiation resistance. This work will be in collaboration with the work of RCA Mountain Top Laboratory Contract. (4) Measurements of solar cell characteristics before and after .1 to 6 mev electron and .1 to 100 mev proton radiation. The behavior of cells of varying resistivity, materials and construction will also be studied.

At RCA, Mountain Top, investigations are concerned with the effects of crystallographic orientation and crystal perfection of the base material on solar cell radiation stability, the effects of particular dopants and their concentration, and the effects of front surface carrier collection.

The work at STL will be concerned with: (1) The energy dependence of radiation damage produced by low energy protons and .1 to 40 mev electrons in silicon, gallium arsenide, and cadmium sulphide solar cells. These studies will include the determination of the practical range limited proton energy dependence for devices in addition to the bulk damage energy dependence for photovoltaic materials. (2) The dependence of charged particle radiation effects in silicon on base material resistivity. This dependence will be investigated in the resistivity range from 0.1 ohm-cm to 100 ohm-cm for both p-type and n-type silicon. (3) Experimental and

theoretical studies on the defect configurations and energy levels produced in silicon by electron and proton bombardment. These studies will include measurements of Hall parameters, minority carrier lifetimes and diffusion lengths, and annealing kinetics. Recombination statistics will be studied in an effort to determine the relationship between the observed energy levels and the dominating recombination centers resulting from charged particle irradiation.

The objectives of the program at General Atomics are to identify the defect levels in silicon which reduce carrier lifetime, to evaluate the production rates of important defects due to different types or radiation, and to achieve an understanding of the kinetics of the production and annealing of the important defects, in order to deduce methods of doping which would alter the annealing kinetics, resulting in defects which have less effect on the excess carrier lifetime, The program will undertake: (1) Excess carrier lifetime studies. From the experimental determinations of both the low-injection and high-injection lifetimes, together with theoretical work being performed, the detailed nature of the recombination defect, including its ionization energy and electron and hole capture cross sections, will be evaluated. Experiments carried out in this program allow one to apply the theory of Shockley and Read without making the approximations made by them. Therefore, one can examine more critically the range of validity of the theory. (2) Electron spin resonance studies. Samples for electron spin resonance (ESR) studies will be prepared by measuring the temperature dependence of the Hall coefficient.. Samples of n-type material will be prepared with exhaustion levels at the donor center and at each of the deeper acceptor levels by successively longer irradiations. P-type material samples will be prepared with exhaustion levels at the acceptor and at 0.27, and at other important donor levels. These samples will be prepared by irradiating with 30 mev electrons. ESR measurements will include orientation and hyperfine interaction studies to determine detailed structural characteristics of the defects. (3) Production annealing studies. The important defects in silicon, having been defined, the rate of production of each will be measured by carrier lifetime and ESR studies as appropriate for irradiation with electrons of 1, 5, 30, and 45 mev energy. The annealing processes in the temperature range between 90° and 380°K will be studied. In addition, the rates of introduction of defects will be compared for a high-temperature irradiation and for a low-temperature irradiation followed by a high-temperature anneal.

The work at the University of Illinois is concerned with minority carrier lifetime measurements in silicon. This experiment locates the energy level of the defect relative to the band edges. Measurements are being made on n and p-type material of various initial resistivities, oxygen content, and level of irradiation. Minority carriers are generated optically. Thick samples are used in an effort to minimize surface recombination processes. Defects are introduced by irradiation with Co^{60} gamma rays. Preliminary results are quite satisfactory. Useful data on a large number of samples should be obtained in the near future.

As a corollary to the study of minority carrier lifetimes, it is possible that a luminescence will be associated with the recombination of excess electrons and holes. The search for this luminescence is currently underway in neutron irradiated silicon and germanium. Cooled infrared detectors, phase sensitive lock-in amplifiers and high intensity excitation sources are being employed. The indirect recombination luminescence of un-irradiated germanium has been easily seen. Neutron irradiation has resulted in the loss of this luminescence without any new luminescence appearing at wavelengths less than 2.8 microns. It will be necessary to look at longer wavelengths with samples having received different neutron fluxes before it can be conclusively stated that no new luminescence appears.

Defect generation in highly doped materials and in highly doped materials which have various degrees of chemical compensation is being investigated. Since such materials are often used in devices, it is of practical importance to know whether the mechanism of defect formation and the nature of the defect is the same as in material of higher purity. The present study is concerned with germanium, using the properties of impurity band conduction as a measure of the damage introduced by fast neutrons. Electrical conductivity, Hall effect, and photoconductive response are being measured between 77 and $2^{o}K$ with particular emphasis between 15 and $2^{o}K$. Samples of various donor concentration and compensation are being used. Preliminary experiments which measure the thermal annealing of these defects are underway.

SATELLITE EXPERIMENTS WITH SOLAR CELLS

Ramond C. Waddel
Goddard Space Flight Center

INTRODUCTION

Solar cell radiation damage experiments on spacecraft can provide empirical information on the relative merits of various solar cells bearing shields of different thicknesses. They also are useful in testing our ability to predict solar cell damage in orbit. This paper reports on the results of solar cell radiation damage experiments on board Relay I and Relay II, both of which are active at this writing, and indicates the degree of agreement between predictions of radiation damage, based on laboratory damage studies and flux data, and that observed in the spacecraft experiments.

ORBITS

Some orbit parameters of Relay I and Relay II are given in Table I. Note that perigees and apogees bracket the "inner belt" of trapped particles centered at about 3000 Km. The higher perigee of Relay II would be expected to make this orbit somewhat more damaging than that of Relay I.

SOLAR CELLS

The solar cells are listed in Table 2, together with the nature and thickness of shields. The "REV, Si" cells on Relay I were designed to make them very radiation damage sensitive, the front surface being about one diffusion length thick. Shrinking of this length with damage would then leave large numbers of photon produced carriers at a distance from the junction greater than the diffusion length, with consequent rapid drop in cell output. The conventional silicon cells were of about 1 ohm-cm base resistivity. They were selected for uniformity of spectral response and efficiency and are believed to be representative of good commercially available products. The gallium arsenide cells are of interest because, on theoretical grounds at least, this material is potentially more efficient and has a greater radiation damage resistance than silicon.

All cells were mounted on an aluminum panel whose dimensions were about 4.0 by 5.3 by 0.125 inches. Each cell was loaded to approximate short circuit conditions by a resistor selected to give an initial voltage of about 165 millivolts in space sunlight. The maximum output of each cell, during spin, was computer corrected to normal illumination, 25°C, and mean earth-sun distance. These corrected voltages were normalized with respect to initial undamaged values and averaged. From 12 to 18 observations of a given cell type and shield were used in determining each data point.

PAGE 50 INTENTIONALLY BLANK

RESULTS, RELAY I

The results from the first 387 days of observations of the Relay I radiation damage experiments are shown in Figure 1. Solar cell damage in laboratory studies using a constant intensity and energy beam of particles shows degradation, in these log-linear coordinates, as an initial horizontal section bending into a section having approximately constant negative slope. The responses of the shielded cells in Figure 1 show these general characteristics. The responses of the unshielded cells fall in a step-wise fashion during the first few orbits as the spacecraft passed through a fairly well defined region in which highly damaging particles were trapped. This region was at about 30^{o} South latitude at an altitude of 6,100 Km.

The N/P, 0 cells (N on P silicon cells with 0 mils of shield) and the GaAs, 0 cells degraded similarly to about the 50% point, after which the latter cells fell rapidly. It has been pointed out that when cells degrade below about the 50% level the internal resistance rises so much because of majority carrier depletion that currents drawn, even by a zero resistance load, are not truly "short circuit" currents.

The N/P, 0 cells show rapid degradation at about 40 days and 130 days, for reaons unknown. The shielded cells all show plateaus from about 65 to 90 days in orbit, followed by a decline at about 17% per decade of time.

It is obvious that the order of merit for the shielded cells, under the given test conditions, is N/P, 60; N/P, 30; P/N, 60; and P/N, 30. When judged at the 75% level the N/P, 60 cells last about 10 times longer than P/N, 60 cells. Also the N/P, 60 cells last about 2.3 times longer than the N/P, 30 cells. It is evident that doubling the weight of shield is probably less effective in obtaining a given current level after heavy damage than using more of a less heavily shielded type of cell.

Figure 2 shows the responses of the "REVersed" cells on Relay I. All of these cells show initial increases in response followed by a maximum and eventual fall. The time of maximum increases with the shielding thickness. These results were unexpected, and, as yet, unexplained. It is suggested that a drift field was built up under the action of trapped particles. This drift field may initially have increased the collection efficiency (initially low) before a damage mechanism dominated and caused the observed final decline in response. This type of cell thus did not provide the high damage sensitivity that was intended. In the Relay II experiment they were replaced by GaAs cells, as Table 2 indicated.

RESULTS, RELAY II

Figure 3 shows results of the Relay II radiation damage experiment for the first 21 days in orbit. Note the similarity to Relay I results of Figure 1. The step-wise damage of the unshielded cells and the cross-over of the P/N, 0 and GaAs, 0 responses are common to both experiments. The maximum for the N/P, 0 cells in Figure 3 at about 10 days is undoubtedly real, being exhibited by all 3 cells of this type. It may be noted in Figure 1 that a maximum for these Relay I N/P, 0 cells may also have actually occurred at about 10 days, but was not evident because of lack of data between one and 13 days (because of spacecraft malfunction). Annealing or drift field mechanisms may have caused the maxima.

Figure 4 shows results for the Relay II shielded cells. It is striking that the 3 mil shielded GaAs cells (GaAs, 3) appear as damage resistant as the much more heavily shielded cells of this type, or of silicon. This indicates that the principal damaging agent for unshielded cells was either protons of energy less than about 3 Mev or electrons of energy less than about 0.1 Mev.

Because of the small amount of damage that is shown in Figure 4, the only generality to be drawn concerning order of merit is that, of the six types shown, the P/N, 60 cells are inferior.

Selected numerical results from the Relay I and Relay II radiation damage experiments are shown in Table 3. Underlined values are for Relay II. It is evident that the Relay II orbit is considerably more damaging than that of Relay I. Also, extrapolations like that which indicates that it would take 18,000 days (50 years) for N/P, 60 cells to degrade to the 50% level must be viewed with caution.

The numerical results of the Relay I and Relay II radiation damage experiments, discussed above, are of interest to designers of solar cell power supplies. Certainly a design involving a type of cell here reported on, and for an orbit similar to that of Relay (or Telstar) which counts on solar cell lifetimes much different than those here reported should be viewed with suspicion.

PREDICTIONS, UNSHIELDED CELLS

A second use for the data here reported is to attempt to predict them from other considerations. Only when such observations can be predicted with satisfactory accuracy can the design of solar cell power supplies be considered to be on a sound engineering basis.

Figure 5 shows (as heavy data points) the early behavior of the P/N, 0 cells on Relay I, together with the results of a detailed prediction.

Preliminary work indicated that the only possibility of accounting for the very rapid degradation of bare cells was to ascribe it to low energy protons. Both silicon and gallium arsenide cells show a proton damage susceptibility which rises rapidly at low energies. Leo Davis, of Goddard Space Flight Center, has made measurements of the distribution of this type of particle and (in a private communication) provided the writer with a detailed prediction of the cumulative low energy proton flux encountered by Relay I during the first 11 hours of orbit. Under certain assumptions, this flux was converted to equivalent 4.6 Mev protons. The damage data of Cherry and Slifer (NASA TN D-2098) using protons of this energy and solar cells similar to those flown in orbit, was then combined with the orbital proton flux to predict cell response as a function of time. This prediction is shown in Figure 5 as the curve with uncertainty bars. It is seen that fair agreement is obtained, with predicted response being somewhat higher than that observed. The predicted and observed times of occurrence of the first and second damage steps are not in disagreement. These steps occurred as the spacecraft passed through the south latitude extension of the low energy proton distribution, whose main part is above Relay apogee.

Figure 6 shows predicted and observed results for the N/P, 0 cells on Relay I. The agreement is again fair, with predicted responses somewhat lower than observed.

PREDICTIONS, SHIELDED CELLS

Since unshielded cells are so damage sensitive, the above exercise with such cells is instructive, but academic. Prediction of the behavior of shielded cells is of immediate engineering interest.

The 30 and 60 mil shields used on Relay I silicon cells exclude the low energy protons which evidently damaged the unshielded cells. Damage by protons and electrons of higher energy was thus considered. Information on such particles has been accumulated in the form of the GSFC P1 proton grid and the GSFC E8 electron grid in a fashion suitable for computer use.

The Relay I spacecraft was "flown" by computer through each of these two grids for five, two day intervals. The cumulative fluxes were tabulated by 14 second steps. These proton and electron fluxes were averaged, modified under certain assumptions concerning particle spectra, damage susceptibility as a function of particle, energy, angle, and shielding and used to calculate the response of the P/N, 60 and N/P, 60 cells after 300 days in orbit. Cherry and Slifer damage rates were again used. The results are shown in Table 4.

It is evident that the predicted responses under proton or electron damage are somewhat less than those observed. A solar cell power supply designed under such conditions would be unnecessarily "over-designed" from a radiation damage standpoint.

FUTURE WORK

Anyone attempting to make predictions of orbital damage will find a need for (1) up-to-date computer grids of proton and electron distributions in space and energy, (2) more laboratory studies of solar cell damage as a function of cell type, particle type and energy (particularly low energy protons) with complete V/I curves evaluated under a space-sunlight simulator, and (3) some method, of either empirical or theoretical origin, for taking into account the modifications that a shield imposes on particle energy and angular distribution. Further, (4) improved orbital damage experiments should be conducted with solar cells, in which promising cell types, shields, and adhesives should be explored and in which full V/I cell characteristics are measured as the cells degrade. Finally, (5), a continuing effort must be made to improve our understanding of the solid state physics of the radiation damage process in semiconductors.

ORBIT PARAMETERS		
	RELAY I	RELAY II
APOGEE (KM)	7439	7414
PERIGEE (KM)	1321	2088
INCLINATION (DEG)	47.5	46.3
PERIOD (MIN)	185.1	194
ZERO TIME	1962 YR, 348 DAY, 00HR 00MIN, 00SEC, GMT	1964 YR, 21 DAY, 21 HR 42 MIN, 00SEC, GMT

TABLE 1

RELAY RADIATION DAMAGE SOLAR CELLS

CELL TYPE	SHIELD MILS, (CAT. NO.)	NO. OF CELLS ON RELAY I	NO. OF CELLS ON RELAY II
P/N, Si	0	3	3
P/N, Si	30, (7940)	3	3
P/N, Si	60, (7940)	3	3
N/P, Si	0	3	3
N/P, Si	30, (7940)	3	3
N/P, Si	60, (7940)	3	3
REV, Si	0	3	0
REV, Si	30, (7940)	3	0
REV, Si	60, (7940)	3	0
Ga As	0	3	2
Ga As	3, (0211)	0	2
Ga As	12, (0211)	0	4
Ga As	30, (7940)	0	2
Ga As	60, (7940)	0	2

TABLE 2

TIMES IN ORBIT AT WHICH VARIOUS SOLAR CELLS FELL TO GIVEN PERCENT INITIAL VALUES

OUTPUT (%)	P/N, 0 (DAYS)	P/N, 30 (DAYS)	P/N, 60 (DAYS)	N/P, 0 (DAYS)	N/P, 30 (DAYS)	N/P, 60 (DAYS)	GaAs, 0 (DAYS)
90	(0.033) 0.044	(3.2) 2.7	(5.7) 4.6	0.14 0.16	34 16	50 24	(0.06) 0.044
75	(0.044) 0.062	32	47	0.33 0.39	197	(480)	0.25 0.18
60	0.17 0.18	128	300	1.6 1.2	(1800)	(4000)	0.66 0.34
50	(0.28) 0.30	(470)	(1200)	17	(7200)	(18000)	1 0.49

( ) =ESTIMATED. 0.30=RELAY II, OTHERS RELAY I

TABLE 3

PREDICTED AND OBSERVED SOLAR CELL RADIATION DAMAGE AFTER 300 DAYS IN ORBIT–RELAY I

CELL TYPE	SHIELD MILS, (CAT. NO.)	RADIATION INFO. SOURCE	PREDICTED RESPONSE (%)	OBSERVED RESPONSE (%)
P/N, Si	60, (7940)	GSFC P1 PROTON GRID	56	60
N/P, Si	60, (7940)	GSFC P1 PROTON GRID	75	79
P/N, Si	60, (7940)	GSFC E8 ELECTRON GRID	47	60
N/P, Si	60, (7940)	GSFC E8 ELECTRON GRID	75	79

TABLE 4

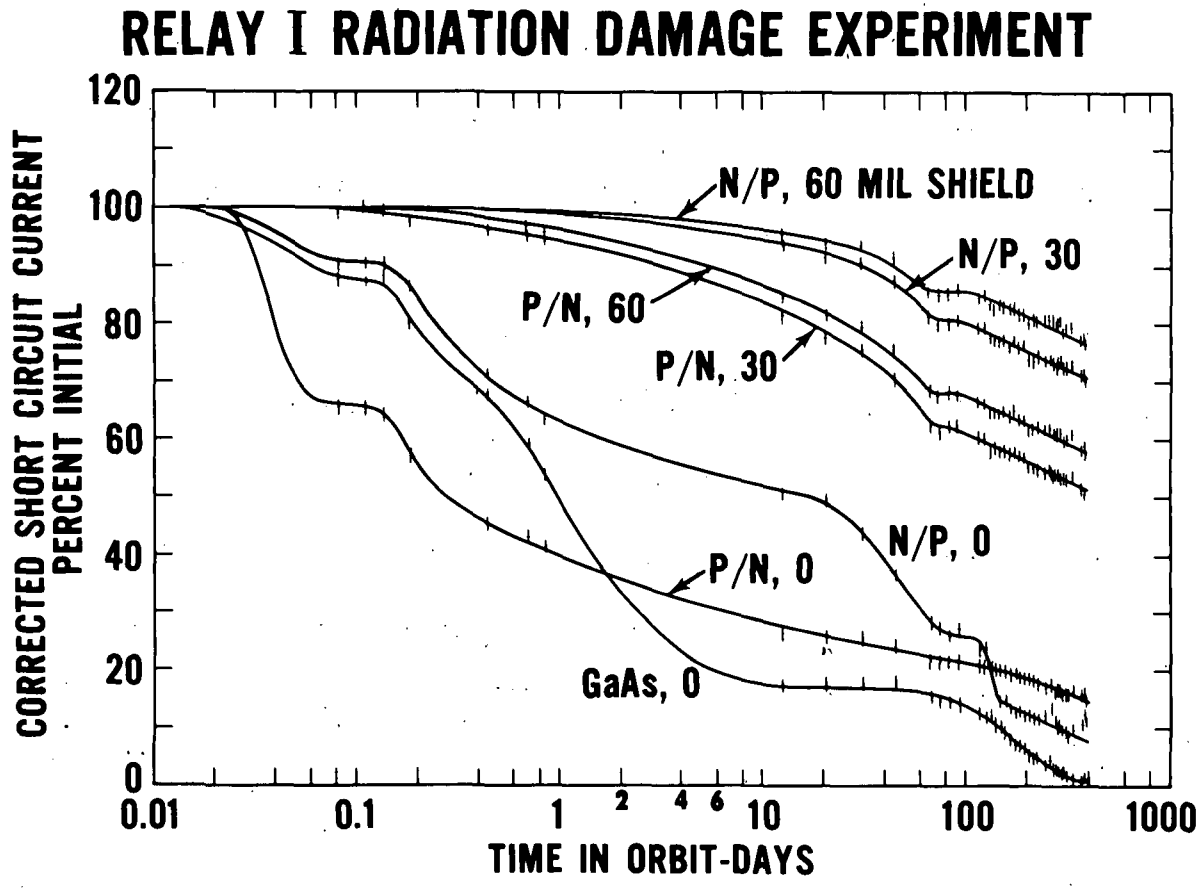
RELAY I RADIATION DAMAGE EXPERIMENT
CORRECTED SHORT CIRCUIT CURRENT
PERCENT INITIAL
120
100
80
60
40
20
0
0.01
0.1
1
2
4
6
10
100
1000
TIME IN ORBIT-DAYS
N/P, 60 MIL SHIELD
N/P, 30
P/N, 60
P/N, 30
N/P, 0
P/N, 0
GaAs, 0

FIGURE 1

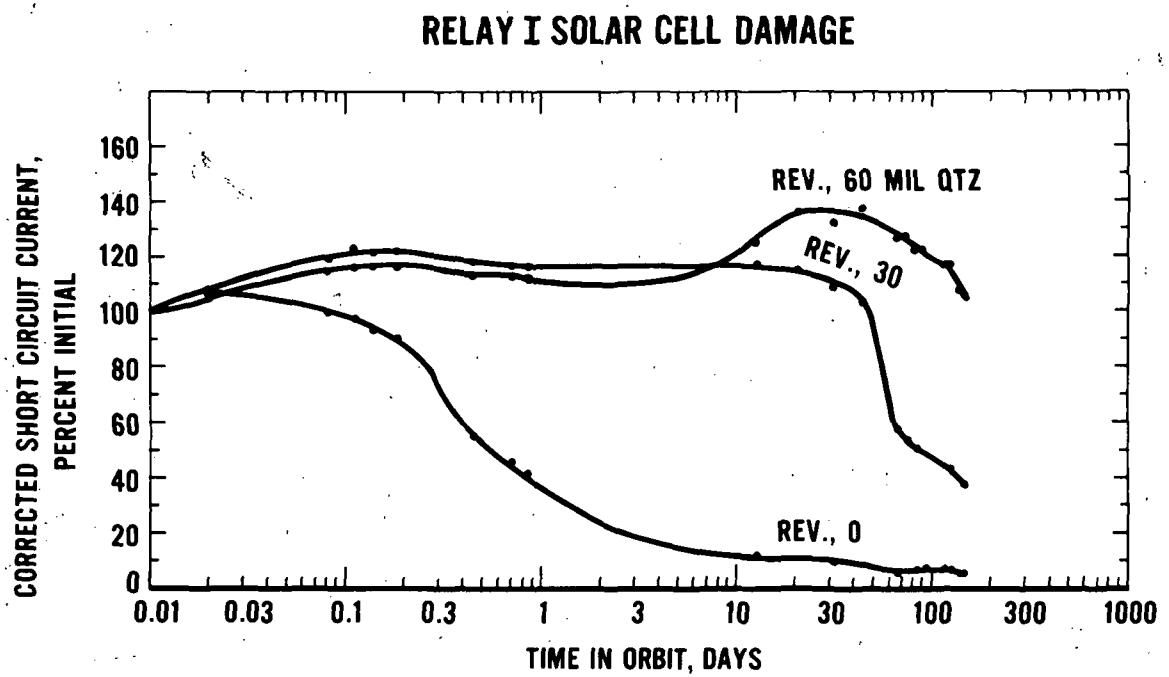
RELAY I SOLAR CELL DAMAGE
CORRECTED SHORT CIRCUIT CURRENT, PERCENT INITIAL
160
140
120
100
80
60
40
20
0
REV., 60 MIL QTZ
REV., 30
REV., 0
0.01
0.03
0.1
0.3
1
3
10
30
100
300
1000
TIME IN ORBIT, DAYS

FIGURE 2

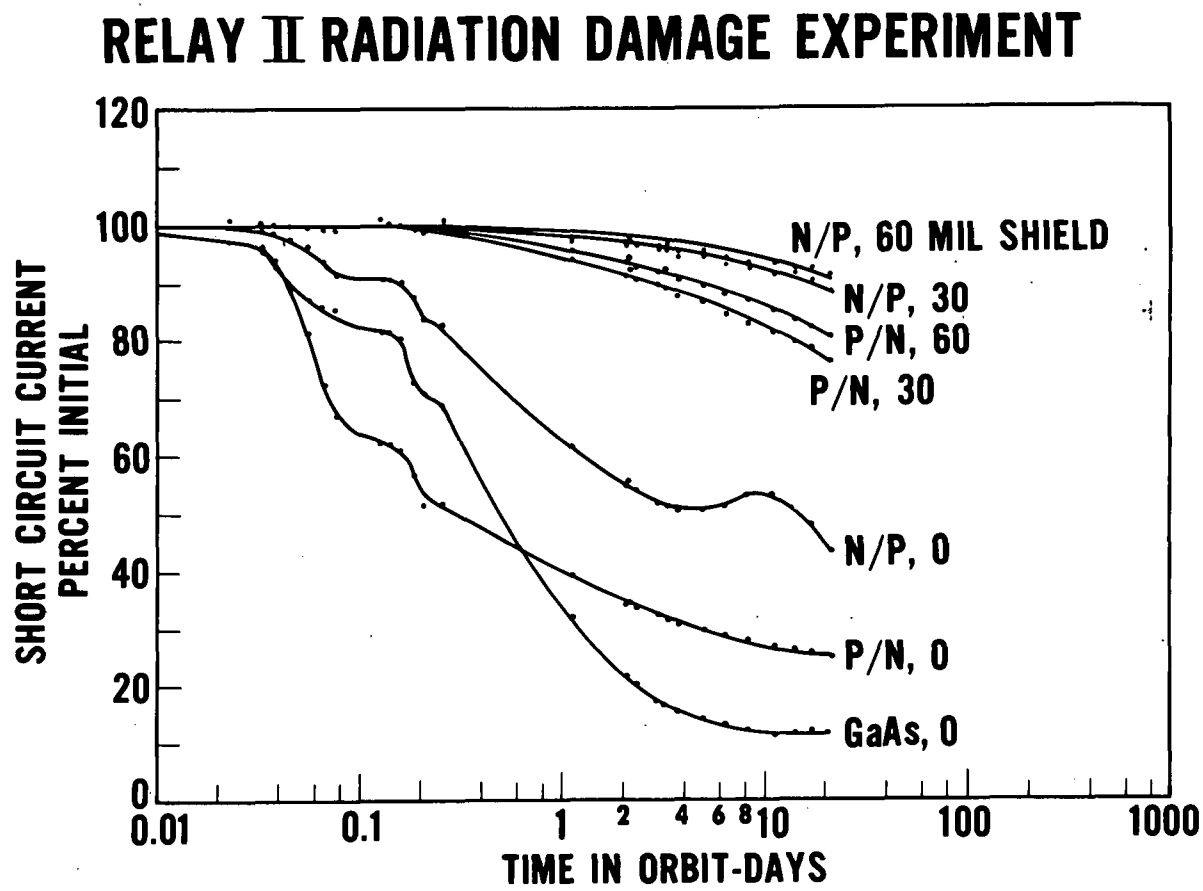
RELAY II RADIATION DAMAGE EXPERIMENT
SHORT CIRCUIT CURRENT
PERCENT INITIAL
120
100
80
60
40
20
0
0.01
0.1
1
2
4
6
8
10
100
1000
TIME IN ORBIT-DAYS
N/P, 60 MIL SHIELD
N/P, 30
P/N, 60
P/N, 30
N/P, 0
P/N, 0
GaAs, 0

FIGURE 3

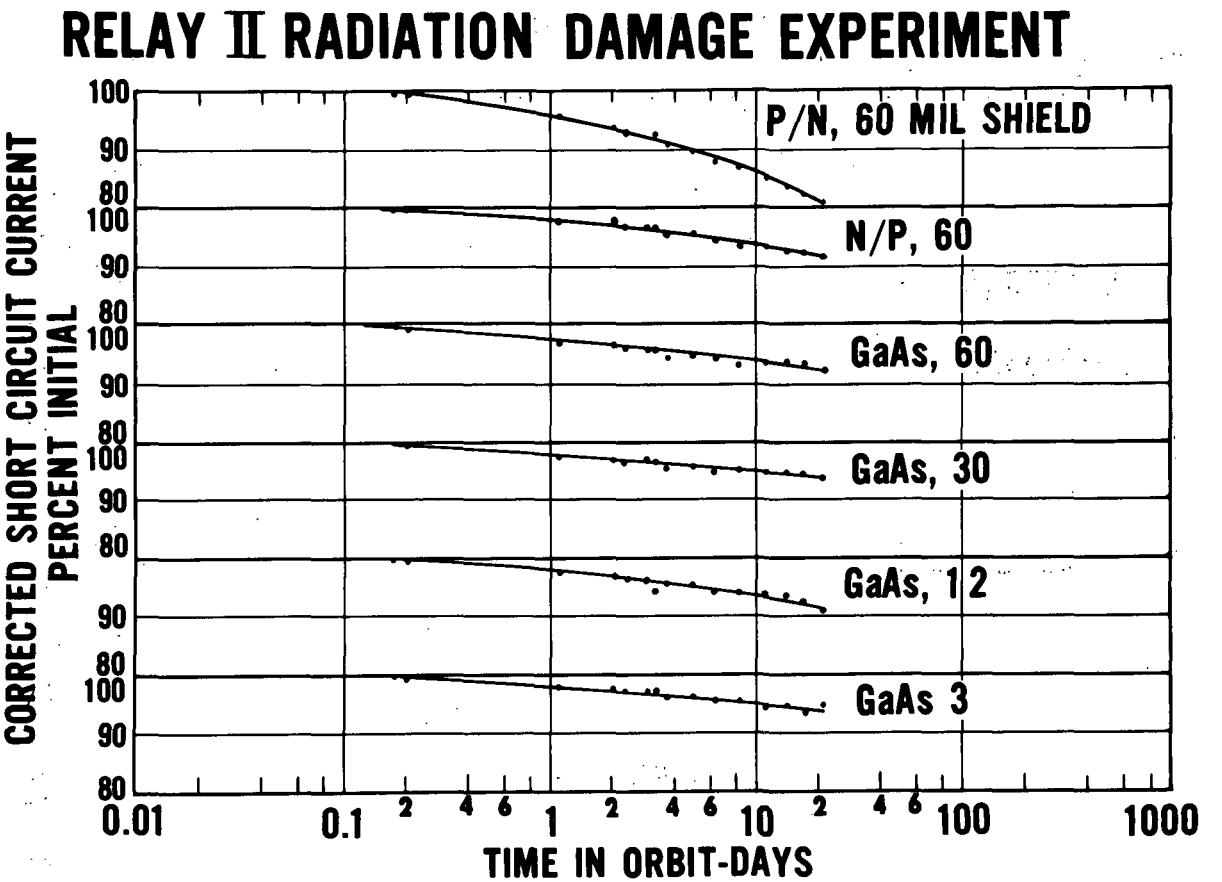
RELAY II RADIATION DAMAGE EXPERIMENT
CORRECTED SHORT CIRCUIT CURRENT
PERCENT INITIAL
P/N, 60 MIL SHIELD
N/P, 60
GaAs, 60
GaAs, 30
GaAs, 12
GaAs 3
100
90
80
0.01
0.1
1
10
100
1000
2
4
6
TIME IN ORBIT-DAYS

FIGURE 4

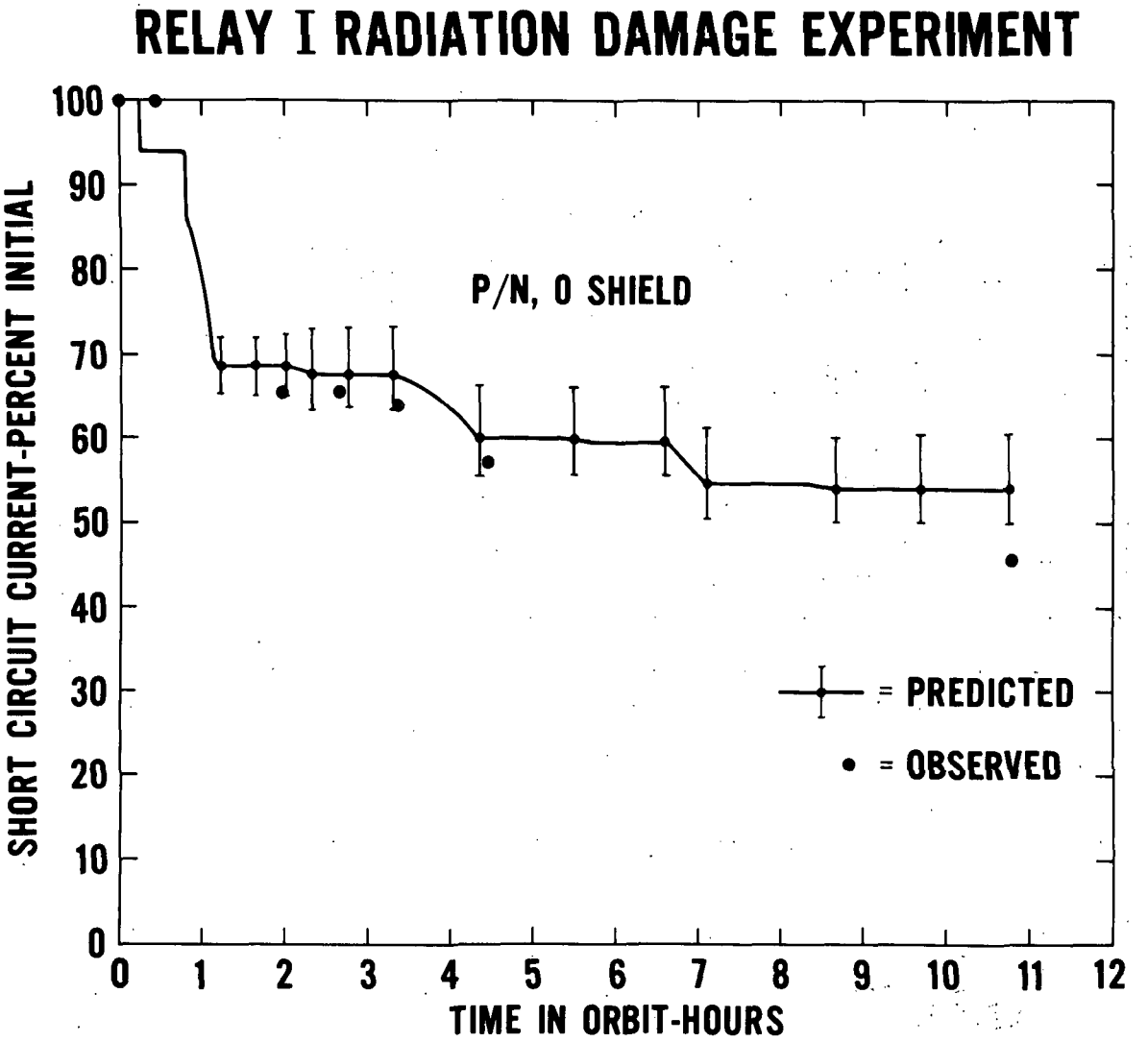
RELAY I RADIATION DAMAGE EXPERIMENT
SHORT CIRCUIT CURRENT-PERCENT INITIAL
100
90
80
70
60
50
40
30
20
10
0
P/N, 0 SHIELD
= PREDICTED
= OBSERVED
0
1
2
3
4
5
6
7
8
9
10
11
12
TIME IN ORBIT-HOURS

FIGURE 5

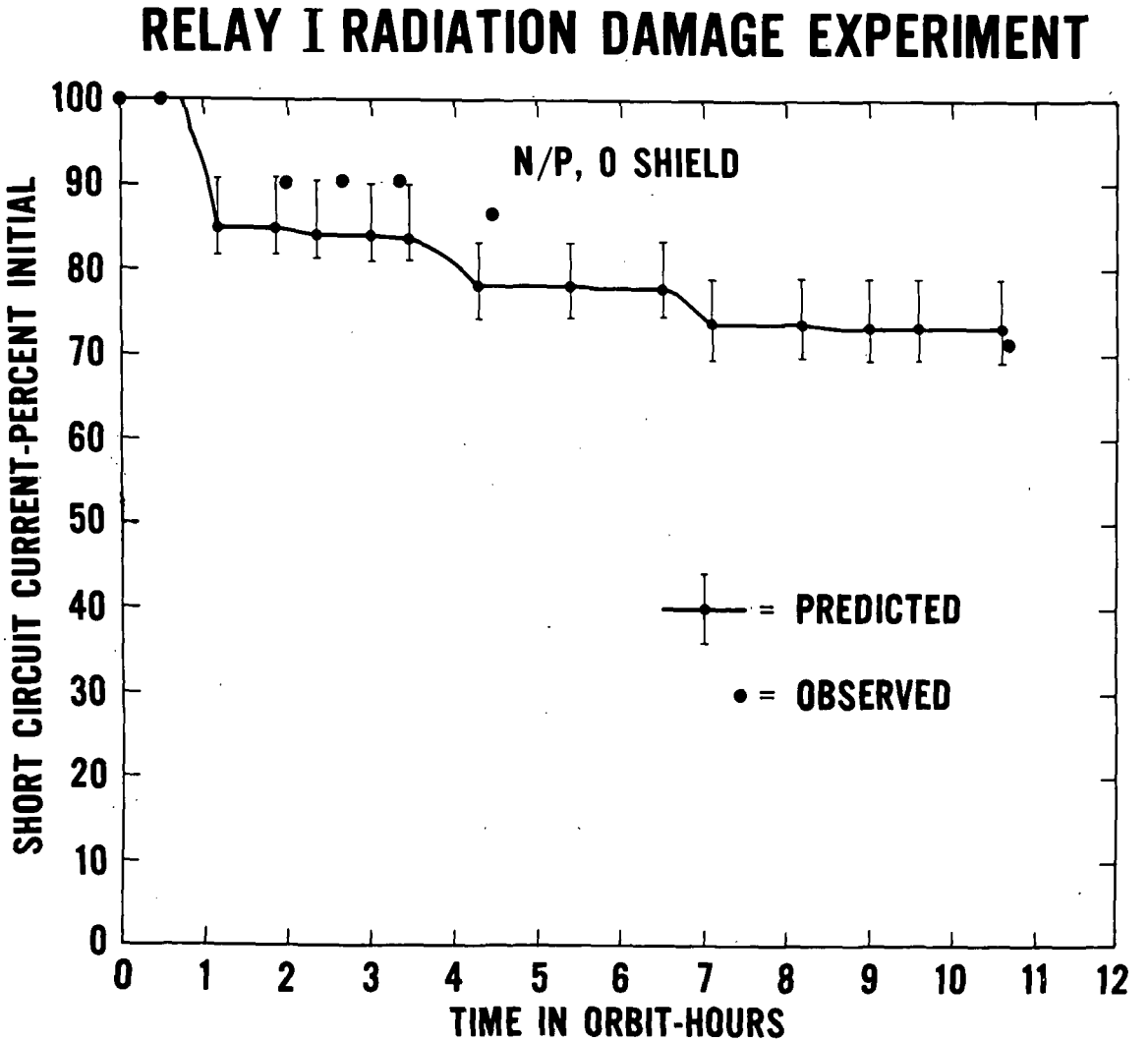
RELAY I RADIATION DAMAGE EXPERIMENT
N/P, 0 SHIELD
= PREDICTED
• = OBSERVED
SHORT CIRCUIT CURRENT-PERCENT INITIAL
TIME IN ORBIT-HOURS
100
90
80
70
60
50
40
30
20
10
0
0 1 2 3 4 5 6 7 8 9 10 11 12

FIGURE 6.

EFFECT OF ELECTRON RADIATION ON TV LENS COMPONENTS

By Lawrence Kobren - Goddard Space Flight Center

Introduction

Orbiting scientific satellites containing optical systems such as television, telescopes, and star trackers will be required to operate for considerable periods of time in a radiation environment. This environment will consist primarily of electrons and protons which make up the Van Allen belts. It has been observed that glass exposed to x and gamma radiation is subject to production of color absorbing defects which decrease the amount of light transmitted by the glass. Because the glass elements of an orbiting optical system will generally be on the surface of a satellite, the glass will be exposed to direct bombardment by electrons and protons. It then becomes important to determine whether electron and proton irradiation have the same effect on glass as does x and gamma radiation and, if so, what effect does this radiation have on the actual performance of the optical system. This paper describes the effect that electron radiation has on the transmissivity of a television lens system which was designed for use on a Nimbus Weather Satellite. Future studies will investigate the effect of proton radiation, and a combination of electron-proton radiation on the transmissivity of the system.

Radiation Exposure

The radiation levels to which the TV lens was exposed simulated as close as possible the actual radiation environment to which the Nimbus satellite would be exposed in its orbit through the Van Allen belt. Based on an altitude of 800 K m (500 mi) in a circular orbit inclined 90° to the equator, the initial value of electron flux was calculated as 6×10^{12} electrons/cm^2/day. This value was later corrected to 4.5×10^{11} electrons/cm^2/day.(1) The electron energies in this orbit range from 0.5 MEV to 8 MEV, however, 45% of the electrons have energies between 0.5 MEV and 2 MEV and a total of 85% have energies less than 3 MEV. From these figures, it was believed that electron energies of 1 MEV and 2 MEV would include the major portion of electrons that would bombard the satellite and, therefore, irradiation was performed at these energies, with most of the work done at 2 MEV. All irradiation was done at room temperature in air. The time required for irradiation varied from 55 seconds for 1 MEV electron to 27 seconds for 2 MEV electrons. This exposure was equivalent to the exposure received by the satellite in two days.

Procedures

The lens system used in this study is shown in figure 1. It consists of a series of glass lenses cemented together in an aluminum frame. The first glass element in the lens system was Dense Barium Crown and was followed by Extra Dense Flint Glass. Since the lens assembly was cemented together and could not be dismantled for examination of the individual elements, the entire lens system was irradiated and transmissivity measurements were made on the integral unit.

(1) Personnel correspondence from G. Stassinopoulos, Goddard Space Flight Center.

PAGE 66 INTENTIONALLY BLANK

Transmissivity measurements before irradiation and after each exposure were made on the lens system using a Cary Recording Monochrometer. Measurements of transmissivity vs. wavelength were continuously recorded for wavelengths between 5400A° and 6400A°. Due to the focusing effect of the lens which prevented all of the transmitted light from reaching the photomultiplier tube of the instrument, some modifications in measuring procedures were necessary. Using this modification, transmissivity vs. wavelength curves were obtained which, while not giving an absolute value of transmissivity, could be compared with previous curves similarly obtained and changes in transmissivity with radiation could be determined.

Exposure of the lens to 1 MEV electrons resulted in an appreciable decrease in transmissivity. The total loss in transmissivity after electron exposure equivalent to eight days in orbit was 47%. For ease in presentation, one particular wavelength (6100A°) was picked and the data showing the loss in transmissivity vs. exposure is presented in Table I. The values are plotted in Figure 2.

Exposure (Days) vs. % Change in Transmission

Exposure (Days)	Relative Transmissivity (at 6100A°)	% Change
0	31	--
2	22.4	27.8
4	19.5	12.9
6	17.4	10.8
8	16.4	5.8

The rate of loss in transmissivity which was quite rapid initially became less rapid after the second exposure (4 days) and leveled off with increasing exposure. After transmissivity measurements were made after the final exposure (8 days) the entire lens system was annealed at 85°C for 63 hours. Transmissivity measurements made after this annealing period showed that substantial recovery had occurred in the lens. (Figure 2)

To determine the effects of higher energy electrons, the annealed lens was exposed to 2 MEV electrons. The flux used was the same ($6 \times 10^{12} e/cm^2/day$) and the total exposure was equivalent to 2 days in orbit. The results of post-irradiation transmissivity measurements indicated a reduction in transmissivity of 42%. (Figure 2)

In order to prevent radiation damage to the lens system, a .645" thick optically flat piece of radiation resistant fused quartz was installed over the front of a new lens system. The entire lens system was then exposed to electron radiation. The energy of the electrons was 2 MEV and the flux used was the corrected value of $4.5 \times 10^{11} e/cm^2/day$. The total exposure was equivalent to 140 days in orbit. Absolute transmissivity measurements were made on this lens system by the National Bureau of Standards before and after radiation exposure. Results,

tabulated in Table 2 and plotted in Figure 3 show a loss in transmissivity of 8.4% after 140 day exposures.

Table II

	Transmissivity	
	Before	After
Lens with Fused Quartz Cover Plate	88.3%	79.9%

To determine the amount of protection the fused quartz cover plate provided the lens components, one additional test was performed. A mock lens system (Figure 4) was fabricated. The system consisted of a hollow aluminum cylinder containing three optically flat glass plates arranged in series behind the fused quartz cover plate. The components were made from Dense Barium Crown, and Extra Dense Flint Glass. Three sets of glass elements were made, the only difference in the sets was in the thickness of fused quartz used for the coverplate. The unit was designed to be easily dismantled so that after each radiation exposure an accurate optical density measurements could be made on each optical element. The thickness of the fused quartz was 0.205", 0.131" and 0.065". Optical measurements were made after exposures equivalent to 2, 4, 6, 8, 12 and 16 days in orbit.

Results of the test showed no significant change in the transmissivity of the fused quartz regardless of its thickness. There was, however, considerable loss in transmissivity of the glass elements directly behind the 0.131" and the 0.065" thick fused quartz cover-plates.(Figure 5) Some loss in transmissivity was noted in the glass element directly behind the 0.205" thick fused quartz cover-plate; however, the loss was considerably less than that which occurred in the other two similarly located elements. The maximum loss in transmissivity occurred in the glass element directly behind the 0.065" thick fused quartz cover-plate. The transmissivity in this element was reduced from an initial value of 91.2% to 22.4% after an exposure equivalent to 16 days. The transmissivity of the glass element behind the 0.131" fused quartz cover-plate was reduced from 89.1% to 40.7% whereas the glass element behind the 0.205" thick cover-plate was reduced from 91.2% to 79.4% with similar exposure. Some loss in transmissivity was noted in the second and third glass elements behind the fused quartz plate. The maximum loss in transmissivity for these elements was 11% after 16 day equivalent exposure. This loss was noted in the second element behind the 0.065" fused quartz plate. The loss in transmissivity for all the remaining elements were less than the values.

After the final electron exposure, the glass elements were allowed to remain at room temperature. Transmissivity measurements were taken at intervals of 1.5 hours, 17 hours, and 4 days. Results plotted in figure 5 show a marked recovery in all specimens.

Discussion and Conclusions

Results of these tests have shown that the optical glass intended for use as lenses in a television camera on a future weather satellite was significantly affected by 1 and 2 MEV electron radiation. The transmissivity of these lens components was reduced to such an extent that the usefulness of these components in a workable satellite is doubtful. The amount of damage (loss in transmissivity) is apparently directly related to the amount of electron exposure. An examination of Figures 2, 3, and 5 indicated that the amount of damage increased quite rapidly with increased exposure. However, it appears that the amount of damage reaches some specific level and changes very little with further exposure.

It was found that radiation protection for the lens system could be provided by incorporating a radiation resistant fused quartz cover-plate over the lens. It was further shown that significant radiation damage occurred only in those lenses directly behind a cover-plate less than 0.205" thick, and that more complete protection could result with a thicker cover-plate (e.g. the .645" thick cover-plate on the second lens system).

One rather significant observation noted was the rapid recovery exhibited by all the lens elements as a result of annealing even at room temperature. Since the recovery time is so rapid, it is possible that the lens in orbit, since it is exposed to electron bombardment at a much lower rate than the rate used in the laboratory, might recover a significant percentage of the damage nearly as rapidly as damage occurred. This would result in only a very slow increase in damage with time. These theories, however, would require further study.

It is believed, however, that whether recovery in orbit occurs or not, it would be unwise to ignore the fact that damage to the glass elements can occur as a result of exposure to electron radiation. It is also believed that an increase in reliability resulting from incorporation of a radiation resistant cover-plate or the use of radiation resistant glass for the lens elements would not be extravagant.

FIGURE 1

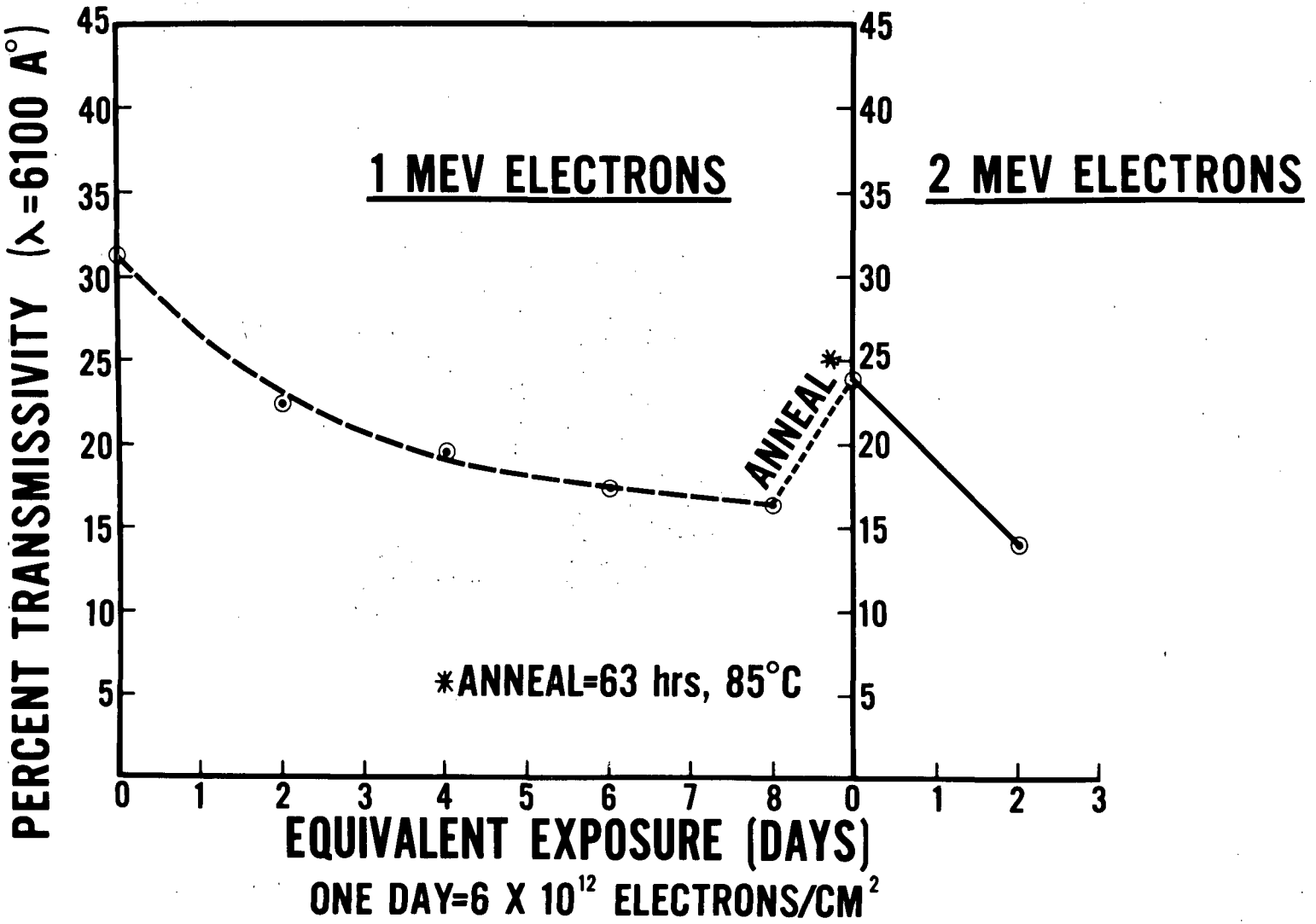
NIMBUS TV LENS SYSTEM
TRANSMISSIVITY VS. ELECTRON EXPOSURE
PERCENT TRANSMISSIVITY (λ=6100 A°)
45
40
35
30
25
20
15
10
5
1 MEV ELECTRONS
2 MEV ELECTRONS
ANNEAL*
*ANNEAL=63 hrs, 85°C
0 1 2 3 4 5 6 7 8 0 1 2 3
EQUIVALENT EXPOSURE (DAYS)
ONE DAY=6 X 10^12 ELECTRONS/CM^2

FIGURE 2

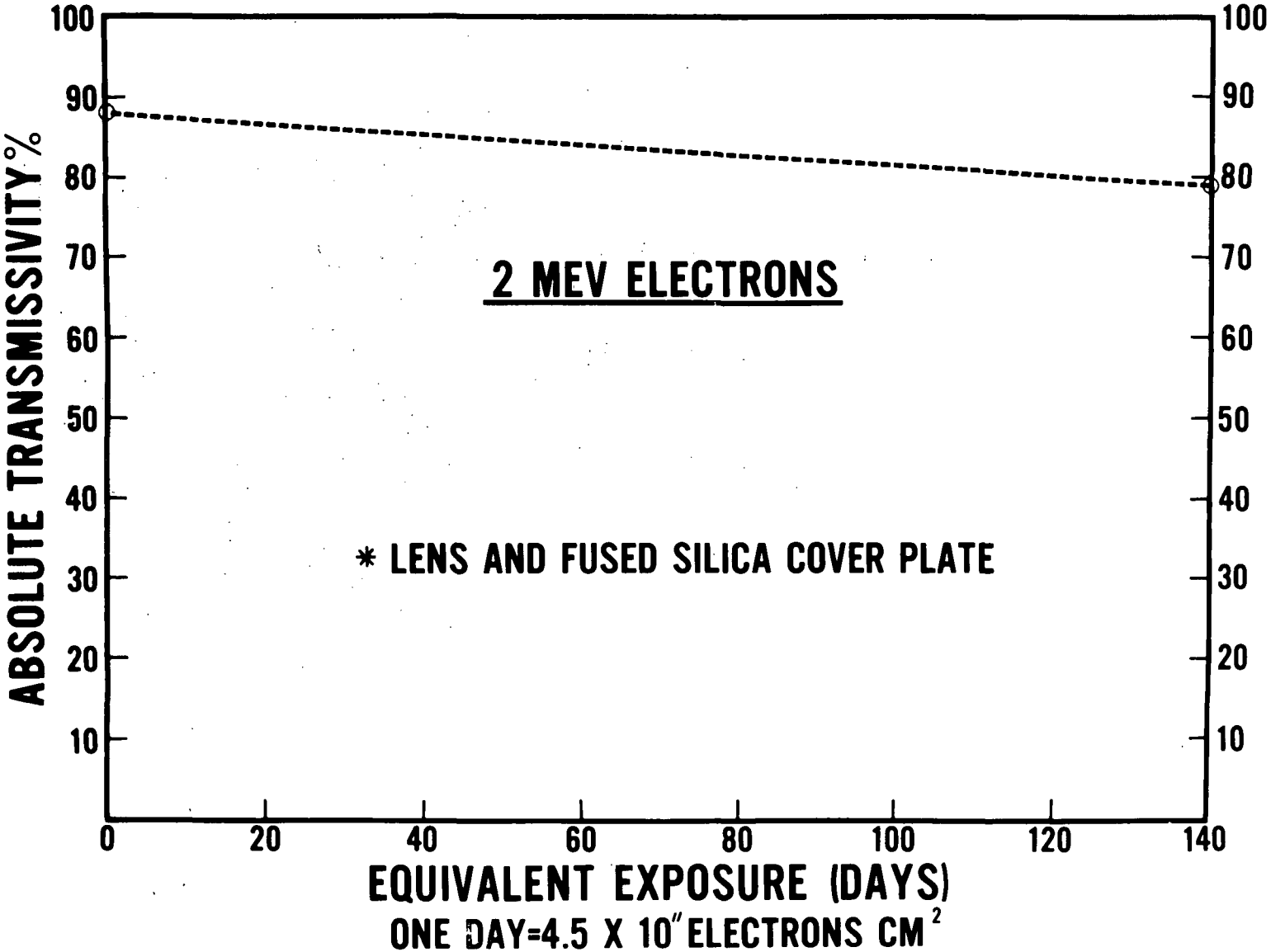
NIMBUS TV LENS SYSTEM*
TRANSMISSIVITY VS. ELECTRON EXPOSURE
ABSOLUTE TRANSMISSIVITY%
100
90
80
70
60
50
40
30
20
10
2 MEV ELECTRONS
* LENS AND FUSED SILICA COVER PLATE
0
20
40
60
80
100
120
140
EQUIVALENT EXPOSURE (DAYS)
ONE DAY=4.5 X 10" ELECTRONS CM 2

FIGURE 3

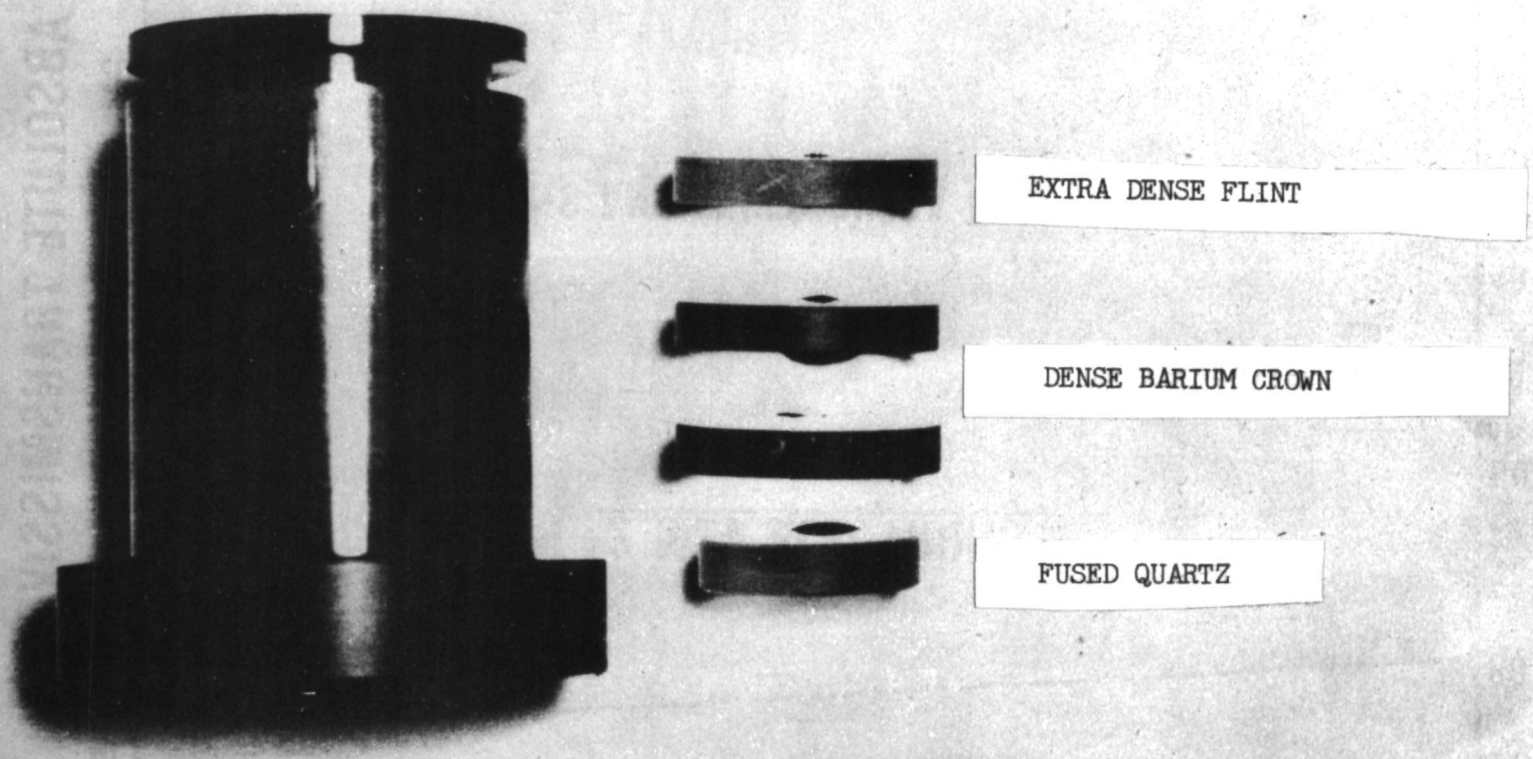

FIGURE 4

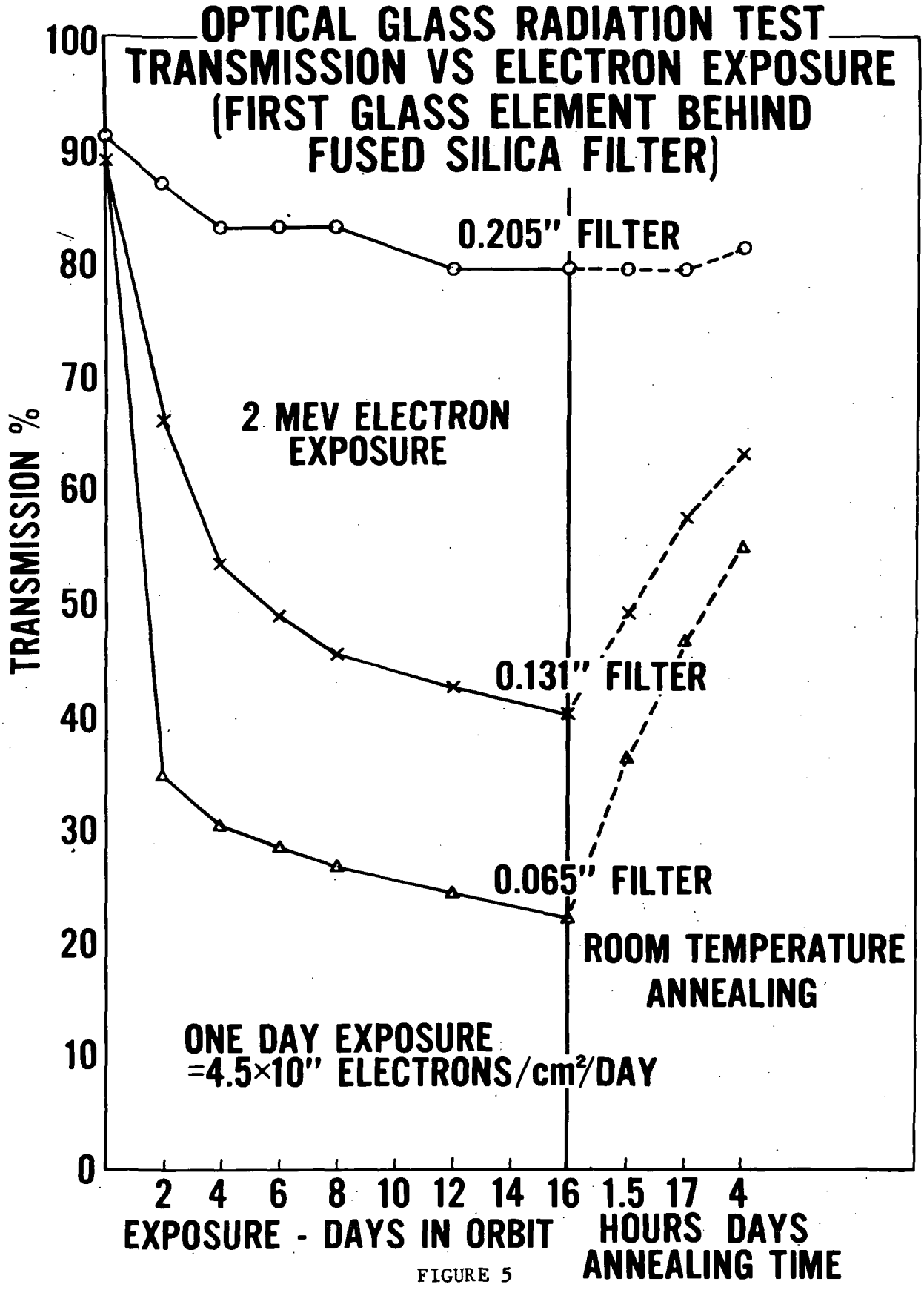
OPTICAL GLASS RADIATION TEST
TRANSMISSION VS ELECTRON EXPOSURE
(FIRST GLASS ELEMENT BEHIND
FUSED SILICA FILTER)
0.205" FILTER
2 MEV ELECTRON
EXPOSURE
0.131" FILTER
0.065" FILTER
ROOM TEMPERATURE
ANNEALING
ONE DAY EXPOSURE
=4.5×10" ELECTRONS/cm²/DAY
TRANSMISSION %
100
90
80
70
60
50
40
30
20
10
0
2 4 6 8 10 12 14 16 1.5 17 4
EXPOSURE - DAYS IN ORBIT
HOURS DAYS
ANNEALING TIME

FIGURE 5

Preliminary Study on the Effect of Electron Radiation on Echo II Balloon Material

By Lawrence Kobren - Goddard Space Flight Center

A study is underway to determine the effect of electron radiation on Echo II balloon material. Essentially, this material is a metal polymer composite consisting of a 0.35 mil mylar film sandwiched between two sheets of 0.18 mill aluminum. The total thickness of the composite, including the polyester adhesive is approximately 0.80 mils. Since the Echo material is subjected in practice to biaxial stresses, we have determined that more meaningful data could be obtained by simulating this same stress condition in the laboratory.

For this purpose, a device was designed and constructed to permit biaxial stressing of a 12" diameter diaphram. By employing a vacuum, the specimen is subjected to a homogeneous pressure distribution on its surface (the atmosphere). Figure 1 shows the equipment used for this study. During the test, a continuous measurement of chamber pressure is recorded. The difference between the initial pressure in the chamber (atmospheric) and the final pressure recorded corresponds to the burst pressure. This pressure could be converted to stress if so desired, however, it is not necessary for our purposes since the burst pressure is directly related to the stress and since we are only interested in comparing one value with another. Also shown in the Fig. 1 is a proximity device which automatically follows the surface of the specimen as it is deflected and this movement is also continuously recorded. This deflection can be related to strain.

The material was exposed to 2 MEV electrons at a flux of $2.3 \times 10^{12} e/cm^2/day$ which closely simulates the orbital environment of Echo II. The results of this exposure is shown in Figure 2. There is an increase in burst strength to a maximum of 122.3 mm Hg after an equivalent of 180 days in orbit. This is an increase of 7% from the initial non-irradiated value of 114.5 mm Hg. This improvement in burst strength degrades to almost nil after an equivalent of 360 days in orbit.

To determine which component of this laminate (metal, polymer or adhesive) was most affected by the radiation, additional radiation tests are being performed on the 0.35 mil mylar and on the adhesive. Preliminary results after irradiation of the mylar are shown in Figure 3. The results indicate a gradual loss in strength with increasing radiation, however, due to the scatter in burst strength data, it is not possible at this time to quantitatively evaluate the extent of this trend.

Further work on the adhesive, which is believed to be affected by the radiation to the greatest degree is being initiated. Sheets of the adhesive are being cast and tensile specimens are being made and tested. Preliminary results indicate that the tensile strength increases 10% and the ductility is reduced a like amount after an equivalent exposure of 135 days. We intend to prepare sheets

PAGE 76 INTENTIONALLY BLANK

of the adhesive large enough to be tested under biaxial stress conditions on the bulge tester. In addition to testing the adhesive properties, peel specimens have been prepared and irradiated, however, results from these tests are not ready at this time.

If the improvement noted in the composite material is real, it might be possible to irradiate this material at some point in the fabrication process which would result in a product with higher strength.

FIGURE

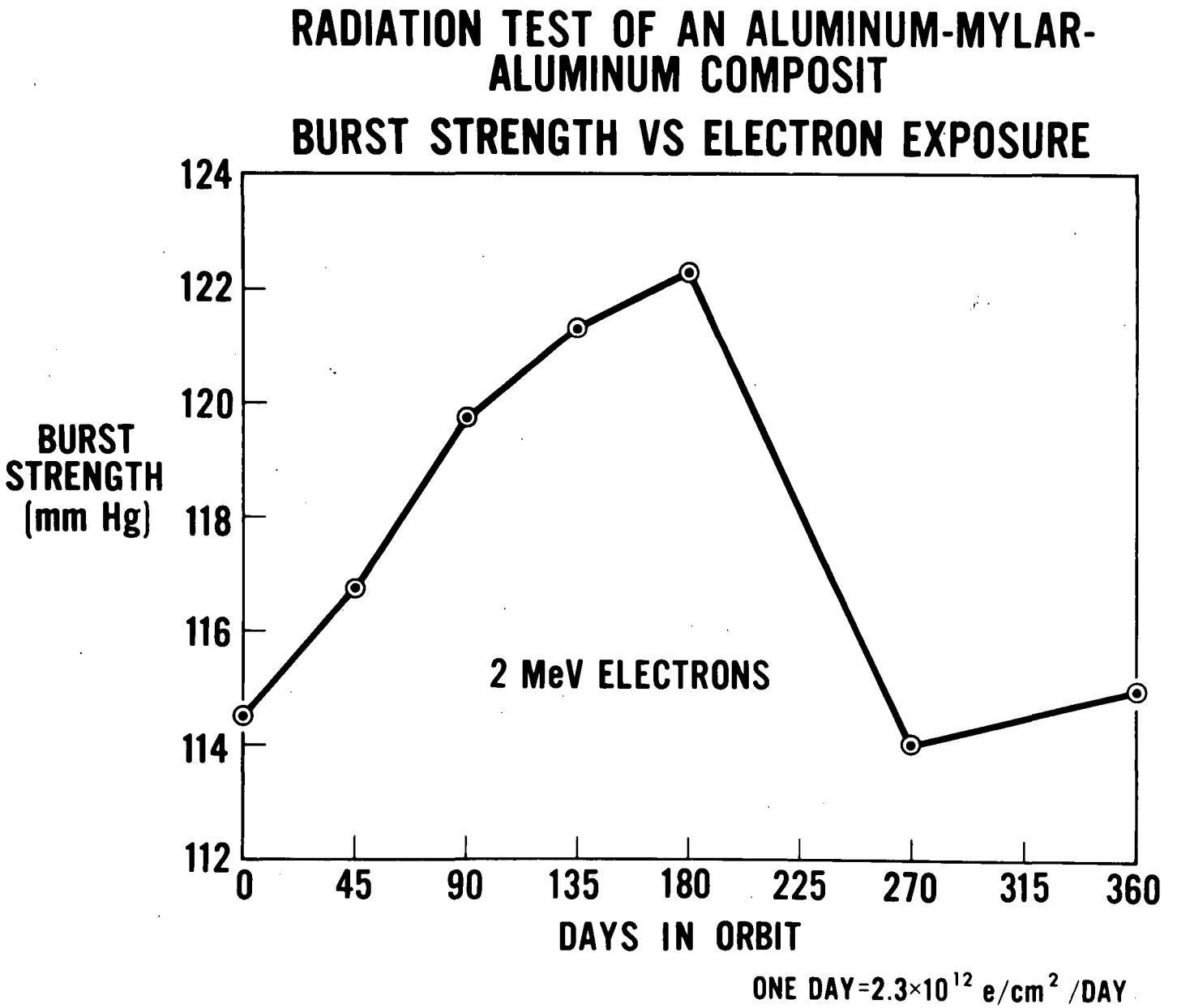
RADIATION TEST OF AN ALUMINUM-MYLAR-ALUMINUM COMPOSIT
BURST STRENGTH VS ELECTRON EXPOSURE
BURST STRENGTH (mm Hg)
124
122
120
118
116
114
112
2 MeV ELECTRONS
0
45
90
135
180
225
270
315
360
DAYS IN ORBIT
ONE DAY=2.3×10^12 e/cm^2 /DAY

FIGURE 2

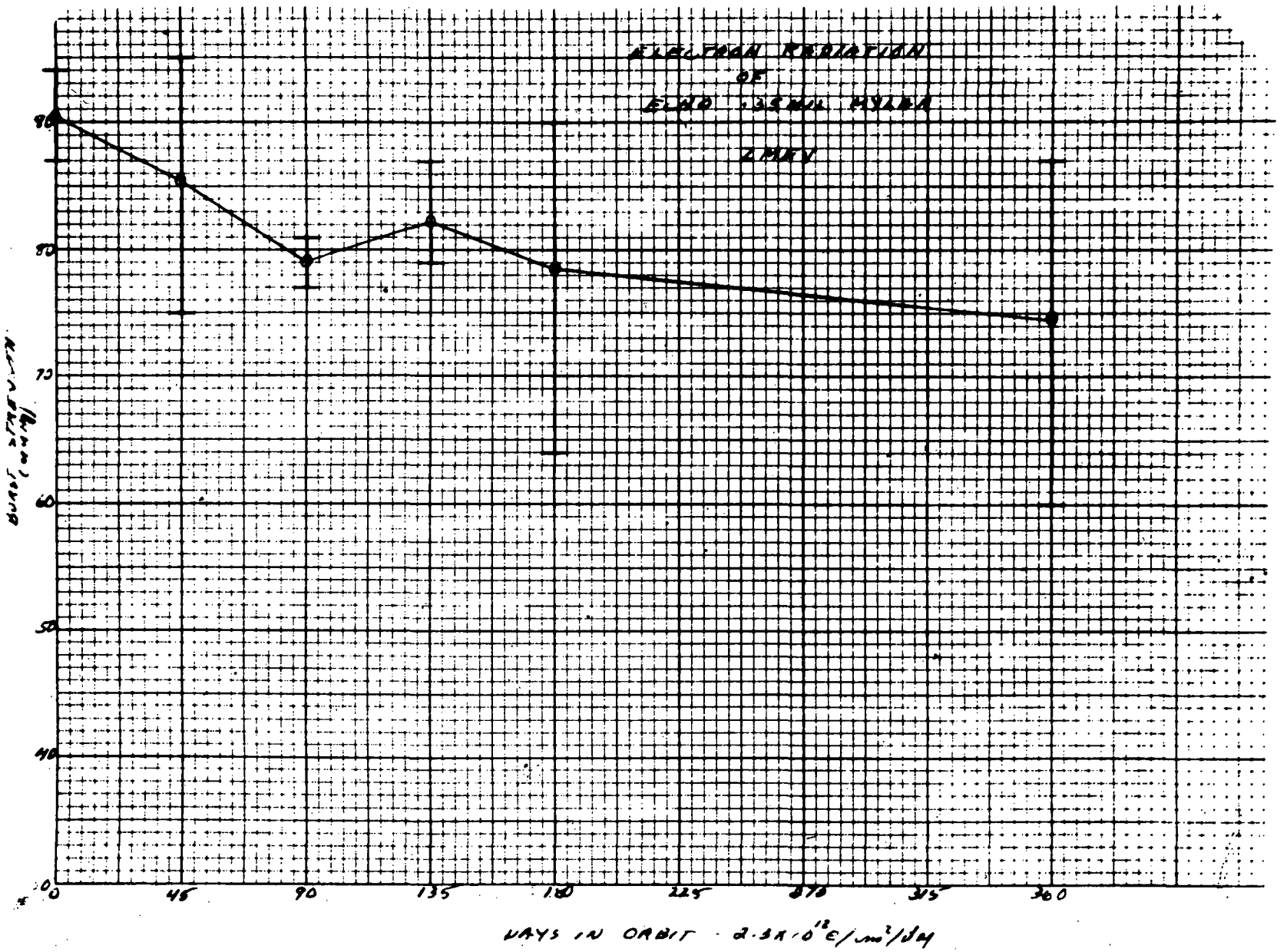
ELECTRON RADIATION
OF
ALUMINUM HYDRA
2 MEV
100
90
80
70
60
50
40
30
0
45
90
135
180
225
270
315
360
DAYS IN ORBIT · 2.3X·10¹² E/cm²/day

FIGURE 3

RADIATION EFFECTS EXPERIMENT ON MICROPOWER MICROELECTRONICS

By Marjorie Townsend
Goddard Space Flight Center

The future of reliable telemetry systems lies in pulse code modulation (PCM) techniques. One such system has been developed for storage of medium resolution radiation data on board meteorological spacecraft. It was designed using microelectronic circuits, primarily the Texas Instruments Series 51 modules. In addition, we had developed in microelectronic form by CBS Laboratories record and playback amplifiers for use with an eight track digital tape recorder, and an analog-to-digital converter in which the logic portion is microelectronic and the analog comparator circuits are constructed of discrete components.

A considerable amount of effort has gone into testing the T.I. modules, and it was felt that an investigation should be made into the radiation resistance of the CBS Laboratories' circuits. To this end, typical circuits are being purchased from CBS Laboratories which represent the types of transistors, diodes, resistors, and capacitors being used in these circuits, but which have leads brought out for testing in order to measure degradation as well as catastrophic failures.

Three different types of modules are being purchased. The first has NPN transistors with betas of 30 and 100 diffused into a common silicon substrate. Capacitors, which are PN junctions, are also diffused into the same substrate. One is a 150 pf polarized capacitor; another one is non-polarized and consists of two of the polarized capacitors back to back. The resistors are 200 K $\pm$ 20% and are deposited over the substrate using a 1.5 mil line width.

The second module has a diode which is the emitter-base junction of a transistor and is diffused into the same substrate as two transistors whose characteristics are the same as the transistors in the first module. The resistors, however, are 860 $\pm$ 5% ohms. A field effect transistor is diffused into a separate chip, and then connected into the module.

The third module has resistors in a ladder network. They have a tolerance of 5%, but are matched so that the voltage divider action of the resistors is accurate to 0.5%. In addition, the module contains 10 K ohm resistors. The ladder network will be operating, but separate resistors will not be energized in any manner so that we may check for changes in resistance due to radiation only.

PAGE 82 INTENTIONALLY BLANK

The purpose of this experiment is to determine the effects of electron bombardment on the parameters and operating characteristics of these particular components, the effects of shielding, and the effects of time of exposure. A very important consideration in such a test is to have a good experimental design. Without one, the results obtained may be meaningless. Such a design has been completed, so that variations which occur entirely by chance will be ruled out.

The simulated environment is that of a 1000 Km orbit. Radiation levels will at three levels between 0 and 3 mev. This band contains more than 80% of the electron energy. The exposure time of eight hours will simulate between 3 and 10 years depending on the latest data on the radiation belt. Five thicknesses of aluminum shielding will be used: 0, 25, 50, 100, and 200 mils. The measurement acquence will be based on a 6 x 6 Latin square to eliminate bias between individual measurements. Thus the measurements will be taken in a variable sequence.

Knowing the effects of radiation and shielding on these specific components will enable us to improve the microelectronic modules, design around their limitations, or build in the required shielding to provide for a long-life, reliable experiment in space.

STATUS REPORT A. ESCRIPTION OF THE NASA SPACE RADIATION EFFECTS LABORATORY

By Emanuel Rind*
NASA Langley Research Center

NASA Langley Research Center personnel of the Instrument Research Division had been conducting various investigations prior to 1960 using X and gamma radiation. As NASA's Space Program accelerated and it became apparent that man and equipment would be exposed to the space particulate radiation of the radiation belts, solar flares, cosmic rays, and of manmade origin, a radiation program was begun to see if these radiations could detrimentally affect space missions. Initial proton experiments on semiconductor devices, insulators, coatings, and similar items used in space missions, indicated that radiation adversely affected most of these. The experiments were continued on the items exhibiting greatest sensitivity to the radiation. The experiments posed a problem because most of the particle accelerators were being used for basic research. This made it rather difficult to obtain time for engineering experiments. Eventually, however, experiments were conducted at McGill University, Carnegie Institute of Technology, University of Rochester, University of Minnesota, Oak Ridge National Laboratories, and Harvard University. The increasing need for experimental beam time led LRC to propose a Space Radiation Effects Laboratory (SREL) which would simulate most of the space particulate radiation and could be used as an engineering research tool with regard to the space radiation problem. The construction of SREL and funding was approved by Congress in Fiscal Year 1963 for a cost of approximately $12,400,000 and all contracts for its construction were let by August 1963. SREL occupies approximately 60,000 square feet of floor space, including offices, and contains three particle accelerators which include one 600 Mev proton synchrocyclotron and two electron accelerators with ranges from less than 0.25 Mev to 600 Mev.

THE SREL PARTICLE ACCELERATORS

The Proton Accelerator

The CERN, Geneva, Switzerland, 600 Mev, proton synchrocyclotron was chosen as the basis for the SREL proton accelerator design because it was the most modern, included the best features of the other existing accelerators, was reliable, and had the needed flux and energy for producing the variable energy and flux for simulating most of the space proton spectra. Figure 1 illustrates the CERN accelerator. Its magnet is 36 feet wide, 21.3 feet deep, and 20 feet high. It is made up of 54 forgings weighing approximately 46 tons each with a total weight of 2500 tons. A duplicate of this is presently under construction for SREL by Bethlehem Steel Corporation and is scheduled to be installed in the facility by April 1964. The beam height above the floor is 4.6 feet.

---

*Aerospace Technologist.

The coils being fabricated by the General Electric Co., figure 2, are almost completed and will be ready for installation May 1964. They consist of two complete coil assemblies, including coil formers, made up of nine pancakes each. Each pancake is wound from one continuously extruded length of hollow aluminum conductor with no joints or splices. The coils are formed by series-connecting the pancakes. Each pancake contains 37 complete turns arranged in two layers. The total resistance of a coil is less than 0.112 ohm at 20° C. Water coolant is used flowing at a rate of more than 7.66 gallons per minute through each pancake. The coils are about 25 feet in diameter, weigh about 60 tons each, and will produce about 0.75 megawatt of heat at 1750 amperes. The maximum radius R of proton path (n = 0.2) is $89\frac{1}{2}$ inches. The magnetic field at this radius is 17.9 kilogauss.

The vacuum chamber housing the Dees and connections are made of welded stainless steel and has a volume of 813 ft^3. It operates at $3 - 5 \times 10^{-6}$ torr using two 32-inch oil diffusion and two 130-cfm roughing pumps used in conjunction with a Roots blower.

The radio-frequency 3/4 λ system, being constructed by Phillips, Holland, has a sweep frequency of 30.0 to 16.4 mc with a modulation frequency of 54 cps. The Dee voltage variation corresponding to the higher frequency starts at 4 kv and goes to 12 kv. Modulation frequency is produced by a variable capacitor consisting of a water-cooled tuning fork. The Dee liner and dummy Dee are made of 1-mm-thick copper sheet.

The ion source is a cold cathode Penning type which operates at 1000 volts in synchronization with the radio frequency and at a controllable phase. The position is adjustable in two directions and is remotely controlled. The flow of each gas is independently variable by means of valves at the cyclotron, remotely controlled.

Target systems, shown in figure 3 are those used at CERN. They consist of: (1) A probe target with variable radius control but fixed in azimuth. (Targets can be interchanged without breaking vacuum.) (2) A universal target, trolley mounted, with provision for changing radius and azimuth is remotely positioned and its position is remotely read. It is equipped with adjustable stops to limit its travel. (3) Six flip targets for producing neutrons at radii corresponding to proton energies of 110 to 600 Mev.

Miscellaneous beam devices consist of a beam clipper which is a carbon absorber used for eliminating parts of the internal beam whose amplitude of vertical oscillation might cause it to strike the Dees or pole tips, a beam chopper which permits varying the beam intensity from zero to a maximum and a peeler regenerator magnetic deflector used for obtaining the external beam. Only some of these target systems will be immediately available in the SREL synchrocyclotron.

VARIABLE ENERGY

The SREL accelerator has been modified and a beam transport system designed to provide variable energy. There are two primary extractions, one at 600 Mev and the second at about 300 Mev. Intermediate energies between 600 and 300 Mev and from 300 Mev to below 100 Mev are obtained by suitable energy degraders. A unique achromatic beam transport system has been designed to handle any discrete energy over this wide energy range. Electrons from the electron accelerators may also be bent into the terminus of the proton beam pipe by means of a Helmholtz coil thus providing a combined electron and proton beam. The proton beam characteristics are summarized in figure 4.

ELECTRON ACCELERATORS

A Dynamitron of 0.5 to 3 Mev has been temporarily installed at NASA, Langley Research Center. A drawing of this accelerator is shown in figure 5. This is a d-c machine with an energy spectrum controllable to ±1 percent. Acceleration occurs by a single voltage drop. It is possible to equip this machine for pulsing. The control of the pulse length and frequency is similar to that achieved with a linac. It is also possible to convert it for proton use.

The electron linear accelerator or linac (fig. 6) is being supplied by Arco. Its energy range is from 2 to 10 Mev. This is an a-c machine which accelerates electrons on an RF wave. The electrons are accelerated through a small voltage drop which travels down a wave guide and keeps pace with the electrons so that the electrons are continuously accelerated. Because of bunching effect associated with the RF accelerator and excessive power requirements the linac is pulsed and does not produce a continuous beam. The duty factors for the linac lies between one and three parts in one thousand. The electron beam characteristics are summarized in figure 7.

PLAN OF SREL

The Space Radiation Effects Laboratory plan view as shown in figure 8 occupies 33,000 square feet exclusive of the support building. It contains the synchrocyclotron cave which is surrounded by 24-foot-thick permanently placed concrete. Adequate space is provided around the accelerator so that major components, like the RF system, can be removed within the cave for repair. The two electron accelerator caves immediately adjacent to it have 7-foot fixed concrete shielding. The remainder of the area is made up of the magnet hall and two target areas. This allows flexibility of operation by permitting the space of these areas to be changed for different experiments. The magnet hall contains the beam transport system and the far wall on the left of the building can be removed for irradiating very large targets. The target area adjacent to the electron caves can be supplied with a combined electron and proton beam.

The electron beam is bent into the proton pipe by means of a Helmholtz coil. Each of the large target areas is provided with a massive iron beam stop embedded in the wall. The shielding around each target area and the electron caves makes each of these areas independent of the others. Thus, experiments can be set up or run in any one of these spaces while work is going on in any other. Massive sliding doors provide access to these areas from the set-up area. The set-up area with its low radiation levels is used for experimental set-ups, calibrations, etc.

The support building has two floors and a half basement with a floor area of 21,000 square feet. Nine thousand square feet on two floors is used for the mechanical and electrical utilities supporting the accelerators. The remaining space is used for offices, shops, the control room, data acquisition, and other areas pertinent to laboratory support.

A vertical view (fig. 9) shows the 8-foot overhead shielding which extends down the magnet hall and minimizes sky shine radiation effects. This view taken through the synchrocyclotron cave also shows the tunnel which houses the electrical cabling and other supply lines for the cyclotron as well as the two 25-ton overhead crane hooks. The crane travels the entire length of the laboratory. An auxiliary 5-ton hook will be added to one of the 25-ton hooks for small loads.

SAFETY FEATURES

The control room located in the support building is shielded to receive minimal radiation. It is being provided with capability for remotely positioning, monitoring, and controlling the accelerator beams, target systems, and other important parameters. Suitable warning systems, visible or audible, to the operator at all times, will make any hazardous condition known immediately. Indications, in the control room, of current and voltage in all major circuits of the accelerators, are provided. Pilot lights will indicate that all interlock chains are complete as well as the presence or absence of voltage on the various circuits. They will also indicate the positions of the contactors. Additional features included are TV monitoring from the control room, hot storage designed into the accelerator cave wall, and remote indications of radiation levels in the various shielded enclosures. All systems are designed fail safe.

Figures 10 and 11 are recent photographs showing the extent of the present construction.

OPERATION OF THE LABORATORY

The laboratory is a facility of the NASA, Langley Research Center. The Virginia Associated Research Center (VARC) formed by the College of William and Mary, the University of Virginia, and the Virginia Polytechnic Institute, will supply, under contract to NASA, the accelerator operators, maintenance crews,

and the various other personnel needed for the housekeeping and knob turning operations of the facility. In return, VARC will receive half the beam time to conduct research in basic physics under grants or contracts which may be self-initiated. NASA, Langley Research Center, will conduct its own basic research and experimental engineering programs in radiation effects.

CONCLUSIONS

A Space Radiation Effects Laboratory (SREL) is being built on a 100-acre site, in the City of Newport News, located about 10 miles from the Langley Research Center. An architect's rendering of this facility is shown in figure 12. All construction schedules are being met and it is anticipated that SREL will be operational in the latter part of 1965.

FIG.1 CERN 600 MEV SYNCHROCYCLOTRON

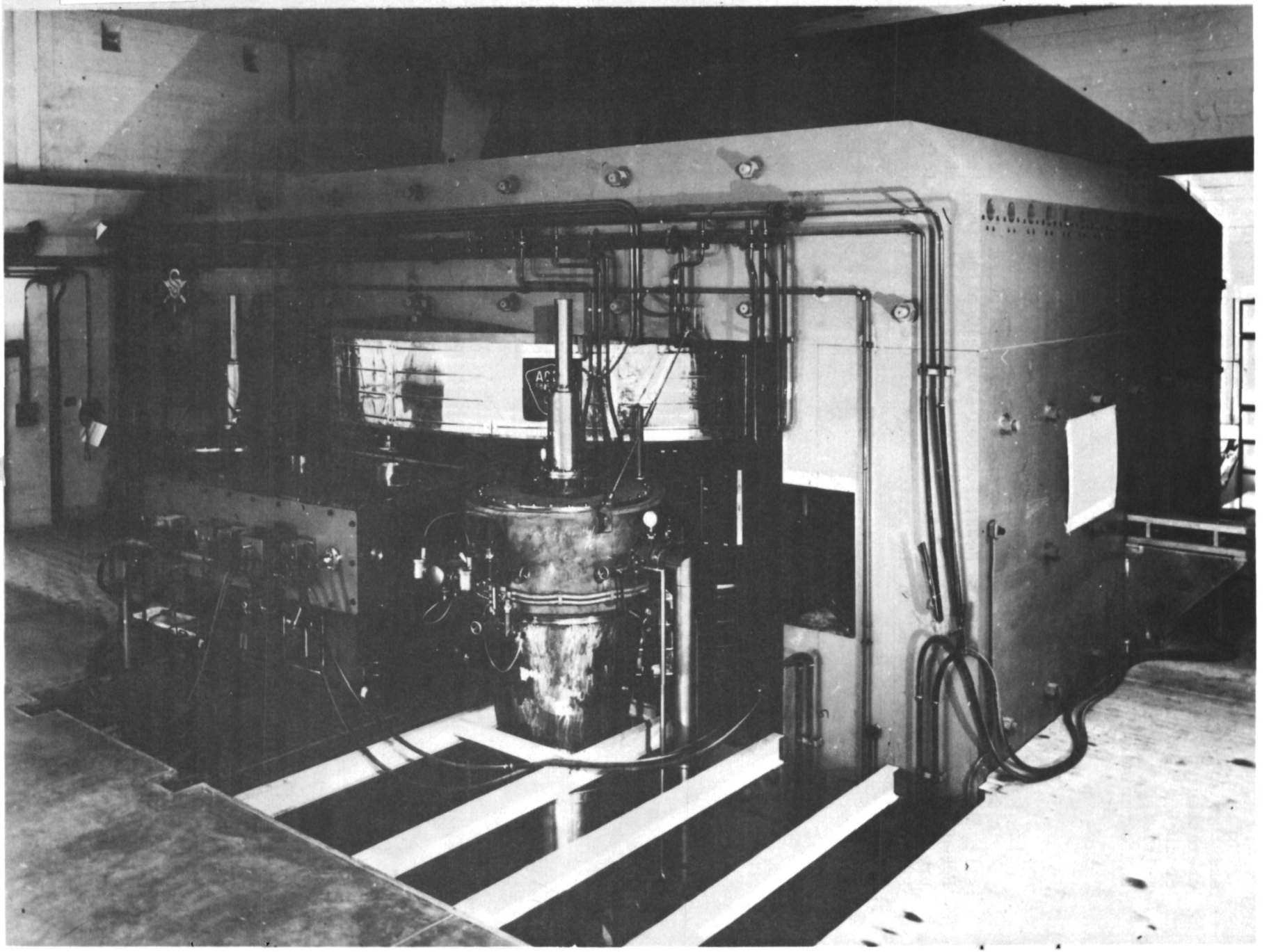

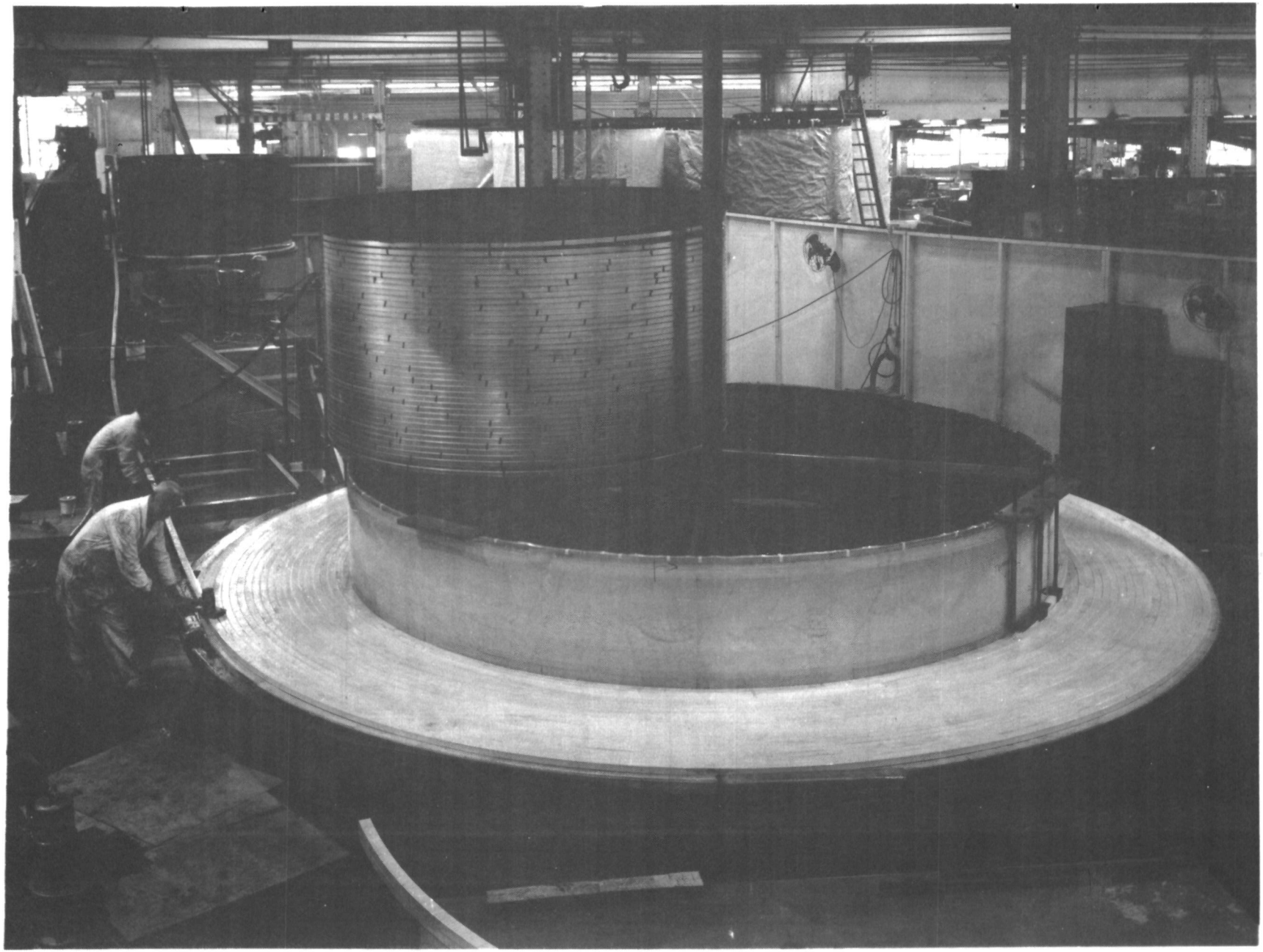

FIG 2. THE SREL 600 MEV MAGNET COIL, INSULATED AND BEING WOUND INTO PANCAKES

FIG. 3 THE CERN
PROTON INTERNAL TARGET SYSTEM

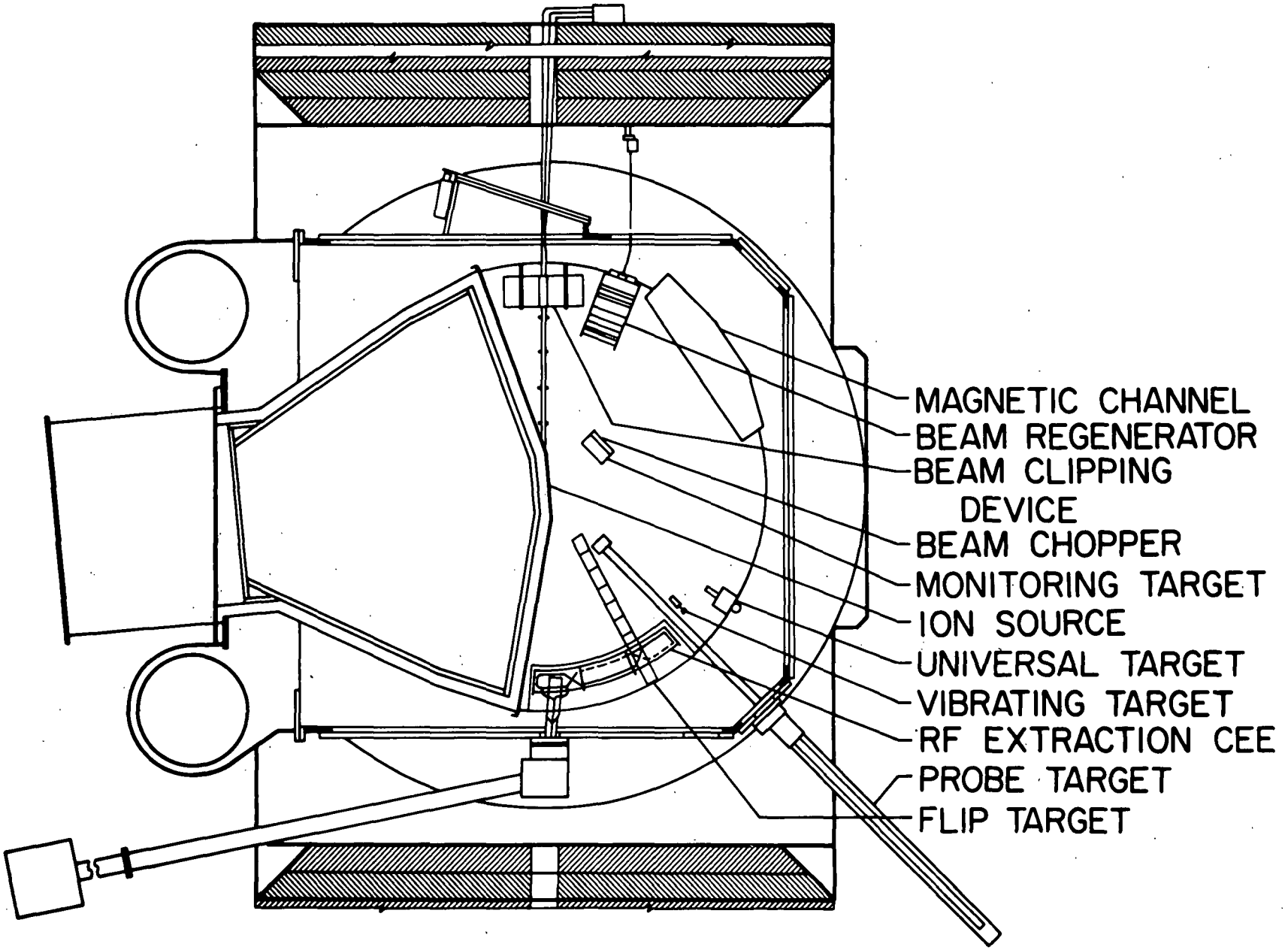

FIG. 4 SUMMARY OF THE SREL PROTON ACCELERATOR BEAM FEATURES

INTERNAL BEAM CURRENT: $\approx 0.5\ \mu$ AMP

EXTERNAL BEAM

- PRIMARY ENERGIES: 300 AND 600 MEV
  - FLUX 10^{11} - 10^{12} PROTONS/SEC
  - ENERGY SPREAD: $< \pm 1\%$
- INTERMEDIATE-LOW ENERGIES: CONTINUOUSLY VARIABLE
  - FROM 600 MEV TO AT LEAST 100 MEV
  - FLUX: NOT LESS THAN 10^{10} PROTONS/SEC
  - ENERGY SPREAD: $< \pm 5\%$

TARGET PLANE

- INTENSITY DISTRIBUTION: $< \pm 5\%$
- AREA: CONTINUOUSLY VARIABLE FROM 15 CM^2 - 900 CM^2

PROVISION FOR AUXILLIARY DEE

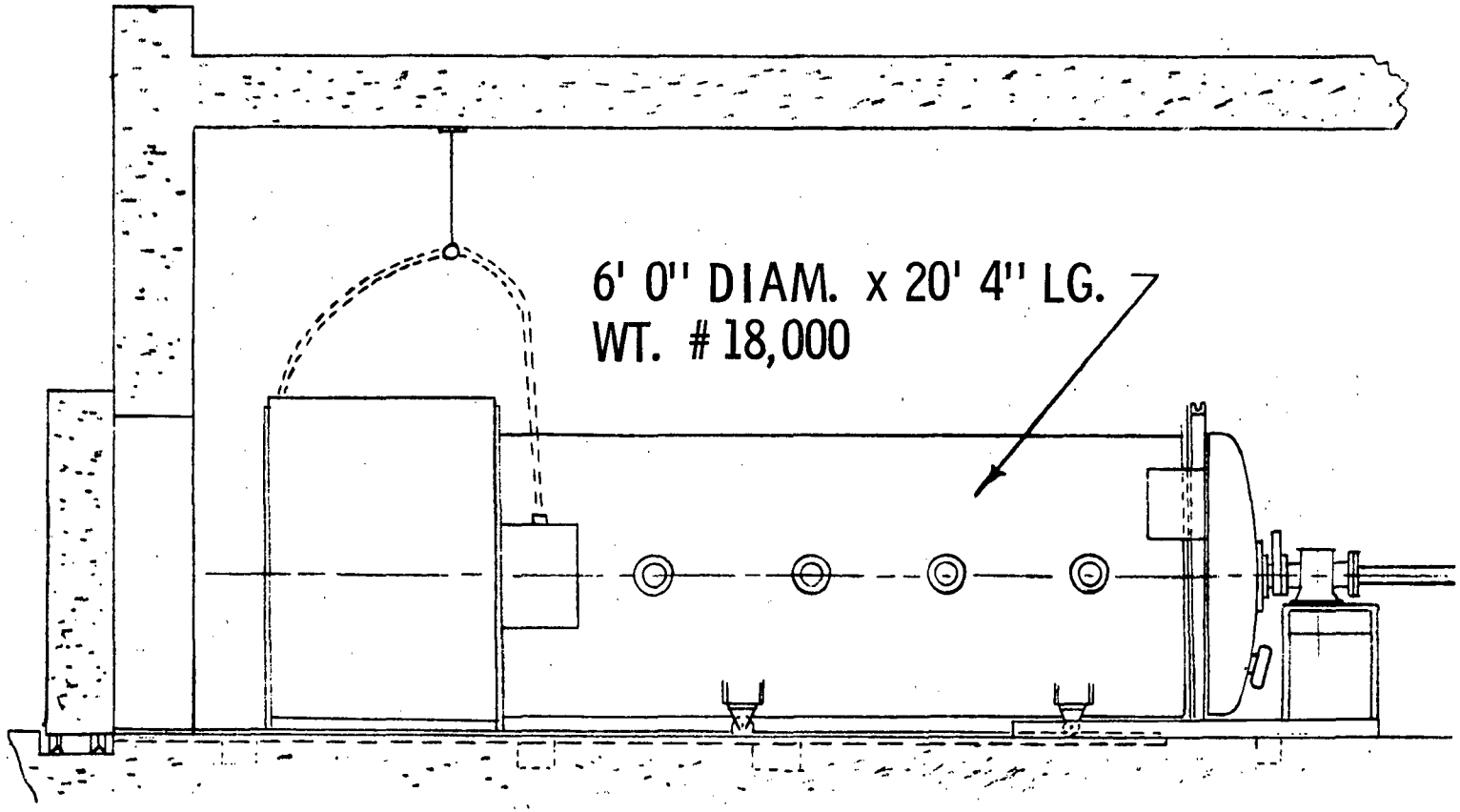

FIG. 5 HORIZONTAL LAYOUT
OF THE 3 MEV DYNAMITRON

FIG. 6 LAYOUT OF THE SREL 10 MEV ELECTRON LINAC

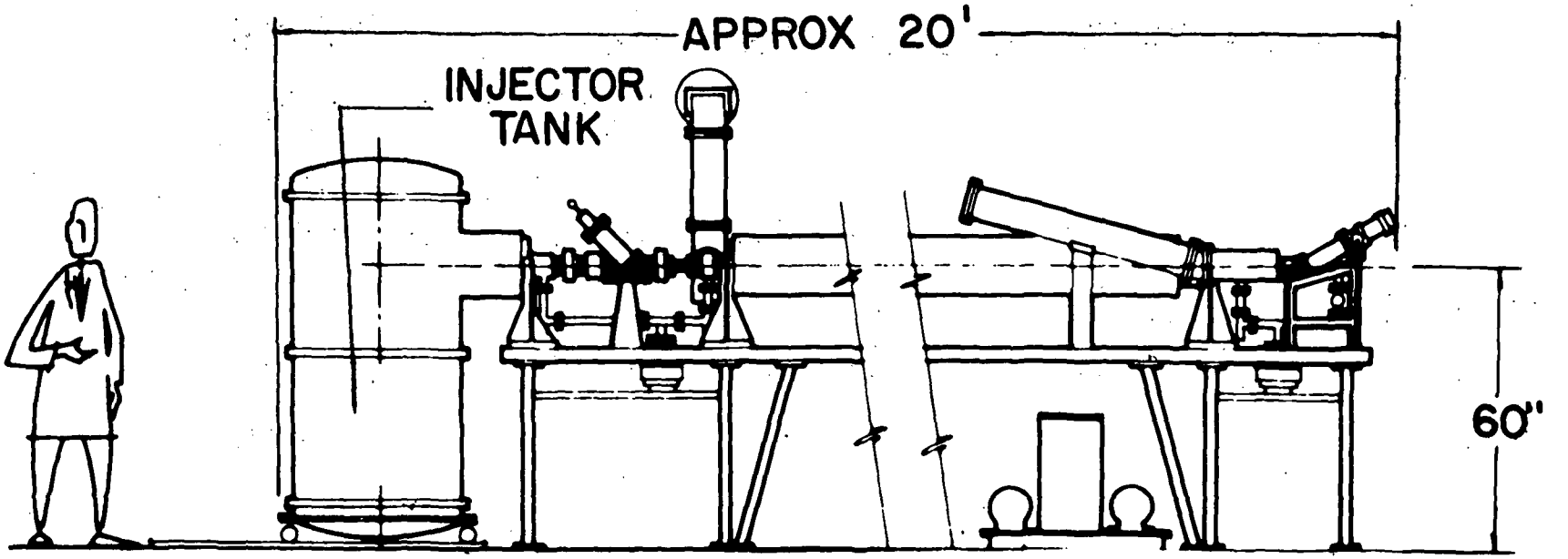

FIG. 7 SUMMARY OF THE SREL ELECTRON ACCELERATOR BEAM FEATURES

LOW ENERGY

RANGE: 0.5 – 3 MEV

CURRENT: 1 MICROAMP – 10 MILLIAMPS

TARGET SCAN RATE: 7–24 ~/SEC OVER 24" LENGTH

POSITIVE ION CAPABILITY

HIGH ENERGY

RANGE: 2–10 MEV EXTENDABLE TO 30 MEV

AVER. D.C. CURRENT: 0–250 μ AMP AT 3 AND 10 MEV
0–1000 μ AMP AT 7 MEV

PULSE LENGTH: .1–6 μ SEC, CONTINUOUSLY VARIABLE
.01–.1 μ SEC, STEPWISE

REPETITION RATE: 10–720 PULSES/SEC

SINGLE PULSE OPERATION

FIG. 8 PLAN OF SPACE RADIATION EFFECTS LABORATORY

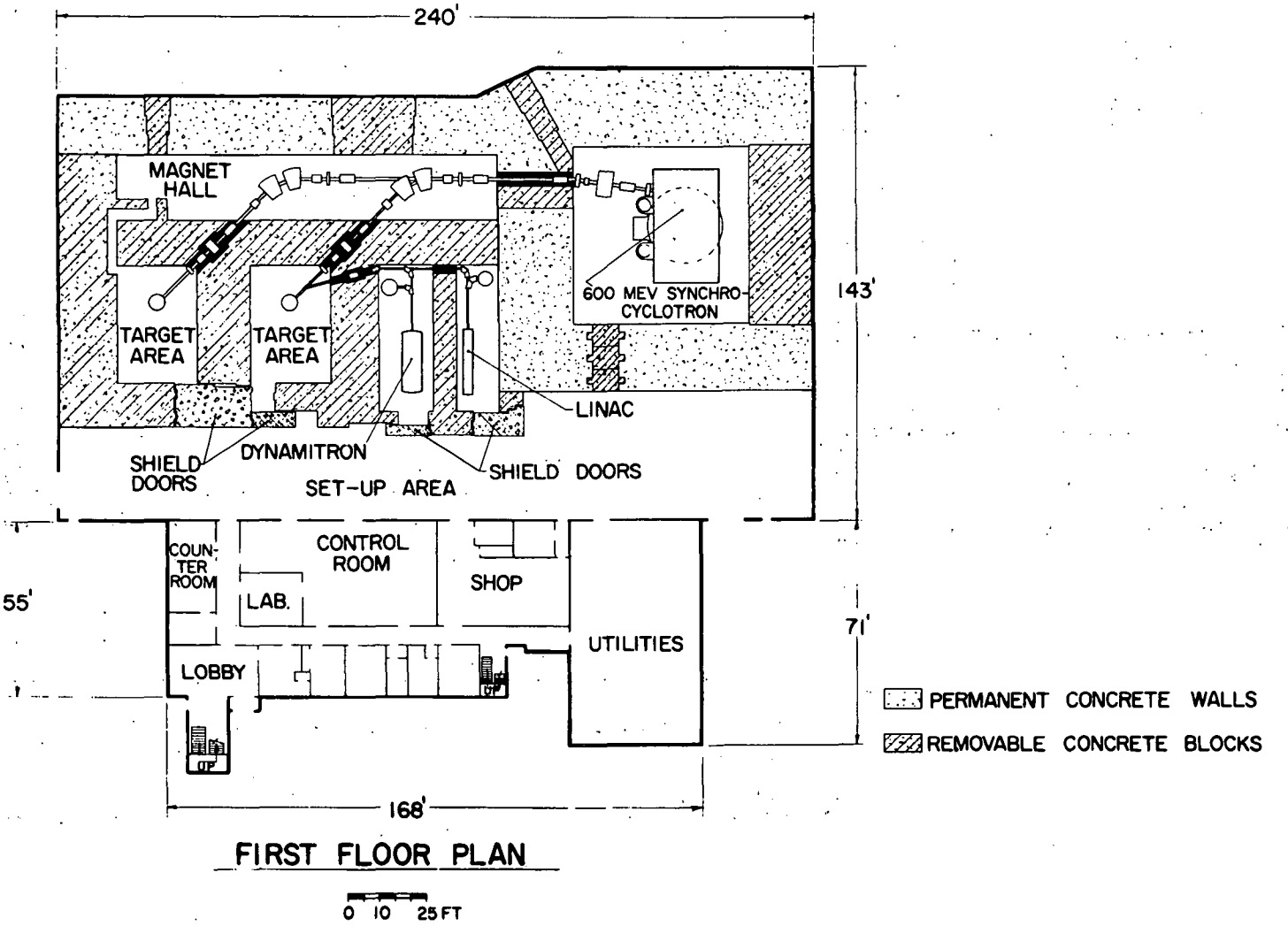

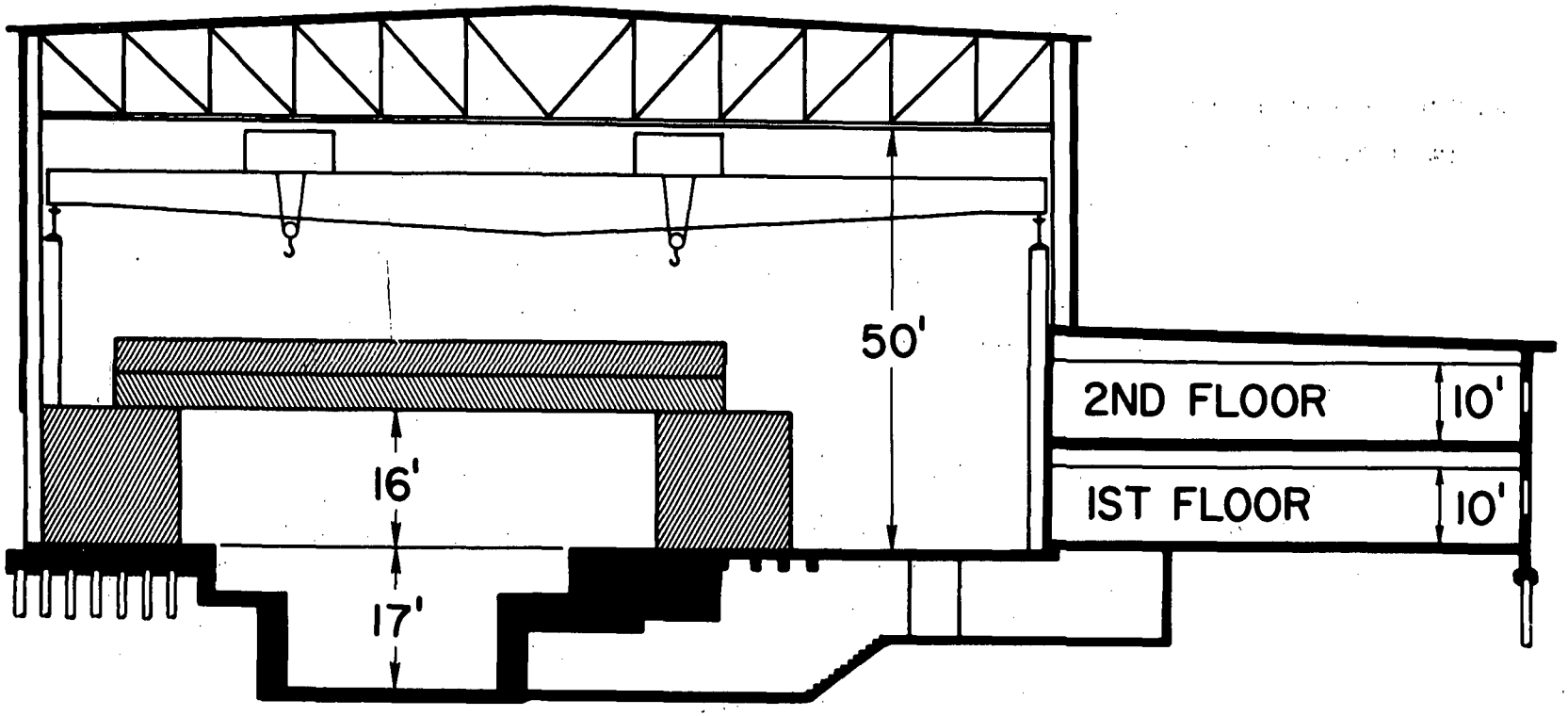

FIG. 9 SECTION THRU THE SYNCHROCYCLOTRON CAVE, SPACE RADIATION EFFECTS LABORATORY

FIG. 10 INTERIOR VIEW OF SREL SHOWING THE 50 TON CRANE INSTALLED

FIG. 11 EXTERIOR VIEW OF SREL SHOWING THE SUPPORT AND ACCELERATOR BUILDINGS

FIG. 12 ARCHITECT'S RENDERING, SPACE RADIATION EFFECTS LABORATORY

RADIATION EFFECTS ON AROMATIC MAIN CHAIN POLYMERS

by

George F. Pezdirtz, Howard L. Price, and Vernon L. Bell

NASA-Langley Research Center

INTRODUCTION

Molecular Weight Considerations

One of the most important properties of any polymeric material is its average molecular weight (molecular size). Unlike common non-polymeric materials such as iron, graphite, silicon, gallium arsenide, water, hydrogen, butane, etc., polymers do not have a single molecular weight. Polymers are composed of long chain molecules with a wide range of lengths or molecular weights. Many of the useful properties of polymers such as their strength, elongation, viscosity in solution, melting point, and vapor pressure are related to their molecular weight in an exponential fashion as shown in Figure 1. Nobel Laurate Staudinger was one of the first to realize this relationship between molecular weight and physical property. As the molecular weight of a given polymer increases, the values of its physical properties rise asymptotically to some limiting value. (Reference 1). In the region of the inflection in Figure 1 a doubling or tripling of the molecular weight may result in only a 10 percent increase in a particular physical property for a given polymer. However, if the molecular weight is reduced to 1/2 or 1/3 its original value at the inflection point, the property may decrease by a factor of 100 or even 1000.

---

[1]H. Staudinger, Die Hochmolekularen Organishen Verbindungen, p. 186, J. Springer, Berlin, 1932.

PAGE 102 INTENTIONALLY BLANK

Gross Effects of Radiation

In a gross sense, high energy ionizing radiation can change the average molecular weight and the molecular weight distribution of a polymer in either of two fashions:

(a) The molecular weight may be increased by forming cross-links (formal molecular bonds) between the chains.

(b) The chains may be ruptured by irradiation as illustrated in Figure 2.

These are permanent effects and can be measured in the laboratory. Cross-linking may lead to surface and bulk crazing of the polymer, loss of physical integrity, and dielectric breakdown. At the other extreme, random chain rupture may result in several undesirable consequences such as off-gassing and contamination of man and/or instruments by small molecular fragments.

Molecular Weight Distribution

Real polymeric materials rarely behave in such a simple manner as just described. Subtle changes in their molecular weight distribution can also accompany radiation damage. The distribution of the various polymer chains of different lengths present in any polymeric material may be characterized by a normal distribution curve as shown by curve No. 2 in Figure 3. In the two extreme cases just discussed, cross-linking may produce a shift of the molecular weight distribution to higher values of molecular weights and some distortion in the shape of the curve as shown by curve No. 3 in Figure 3. At the other extreme, complete random chain rupture will shift the molecular weight distribution curve to lower value of average molecular weight, but generally the shape of the curve will be

retained. These two extreme cases are not too common and frequently both cross-linking and chain rupture will occur simultaneously when polymeric materials are irradiated. This produces a broadening of the molecular weight distribution as shown by curve No. 4 in Figure 3.

The shape of these curves can be determined experimentally by measuring the average molecular weight using two different weighting factors and comparing the ratio of the weight average and number average molecular weights. For the most probably molecular weight distribution the ratio of the weight average molecular to the number average molecular weight (Mw/Mn) will be approximately 2. If the molecular weight distribution is considerably broadened as shown in curve No. 4 of Figure 3, this ratio (Mw/Mn) may be increased to 15 or greater.

THEORETICAL BACKGROUND

Influence of Molecular Structure on Radiation Effects

Most of the polymers of commerce can be classified as addition polymers, that is, they are made up of simple repeating units based upon ethylene or substituted ethylene groups (vinyl polymers). The molecular structure of a polymer is one key to its resistance to change during irradiation. For the large class of addition polymers some general ground rules for predicting radiation damage effects have been developed over the past decade. In Figure 4 the two types of repeating units for most addition polymers are shown schematically. If the repeating unit of the polymer has a vinyl side group (a single side group, other than hydrogen, on every other carbon atom), then the polymer will predominately cross-link. On the other hand, if the repeating unit of the polymer has vinylidene side groups (two side groups, other than hydrogen, on every other carbon atom), then the polymer will

predominately rupture when irradiated. Wall (reference 2) has explained this in terms of internal molecular strain along the polymer chain.

In the case of the vinyl structure, the side groups have sufficient freedom to arrange themselves in space along the chain in such a way that there is little or no interaction between them and as a consequence little or no strain in the chain. Typical vinyl polymers are polypropylene, polyvinyl chloride, polyvinyl fluoride, and polystyrene, and polyvinyl alcohol. In the case of the vinylidene structure, the two side groups on alternate carbon atoms are unable to find a geometric position in which they will not interact with each other. This produces an internal molecular strain along the chain and as a result when the chain is broken by ionizing radiation, this molecular strain causes the ruptured fragments to effectively fly apart and prevents "rehealing" of the broken chain. Typical examples of vinylidene polymers are polyvinylidene chloride (Saran), polyisobutylene (Butyal rubber), polymethyl methacrylate (Lucite, Plexiglas), and polyvinylidene fluoride (Kynar).

Several years ago we analyzed these ground rules and felt that there should be a single exception to the general rule that radiation induces rupture in vinylidene type polymers. If the two side groups on such a polymer were small enough so that their spatial requirements could be satisfied without any steric intereaction along the chain, then there would be no molecular strain in the chain and the polymer would cross-link rather than degrade during irradiation. The only case where this condition of small sized side groups would be possible is in the polymer,

---

[2]L. Wall, "Factors Influencing the Behavior of Irradiated Polymers," J. Polymer Science, 17, 141 (1955).

polyvinylidene fluoride, which has two fluorine atoms on every other carbon atom along the polymer chain (CH_2-CF_2). At that time we were unable to obtain any polyvinylidene fluoride to experimentally confirm this hypothesis. In recent times polyvinylidene fluoride has become available and is now sold under the trademark Kynar. We were able to confirm our hypothesis about a year ago by irradiating Kynar and observing that cross-linking and not rupture was the predominate reaction. Cross-linking produces a three-dimensional network molecule which makes a polymer insoluble in its normal solvents. This was the case for irradiated Kynar.

Energy Sinks and Their Protective Effect

In addition to these structural guidelines another ground rule for predicting the radiation effects on polymers is based on the electronic nature of small molecular groups which may be present in a particular polymer and can act as "energy sinks" to protect the polymer from damage during irradiation. One of the most notable examples of this protective effect is found in the benzene or aromatic ring. Burton has noted (reference 3) that:

(1) The greater the molecular complexity,

(2) the greater the degree of electronic resonance, and

(3) the closer the excited and ground states structure resemble each other, the less the molecule is ultimately affected by radiation.

(a) Mechanism of Protection

The mechanism of this protective effect in the case of benzene-like rings is not fully understood. It is believed that the π electrons,

---

[3] M. Burton, "Effects of High Energy Radiation on Organic Compounds," J. of Physical and Colloid Chem., 51, No. 3, 787 (May 1947).

which are delocalized among the six carbon atoms of the ring, are able to absorb the energy or radiation, either directly or indirectly, and are exicted to a triplet state (or states). In the triplet states the electrons are unpaired but not unbonded (the molecular bonds are essentially still intact). Since these electrons are not associated with only one or two carbon atoms in the ring, but rather are delocalized or "smeared out" over six carbon atoms, this highly energetic state does not lead to bond rupture. Within a very short time (milliseconds or microseconds) the ring is able to degrade this energy by internal conversion, giving off heat and light, thereby returning to the ground state without undergoing any permanent damage. (See Figure 5.)

There are several aspects of this mechanism which are not well understood. For example, very little is known about the effect of the electron density of the ring or the position of the ring in relation to a polymer chain. We are presently preparing several substituted polyethylene terephthalates (Mylar). Some will have increased and some will have decreased electron densities in the aromatic rings along the chain. Dr. Sands will discuss this aspect of our work in more detail in the following paper.

Charlesby has shown (reference 4) that the benzene ring can exert its protective effect over about six carbon atoms. It is not known how the position of the ring with respect to the polymer chain influences this protective effect. The ring may be attached to the side of the polymer chain itself as in the case of polyethylene terephthalate (Mylar). Figure 5 illustrates some of the differences in molecular structure between polymers with the ring in the chain and attached along the side of the chain.

---

[4]P. Alexander and A. Charlesby, "Energy Transfer in Macro Molecular Systems Exposed to Radiation," Nature, 173, 58 (1954).

(b) Effect of the Position of the Ring

Recent interest is growing to develop new condensation polymers which have complex repeating units and contain aromatic rings within the chain. These polymers are highly polar and are only slightly soluble in polar solvents. They have very desirable high temperature stability and excellent dielectric properties. Mylar represents a moderately complex aromatic main chain polymer which has been available for a number of years. Polystyrene represents a relatively simple aromatic side chain polymer. As the number of aromatic rings within a polymer chain is increased, the radiation resistance of the polymer also increases.

The extremes of aromatic main chain polymers might be represented by polyphenyl and polyacene type polymers (figure 6). In the case of polyphenyl the rings are joined in a "head to tail" fashion and would be expected to have considerable radiation and thermal stability. Evidence for this kind of stability can be found by considering terphenyl (which has a simple molecular structure composed of three benzene rings joined "head to tail") which is used as the organic moderator in some nuclear reactors. A more complex arrangement of aromatic rings along a chain is represented by polyacene (figure 6). In this case the rings are fused together side by side. This material has never been made in high molecular weights. The small molecular analog of polyacene is anthracene which has been studied in recent years for its semiconductive and photo conductive properties (reference 5). Polyacene also represents a simplified version of a "ladder" polymer. The π electrons of the polyacene rings are highly delocalized along the chain

---

[5](a) R. G. Kepler, "Charge Carrier Mobility and Production in Anthracene," Organic Semiconductors, p. 1, The Macmillan Company, 1962.
(b) O. H. LeBlanc, Jr., "Electronic Transport in Anthracene and Other Organic Systems," Ibid, p. 21.
(c) M. Silver, "Carrier Generation and Electrode Contact Effects in Photoconducting Anthtacene," Ibid, p. 27.

and it would be expected that polyacene would exhibit excellent radiation and thermal stability. This material would also probably be a very interesting semiconducting polymer. A simplified molecular model of graphite is also shown in figure 6 for comparison.

RESULTS AND DISCUSSION

Many of the new complex polar condensation polymers are not soluble even in exotic polar solvents. This makes it difficult to analyze their properties and study the mechanism of radiation damage using the traditional solution properties such as solution viscosity. New techniques are required to analyze the polymer in the solid state using its bulk properties in an attempt to determine the mechanism of radiation damage. Two examples which illustrate this point and represent the current studies in the Spacecraft Materials Section at Langley are: (1) the radiation effects on polyimides and (2) thermal control coatings.

Polyimides

A new class of polyimides represented by polypyromellitimides (H-Film) have outstanding thermal and radiation stability. This polymer has a highly complex molecular structure and cannot be dissolved without being degraded. One technique for attempting to understand the effects of radiation on this material is to study its infrared absorption spectra as shown in figure 7. This data should be considered as preliminary in nature and is presented as an example of one of the techniques used to study the radiation effects on the bulk properties of polymers. A detailed analysis of this spectra is still pending. As a first approximation, it can be seen that this material

is quite resistant to change by radiation. There are some indicated differences in the absorption spectra which require further resolution. The absorption bands indicated by (1) in figure 7 are assigned to the imide group indicated by (1) in molecular structure above the spectra. The absorption bands attributed to the diphenyl ether group are indicated by (2).

Another technique for analyzing this polyimide in the solid state is to study the changes in its mechanical properties as a function of radiation dose in vacuum and in air. This data is shown in figure 8 and is compared with Mylar film. The polyimide used in this study is known as H-Film and will be commercially available in the fall of 1964 from DuPont. In comparing the radiation resistance of H-film with that of Mylar, one should keep in mind that Mylar is one of the strongest and most radiation resistant films presently available commercially. It has a tensile strength around 23,000 psi. The radiation resistance of H-film is more than two orders of magnitude greater than that of Mylar. Its mechanical properties are quite comparable to those of Mylar. Mylar is a highly crystalline biaxially oriented (pre-stretched in two directions) plastic film. Its strength is in a large part due to its high crystallinity and its biaxial orientation. On the other hand, H-film is an amosphous, unoriented film and may, in future years, be made with a tensile strength in excess of its present 25,000 psi through biaxial orientation.

Thermal Control Coatings

The second example of our radiation damage studies also requires analysis in the solid state to understand radiation effects. This is illustrated by some initial exploratory results of the radiation damage to thermal control coatings listed in figure 9. These preliminary results (reference 6) show

[6]G. F. Pezdirtz and R. A. Jewell, "A Study of the Photodegradation of Selected Thermal-Control Surfaces," Proceedings of Symposium on Thermal Radiation of Solids, Session IV, San Francisco, Calif., March 4,5,6, 1964.

the magnitude and comparative effects of ultraviolet and gamma radiations on some "stable" white thermal control paints. These paints range in stability from the relatively unstable titanium dioxide-epoxy paints to the relatively stable zinc-oxide in potassium silicate. As a first approximation, this data indicates that the effects of ultraviolet and gamma radiation are comparable in magnitude and direction but differ in equivalent space or sun hours (ESH). The ultraviolet radiation generally produces a greater change in solar absorptance during a short exposure (300 ESH) than the gamma radiation equivalent to many weeks of simulated absorbed dose. Further evidence for the similarity of the observable damage from both ultraviolet and gamma radiation on these coatings can be ascertained by studying the absolute spectral reflectances as a function of wavelength shown in figure 10. In general, we feel that this spectral evidence indicates that the overall changes in solar absorptance (darkening) of the white paints is comparable for the two forms or radiation. The molecular and electronic mechanisms of energy absorption, etc., are undoubledly quite different. The energetics of these reactions have yet to be analyzed. We hope to be able to attack this problem in the near future.

CURRENT AND FUTURE WORK

Some of our future plans in the area of radiation effects on polymers are outlined in figure 11. We are presently synthesizing new polymers of known molecular structure in order to study the effect of polyaromatic ring structure on the physical and chemical properties of these materials. We have recently initiated work to study the effect of radiation on this crystallinity of polymers by using low angle x-ray diffraction techniques.

We intend to use electron spin resonance as a technique to identify the kind and number of free radical fragments produced when polymers are irradiated in the solid state. Differential calorimetry will provide some insights into changes in the heat taken up to given off by the morphological and chemical reactions of irradiated polymers. Additional studies on a more basic level are presently anticipated to understand the damage mechanisms of ultraviolet and high energy ionizing radiation.

REFERENCE TEXTS

F. A. Bovey, The Effects of Ionizing Radiation on Natural and Synthetic High Polymers, Interscience Publishers, Inc., New York, 1958.

R. O. Bolt and J. G. Carroll, Radiation Effects on Organic Materials, Academic Press, New York, 1963.

A. Charlesby, Atomic Radiation and Polymers, Pergamon Press, New York, 1960.

A. Chapiro, Radiation Chemistry of Polymeric Systems, Interscience Publishers, New York, 1962.

A. J. Swallow, Radiation Chemistry of Organic Compounds, Pergamon Press, New York, 1960.

PROPERTY - MOLECULAR WEIGHT

RELATIONSHIP

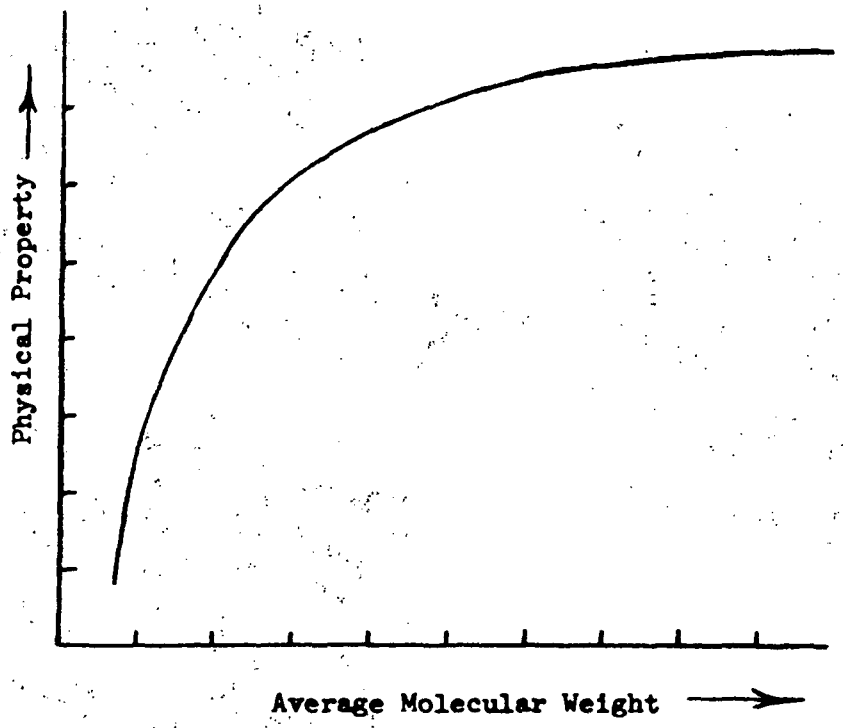

FIG.1

GENERAL EFFECT OF RADIATION ON POLYMERS

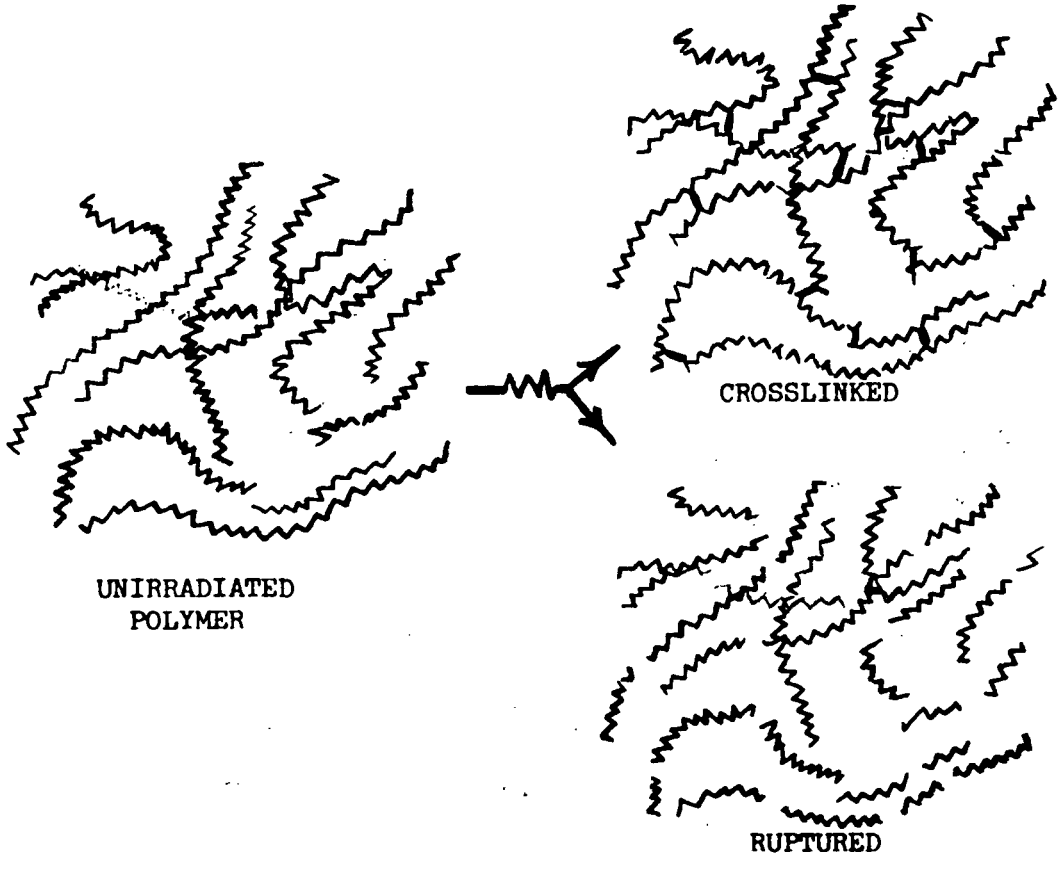

FIG 2

RADIATION EFFECT ON MOLECULAR DISTRIBUTION

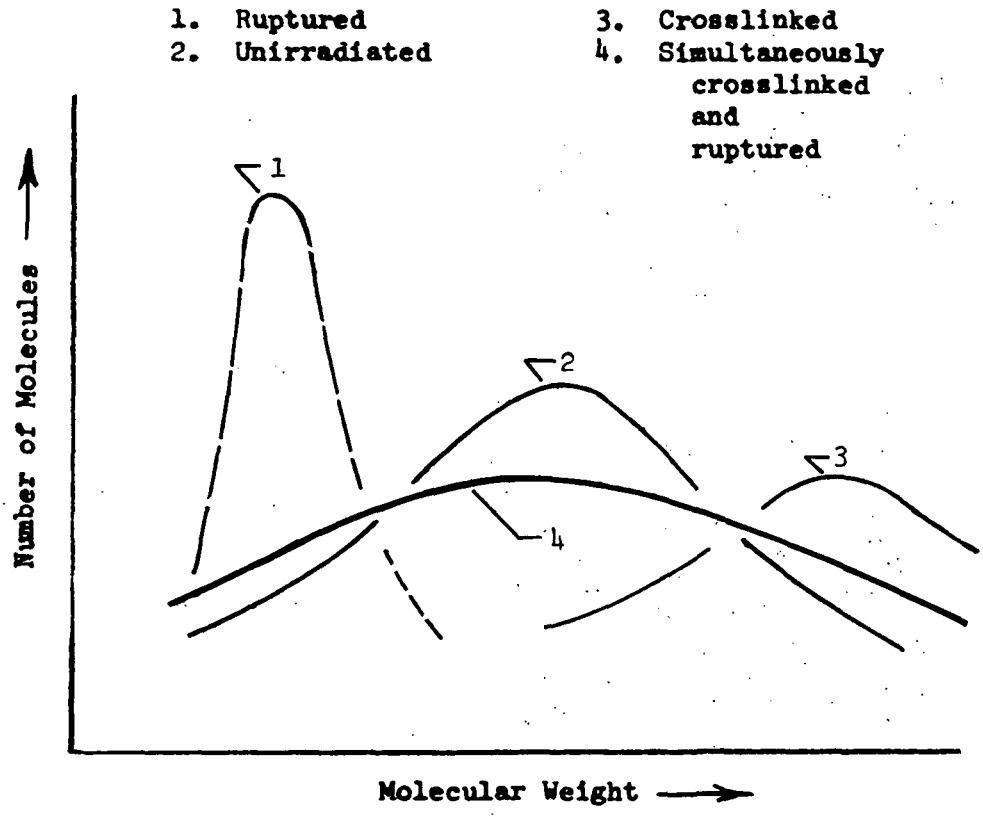

FIG 3

STRUCTURAL INFLUENCE ON RADIATION DAMAGE
TO ADDITION POLYMERS

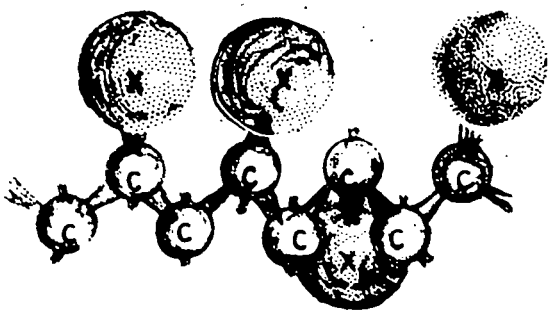

VINYL STRUCTURE
CROSSLINKS

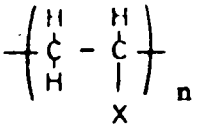

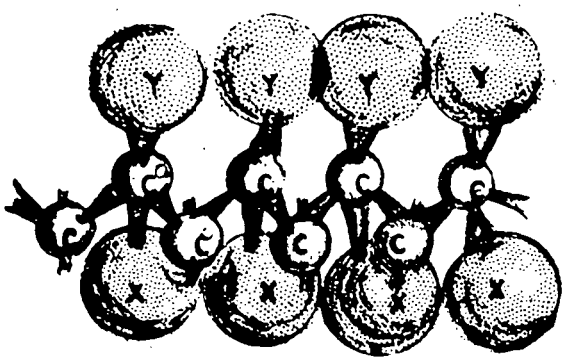

VINYLIDENE STRUCTURE
RUPTURES

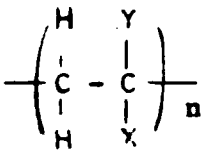

FIG 4

PROTECTIVE MECHANISM
OF
AROMATIC RING

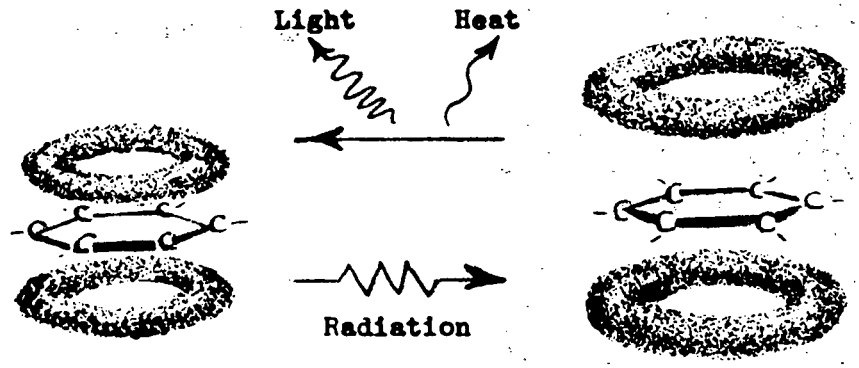

Ground State

Excited State

π Electrons Spin

singlet

triplet

F16

STRUCTURAL COMPARISON OF AROMATIC POLYMERS

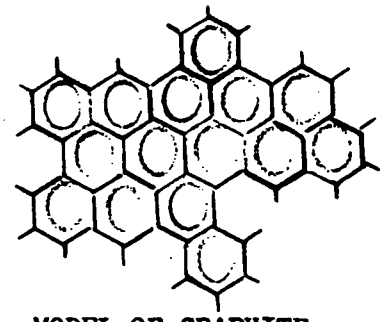

MODEL OF GRAPHITE

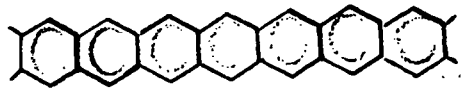

POLYACENE

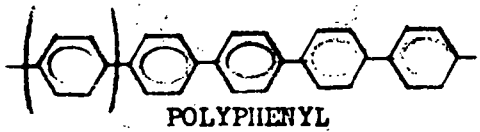

POLYPHENYL

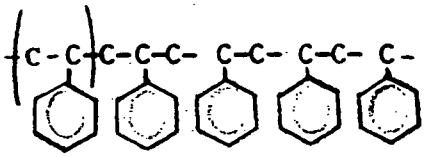

POLYSTYRENE

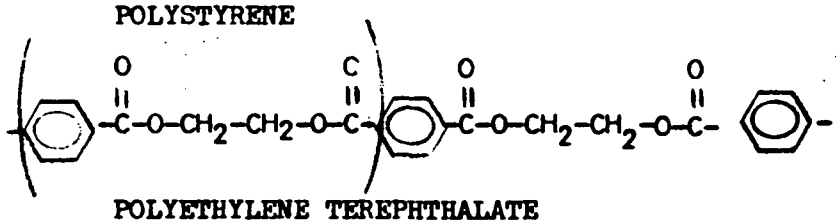

POLYETHYLENE TEREPHTHALATE

INCREASING RADIATION STABILITY

FIG. 6

INFRARED SPECTRA OF POLYIMIDE

POLYPYROMELLITIMIDE

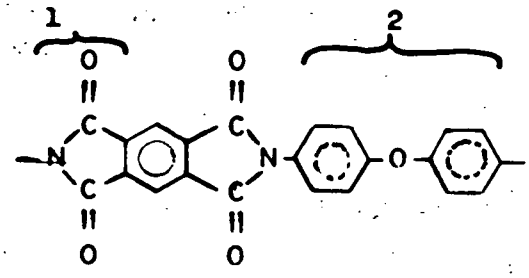

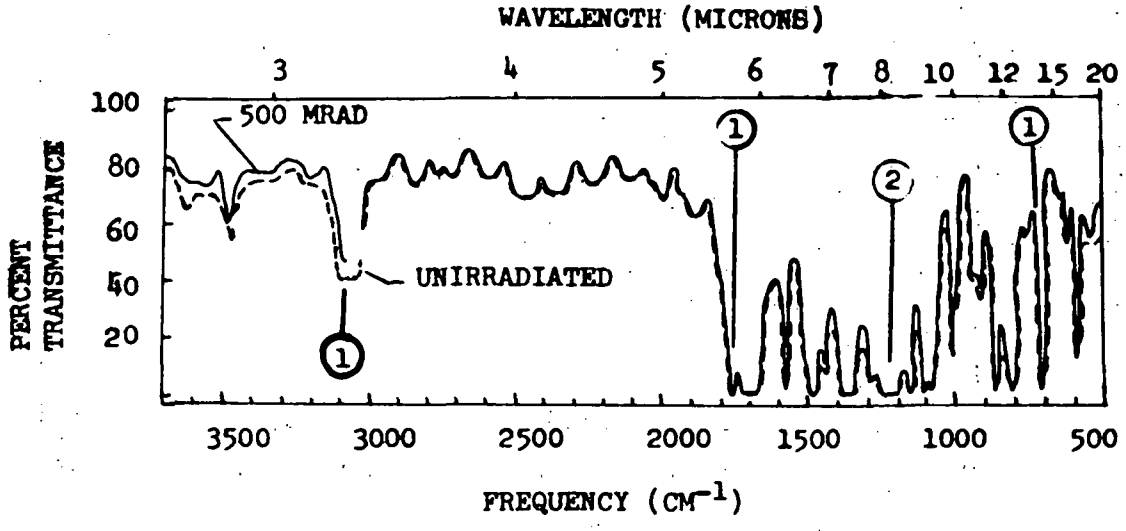

FIG 7

EFFECT OF GAMMA RADIATION ON
PHYSICAL PROPERTIES OF AROMATIC POLYMERS

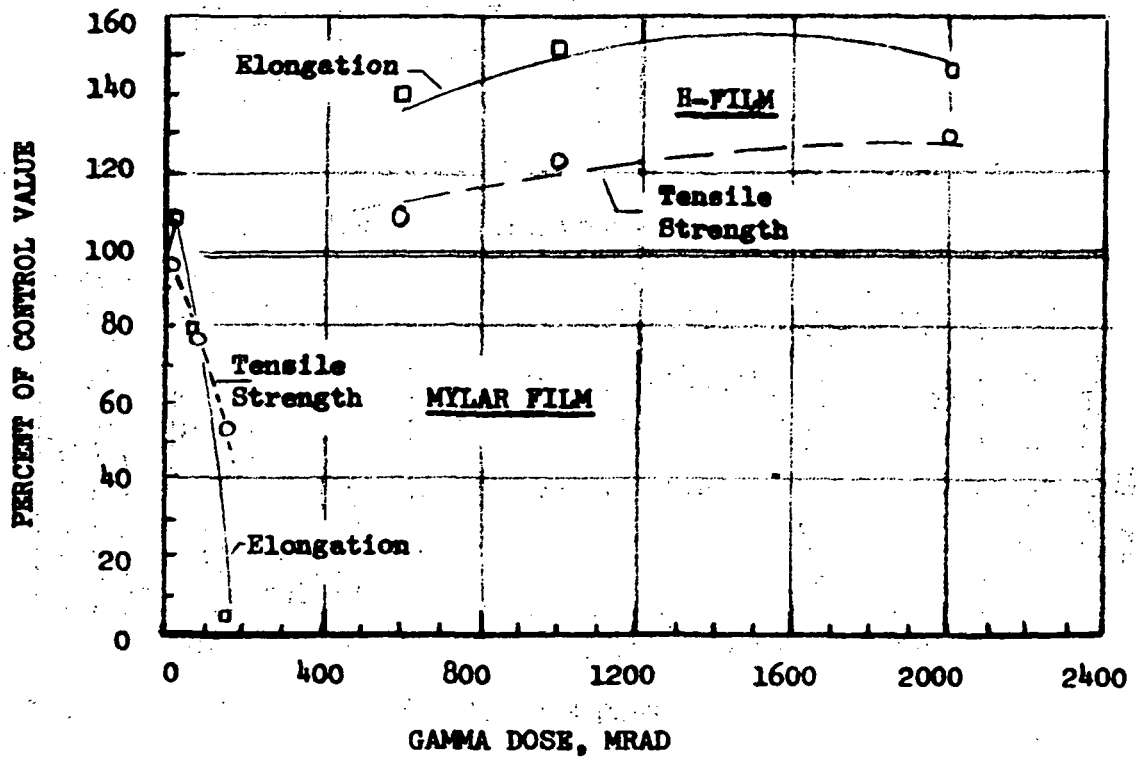

FIG 8

COMPARATIVE EFFECT OF GAMMA & ULTRAVIOLET RADIATION ON SOLAR ABSORPTANCE OF THERMAL CONTROL COATINGS

COATING		SOLAR ABSORPTANCE, α_s			
		ORIGINAL VALUE	INCREASED, $\Delta\alpha_s$		
			GAMMA MRAD		ULTRAVIOLET, ESH
PIGMENT	VEHICLE		77*	385*	300*
Zinc Oxide	Silicone plus Catalyst	0.17	0.04	0.04	0.04
Zinc Oxide	Potassium Silicate	0.14	0.04	0.04	0.01
Titanium Dioxide	Silicone Resin	0.25	0.12	0.18	0.03
Titanium Dioxide	Epoxy Resin	0.20	0.22	0.27	0.19
Antimony Oxide	Potassium Silicate	0.26	0.10	0.26	0.08

Approximate Surface Exposure in Space

Note:	Dose	
(1)	77 MRAD	12 Weeks
(2)	385 MRAD	60 Weeks
(3)	300 ESH	2 Weeks

FIG 9

EFFECT OF RADIATION ON
THERMAL CONTROL COATINGS

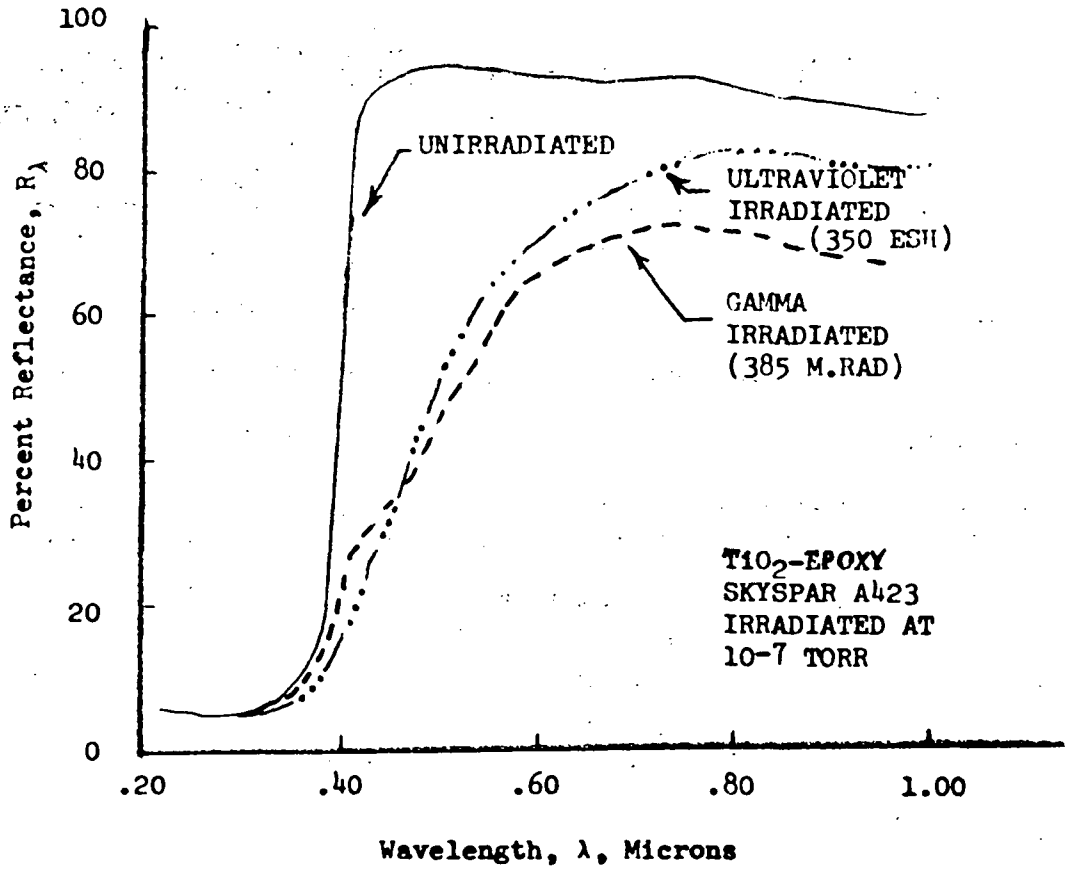

FIG 10

CURRENT AND FUTURE EXPERIMENTS

1. SYNTHESIS OF NEW AND MODEL POLYAROMATIC STRUCTURES.
2. STUDY POLYMERS IN THE SOLID STATE
   - A. X-RAY DIFFRACTION
   - B. ELECTRON SPIN RESONANCE
   - C. DIFFERENTIAL CALORIMETRY
3. COMPARE PHOTO AND RADIATION EFFECTS ON OPTICAL PROPERTIES.

FIG II

EFFECTS OF GAMMA RADIATION ON POLYESTERS

by

George D. Sands, Howard L. Price, and George F. Pezdirtz

NASA-Langley Research Center

INTRODUCTION

A study was conducted on the effects of gamma radiation on polyesters, represented by the commercial polymers Mylar, Dacron, Videne, and Kodar. The three objectives of the study are: To measure the effects experimentally, to deduce the mechanisms of the reactions involved, and to use this information to use polymers to the best advantage in space and to suggest new polymer structures with improved properties. (See Figure 1).

Mylar was studied most extensively, for the following reasons. (See Figure 2). Of the plastic materials available, Mylar ranks among the best in mechanical, electrical, and chemical properties. Its tensile strength is 23,000 pounds per square inch, about one-third the value of machine steel, and slightly greater than the tensile strength of aluminum. The polymer exhibits high radiation resistance, and it is available in a wide variety of thicknesses and widths. These properties led to its use in Echo I and Echo II, and in a number of other structural and electrical uses in space vehicles.

In addition to the "applied" reasons enumerated above, there is a fundamental reason for its choice. Mylar represents a "transition" polymer between polystyrene on the one hand and H-film on the other. Polystyrene is easy to put into solution and characterize; but its mechanical properties are poor. H-film has very good mechanical and radiation-resistant properties,

PAGE 126 INTENTIONALLY BLANK

but is so intractable that there are no known solvents.

Polystyrene is an addition polymer with a simple and well-known structure, while H-film is a more complex condensation polymer with a highly aromatic structure. Mylar is intermediate between the two, with respect to properties and structure. It can be characterized with difficulty, and the objective was to extrapolate the techniques and information developed for Mylar to speculate about the mechanisms of radiation effects for H-film.

EXPERIMENTAL

Table III lists the experimental conditions of irradiation. Sealed glass tubes containing pre-cut polymer strips one-half inch wide and six inches long were placed in a Gammacell-220 irradiation facility. The Gammacell contains 24,000 curies of cobalt-60, which gives an intensity in the irradiation chamber of 1.6 megarads per hour of 1.33 and 1.17 Mev gamma rays.

The samples were degassed for 72 hours at 50°C and 10^{-6} torr before sealing off in order to remove oxygen, water, and other volatile contaminants. This is a critical step because of the vast difference in behavior exhibited by a given material on being irradiated in air versus in vacuo. Teflon, for example, decreases in tensile strength from 100% to 0% after a dose of 16 megarads in air, while in vacuo it still remains 50% of its original tensile strength after 100 megarads.

The samples were annealed for 16 hours at 85°C after irradiation and then stored under argon at 3 pounds per square inch. This treatment was

an attempt to anneal out the free radicals formed during irradiation and minimized any post-irradiation effects which might mask those effects produced during the irradiation.

The properties measured are shown in Figure 4, under two headings, bulk and solution. Mechanical properties measured include ultimate tensile strength and elongation determined on a TT-C type Instron testing machine. The ultraviolet spectrum in the range 1800 A° was measured with a Cary 14 spectrophotometer. A Perkin-Elmer 421 Spectrophotometer was used to study the infrared spectrum in the range 2.5 to 18 microns.

Solution properties measured include solubility and intrinsic viscosity in orthochlorophenol. Light-scattering and fluorescence measurements were also made.

RESULTS AND DISCUSSION+

Influence of Molecular Structure

Figure 5 indicates three possible cross-linking modes and three possible scission modes in the degradation of Mylar. Evidence to be cited later indicates that scission modes 4 and 6 probably predominate.

To get an indication of the particular structural features of Mylar which give it its high radiation resistance, its radiation resistance and structure were compared with two other polyesters of known structural differences. The comparative structures of Mylar, Kodar, and Videne are shown in Figure 6. Both Mylar and Kodar are crystalline and biaxially oriented, while Videne is amorphous and unoriented. The six-membered ring in the shaded area in the Kodar molecule is saturated and hence does not afford radiation protection as do unsaturated or aromatic rings. As

indicated in the figure, the glycol portion of the chain is different in each polymer, being ethylene glycol in Mylar, p-cyclohexyl dimethylene glycol in Kodar, and neopentyl glycol in Videne.

The relative radiation resistance of the three polyesters is shown in Figure 7. Mylar is intermediate between Videne and Kodar in radiation resistance. To find that Mylar is more radiation resistant than Kodar is not surprising. In general, a benzene ring will offer protection to six carbon atoms in an attached side chain, and in Mylar, each ring has four aliphatic chain carbon atoms to protect, while in Kodar, each benzene ring must protect ten aliphatic chain carbon atoms.

Reasons for the higher radiation resistance of Videne that Mylar are not so apparent. Videne has a less favorable ratio of benzene rings to aliphatic carbon atoms (1/7) than does Mylar (1/4). The difference may lie in the fact that Videne is amorphous and unoriented, while Mylar is crystalline and biaxially oriented. Another commercial polyester, Scotchpak, will be studied, and polyesters with known structual features will be synthesized in order to learn more about how the benzene ring imparts radiation protection.

Figure 8 shows the change in several properties of Mylar with increasing radiation dose. It should be emphasized that the threshold dose for detectable damage in Mylar is about 10 megarads, or the dose received by Echo II in 10 days at its altitude of 600 to 800 statute miles, a sizeable dose; the dose range covered by the figure corresponds to a three year dose for Echo II. In the initial stages of irradiation, the curves depicting molecular weight, tensile strength, and elongation decrease with increased dose in the same general way. The mechanical properties of a polymer depend

upon the combined effects of the mechanical and Van der Waals interactions among the individual high molecular weight chains. As gamma radiation cleaves some of these chains, the molecular weight decreases, and this is reflected in the observed tensile strength and elongation values.

Influence of Temperature

All irradiated samples have shown complete solubility; i.e., no gel has been observed. Thus, all the evidence accumulated to now suggests that simple cleavage of the polymer chains occurs.

Hellwege (reference 1) and Sobue (references 2 and 3) have observed gelation in Mylar which has received 300 to 1200 megarads of 1 Mev electrons. Damage to polymers from ionizing radiation is generally considered to be dependent only on the total dose absorbed and not on the type of radiation. Since our samples exhibited no gel even at 5000 Megarads, it was concluded that the fact that Hellwege and Sobue used such high irradiation rates that local heating may have occurred and caused gel.

To investigate this point, the Gammacell-220 was fitted with an oven to permit irradiation at elevated temperatures, and samples of Mylar were irradiated at doses up to 1500 megarads. Even at 100°C, about 15°C above the glass transition temperature, no gel was observed. A comparison of the change in viscosity with dose is shown in Figure 9. The curves depicting

---

[1] V.K-H. Hellwege, U. Johnsen, W. Seufert, "Vernetzing and Abbau von Polyathylenterephthalate durch Electronenbestrahlung", Kolloid-Feitschrift and Feitschrift Lur Polymere, 188, No. 1, 11, (March 1963).

[2] H. Sobue and A. Kajira, "Effects of Electron-Beam Irradiation of Polyethylene Terephthalate", Kogyo Kagaku Zasshi, 62, 1171 (1959) (Translated in NASA TT F-8449.)

[3] H. Sobue, Y. Tabata, M. Hiraoka, "Effects of Ionizing Radiation on Polyethylene Terephthalate", Kogyo Kagaku Zasshi, 64, 372 (1961) (Translated in NASA TT F-8450).

behavior at the normal chamber temperature of 47°C and at 100°C follow the same general form; the 100°C curve indicates that degradation occurs at a slightly higher rate at this temperature than at 47°C, as might be expected.

CURRENT AND FUTURE WORK

Figure 10 lists some of the current and future experiments designed to provide more information about the fundamental processes which occur as Mylar undergoes radiation damage, including the specific way in which the benzene ring provides protection against radiation. Having investigated most of the polyesters which are commercially available, synthesis of polymers containing known structural elements is being conducted. The radiation resistance of these polymers will be determined and will be correlated with the structural elements present.

A number of structural features will be varied, including the location of the benzene ring in a side chain, as part of the acid residue, or as part of the glycol residue. The effect of electron deficiency or electron excess in the benzene ring of the acid residue is being determined (see Figure 11). This is being done by introducing chlorine atoms in place of hydrogen in the ring to withdraw electrons from the aromatic ring and determining what effect this change has on the radiation stability of the polyester. Other changes which are being made to study the effect of the electron-poor condition and the electron-rich condition on radiation resistance of polyesters are indicated in Figure 11.

Other structural variations which are being studied include variation of the size of the acid group, alteration of the size of the glycol group, and varying the degree of crystallinity.

To gain the maximum amount of information from these polymers which have been synthesized, additional property measurements are being made. They include small angle x-ray diffraction measurements to indicate degree of crystallinity and other morphological features. Electron spin resonance values will be measured to indicate the concentration and kind of free radicals present. Differential scan calorimetry will indicate what phase transformations take place in the polymer as a function of temperature, and analysis of the gases evolved during irradiation will indicate at what point in the chain rupture is taking place.

At the conclusion of the study there will be a better understanding of the mechanism by which the benzene ring protects a polymer against radiation, and it will be possible to specify which structural elements should be included in a polymer to give the maximum radiation resistance.

EFFECTS OF GAMMA RADIATION ON POLYESTERS

PURPOSE OF STUDY

1. MEASURE EFFECTS.
2. DEDUCE MECHANISMS.
3. POINT WAY TO NEW MATERIALS.

FIGURE 1

REASONS FOR CHOOSING MYLAR

1. APPLIED

   a. GOOD MECHANICAL, ELECTRICAL, AND CHEMICAL PROPERTIES.

   b. GOOD RADIATION RESISTANCE.

   c. COMMERCIAL AVAILABILITY.

2. FUNDAMENTAL

   MYLAR IS A GOOD EXAMPLE OF A TRANSITION POLYMER, BOTH IN STRUCTURE AND PROPERTIES.

FIGURE 2

IRRADIATION CONDITIONS

1. GAMMACELL-220 ^{60}Co
   1.33, 1.17 MEV
   24,000 CURIES; 1.6 MRAD/HR.

2. 0 TO 5,000 MEGARADS.

3. DEGASSED 72 HRS. AT 50°C & 10^{-6} TORR.

4. ANNEALED 16 HRS. AT 85°C.

5. STORED UNDER ARGON AFTER IRRADIATION.

FIGURE 3

PROPERTIES MEASURED

BULK	SOLUTION
1. TENSILE STRENGTH	1. SOLUBILITY
2. ELONGATION	2. INTRINSIC VISCOSITY
3. UV SPECTRA, 1800 TO 3600 Å, CARY 14	3. (LIGHT SCATTERING).
4. IR SPECTRA, 2.5 TO 18 μ, PE 421	4. (FLUORESCENCE).

FIGURE 4

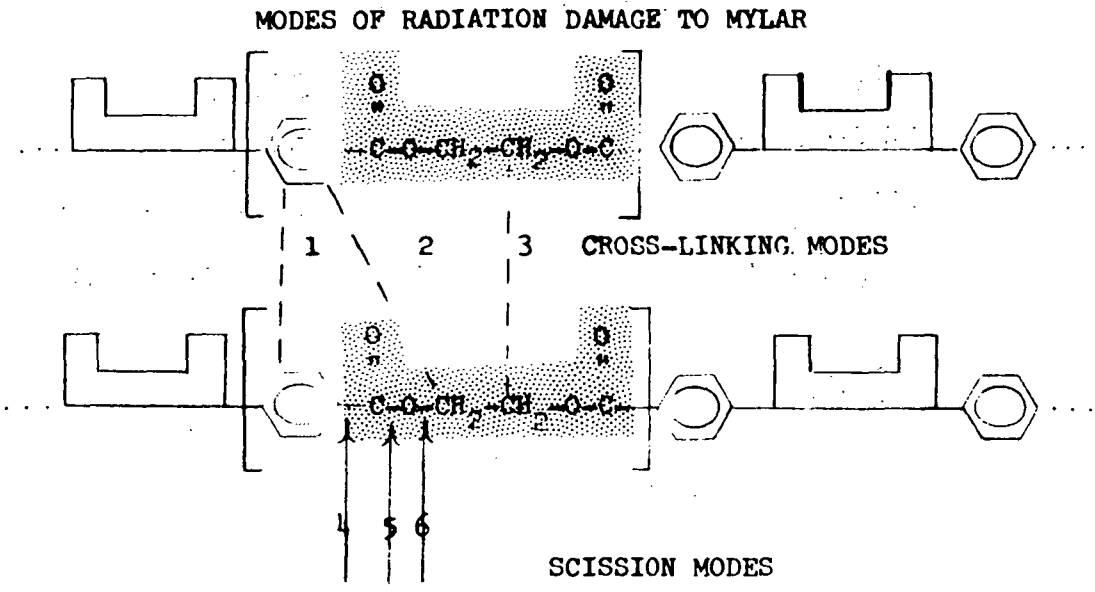
MODES OF RADIATION DAMAGE TO MYLAR
1
2
3
CROSS-LINKING MODES
4
5
6
SCISSION MODES

FIGURE 5

COMPARATIVE STRUCTURES OF MYLAR, KODAR, AND VIDENE

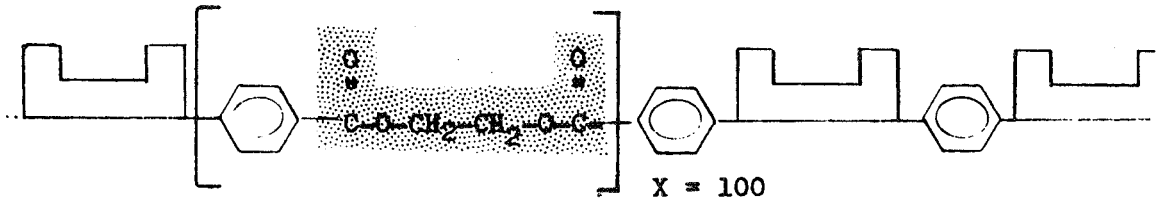

MYLAR (CRYSTALLINE, BIAXIALLY ORIENTED)

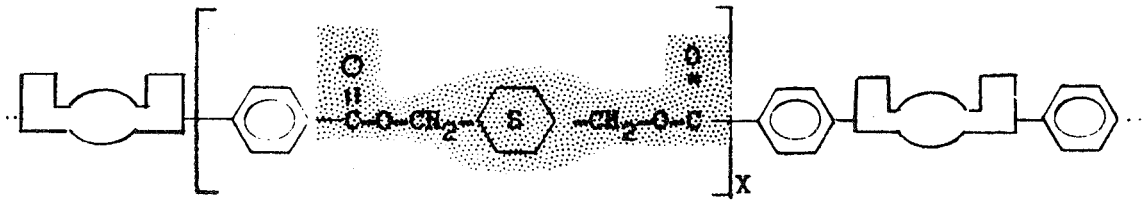

KODAR (CRYSTALLINE, BIAXIALLY ORIENTED)

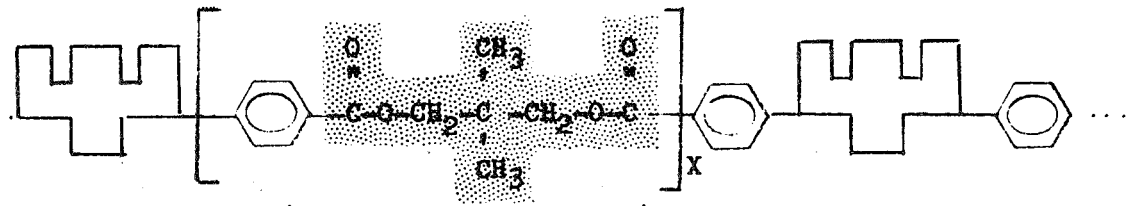

VIDENE (AMORPHOUS, UNORIENTED)

FIGURE 6

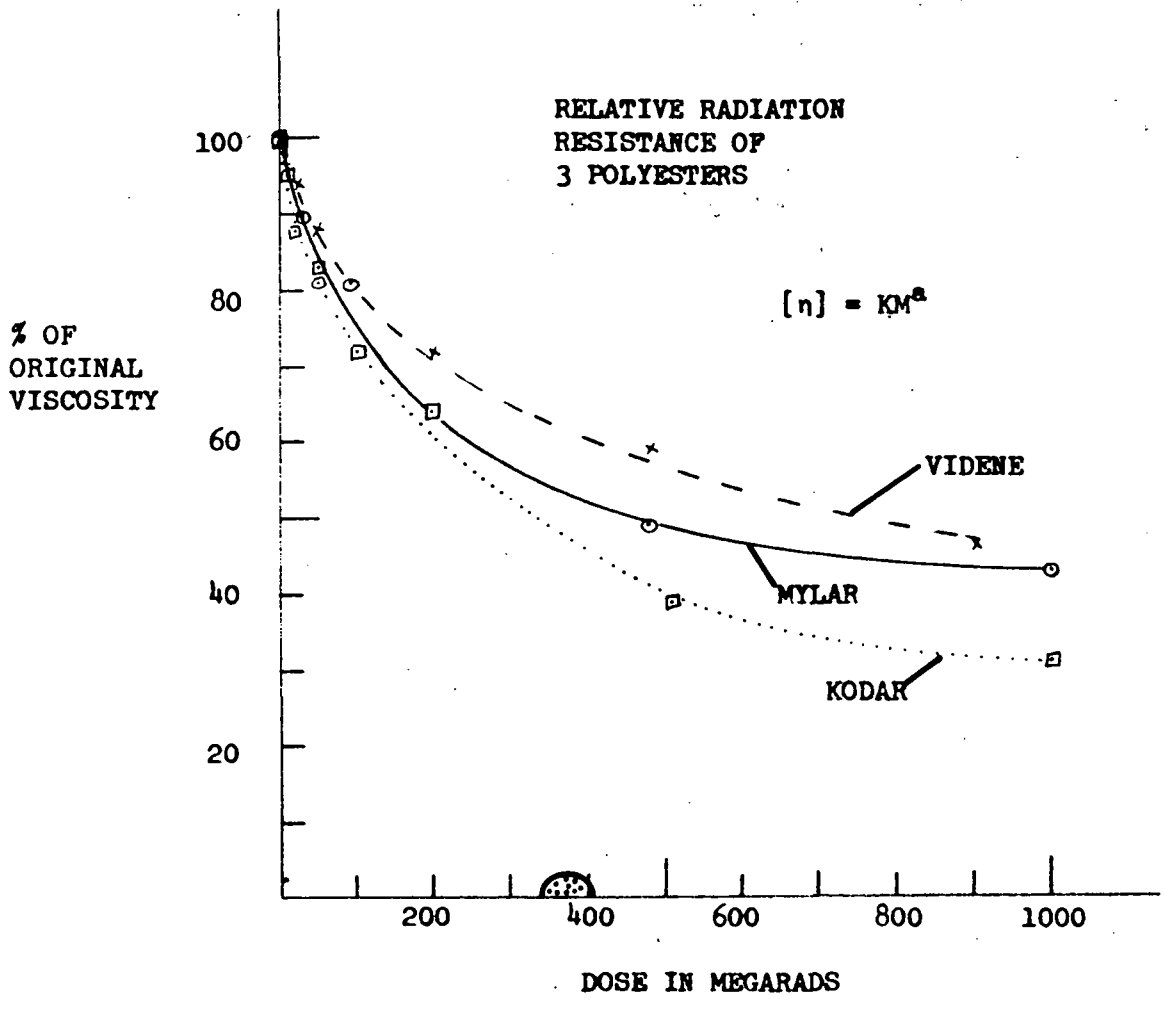
RELATIVE RADIATION
RESISTANCE OF
3 POLYESTERS
[n] = KM^a
% OF
ORIGINAL
VISCOSITY
100
80
60
40
20
VIDENE
MYLAR
KODAR
200
400
600
800
1000
DOSE IN MEGARADS

FIGURE 7

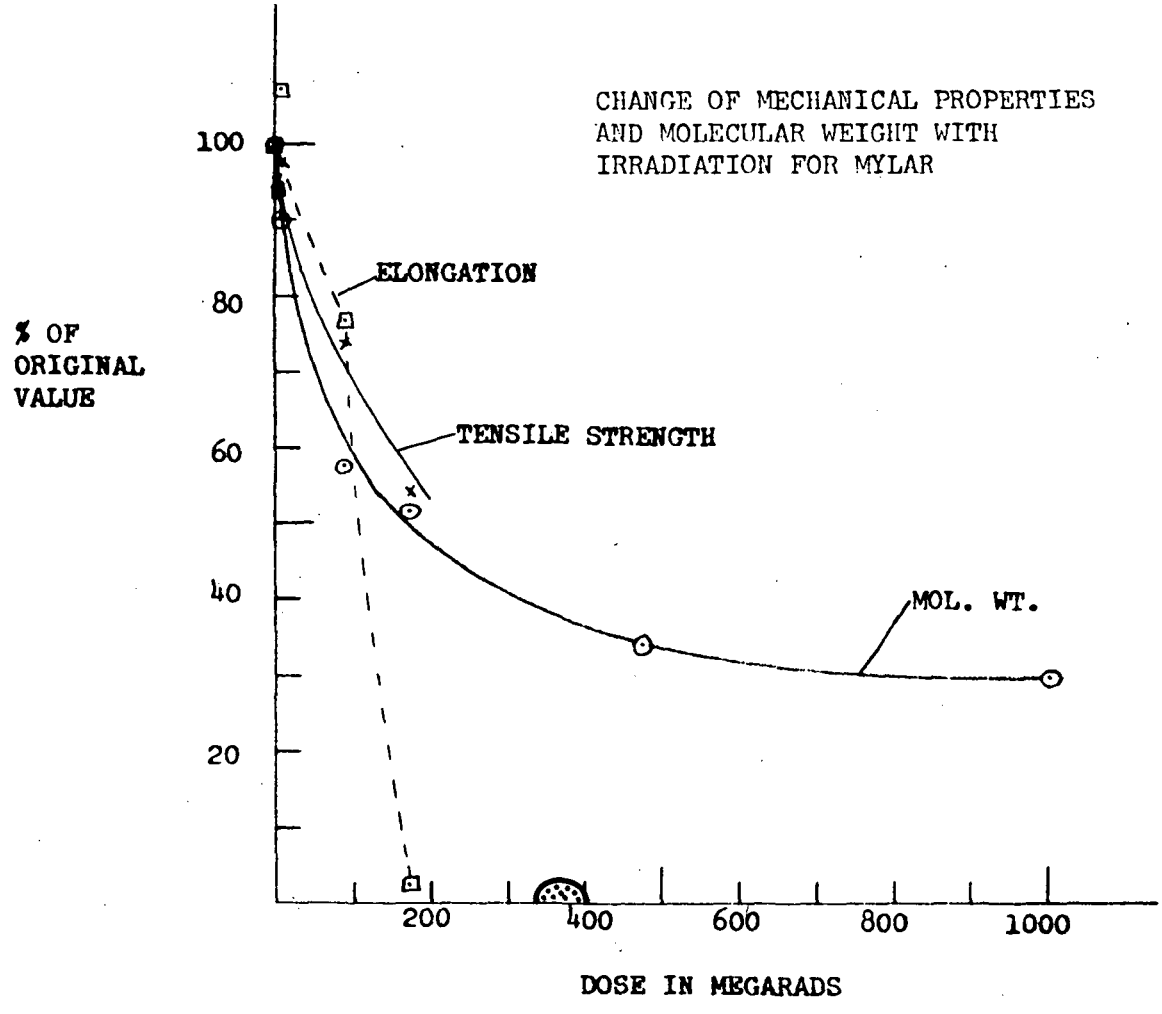
CHANGE OF MECHANICAL PROPERTIES
AND MOLECULAR WEIGHT WITH
IRRADIATION FOR MYLAR
% OF
ORIGINAL
VALUE
100
80
60
40
20
ELONGATION
TENSILE STRENGTH
MOL. WT.
200
400
600
800
1000
DOSE IN MEGARADS

FIGURE 8

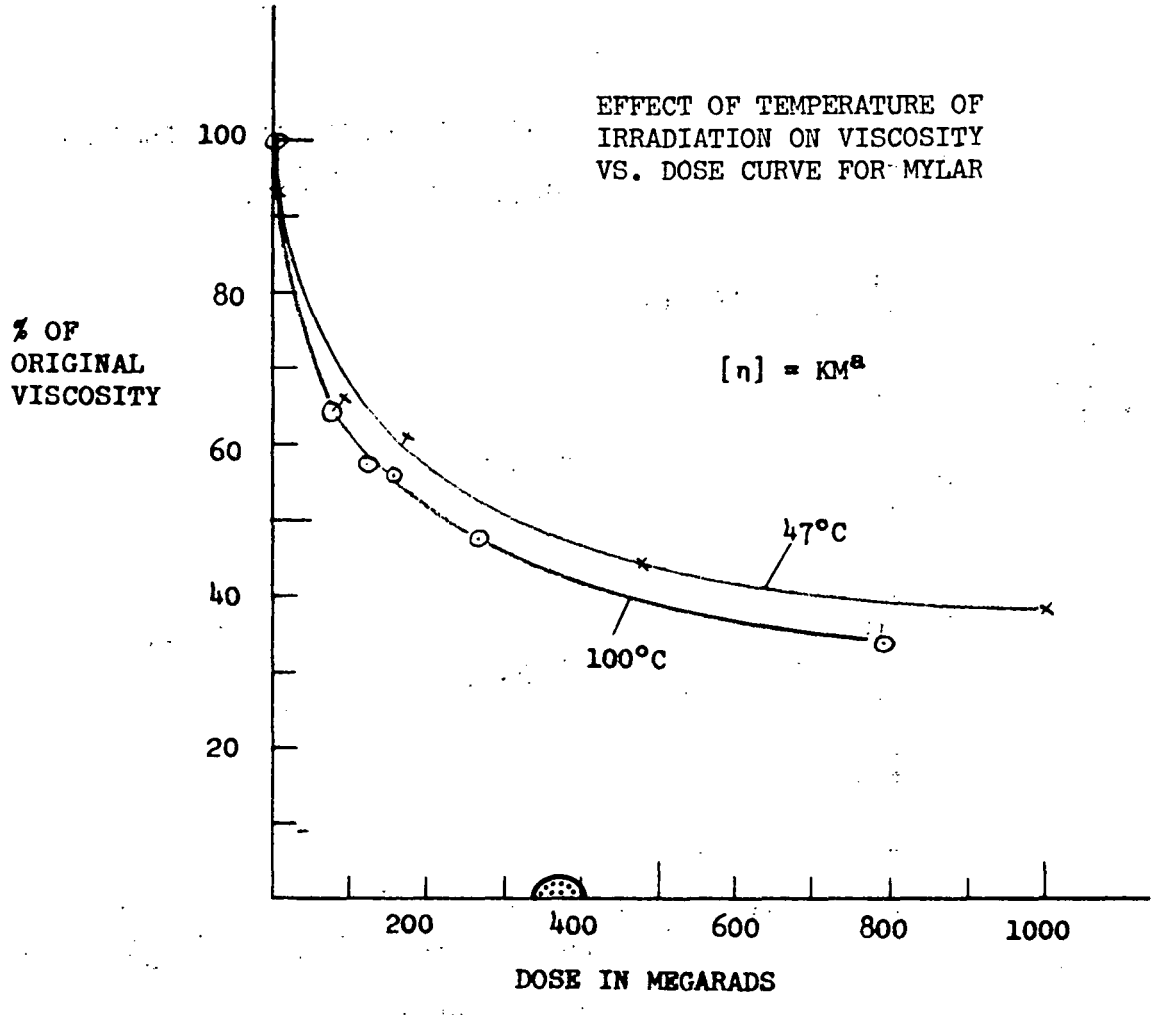
EFFECT OF TEMPERATURE OF
IRRADIATION ON VISCOSITY
VS. DOSE CURVE FOR MYLAR
% OF
ORIGINAL
VISCOSITY
100
80
60
40
20
[η] = KM^a
47°C
100°C
200
400
600
800
1000
DOSE IN MEGARADS

FIGURE 9

CURRENT AND FUTURE EXPERIMENTS

1. ADDITIONAL PROPERTY MEASUREMENTS.
    a. SMALL ANGLE X-RAY DIFFRACTION.
    b. ELECTRON SPIN RESONANCE.
    c. DIFFERENTIAL SCAN CALORIMETRY.
    d. GAS ANALYSIS.
2. SYNTHESIS OF POLYMERS OF KNOWN STRUCTURE.
    a. LOCATION OF AROMATICITY.
    b. ELECTRON-RICH VS. ELECTRON-POOR AROMATIC RING.
    c. VARY SIZE OF ACID GROUP AND OF GLYCOL GROUP.
    d. VARY DEGREE OF CRYSTALLINITY.

FIGURE 10

VARIATION IN ELECTRON DENSITY IN AROMATIC RING

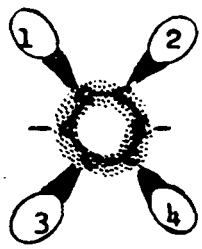

ELECTRON POOR

1	2	3	4
H	Cl	H	Cl
Cl	Cl	Cl	Cl
CN	H	CN	H
CN	CN	CN	CN

NORMAL

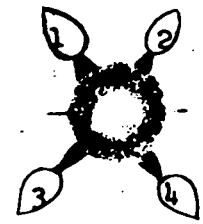

ELECTRON RICH

1	2	3	4
CH_3	H	CH_3	H
OCH_3	H	OCH_3	H

FIGURE 11

THE EFFECTS OF ELECTRON RADIATION ON THE OPTICAL TRANSMISSION OF SEVERAL TRANSPARENT MATERIALS

BY

Gilbert A. Haynes
NASA Langley Research Center

INTRODUCTION

The particulate radiation of the earth radiation belts poses a serious problem to many components of earth orbiting satellites. Components such as solar cells, transparent materials used in optical instruments, and spacecraft windows are especially sensitive to radiation. A study was undertaken by the Langley Research Center to provide data on electron radiation effects on commercially available transparent materials for the aforementioned uses. Tests were made on the optical transmission of samples of each material before and after irradiation. The spectral range of these tests was 0.25 microns (μ) to 2.7 μ. Wide-band tests were made over the silicon solar cell response band (0.4 μ to 1.2 μ). Irradiation was done employing 1.2 Mev electrons, and also 0.25 and 2.4 Mev electrons. Materials tested include synthetic sapphire, synthetic fused silica and several other silica glasses.

APPARATUS AND TEST PROCEDURE

The particle accelerators used were 1 and 3 Mev dynamitrons located at the Langley and Lewis Research Centers respectively. Pre- and post-irradiation tests on the optical transmission were made using a Beckman DK-1 spectrophotometer and a wide-band transmission monitor consisting of a silicon solar cell, a tungsten lamp and a readout instrument. The resolution of the spectrophotometer was about 10 Å maximum and repeatibility was within 2 percent. Wide-band tests were repeatable within 0.5 percent.

Fluorescence tests were made by exposing the samples to ultraviolet light and visibly noting flourescence. The visible appearance of the samples was also noted before and after irradiation.

Tests were made to check the bleaching of the discolored materials by heat and ultraviolet light. Temperatures up to 600°F were employed in the heat tests, and a B-H6 high intensity mercury lamp was employed in the ultraviolet tests.

RESULTS AND DISCUSSION

The materials tests were chosen primarily for their transmission characteristics in the ultraviolet, visible and near

infrared regions. Thicknesses of the samples varied considerably. Consequently, some results cannot be compared directly. The range of 1.2 Mev electrons in SiO_2 is 0.480 g/cm^2 (corresponds to 0.086 inches in thickness). As a result samples of thickness greater than 0.086 inches will absorb practically all of the incident electrons while samples of lesser thickness will only absorb a portion. Thus, the full effect of the electrons of a given dose may not develop. For this reason direct comparison is limited to samples with sufficient thickness to absorb the majority of the irradiating electrons.

Results are presented for a sample of most materials tested.

1.2 MEV ELECTRON IRRADIATION TESTS

A large cross-section of the commercially available transparent materials were tested at this energy. These materials represented a large number of manufacturers. A general description of a sample of each material and results of wide-band transmission tests on each is given in Slide 1. As indicated in the table the materials were sapphire, synthetic fused silica, fused quartz, radiation shielding glass, microsheet, solex and pyrex. All samples in this table were irradiated with 2.7×10^{15} e/cm^2 except the starred sample - 1.0×10^{17} e/cm^2. Most of these samples exceed the range of electrons in the material.

The sapphire sample listed is synthetic annealed crystalline sapphire and has a purity of 99.99+ percent. Synthetic fused silica is a material manufactured by a vapor deposition method where $SiCl_4$ is oxidized at high temperatures. Materials produced by this method may contain as little as 0.2 ppm impurities. Fused quartz is manufactured by fusing natural quartz crystals at high temperatures. By this method purities of 99.8 percent have been obtained in commercially available quartz. Corning #8362 is a cerium doped lead glass, and Corning #8365 is a cerium doped lime glass. Cerium tends to inhibit radiation darkening of glass and also enhance recovery. Corning #0211 or Micro-Sheet is a fire-polished drawn glass available in thickness from 0.006 to 0.026 inches. Solex is a glass with a large iron content. Furrex is a Pyrex glass. In materials other than sapphire and quartz the silica content is betwen 50 and 85 percent approximately.

The wide-band transmission results indicate that the listed dose causes no measurable damage over the solar cell response region in sapphire or synthetic fused silica. A heavy dose

will cause less than 2 percent damage in synthetic fused silica (starred sample). Only two samples of the several kinds of fused quartz are represented. These are a slightly damaged sample and a heavily damaged sample. Other types tested that lost less than 7% in wide-band transmission were Amersil infrasil, GE 105, and GE 106. GE 104 lost less than 1 percent in transmission at the listed dose.

Three types of radiation shielding glass were tested. The samples of Corning #8363 and #8365 did not change in transmission in the solar cell response band. However the sample of Corning #8362 developed electron discharge patterns or Litchenberg Figures after a dose of about 7.4×10^{14} e/cm^2. Such imperfections cause attenuation of light being transmitted by the sample, thus, a loss in transmission is seen. The densities of these materials are relatively high so the penetration depth of electrons in them is less than in quartz.

The sample of Corning #0211 listed was 0.026 inches thick. By virtue of its thinness the majority of the incident electrons electrons were transmitted. There were samples of this material irradiated that were only 0.006 inches thick. These samples lost only about 2 percent in wide-band transmission. The solex tested exhibited good radiation resistance. However, Furrex, suffered substantial loss in wide-band transmission.

Slides 2 through 5 show the spectral transmission of some of the materials before and after irradiation. Slide 2 represents sapphire. At a dose of 2.7×10^{15} e/cm^2 no change occured in the transmission. However, after a dose of 1.0×10^{17} e/cm^2 a very small decrease in ultraviolet transmission occurs. Sapphire also developed a slight discoloration (color indeterminate). There was no pre- or post-irradiation fluorescence.

Slide 3 represents synthetic fused silica before irradiation and after several doses. Notice that at a dose of 1.0×10^{15} e/cm^2 the transmission degradation is primarily in the ultraviolet. But as the dose increases the degradation extends into the visible. Associated with the spectral transmission degradation is a slight bluish visible discoloration. The depth of this discoloration in the material appears to approximate the penetration depth of 1.2 Mev electrons in SiO_2. Other tests indicate that synthetic fused silica fluoresces (red) after irradiation, but does not fluoresce before irradiation.

Slide 4 represents a lightly damaged sample of fused quartz. There is degradation of transmission in the UV, and visible regions

with some degradation in the infrared. Notice that an absorption maximum appears to be centered at 0.55 . Damage to other types of fused quartz differed in degree only from that shown in the figure. The absorption maximum and the spectral range of the damage were characteristically the same. Associated with this absorption maximum in the visible is a discoloration, that is proportional to the degree of absorption. It varies from a faint brownish color for the lightly damaged samples to a deep purple for the heavily damaged samples. This material fluoresces (red) before and after irradiation.

Slide 5 represents Corning #8363 high density lead glass. A dose of 2.7×10^{15} e/cm^2 causes very little damage in the region of the spectral cut-off for the sample. The transmission decrease in the solar cell response region is minute thus explaining negligible wide-band transmission loss for this sample. Even less damage occurred in Corning #8365. The Corning #8362 sample showed a substantial decrease in spectral transmission. However, this decrease was not due to discoloration, but to electron discharge patterns as discussed earlier. No recovery tests were made in conjunction with this study. Corning #8362 and 8365 fluoresced (yellow) before and after irradiation.

Most of the damage to Corning #0211 occurs in the visible region. This material has a spectral-cut-off in the ultra-violet. It also had a brownish visible appearance after irradiation. It fluoresced (yellow) before and after irradiation.

Slide 6 shows damage versus flux curves for several materials. These curves show that damage to materials is non-linear, and the damage occurs at relatively low fluxes as pointed out by curves c and d.

It is believed that the impurities in the materials are the main cause of discoloration or absorption in the visible. Damage to UV transmission is thought to be caused by defects in the atomic structure of the material. These theories are borne out in the quartz tests. The very pure synthetic fused silica degraded relatively little while the less pure fused quartz degraded substantially. There are exceptions in the cases of the radiation shielding glasses, and solex which have high impurity contents.

COMPARISONS AT SEVERAL ENERGIES

Shown in Slide 7 is a tabulation of the effects of 2.4, 1.2, and 0.25 Mev electrons on the wide-band transmission of 4 materials. Not all materials were irradiated at all energies. However, from data in the table the damage to the optical transmission of the

materials appears to be more energy dependent, than flux dependent. Notice that for sapphire the extremely large dose of 1.0×10^{17} at 1.2 Mev causes no wide-band transmission damage while at one tenth the dose with 2.4 Mev electrons the transmission degrades. There is a similar occurence for all of the samples listed.

BLEACHING TESTS

Some bleaching tests were made on samples of synthetic fused silica and fused quartz. Slide 8 illustrates the effect of heat on a radiation damaged sample of fused quartz. This sample was heated at temperatures up to 600°F approximately for 32 hours. Recovery was almost complete. A sample of synthetic fused silica (damaged in UV transmission) was heated for approximately 8 hours at 600°F and recovery was complete. When exposed to a mercury lamp for approximately 91 hours recovery of fused quartz was almost complete. When exposed to the B-H6 lamp for approximately 40 hours recovery of synthetic fused silica was approximately 50 percent complete.

CONCLUSIONS

1. For practical doses sapphire is very radiation resistant in transmission. It is an optical quality material that has been used as a solar cell cover, and may be used in optical instruments and spacecraft windows to the extent that cost is not prohibitive.

2. Damage occurs primarily to the ultraviolet transmission of synthetic fused silica. It is excellent for use as solar cell covers, but it must be used with caution for applications involving ultraviolet transmission.

3. Some types of fused quartz are quite radiation resistant in the visible and near IR. These types may be considered for use in these regions.

4. Micro-Sheet Corning #0211 is radiation resistant somewhat by virtue of its thinness.

5. High density lead glass and non-browning lime glass showed good radiation resistance as did solex.

6. Impurities appear to affect radiation resistance.

7. Ultraviolet light and heat have a bleaching effect on darkened silica materials.

GAHaynes:cdl
(4/8/64)

TABLE I EFFECT OF 1.2 MEV ELECTRONS ON SEVERAL MATERIALS. DOSE 2.7×10^{15} e/cm^2

MANUFACTURER	TRADE NAME	TYPE	WIDE-BAND TRANSMISSION LOSS (%)
LINDE COMPANY	SAPPHIRE	ANNEALED SAPPHIRE	0
CORNING GLASS WORKS	CORNING #7940	SYNTHETIC FUSED SILICA	0
*DYNASIL CORP.	DYNASIL OPTICAL GR.	SYNTHETIC FUSED SILICA	1.5
AMERSIL QUARTZ DIVISION, ENGELHARD	AMERSIL OPTICAL GR.	FUSED QUARTZ	1.8
AMERSIL QUARTZ DIVISION, ENGELHARD	—	FUSED QUARTZ	41.6
CORNING GLASS WORKS	CORNING # 8362	NONBROWNING LEAD GLASS	2.4
CORNING GLASS WORKS	CORNING # 8363	HIGH DENSITY LEAD GLASS	0
CORNING GLASS WORKS	CORNING # 8365	NONBROWNING LIME GLASS	0
CORNING GLASS WORKS	CORNING # 0211	DRAWN GLASS	7.6
—	SOLEX	HEAT ABSORBENT GLASS	2.7
BLUE RIDGE GLASS CORP.	FURREX	PYREX	25.2

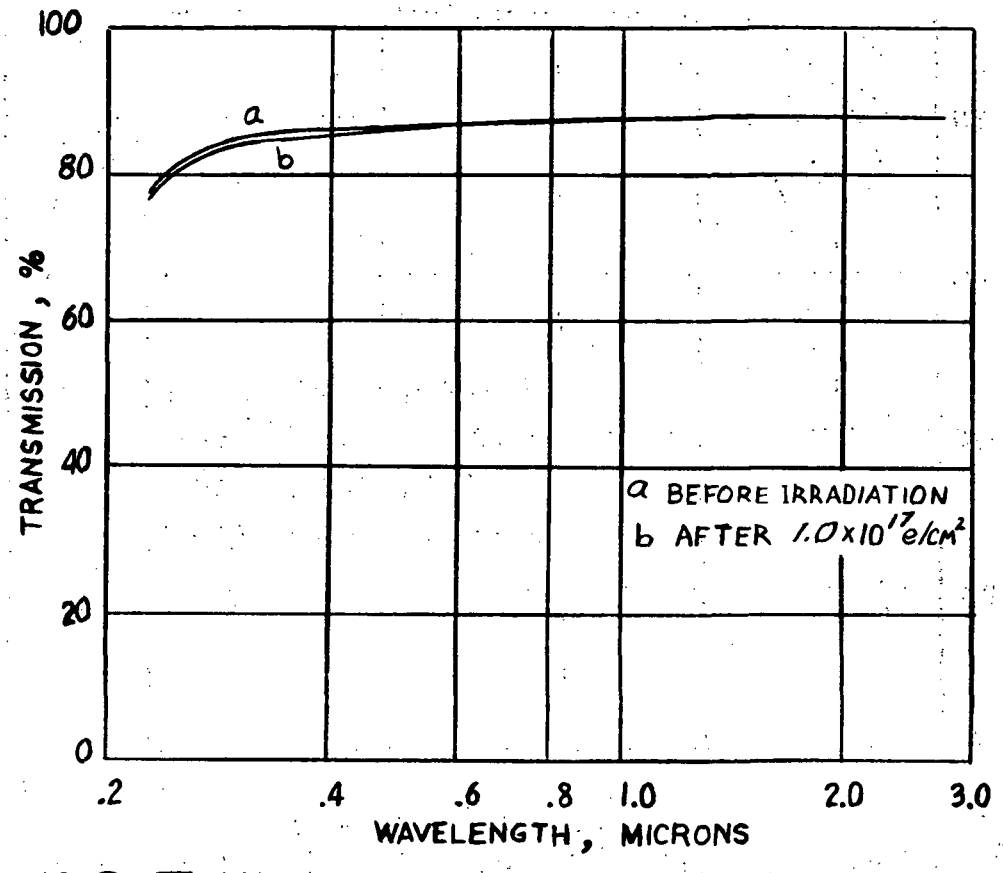

FIG. 2 TRANSMISSION OF ANNEALED SAPPHIRE BEFORE AND AFTER IRRADIATION WITH 1.2 MEV ELECTRONS

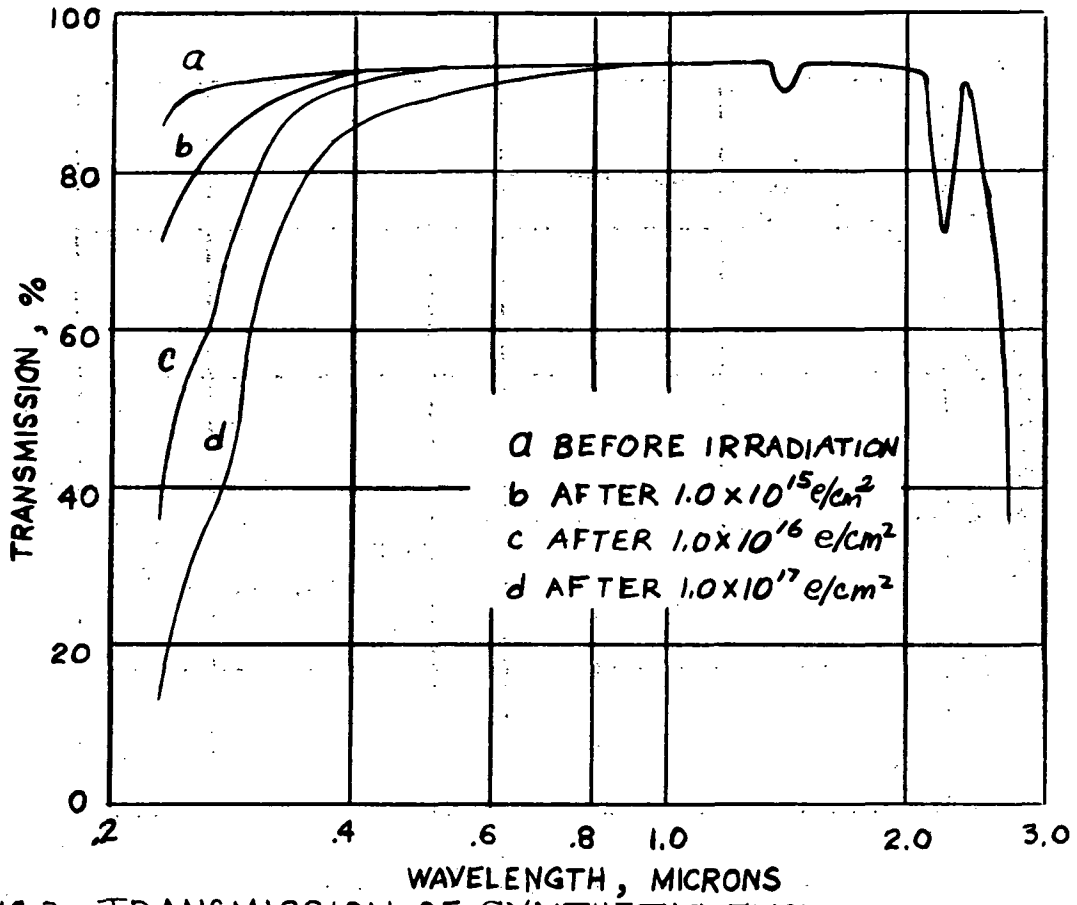

FIG.3 TRANSMISSION OF SYNTHETIC FUSED SILICA BEFORE AND AFTER IRRADIATION

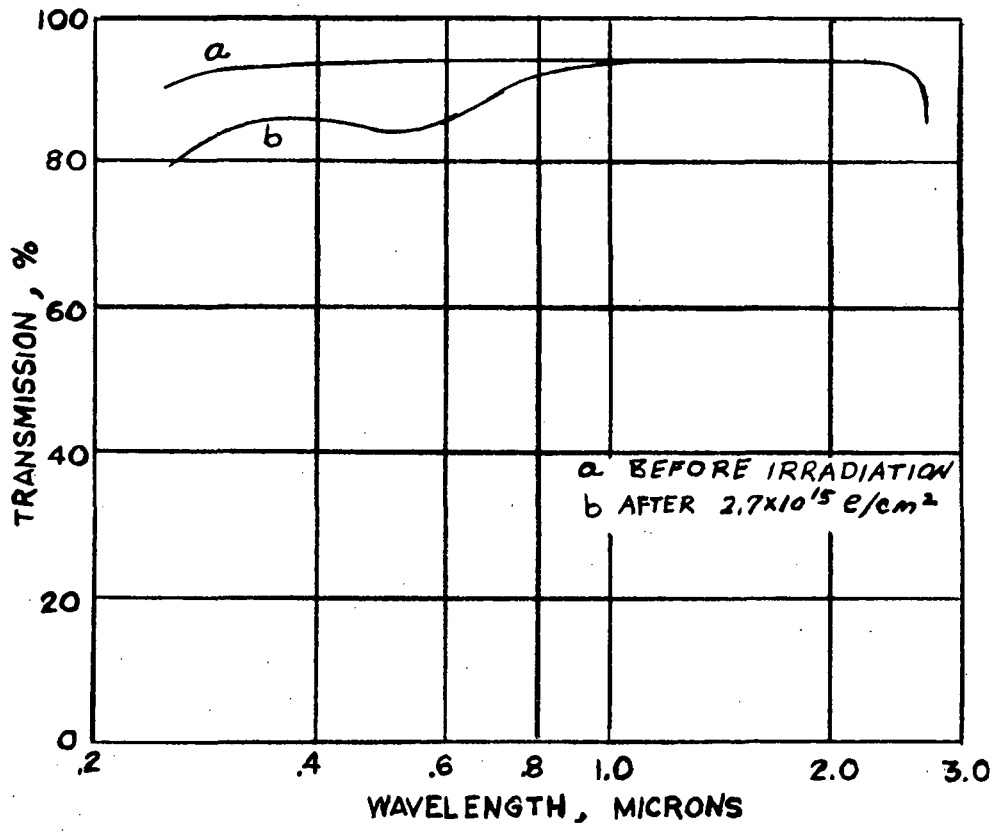

FIGURE 4 TRANSMISSION OF FUSED QUARTZ BEFORE AND AFTER IRRADIATION WITH 1.2 MEV ELECTRONS

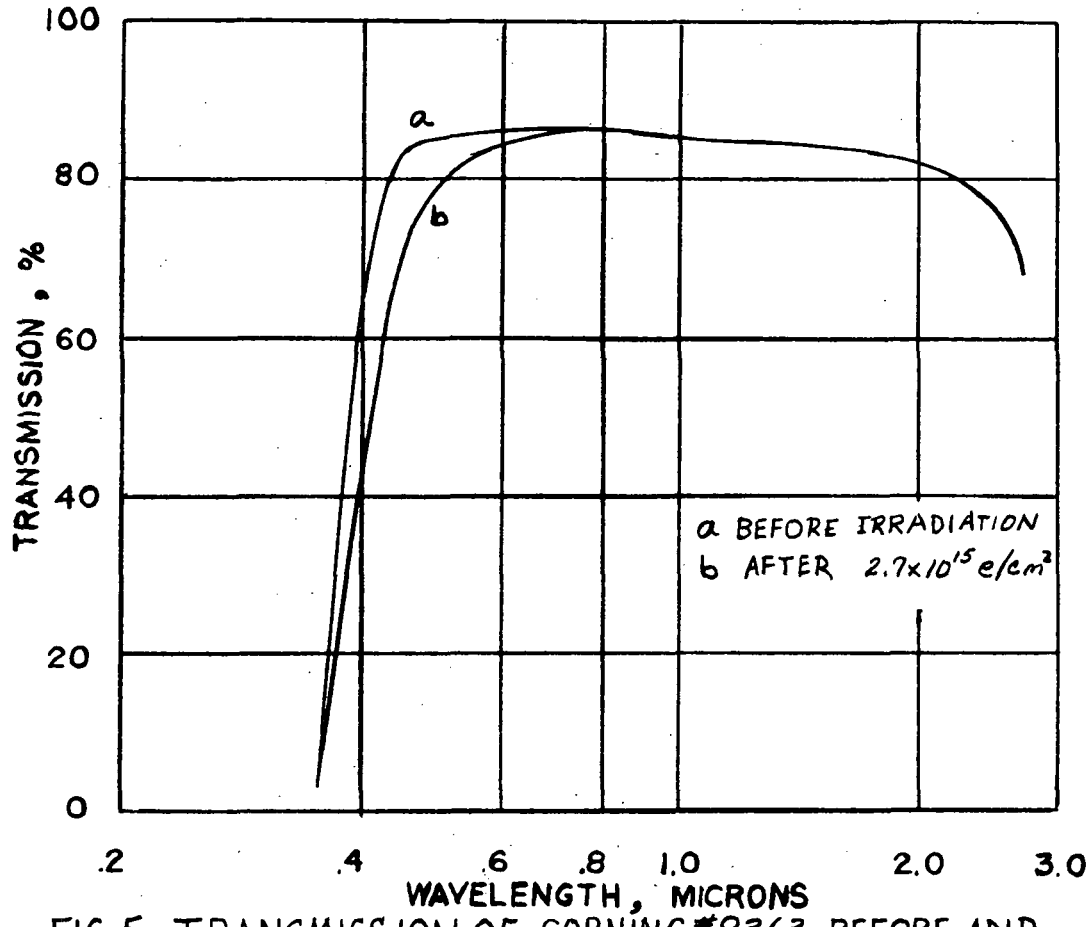

FIG. 5 TRANSMISSION OF CORNING #8363 BEFORE AND AFTER IRRADIATION WITH 1.2MEV ELECTRONS

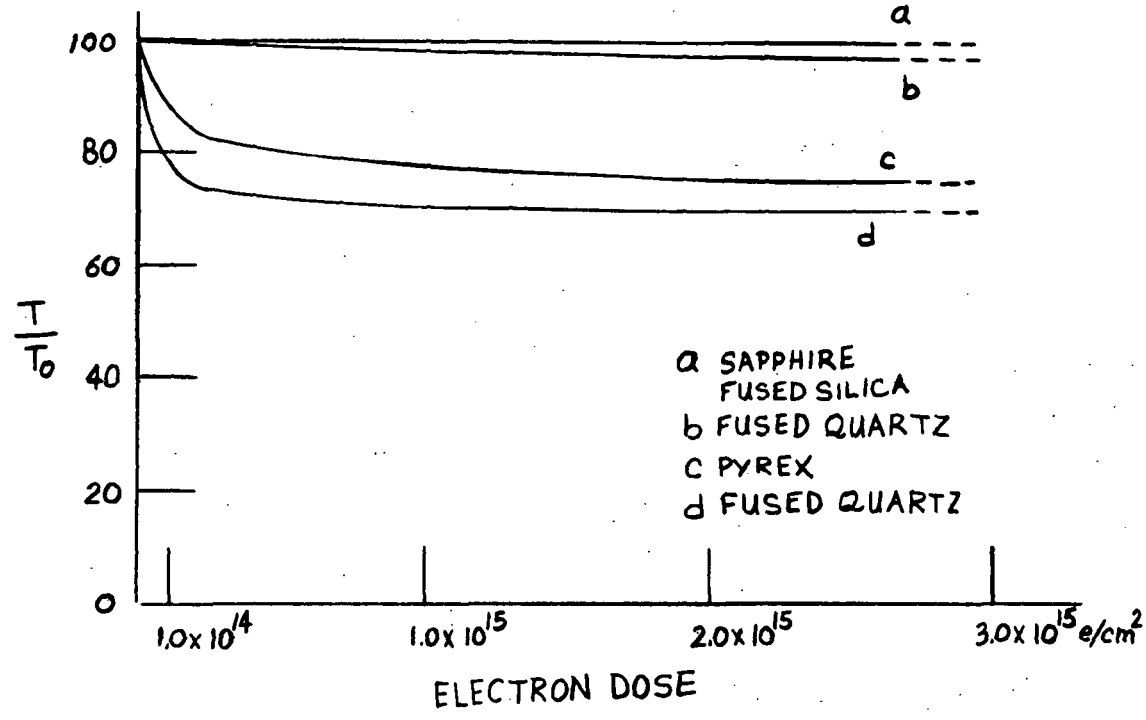

FIG.6 DAMAGE VS. FLUX CURVES FOR 1.2 MEV ELECTRON IRRADIATED MATERIALS

TABLE II COMPARISON OF SEVERAL MATERIALS IRRADIATED WITH ELECTRONS OF SEVERAL ENERGIES

TRADE NAME	THICKNESS (INCHES)	ENERGY (MEV)	ELECTRON FLUX (e/cm²)	WIDE-BAND TRANSMISSION LOSS (%)
ANNEALED SAPPHIRE	0.120	2.4	1.0×10^{16}	0.9
	0.080	1.2	1.0×10^{17}	0
	0.040	0.25	2.7×10^{15}	0
SYNTHETIC FUSED SILICA	0.250	2.4	1.0×10^{16}	3.9
	0.125	1.2	1.0×10^{17}	1.5
	0.125	0.25	2.7×10^{15}	0
FUSED QUARTZ	0.0935	1.2	2.7×10^{15}	30.0
	0.0935	0.25	2.7×10^{15}	5.3
CORNING #0211	0.026	1.2	2.7×10^{15}	7.6
	0.026	0.25	2.7×10^{15}	3.2

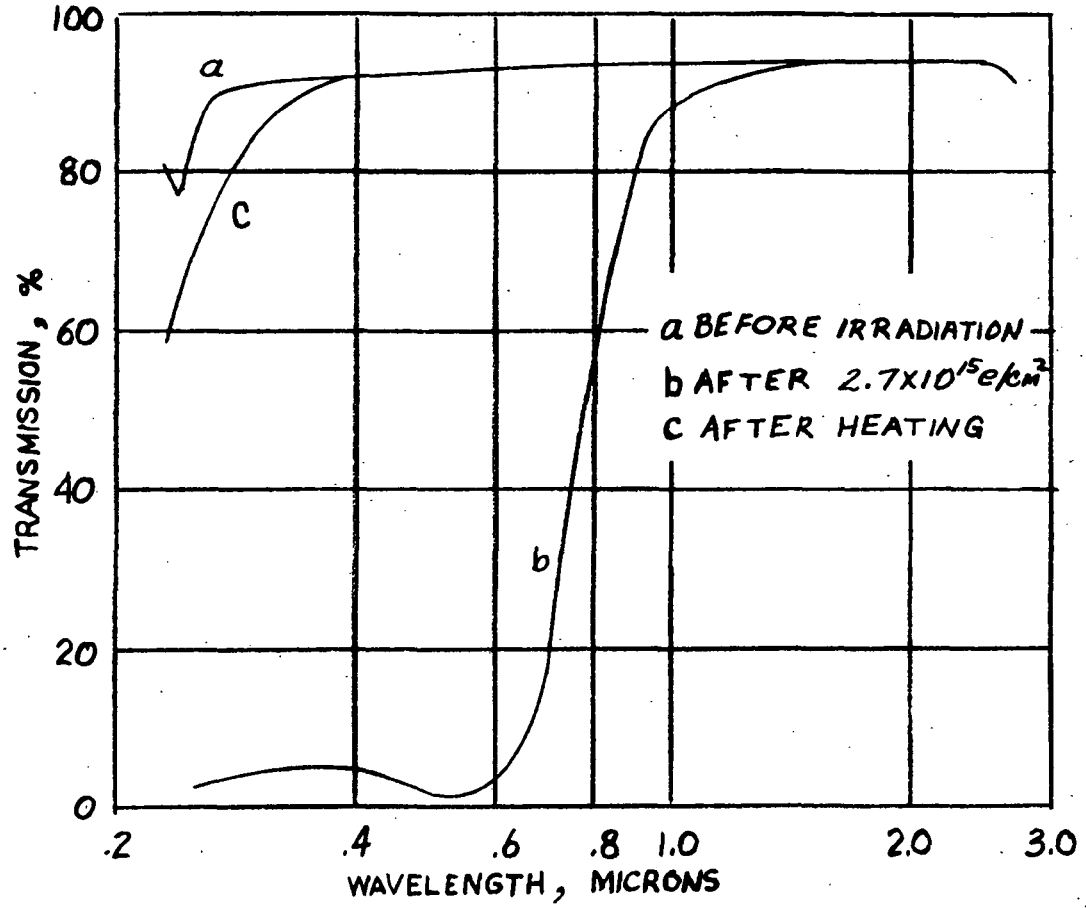

FIG. 8 BLEACHING EFFECTS OF HEAT ON IRRADIATED FUSED QUARTZ

REVIEW OF LANGLEY'S SOLAR CELL DEGRADATION EFFORT

J. L. Patterson and W. E. Ellis
NASA Langley Research Center

The solar cell irradiation work at Langley has primarily been directed toward obtaining the data needed to complement that available from other sources, for support of Langley projects. For this reason, emphasis has been on obtaining complete data for a few types of cells, for power supply lifetime predictions, rather than on comparing certain damage criteria for many types of cells. In addition, we have a test solar cell experiment on the S-55 series of satellites, and we are attempting to correlate the degradation rates in space with those in ground facilities. More recently, we are trying to obtain cell irradiation data of a more general interest.

The first figure lists some of the problem areas involved. Ideally, the accuracy of a solar cell lifetime prediction should be limited primarily by the accuracy to which the space environment has been determined - within a factor of about 3. Actually there are a number of possibly large sources of error connected with solar cell shielding and with ground irradiation parameters and techniques.

One problem associated with the space environment has been and still is obtaining up-to-date data, especially on the changes in the artificial electron belt. Also, in using flux densities computed for a satellite, care must be exercised to arrive at a properly averaged daily dose. (In addition to the problems of averaging the temporal variations of the belts.) Satellites with fairly low elliptical orbits can receive most of their radiation near apogee, particularly when apogee passes through the South Atlantic anomaly. For Explorer XVI, the integrated flux, per orbit, varied as much as four orders of magnitude each day. This either requires integration over a large number of orbits, or making time plots and averaging over one or more daily cycles. The slow progression of the apogee can also have a large effect. The dose rates for Explorer XVI were computed for us by Mr. Vosteen of Langley for three epochs several months apart using the same Goddard data for each. The average number of electrons/day differed by factors up to 15 and protons/day by factors up to 20.

The effectiveness of solar cell shields is another area where care (and research) is needed to avoid large lifetime prediction errors. I will touch on this later. The energetic particles in space must be assumed to be omnidirectional with

PAGE 158 INTENTIONALLY BLANK

respect to solar cell panels, except possible for a magnetically oriented earth satellite. Hence, to correlate shielding effectiveness in space with ground tests, and to allow for shielding by the vehicle structure, orientation factors must be determined. Shields for the light-sensitive side of solar cells must, of course, by transparent, and the transparency could be affected by radiation. Gilbert Haynes discussed this area in a separate paper.

There are many variables associated with radiation damage testing of solar cells in particle accelerators:

Cell Types and Variations - The influence of basic materials such as silicon and GaAs, N-type vs P-type base material, base resistivity, and more recently, dopant materials, on radiation damage have been discussed by others. Much of our testing has been on state-of-the-art cells ordered for specific projects.

Type and Energy of Particles - To date, interest has centered on electrons and protons, although the alphas of solar flares should also be considered. The energies of most interest are those most likely to be encountered in space and not stopped by the shields provided. Our early designs have had shields of 0.3 gms/cm^2 or more, and from 1960 to July 1962, we were most interested in protons with energies between 20 and 500 Mev. At that time, our primary interest switched to electrons with energies of one to several Mev.

Irradiation Parameters - We try to simulate actual conditions, especially as to cell mounting and irradiation temperature. Since electrons scatter badly and generate Bremstralung, mounting materials and spacing are important.

Evaluation Parameters - We have found it necessary to devote considerable effort in this area. When irradiating the early P/N cells with protons, the damage varied considerably among cells, requiring a large number of cells for good averaging. The scatter has been less with electrons, with N/P cells, and with newer, better matched cells. The effects of the cell loading, temperature, and type of illumination used during damage evaluation will be discussed later. Although we have not found damage recovery to be a major factor, it is large enough to be considered - up to 15% in several months.

The list is obviously not complete - measuring the irradiating flux, and solar panel over-design versus shielding, are examples of areas that could be included if time permitted.

In figure 2 we have attempted to show the electron energy spectrum of the artificial belt. We have combined and plotted the upper and lower bounds of the energy data furnished us about a year ago by Dr. Hess of Goddard for the Explorer XVI orbit (perigee 750 km, apogee 1140 km, and inclination 52°) and for circular, 30° orbits with altitudes of 400, 600, 800 and 1,000 km. The curve is thus a roughly averaged energy spectrum expected for satellites having orbits of moderate inclination and between about 400 and 1200 km in altitude. This spectrum is considerably "harder" than the originally assumed fission energy curve which showed 45% of the flux between 0 and 1 Mev, 30 between 1 and 2 Mev, etc.

Also shown is a curve given by Dr. Rosenzweig of Bell Lab, at the 1963 Photovoltaic Specialists Conference showing the effect of electron energy on solar cell damage rates. When dealing with the factors necessary to apply ground irradiation tests to space lifetime predictions, flux ratios rather than damage ratios have been found to be most convenient. In this case, Dr. Rosenzweig gives the "damage equivalent 1 Mev electron flux" as a function of energy. For example, the curve indicates that it takes about 10 one Mev electrons to do the same damage as a single 4 Mev electron.

Below a few kilovolts, electrons have insufficient energy to produce many defects in silicon. The simple atomic displacement theory predicts that the damage rate should increase approximately as shown up to about 1 Mev, and then should almost flatten out. For P/N cells, the curve is not much steeper than predicted, but as shown for the Bell Lab N/P cells, it is quite steep. Limiting testing by ourselves and others indicates that damage rates above 1 Mev may increase even faster for other N/P cells.

If one took the product of these two curves, the resulting curve would peak at about 2.7 Mev. Irradiating bare N/P cells near this energy results in smaller correction factors and minimum uncertainty. In the fall of 1962 when a fission energy spectrum was assumed, the corresponding optimum test energy was throught to be about 1.2 Mev for P/N cells. Shielding the cells tends to increase these energies.

Data on shielding effectiveness if scarce, particularly for electrons by relatively thick shields of materials other than aluminum. We have considered it necessary to make spot checks, and figure 3 gives degradation vs integrated electron

flux for typical N/P solar cells, both unshielded and with several thicknesses of silicon dioxide (fused silica) shields. The Atmospheric Density Satellite (12' sphere) cells are covered with 1/8" shields, the S-55C power solar cell trays have 3/16" windows, and the S-55C solar aspect sensor is protected with 1/4" fused silica.

The particular degradation parameter shown is short circuit current. It was measured using tungsten lamps, but was corrected to that expected in space sun (air mass of AM=o). The 2.4 Mev electron energy was the highest available at the time, but as mentioned earlier, it is reasonably typical of the artificial belt electrons. This energy has a practical range of 1.5 gms/cm^2 in fused silica or slightly over 3/16". The critical flux (that required to give 25% degradation) for the cells behind the 1/8" thick fused silica was increased by a factor of about 3.0. The corresponding factor for 3/16" fused silica was 60, and 1/4" fused silica, it was over 1,000. These factors are considerably larger than those deduced from data given by Marshall and Ward for electron transmission of aluminum foils, especially when the thickness was near the range. Evidently, a large number of the straggling electrons had energies too low to be effective in damaging the cells.

Figure 4 is shown primarily to illustrate why we think it is still necessary to at least spot-check the effects of irradiation on solar cells procured for a space project. Relative short circuit current is plotted vs electron flux, but the data has not been corrected to space sun. The two type cells irradiated with 2.4 Mev electrons are each nominally 10% N/P cells purchased with the same specifications. The critical flux (that required to give 25% degradation) varied by a factor of 2. Each curve represents an average of at least 4 cells, and scatter in damage was less than 2%. For the RCA cells, the critical flux decreased by a factor of 7 (damage rate increased) when the electron energy was increased from 1.2 Mev to 2.4 Mev. This compares with a factor of 3.7 shown on an earlier slide for Bell Lab cells.

Figure 5 is shown to review the old story of the effect of irradiation on the spectral response of solar cells. Because irradiation decreases diffusion length, and because the output resulting from illumination for the longer, more penetrating wavelengths of light is more dependent on diffusion length, there is an apparent shift in response toward shorter wavelengths. Because of their stability, tungsten lights with peak output at about 1.0μ have been used most often to evaluate solar cell damage. Since Johnson's curve for space sun peaks at about 0.50μ, it is obvious that tungsten light measurements give

exaggerated degradation. We have found that spectral response of some cells is a function of light level and exacting techniques are necessary to permit accurate computation of tungsten-light to space-sun degradation correction factors. This ties in with the findings of Denny and Downing of STL, that for cells irradiated with high energy protons, the diffusion length is a function of injection level. We are now evaluating a recently acquired space sun simulator which should avoid some of the time-consuming spectral response work.

Figure 6 gives some I-V curves taken for a typical 10% N/P RCA solar cell purchased for S-55C. Current is plotted vs voltage and the loading was varied from short-circuit to open-circuit conditions. Curves are given for four temperatures before irradiation and after a rather heavy dose of electrons at 1.2 Mev.

The reduction of diffusion length, which is manifested by the reduction in short circuit current, is the principle factor involved. However, changes in junction impedance, which are indicated by the relatively small drop in open circuit voltage, can make a big difference under some load conditions. This is also true with respect to changes in temperature coefficients. After irradiation, the percent change of short circuit current with temperature is comparatively large, probably caused by the introduction of new recombination centers. In the S-55 power supplies, the batteries maintain the solar cell voltages very close to 0.38 volts per cell. Degradation at room temperature at this load was not much greater than that at short circuit, but was considerably greater at elevated temperatures. Higher voltages per cell, where the situation is worse, are used (maximum power at room temperature for this cell is at 0.43 volts). The S-55C test solar cells are loaded with fixed resistors of 6.6 ohms per cell, and their output voltage was monitored. Here we have a case where the temperature coefficient reversed. Before irradiation a temperature increase meant less output, but the reverse was true after irradiation.

The remaining figures show the percent change in output with temperature for specific loads. In each of these figures, percent change in output at the indicated loading is plotted vs temperature in degrees F. An intermediate and more practical dose is also shown, but note that cold temperature readings were not obtained for this dose. In figure 7, note that irradiation caused more percent change in short circuit current than in open

circuit voltage. Figure 8 gives the curves for maximum power, and for the voltage across 6.6 ohms. The slope of the maximum power curve changed very little from its nominal value of 1/2%/°C. The slope reversal is apparent for the case of the fixed resistive load. Figure 9 makes it apparent that, for constant voltage loading and if high irradiation damage and high temperatures are both expected, the cells must be given conservative voltage loading.

We have not attempted to estimate the accuracy to which we can compute solar cell lifetime in space. It is obvious that a number of factors have to be carefully considered to permit estimates much better than a factor of 10. Certainly, a continued effort is needed to improve our knowledge in this field.

Problems Related To The Accurate Estimation Of Solar Cell Lifetime In Space

Space environment
- **obtaining up-to-date data;**
- **estimating average dose rates.**

Solar cell shields
- **shielding effectiveness;**
- **orientation effects;**
- **degradation of transparent shields.**

Radiation testing of solar cells
- **cell types and variations;**
- **type and energy of particles;**
- **irradiation parameters:**
  cell mounting arrangement and temperature,
  beam direction and uniformity,
  in vacuum or air;
- **evaluation parameters:**
  number of irradiation samples,
  cell loading,
  operating temperatures,
  types of illumination,
  damage recovery.

FIGURE 1

Energy Spectrum of Artificial Election Belt
and
Relative Damage of N/P Solar Cells Vs Electron Energy

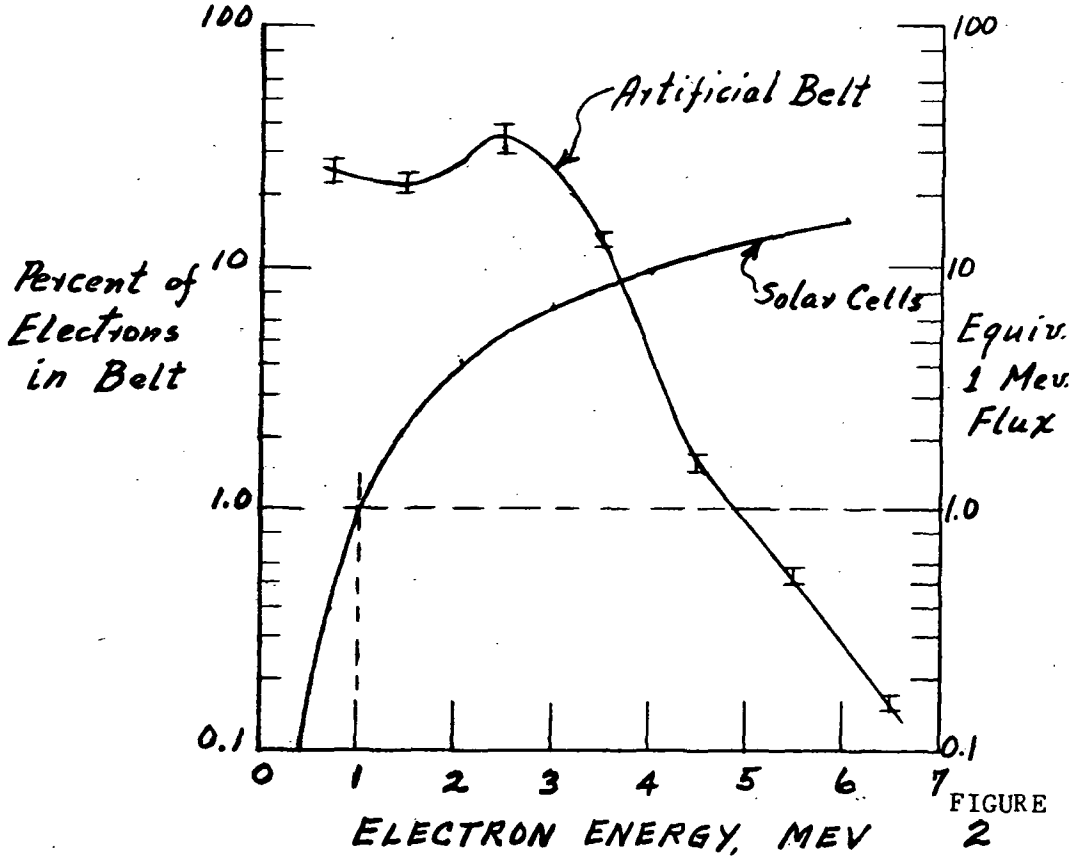

FIGURE 2

Damage Rates of N/P Solar Cells With and Without Shields - 2.4 Mev Electrons

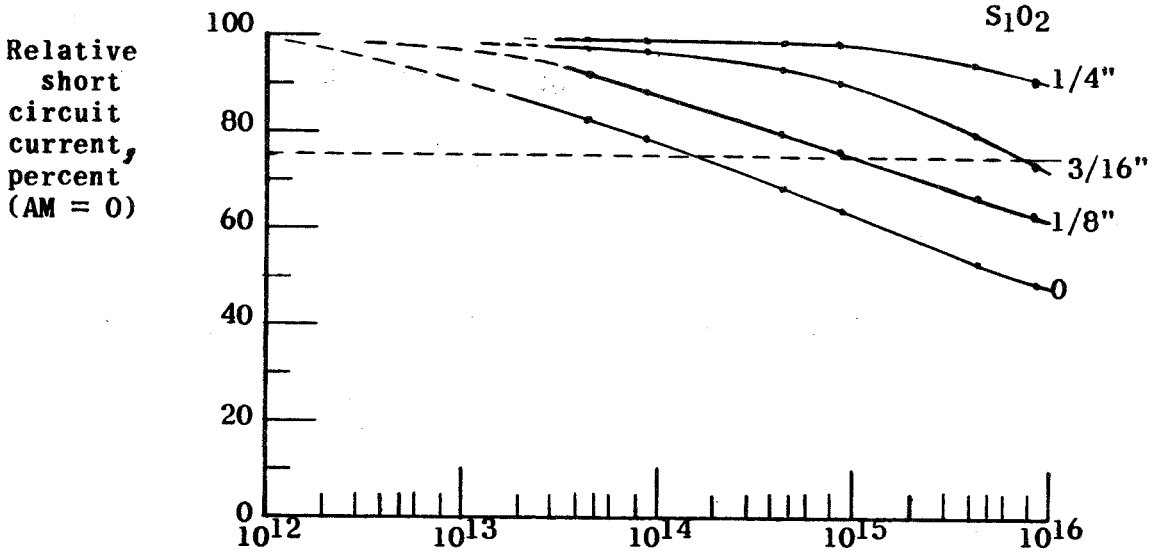

FIGURE 3

Damage Rates of N/P Solar Cells

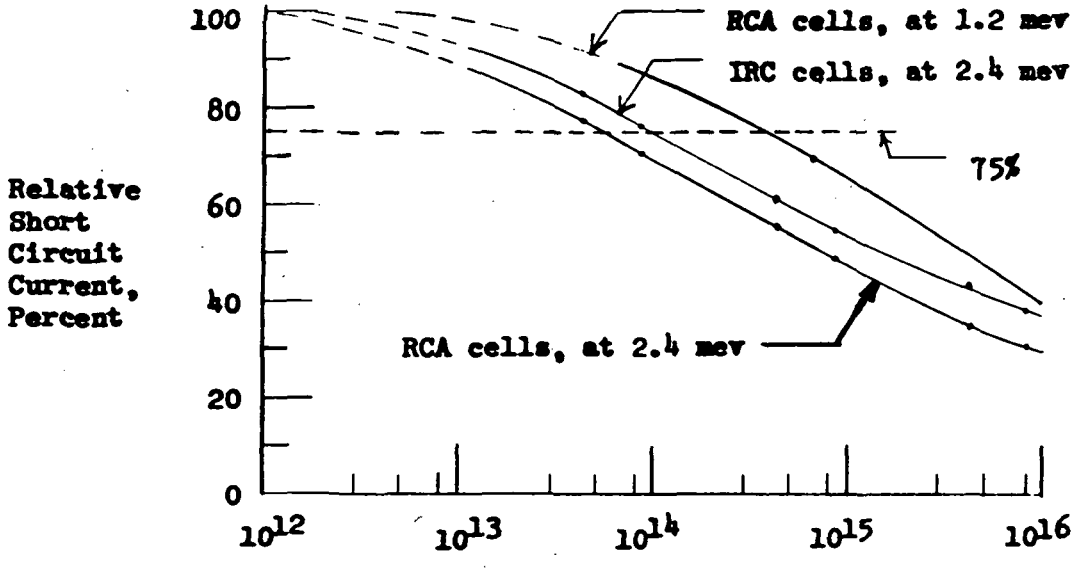

FIGURE 4

Change in spectral response of a typical
Solar Cell
due to Proton irradiation
(7.2 X 10^{n} P/cm^2 at 22 MEV.)

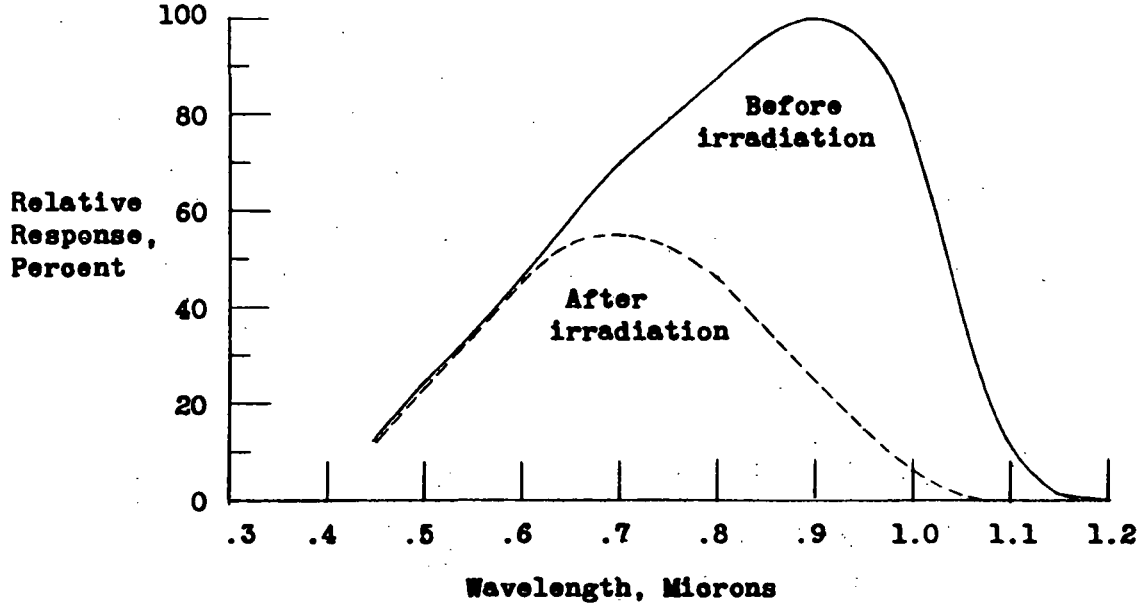

FIGURE 5

Effect of Electron Irradiation on the Load and Temperature Characteristics of N/P Solar Cell

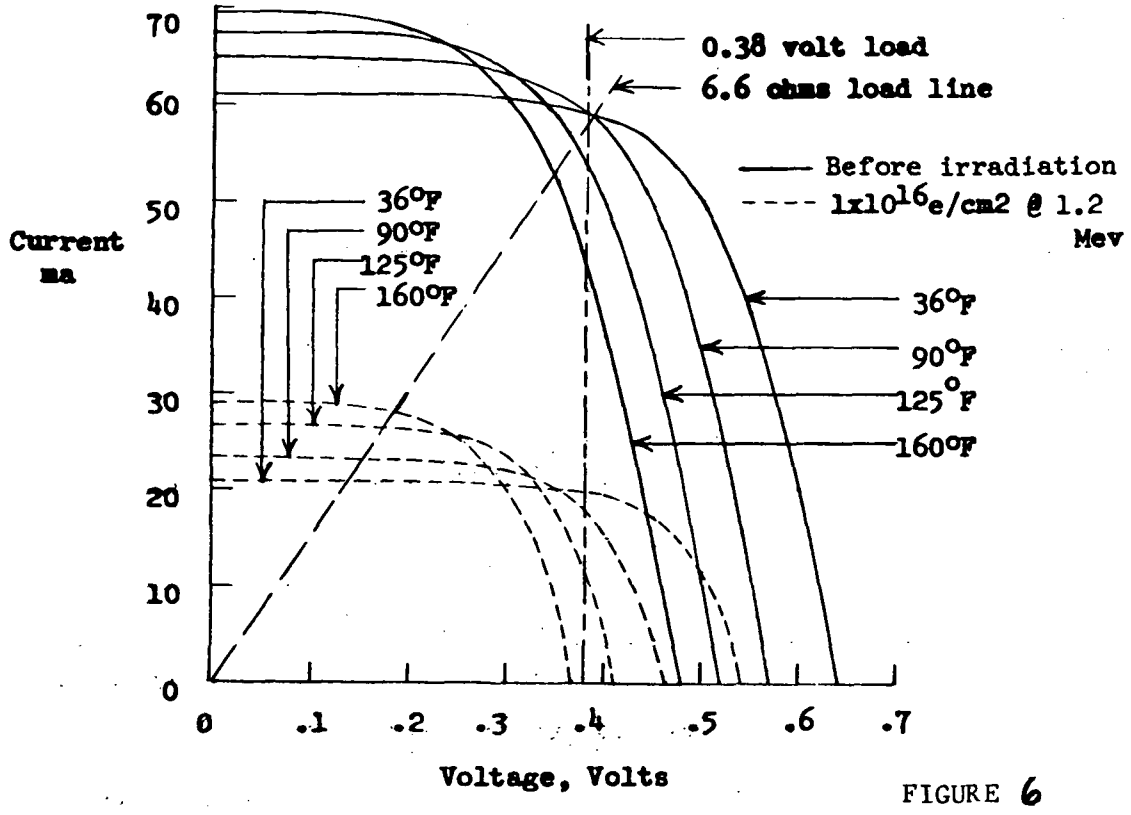

FIGURE 6

Effect of Irradiation on the Temperature Characteristics of Short-Circuit Current and Open-Circuit Voltage

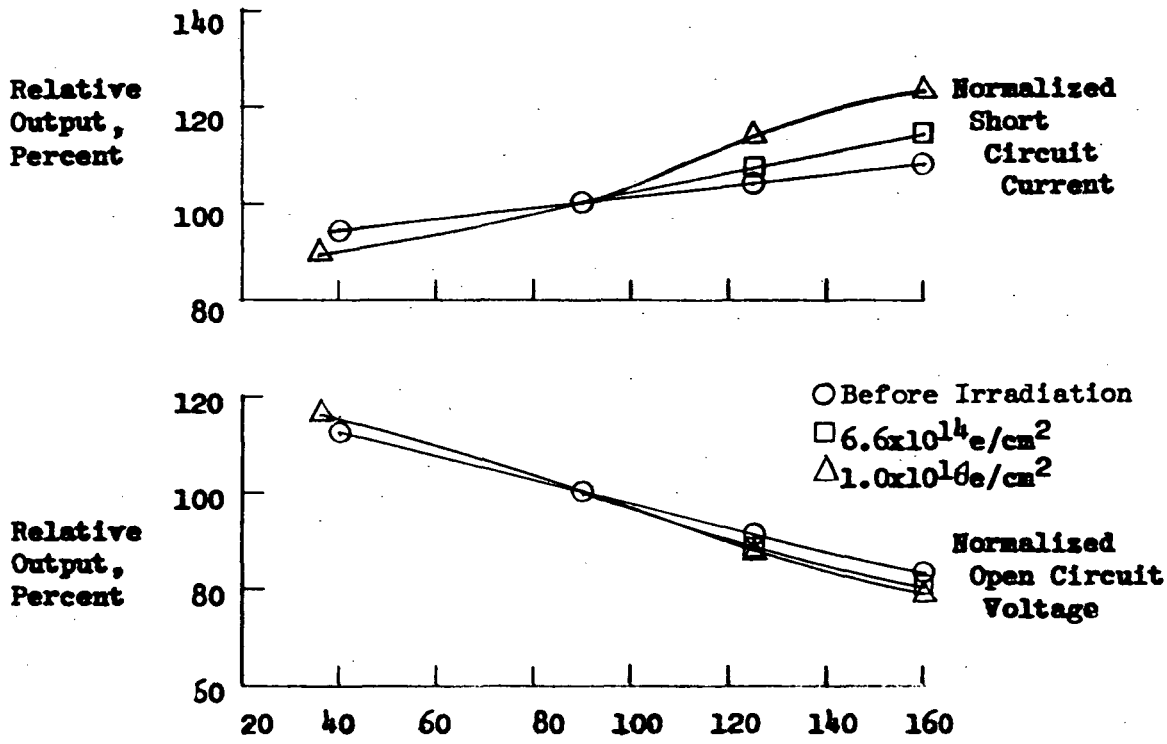

FIGURE 7

Effect of Irradiation on Temperature Characteristics at Maximum Power and at 6.6 ohms load per cell

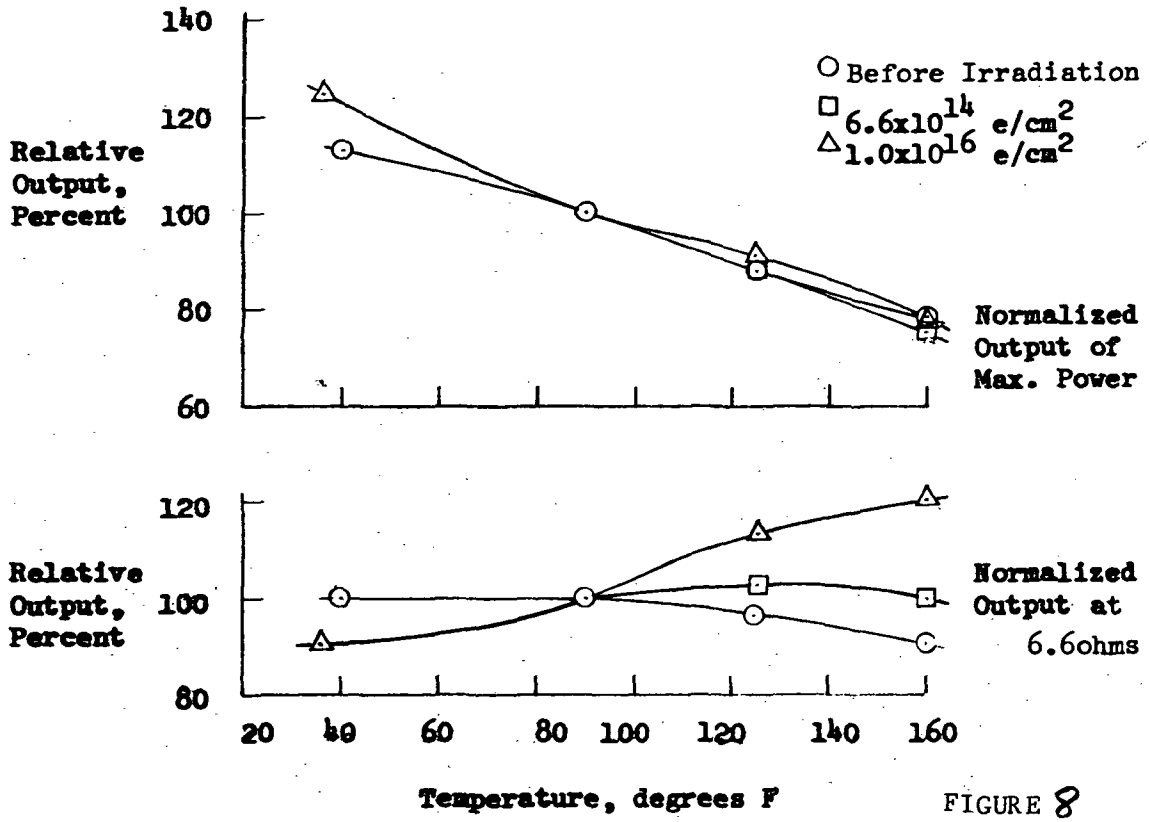

FIGURE 8

Effect of Electron Irradiation on the Temperature Characteristics at 0.38 volts per cell

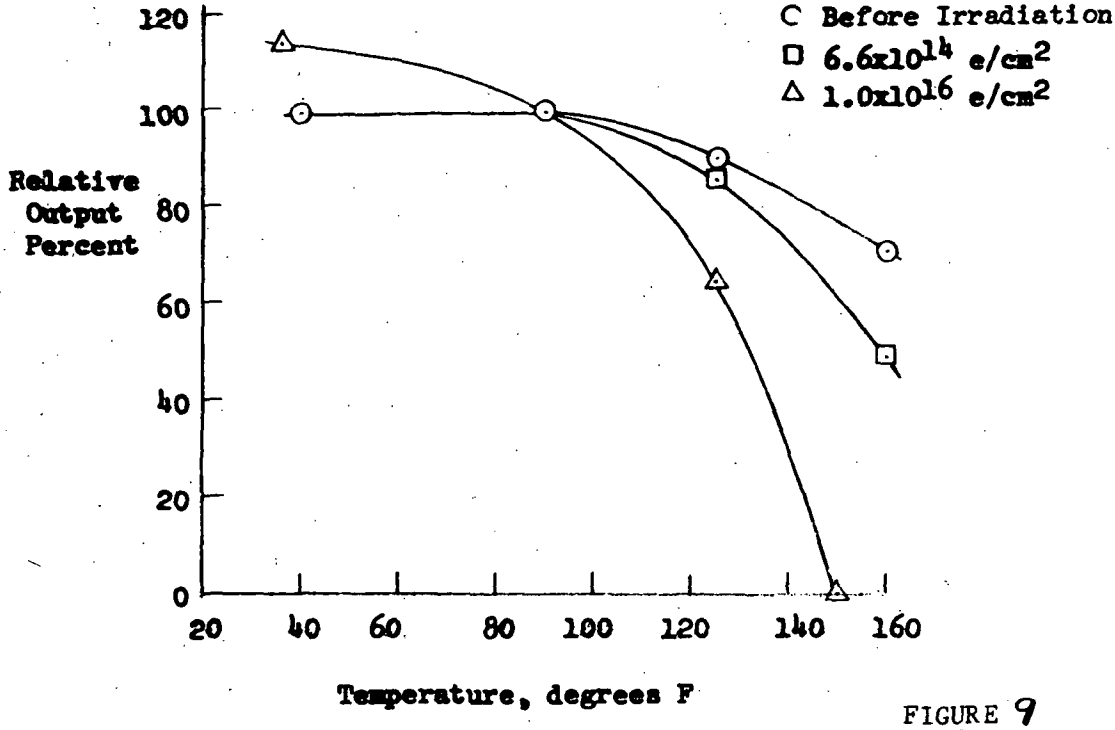

FIGURE 9

Page Intentionally Left Blank

RADIATION EFFECTS ON SEMICONDUCTOR ELECTRONICS

By F. R. Bryant* and W. C. Hulten*
NASA Langley Research Center

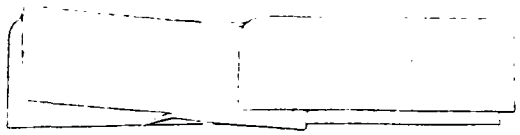

ABSTRACT

Radiation effects on semiconductor devices are discussed and the results of Langley Research Center's effort in the experimental evaluation of proton damage to semiconductors is presented. The use of minority carrier lifetime damage constants in predicting radiation damage to transistors is reviewed. A number of conclusions, concerning proton radiation damage to transistors, arrived at through experiments conducted by LRC are presented.

SYMBOLS

S	recombination velocity of surface carriers over the emitter-base surface
W	base width
A_s	surface area around emitter over which surface recombination of carriers occurs
D_p, D_n	diffusion constants for holes and electrons in the base region
A_e	cross-sectional area of the conduction path which is approximately equal to the emitter area
τ_p, τ_n	minority carrier lifetimes in the base region
σ_b, σ_e	base and emitter conductivities
K_τ	minority carrier lifetime damage constant
τ	minority carrier lifetime
$f_{\alpha co}$	alpha cut-off frequency
ϕ	total integrated flux
β	current gain

---

*Aerospace Technologist.

PAGE 174 INTENTIONALLY BLANK

L_{pb} diffusion length of holes in the base region

L_{ne} diffusion length of electrons in the emitter.

RADIATION EFFECTS ON SEMICONDUCTOR ELECTRONICS

A part of the overall radiation effects program at the Langley Research Center is allotted to the study of radiation damage to semiconductor devices. The effort to date has been concerned primarily with proton radiation effects on semiconductors because of the lack of data available in this area.

The experimental phase of this program has been carried out utilizing proton accelerators at the Oak Ridge National Laboratory and at various universities. The accelerators used to date include ORNL's 22 mev cyclotron, University of Minnesota's 40 mev linear accelerator, Harvard University's 158 mev synchrocyclotron, University of Rochester's 240 mev synchrocyclotron, and Carnegie Institute of Technology's 440 mev synchrocyclotron. The actual irradiation experiments were carried out by LRC personnel at the various accelerator sites.

The early phases of this effort included irradiation of resistors, diodes, capacitors, and conventional bipolar transistors. Recent tests have included field-effect transistors and microelectronic devices. Microelectronic devices include microdiodes, microcapacitors, microtransistors, and integrated circuits. The earlier effort has been documented in NASA Technical Notes D-718 and D-1490 (refs. 1 and 2). Some of the more recent data is being analyzed for future documentation; however, the data will be made available in rough form to interested NASA personnel.

It has been established that three major radiation-induced effects must be considered when evaluating transistors in a radiation environment. The effects are surface ionization, bulk ionization, and atomic displacements. Surface ionization effects can cause appreciable degradation of transistor characteristics at doses low compared to those required for permanent bulk damage. These effects may vary considerably for different device types and even individual units of a given type. Surface effects are not well understood but involve the collection of ionized gas particles or impurities on the surface of the device, thereby producing inversion layers that can alter the shunt leakage paths around the device. This results in a significant increase in the reverse leakage currents. Bulk ionization is the excitation of the electrons within the bulk material of the semiconductor and results in a flow of electrons in the device. The intensity of space radiation is not considered great enough for bulk ionization to be a problem. Ionization effects are considered "transient" effects since they disappear when bombardment ceases.

Atomic displacement due to radiation causes the introduction of vacancy-interstitial pairs in the base region of transistors which act as trapping centers for the minority carriers. The trapping of the minority carriers in the base region decreases minority carrier lifetime, thus decreasing the gain of the transistor:

The common emitter current gain (β) of a transistor is related to the minority carrier lifetime as shown by Webster's equation in figure 1 (ref. 3).

Webster's equation states that for a PNP transistor (substitute n for p and p for n for NPN transistors)

$$\frac{1}{\beta} = \frac{SWA_s}{D_p A_e} + \frac{\sigma_b W}{\sigma_e L_{ne}} + \frac{1}{2}\left(\frac{W}{L_{pb}}\right)^2 \tag{1}$$

where the first term on the right-hand side of the equation is the surface recombination term, the second term is the emitter efficiency term, and the third term is the volume recombination or minority carrier lifetime term. The minority carrier lifetime comes from the relation $L_{pb}^2 = D_p \tau_p$. Using this and the following well-known relations

$$f_{\alpha co} = \frac{1.22}{\pi} \frac{D_p}{W^2} \tag{2}$$

and

$$\frac{1}{\tau_f} = \frac{1}{\tau_i} + \phi K_\tau \tag{3}$$

an expression for the minority carrier lifetime damage constant can be obtained (ref. 4).

$$K_\tau = \frac{f_{\alpha co}}{0.194\phi}\left(\frac{1}{\beta_f} - \frac{1}{\beta_i}\right) \tag{4}$$

This expression is for a transistor having a uniform base and one in which the base width and alpha cut-off frequency does not change. Using equation (4), damage constants were calculated for a number of transistors. Results are as shown in figure 2. Damage constants are plotted for three types of transistors at four different energies. An average of 5 to 8 transistors were taken to obtain each point on the curve. It can be seen that there is considerable variation in the constants which can probably be attributed to variations in device performance as a result of loosely controlled manufacturing processes.

Figure 3 shows a plot of eight 2N526 PNP germanium transistors irradiated with 40 mev protons. The normalized small signal current gain vs integrated flux curves shows the large amount of scatter in data from transistors whose parameters have not been matched before irradiation. This scatter could be minimized by proper control of manufacturing process or matching parameters of transistors to be irradiated. The rise in gain at low flux levels is probably due to excess leakage current caused by surface ionization or impurities on the surface.

Figure 4 shows a plot of several 2N337 NPN-Silicon transistors irradiated with 40 mev protons. Scatter in data here is less, probably due to the better leakage characteristics of silicon. These transistors degraded very rapidly and were down to 40 percent of their initial gain at about an order of magnitude less integrated flux than it took to degrade the 2N526 germanium transistors to an equivalent level.

Figure 5 shows transistor gain as a function of base current. It can be seen that the percent loss is less at the higher base current. At the lower base currents, the current carriers have a tendency to migrate to the surface and recombine. At the higher currents the electric field set up by this current restricts the migration of carriers to the surface thus reducing recombination of carriers and decreasing percentage loss of transistor current gain.

Figure 6 shows some comparative values of integrated flux required to produce equal degradation in a number of different type transistors. The first three transistors are conventional bipolar transistors having alpha cut-off frequencies in the low, medium, and high range. As indicated here, the higher frequency devices have a greater radiation tolerance. The integrated circuit transistors and the microtransistors have radiation tolerances equivalent to conventional high-frequency transistors. The p-channel silicon field-effect transistors require flux values approximately two orders of magnitude higher than a medium-frequency bipolar transistor for equivalent degradation in gain. This compares favorably with data by other investigators utilizing electron and neutron sources (refs. 5 and 6).

A photograph of the experimental setup as used at ORNL and the University of Minnesota is shown in figure 7. Remotely controlled positioning motor was used to position desired specimen in the beam. A closed-circuit television system was used for monitoring specimen number and position after first locating beam with the silver activated zinc sulphide phosphor. A thin window ion chamber placed between beam exit port and target was calibrated with a Faraday cup and was used during the irradiations to monitor beam current. A current integrator was used for obtaining integrated flux.

Data are read out on commercial test equipment, recorders and transistor curve tracers. A typical preirradiation and postirradiation photo of the common emitter collector characteristics of a microtransistor is shown in figure 8. A loss in d-c gain of approximately 25 percent is indicated by these photographs. The transistor was bombarded with 128 mev protons to an integrated flux of 6.25×10^{12} protons/cm^2.

As a result of many experiments, certain conclusions have been arrived at concerning proton damage effects on transistors. These conclusions are:

NPN transistors have greater radiation tolerance than PNP.

Germanium transistors have greater radiation tolerance than silicon transistors.

Thin-base (high-frequency) transistors have greater radiation tolerance than wide-base (low-frequency) transistors.

Protective grease and potting materials produce adverse surface effects causing instability of collector and leakage currents.

Transistors have a greater percentage degradation at low collector currents.

Planar transistors with passivated surfaces have less transient effects.

Field-effect or unipolar transistors require 2 to 3 orders of magnitude greater flux to give the same degree of damage as the conventional bipolar unit.

Integrated circuit transistors are affected to about the same degree as an equivalent discrete transistor.

REFERENCES

1. Hulten, W. C., Honaker, W. C., and Patterson, John L.: Irradiation Effects of 22 and 240 Mev Protons on Several Transistors and Solar Cells. NASA TN D-718, 1961.

2. Honaker, W. C., and Bryant, F. R.: Irradiation Effects of 40 and 440 Mev Protons on Transistors. NASA TN D-1490, 1963.

3. Webster, W. M.: Proc., IRE 42, 914, 1954.

4. Bilinski, J. R., Brooks, E. H., et al.: Proton-Neutron Damage Correlation in Semiconductors. General Electric Co. (NASA Contract No. NAS1-1595); June 10, 1962.

5. Roberts, C. E., and Hoeni, J. A.: Comparative Effects of 1 Mev Electron Irradiation on Field Effect and Injection Transistors. Amelco Semiconductor Division of Teledyne Inc., March 1963.

6. Taylor, Lyndon: TIX 691 Field Effect Transistor Irradiation. Components Division, Texas Instruments Inc., March 15, 1962.

$$1/\beta = \frac{SWA_S}{D_p A_e} + \frac{\sigma_b W_b}{\sigma_e L_{ne}} + \frac{1}{2}\left(\frac{W}{L_{pb}}\right)^2 \qquad (1)$$

$$L_{pb}^{\ 2} = D_p \tau_p \qquad (2)$$

$$f_{\alpha co} = \frac{1.22}{\pi}\left(\frac{D_p}{W^2}\right) \qquad (3)$$

$$\frac{1}{\tau_f} = \frac{1}{\tau_i} + \phi K_\tau \qquad (4)$$

$$K_\tau = \frac{f_{\alpha co}}{0.194\phi}\left(\frac{1}{\beta_f} - \frac{1}{\beta_i}\right) \qquad (5)$$

NASA

Figure 1.- Derivation of transistor radiation damage constants from Webster's gain equation.

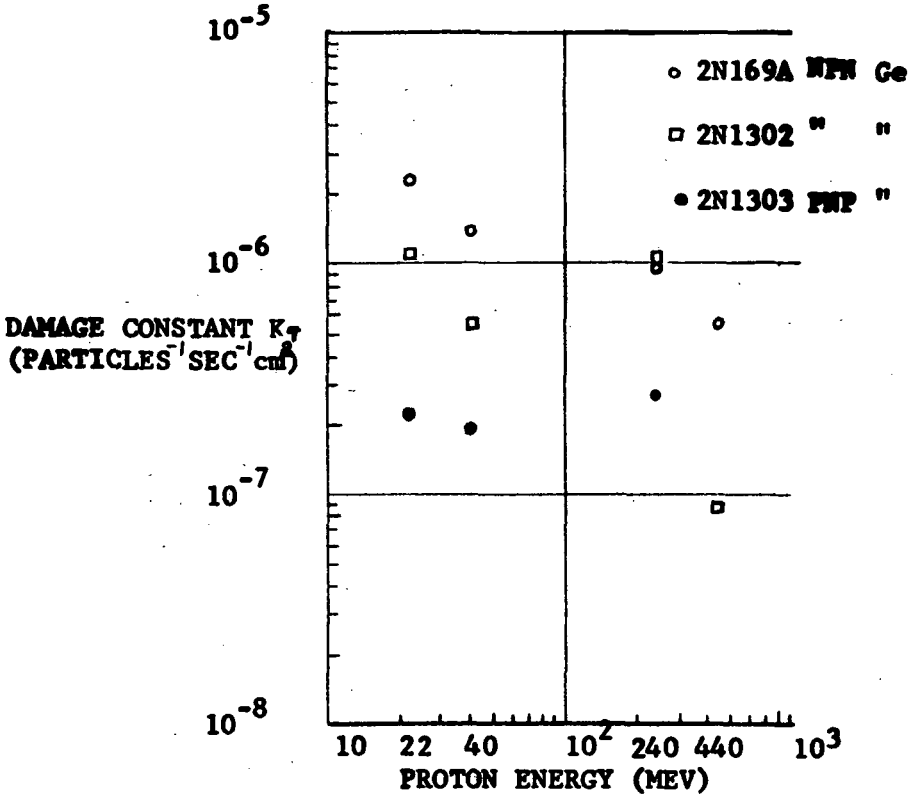

NASA

Figure 2.- Proton damage in germanium transitors.

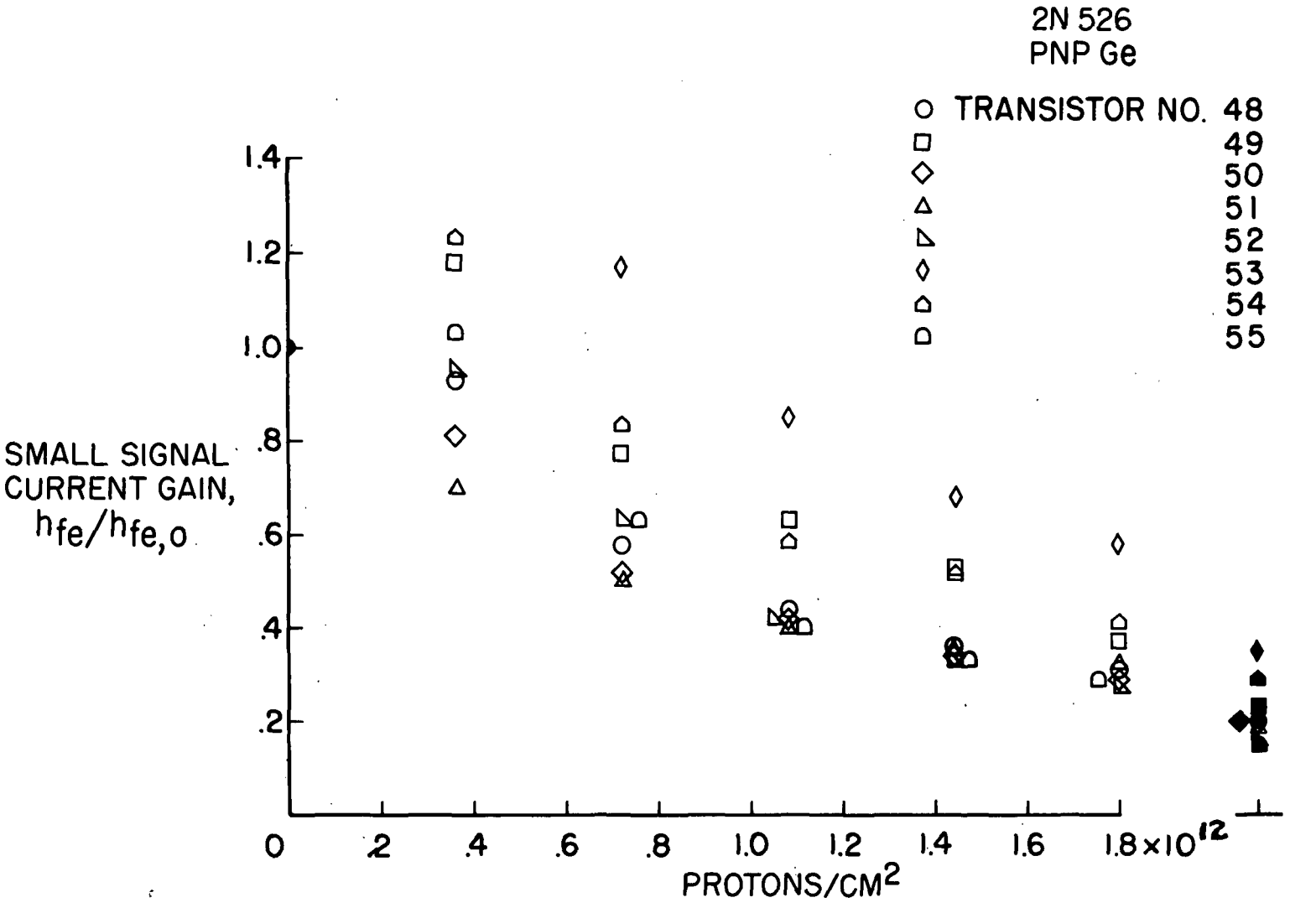

Figure 3.- Variation of small-signal current gain with integrated flux in a 40 Mev proton beam. Filled-in symbols are post check points.

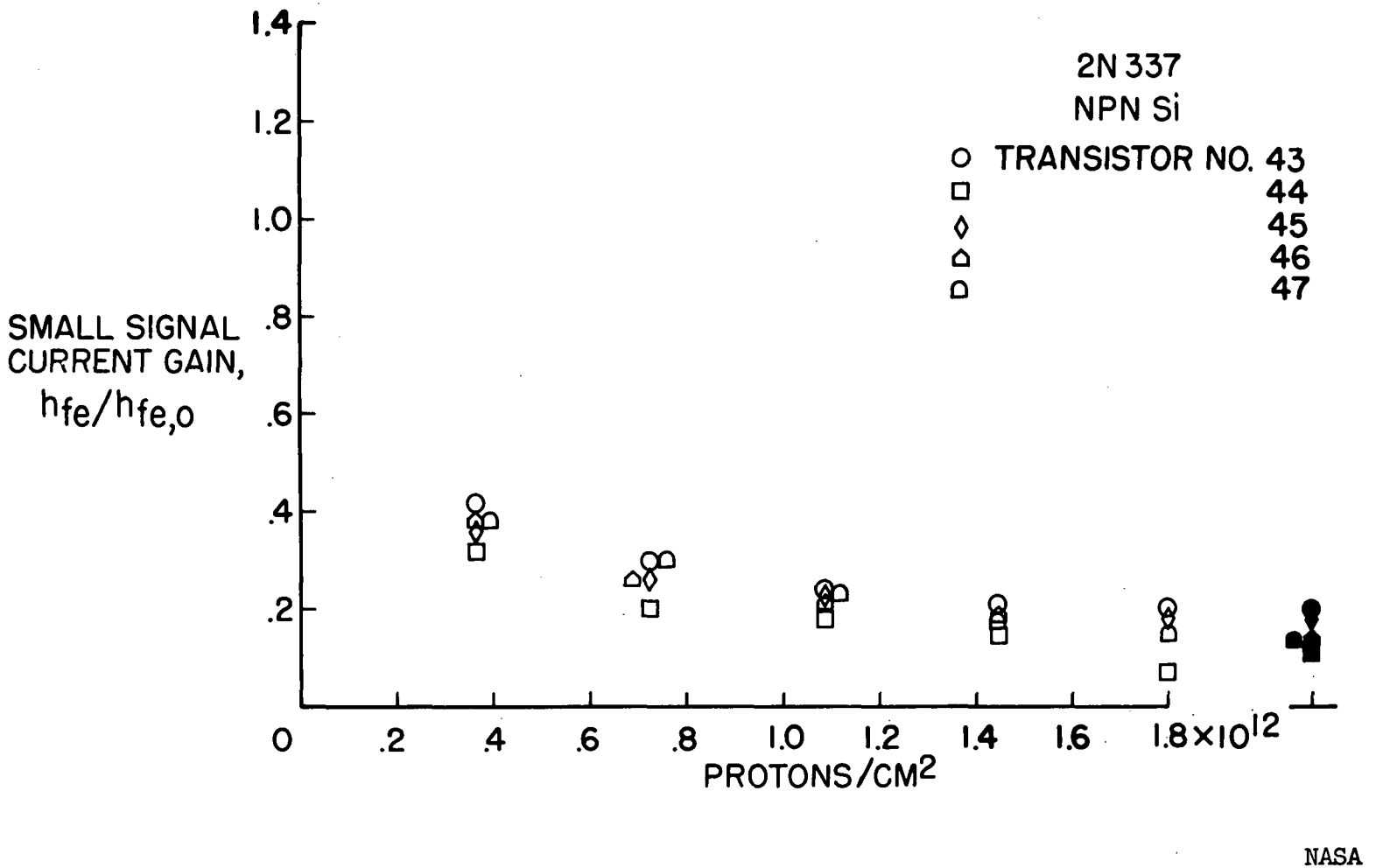

Figure 4.- Variation of small-signal current gain with integrated flux in a 40 Mev proton beam. Filled-in symbols are post check points.

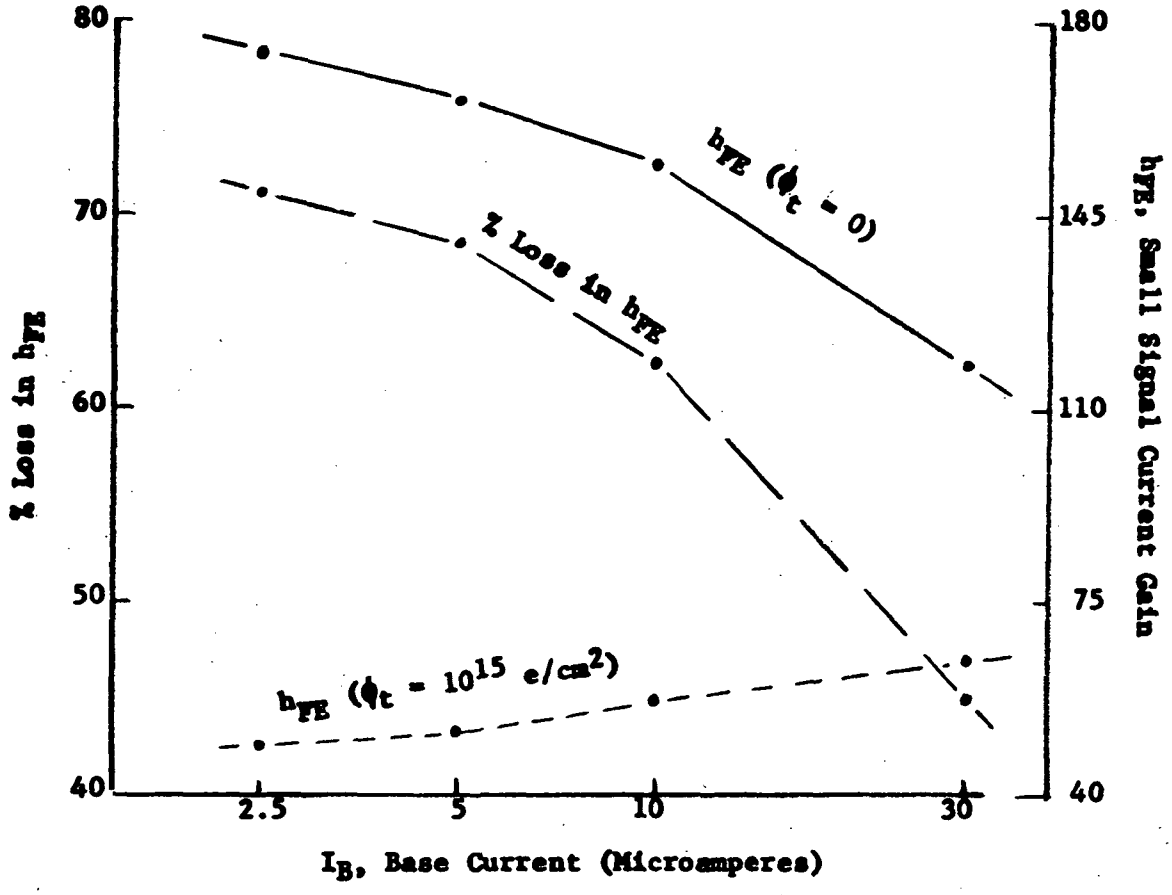

NASA

Figure 5.- 2N393, PNP-Ge transitors, before and after irradiation with 3 Mev electrons.

TRANSISTOR TYPE	ENERGY, Mev	MAX. TOLERANCE FLUX, PROTONS/CM^2	NOM. FREQ., mc	REMARKS
2N224 (PNP-Ge)	40	1.5×10^{11}	0.5	
2N169 (NPN-Ge)	40	7×10^{11}	9	
2N743 (NPN-Si)	40	1.8×10^{12}	400	
μET-1 (NPN-Si)	128	4.5×10^{12} ($h_{FE}/h_{FE,o} = 0.78$)	---	INTEGRATED-CIRCUIT TRANSISTOR
	22	4.1×10^{12}	---	
TMT-843 (NPN-Si)	128	1.4×10^{12} ($h_{FE}/h_{FE,o} = 0.81$)	20	MICROTRANSISTOR
MHM 1101 (NPN-Si)	128	5.6×10^{11} ($h_{FE}/h_{FE,o} = 0.27$)	60	DARLINGTON-CONNECTED
TIX-880	128	6.72×10^{12} ($A/A_o = 0.64$)	---	N-CHANNEL Ge FIELD-EFFECT TRANSISTOR
2N2497	128	3.36×10^{13} ($A/A_o = 0.87$)	---	P-CHANNEL Si FIELD-EFFECT TRANSISTOR
	22	5.34×10^{13} ($A/A_o = 0.64$)		

NASA

Figure 6.- Integrated proton flux for 30-percent loss in h_{FE}.

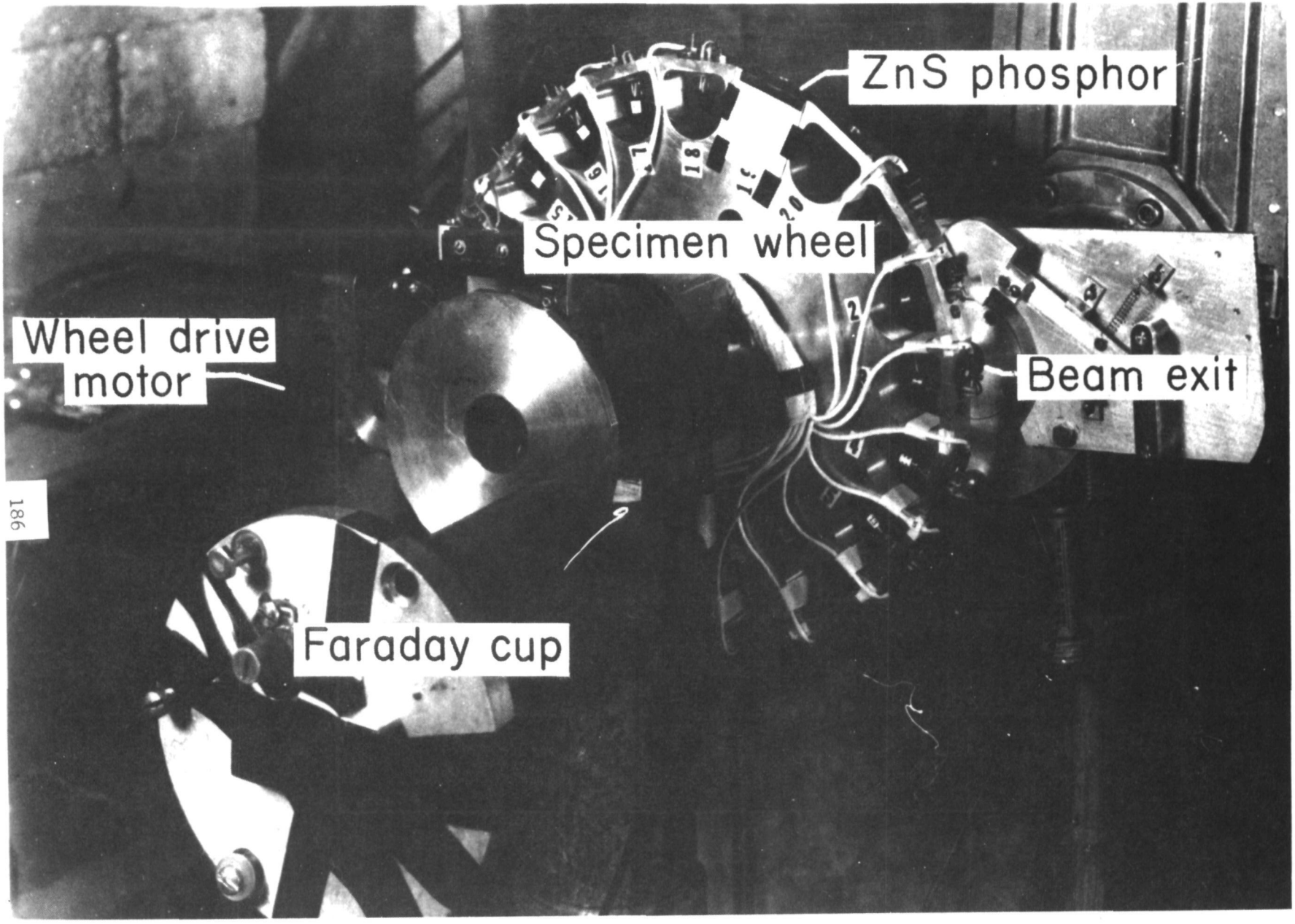

NASA
L-62-1017

Figure 7. - Experimental setup used during irradiation tests conducted at the University of Minnesota.

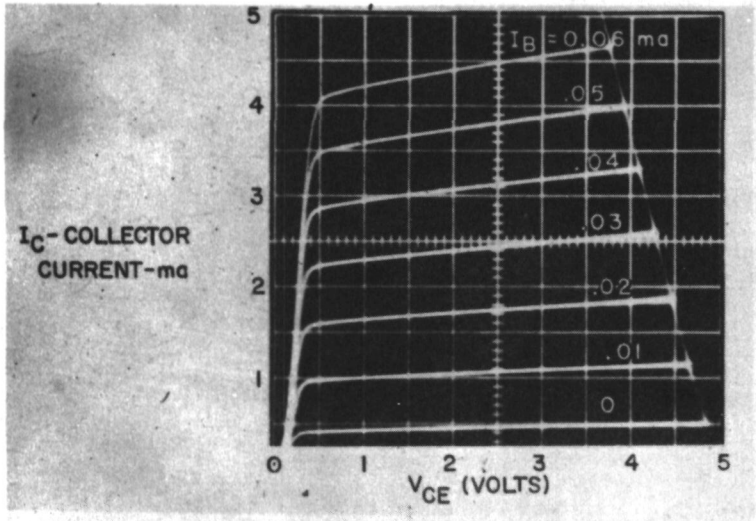

Figure 8(a).- Preirradiation photo of C. E. collector characteristics for μET-1 microtransistor.

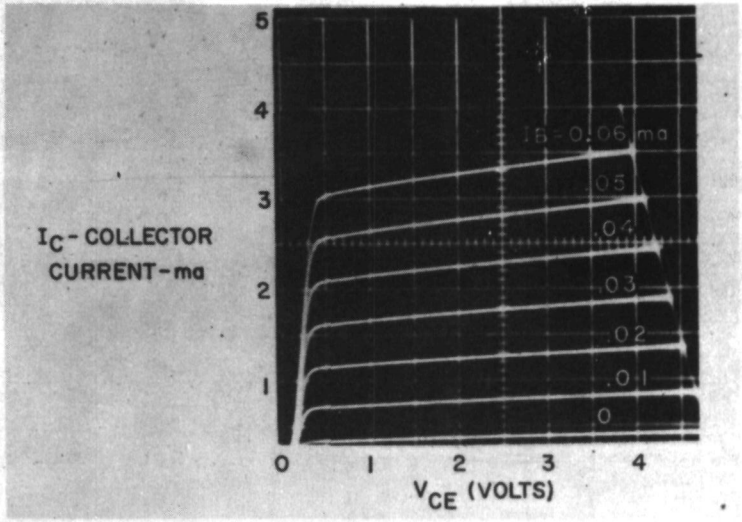

NASA

Figure 8(b).- Postirradiation photo of μET-1 microtransistor.

NATIONAL AERONAUTICS AND SPACE ADMINISTRATION

DAMAGE TO GERMANIUM PRODUCED BY 22 AND 40 MEV PROTONS

By Roger A. Breckenridge and Chris Gross
NASA Langley Research Center

INTRODUCTION

Studies of proton damage to germanium transistors have indicated a need for a better understanding of defects produced in the constituent materials of these devices by high-energy protons (ref. 1). Although extensive radiation damage studies have been conducted with other types of damaging radiation, only a limited amount of work has been done with protons. For this reason the following investigations were initiated.

Measurements were made of electrical conductivity and the Hall coefficient since both are very sensitive to defects produced in the lattice of the semiconductor by radiation. Only permanent defects were considered in these studies, that is, defects arising from the creation of interstituals and vacancies by the incident protons and resulting secondaries. These defects give rise to trapping sites and recombination centers in the germanium. However, in this report we will be concerned only with the trapping of majority carriers from either the conduction band or the valence band.

REVIEW OF RADIATION DAMAGE PHENOMENON IN SEMICONDUCTORS

When an energetic charged particle passes through a solid, it produces ionization and displaced atoms (figs. 1 and 2).* The majority of the energy of the charged particle is lost through the ionization process. In a semiconductor, this ionization is rapidly converted into electron-hole pairs that quickly disappear through the recombination process. The displacement of the lattice atoms from their normal lattice sites to form stable defects give rise to permanent damage in the semiconductor materials. These defects or imperfections in the lattice structure introduce energy levels in the forbidden gap that are capable of trapping the majority carriers.

The simplest form of radiation-produced defect is a lattice vacancy and interstitial atom (Frenkel defect). The defect-energy-level model proposed by James and Lark-Horovitz (ref. 2) for Frenkel defects attributes two acceptor levels to the vacancy and two donor levels to the interstitual (fig. 3). The levels are asymmetrical about the center of the gap, one being above the center while the other three lie below the center of gap. The probability that these levels are occupied with electrons is dependent upon their location in the forbidden gap and the

*Wertheim, G. H., Reprints from "Proceedings of the Symposium on High Power Accelerator Applications", Radiation Effects on Semiconductors, 1961.

PAGE 188 INTENTIONALLY BLANK

position of the Fermi level (fig. 4).* If the Fermi level lies above or below a given defect level, that level is essentially filled or empty, respectively.

DESCRIPTION OF EXPERIMENTAL TECHNIQUE

The germanium used in these studies was obtained commercially in the form of ingots. The ingots were sliced into 25 mil wafers by means of a diamond cutoff wheel. Then bridge samples were cut from these wafers by means of an ultrasonic cutter. (See fig. 5.) The samples were then mechanically lapped to a thickness of approximately 15 mils. Next the germanium samples were etched in a standard chemical etch.** Leads were attached to the tabs of the samples by means of indium alloy solder. The samples were mounted on ceramic slices for ease of handling (fig. 5).

The bombardment phase of the experiment was conducted at Oak Ridge National Laboratory's 22-Mev cyclotron and at the University of Minnesota's 40-Mev linear accelerator. During bombardment the germanium samples were mounted in a Hall magnet and the proton beam was allowed to fall on the sample by passing it through a hole in the pole piece of the magnet. (See fig. 6.) Flux determinations were accomplished by means of a Faraday cup mounted behind the sample for the 40-Mev irradiations. However, for the 22-Mev bombardments the collimator was calibrated against the Faraday cup, and beam current was collected by means of the collimator. The magnetic field strength was 5,000 gauss during this phase of the experiment. Voltage measurements during bombardment were made with a precision digital voltmeter and a precision d-c potentiometer. The electrical parameters that were monitored during irradiation were the electrical conductivity and the Hall coefficient.

The temperature runs prior and subsequent to bombardment were conducted at Langley Research Center. The temperature of the samples was monitored by measuring the output voltage of a copper-constantin thermocouple attached directly to the sample. The voltages for the electrical conductivity and Hall coefficient were measured with a precision d-c potentiometer. The lower temperatures were controlled by means of a liquid nitrogen bath and a heater coil which was wound around the chamber enclosing the sample. For temperatures closer to room temperature, dry ice was substituted for the liquid nitrogen bath. Using this type of temperature control system, the temperature could be maintained to $\pm 1^{\circ}$ C. The magnetic fields used in this part of the experiment were maintained at 3,000 gauss.

**Five parts HF, five parts acetic acid, and eight parts HNO_3.

*Wertheim, G. H., Reprints from "Proceedings of the Symposium on High Power Accelerator Applications", Radiation Effects on Semiconductors, 1961.

RESULTS AND DISCUSSIONS

N-Type Germanium

Samples of n-type, arsenic-doped germanium, resistivities in the range from 0.069 to 12.8 Ω-cm, were irradiated with 22 and 40 Mev protons at room temperature. The Hall coefficient and electrical conductivity were measured at regular intervals during the bombardment. The thicknesses of the samples were such that the proton beam was not appreciably attenuated when it passed through the samples. Examples of results obtained during bombardment are shown in figures 7 and 8. Figure 7 shows changes in the conductivity and Hall coefficient for a germanium sample which had an initial resistivity of 0.76 Ω-cm. This sample was bombarded with 22 Mev protons to an integrated flux of 1.91×10^{13} protons/cm^2. Figure 8 shows changes in the identical parameters for a 0.85 Ω-cm germanium sample irradiated with 40 Mev protons to an integrated flux of 8.88×10^{12} protons/cm^2. It is seen that both the conductivity and reciprocal Hall coefficient decrease under irradiation for both the 22 and 40 Mev bombardments. This behavior is attributed to the trapping of conduction electrons by acceptor levels introduced in the forbidden gap.

The position of the defect energy levels in the forbidden gap may be determined by investigating the temperature dependence of the majority carrier concentration. As the temperature is varied, the Fermi level shifts, thereby changing the probability of occupation of the defect level. When the Fermi level passes over the defect level, the concentration of the carriers available for conduction changes abruptly. If the log of the carrier concentration times the temperature to the minus three-halves power is plotted versus reciprocal temperature, the energy of the defect level will be given by the slope of the curve times Boltzmann's constant. Figure 9 points out the existence of a level in n-type germanium 0.20 ev below the bottom of the conduction band not seen prior to irradiation. This level has been found by other investigators using other types of damaging radiation. Results of Cleland and Crawford indicate that this level acts as an acceptor (refs. 3 and 4).

Bombardment results for both the 22- and 40-Mev irradiations are summarized in table I. As can readily be seen, the removal rate of conduction electrons is a function of the initial Fermi level, ranging from -137.3 electrons/cm/proton for an initial Fermi level of E_c - 0.147 ev to -56.8 electrons/cm/proton for the initial location of the Fermi level 0.287 ev below the bottom of the conduction band for the 22-Mev bombardment. From the table, it is evident that the further the Fermi level is from the conduction band the smaller the removal rate. The explanation for this behavior is as follows. When the Fermi level is close to the conduction band, both acceptor levels are effective in trapping conduction electrons. However, when the Fermi level is moved further away from the conduction band the acceptor level above the center of the gap

(shallow level) becomes only partially effective in trapping electrons. Therefore the removal rate can vary as much as a factor of two depending upon whether the shallow level is filled or empty.

Another method of determining the energy of the shallow defect level in n-type germanium is to fit a theoretical initial removal rate curve assuming two acceptor levels, one of which is always completely filled, to the experimentally measured values. The best theoretical fit was obtained at 0.19 ev below the conduction band for the 22-Mev bombardments and at 0.21 ev below the conduction band for the 40-Mev bombardments (fig. 10). These values are in agreement within experimental errors with the level found from the temperature cycling.

To compare damage at the two energies, it is preferable to use the rate of introduction of Frenkel defects instead of carrier removal rates since the former is independent of Fermi level at room temperature. It is found that the ratio of the number of defect produced by 22 Mev to 40 Mev is 1.78. Simple displacement theory, based on only coulomb interaction, yields a value of 1.72 for this ratio. The fairly close agreement between theory and experiment indicates that coulomb interaction is principally responsible for the production of defects in this energy range.

P-Type Germanium

Several samples of p-type, indium-doped germanium with a range of resistivities from 0.089 to 9.80 Ω-cm were also bombarded with 22 and 40 Mev protons at room temperature. Conductivity and reciprocal Hall coefficient changes during bombardment with 22 Mev protons are shown in figure 11. This particular sample had an initial resistivity of 1.10 Ω-cm. Both the conductivity and the reciprocal Hall coefficient decreased under bombardment due to the fact that holes were being removed from the valence band. A similar plot is shown for a 9.54 Ω-cm sample in figure 12 for bombardment with 40 Mev protons. However, both the conductivity and reciprocal Hall coefficient increased during bombardment indicating that holes were being introduced into the valence band.

The results of the bombardment of p-type germanium are summarized in table II. As can be seen from the table, for the 22-Mev bombardment the removal rate changes from a negative value to a positive value between values of the initial Fermi level of E_V + 0.202 ev and E_V + 0.252 ev. This points out the existence of a limiting value of the Fermi level between these two values.* It can also be seen from tables I and II that the removal rates for holes are much lower than for electrons at a similar resistivity and for the same bombarding particles.

---

*The limiting value of the Fermi level is that value of the Fermi level for which the removal of carriers is zero.

CONCLUDING REMARKS

Results obtained from the 22- and 40-Mev proton bombardment of germanium indicate that displacements are produced mainly by coulomb collisions in the energy range. This result is not too surprising since the cross section for nuclear scattering is quite small compared to the coulomb scattering cross section at these energies.

The existence of the level ~0.2 ev below the conduction band in n-type germanium has been seen with other types of bombarding particles and seems to be a predominate level.

REFERENCES

1. Honaker, W. C., and Bryant, F. R.: Irradiation Effects of 40 and 440 Mev Protons on Transistors. NASA TN D-1490, 1963.

2. James, H. M., and Lark-Horovitz, K.: Zeitshrift für Physikalische Chemie 198, 107. 1951.

3. Crawford, J. H., Jr., and Cleland, J. W.: Jour. App. Phys. 30, 1204. 1959.

4. Billington, D. S., and Crawford, J. H., Jr.: Radiation Damage in Solids. 1961.

IONIZATION PROCESS

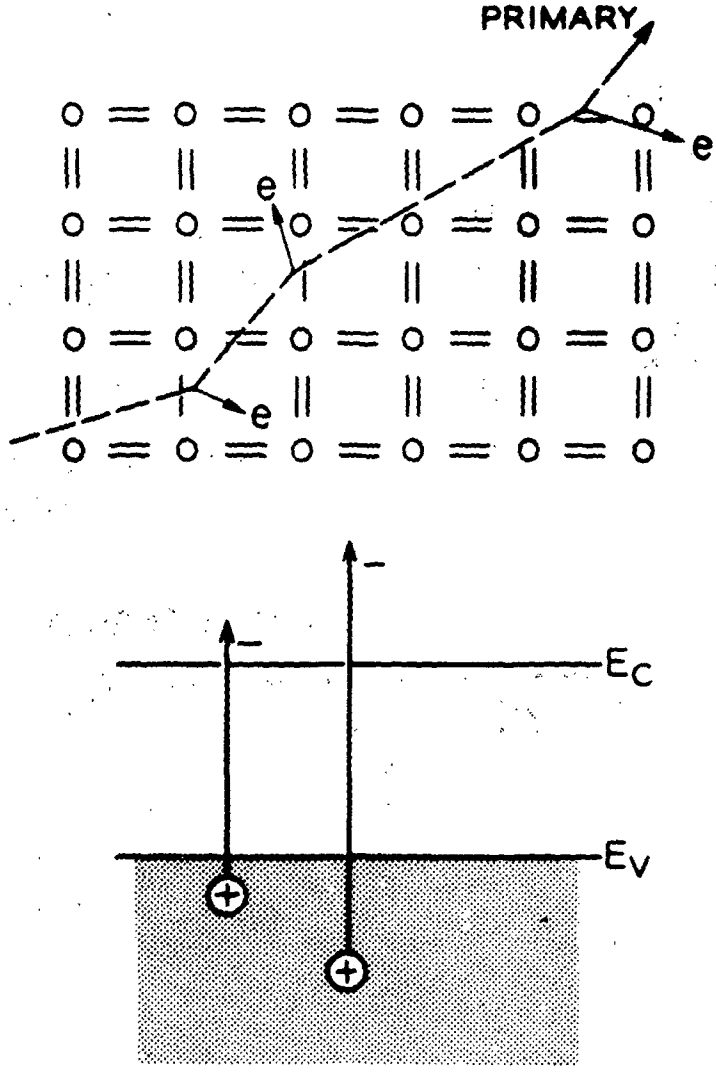

Figure 1.

PREDUCTION OF ATOMIC DISPLACEMENTS BY RADIATION

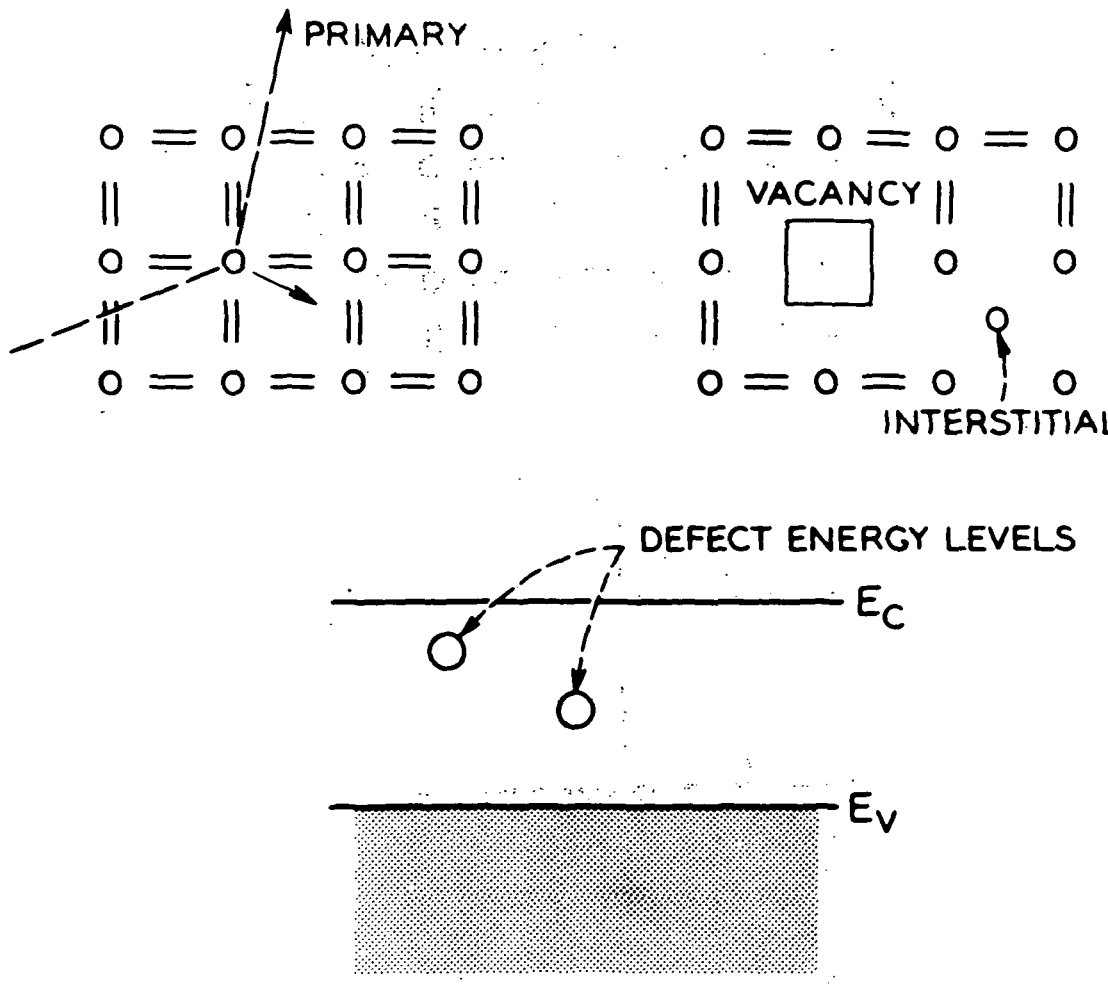

Figure 2.

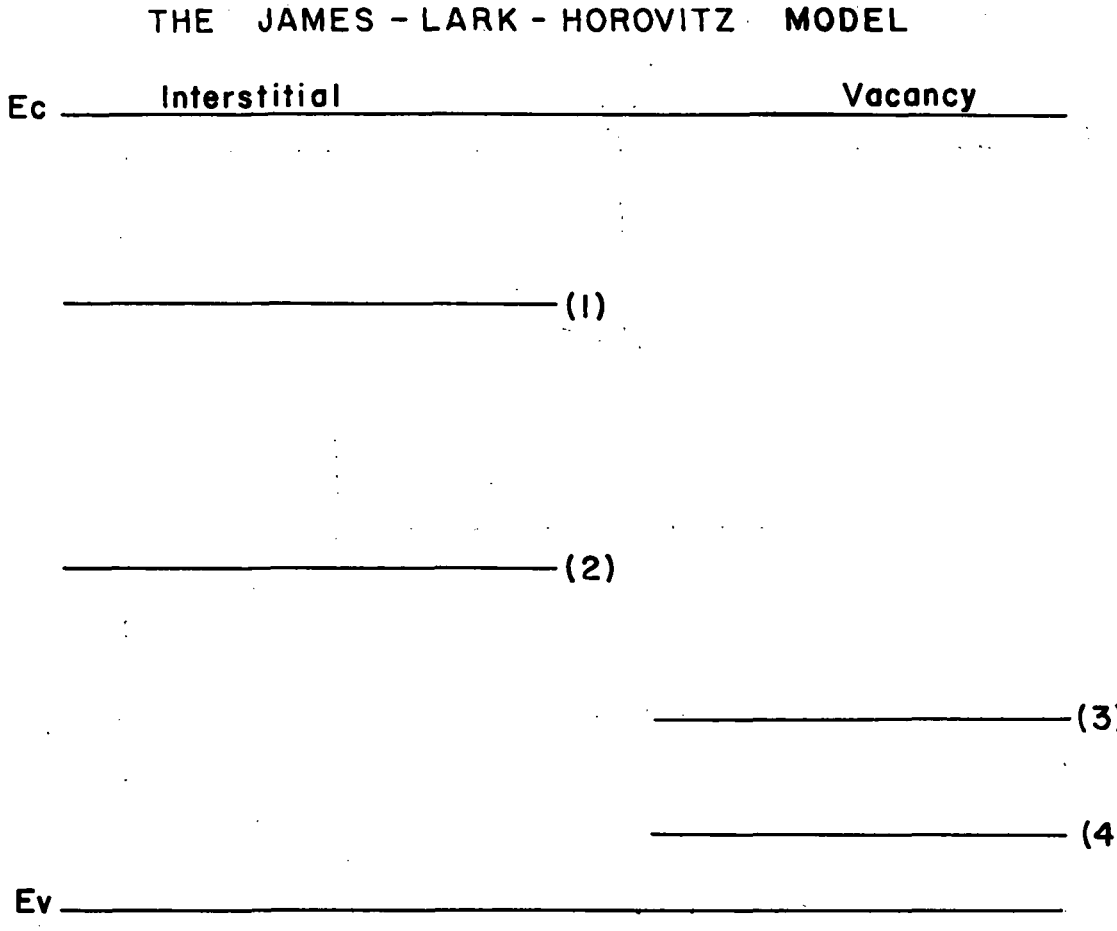
THE JAMES - LARK - HOROVITZ MODEL
Ec
Interstitial
Vacancy
(1)
(2)
(3)
(4)
Ev

Figure 3.

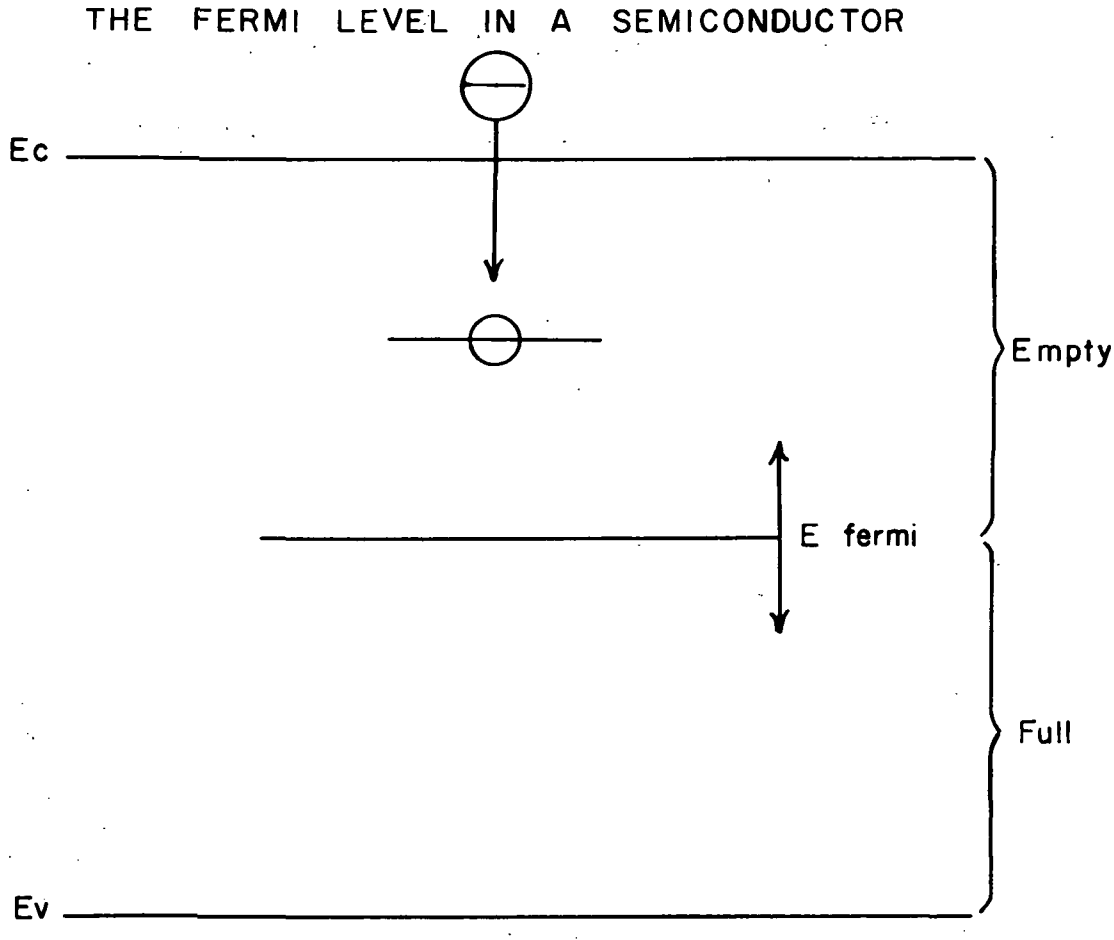

Figure 4.

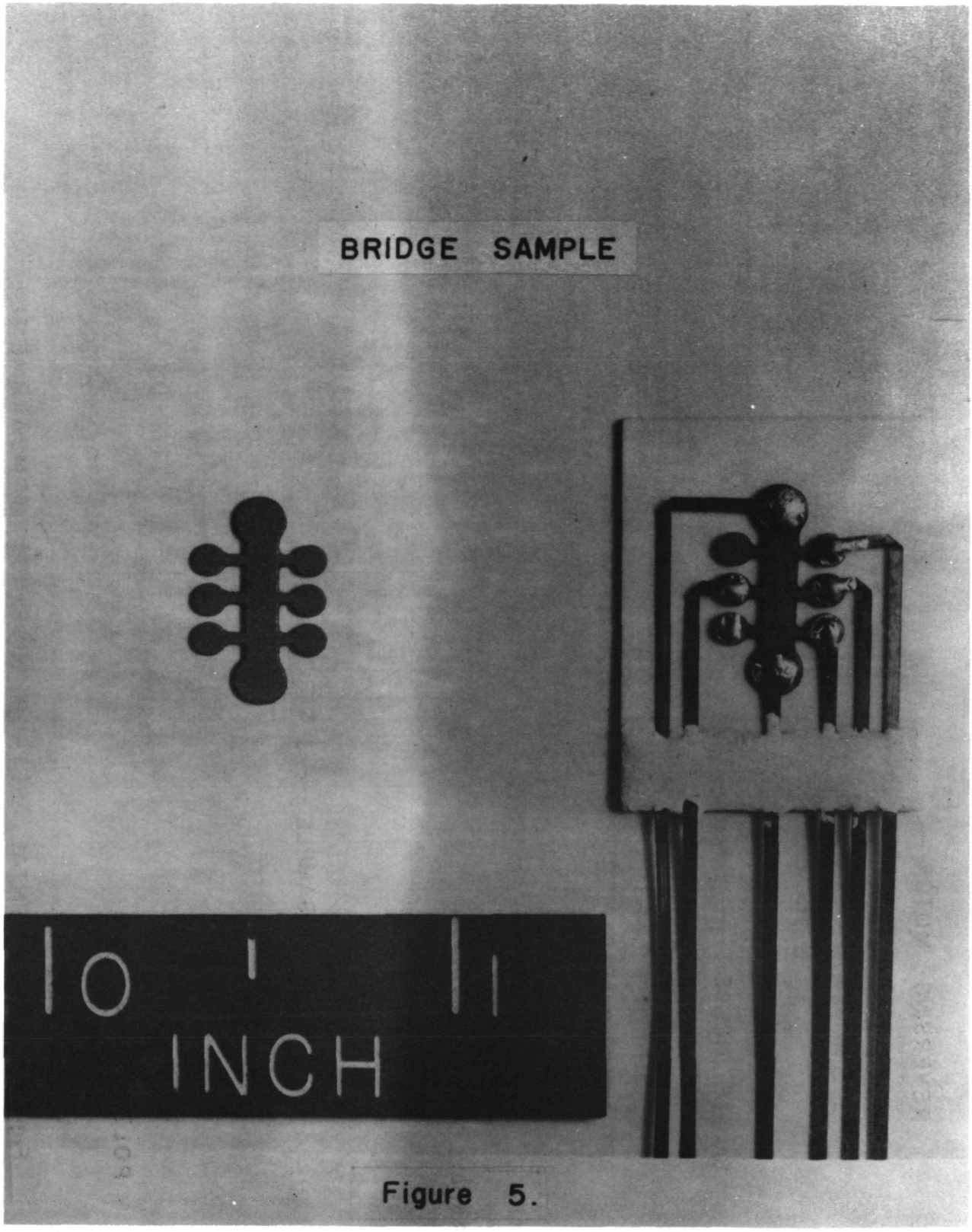

Figure 5.

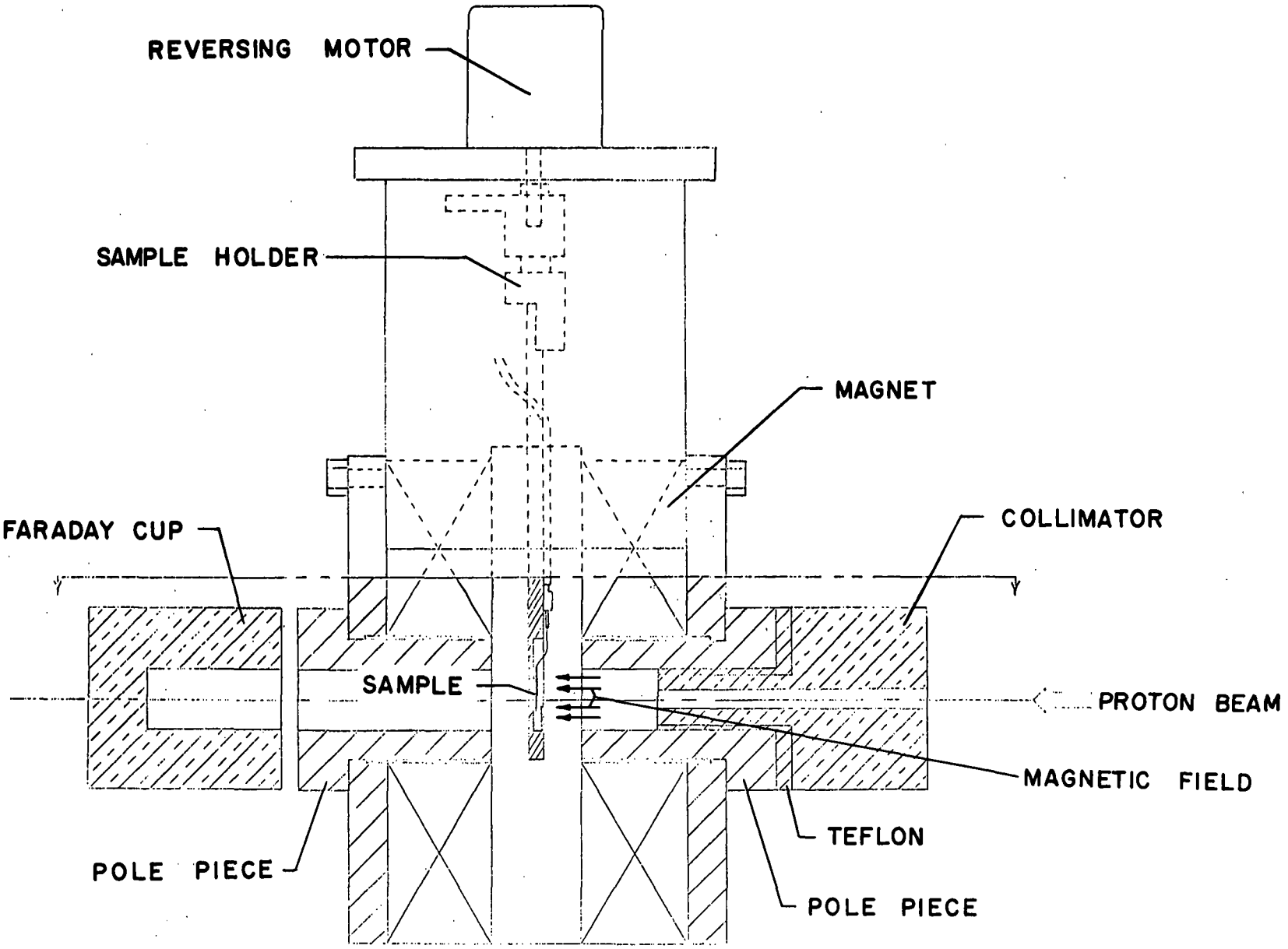

Figure 6. EXPERIMENTAL SET-UP DURING BOMBARDMENT

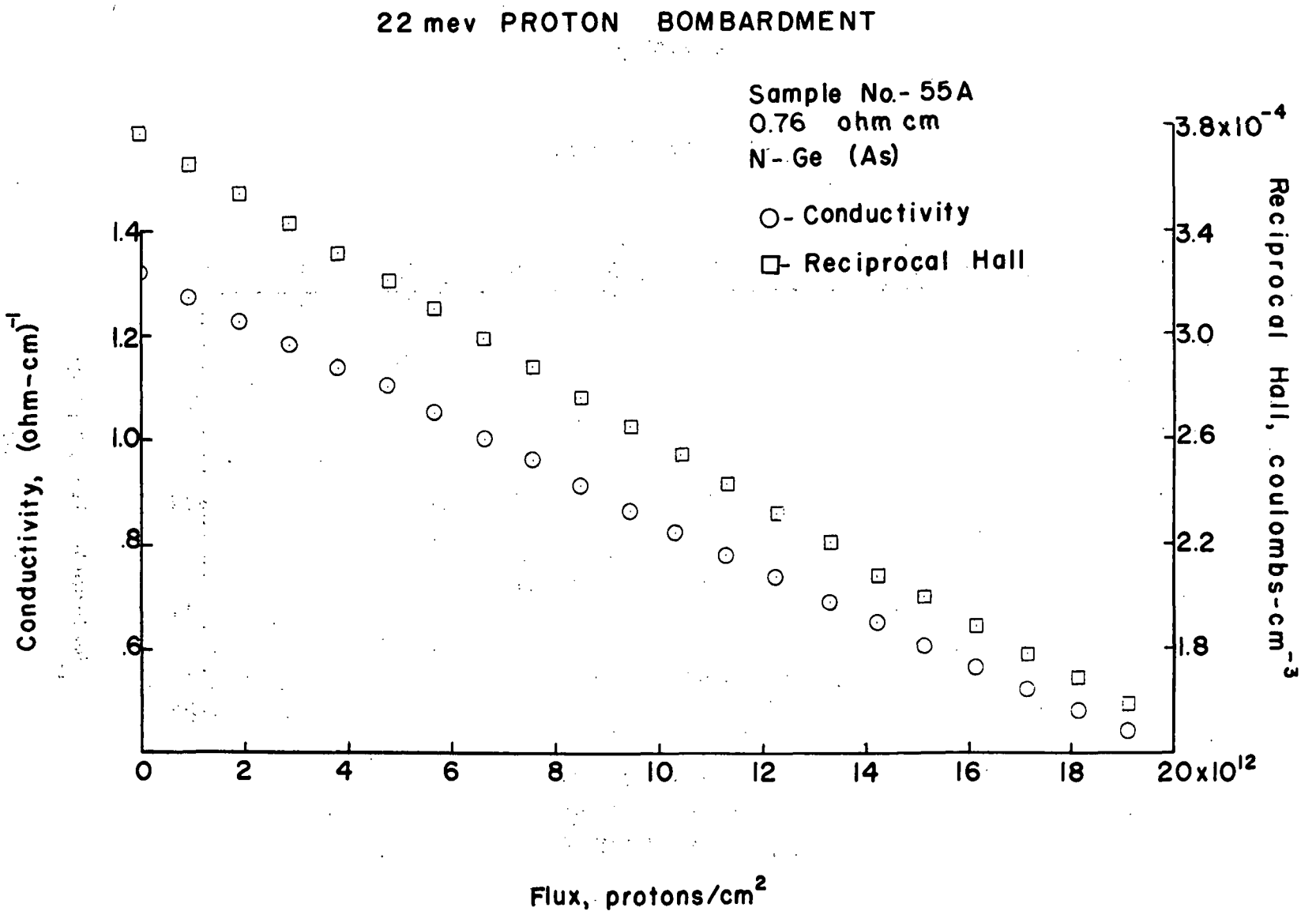
22 mev PROTON BOMBARDMENT
Sample No.- 55A
0.76 ohm cm
N- Ge (As)
○- Conductivity
□- Reciprocal Hall
Conductivity, (ohm-cm)$^{-1}$
Reciprocal Hall, coulombs-cm^{-3}
1.4
1.2
1.0
.8
.6
3.8x10^{-4}
3.4
3.0
2.6
2.2
1.8
0
2
4
6
8
10
12
14
16
18
20x10^{12}
Flux, protons/cm^2

Figure 7.

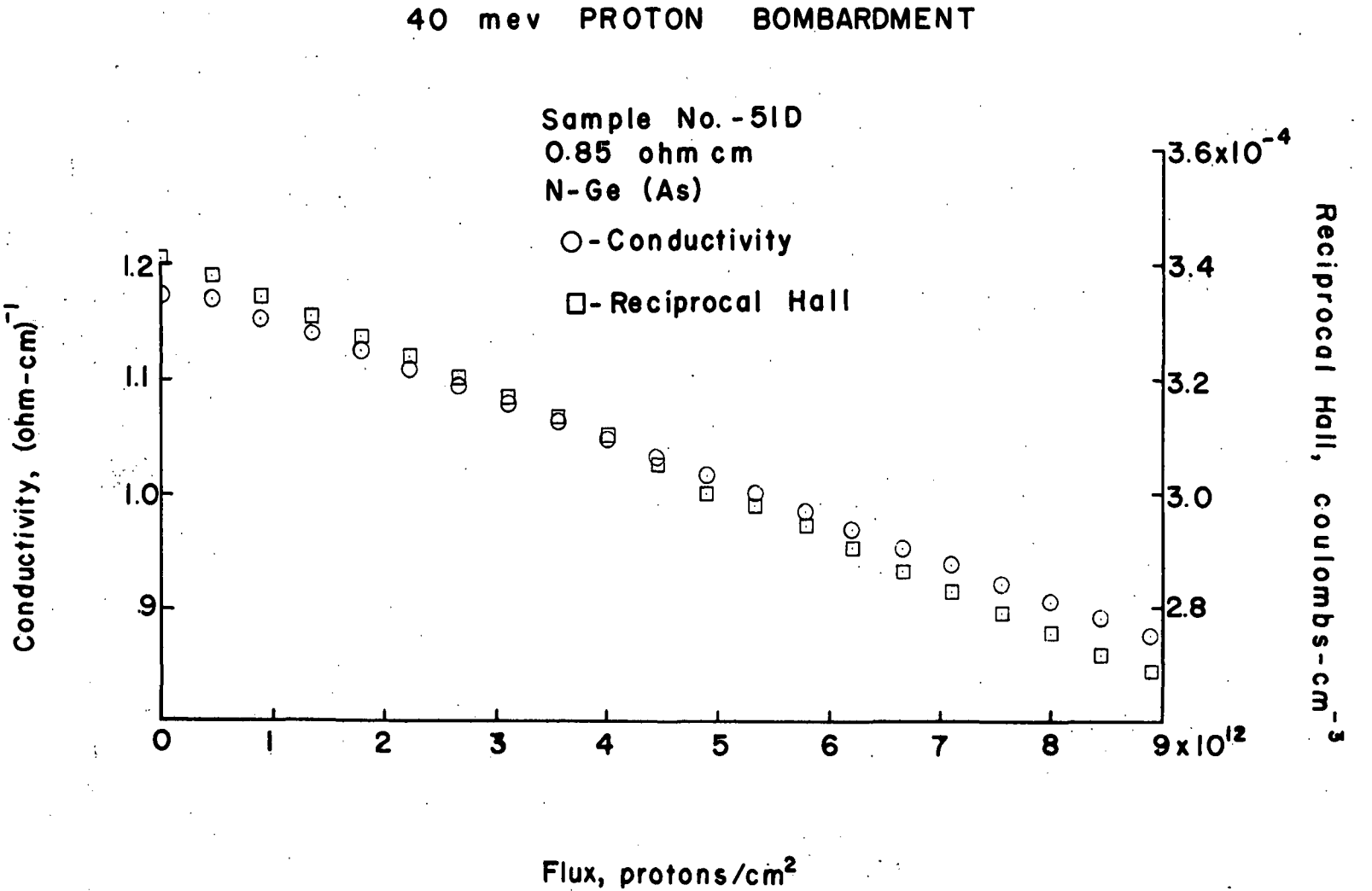
40 mev PROTON BOMBARDMENT
Sample No. -51D
0.85 ohm cm
N-Ge (As)
○ - Conductivity
□ - Reciprocal Hall
Conductivity, (ohm-cm)⁻¹
Reciprocal Hall, coulombs-cm⁻³
1.2
1.1
1.0
.9
3.6x10⁻⁴
3.4
3.2
3.0
2.8
0
1
2
3
4
5
6
7
8
9x10¹²
Flux, protons/cm²

Figure 8.

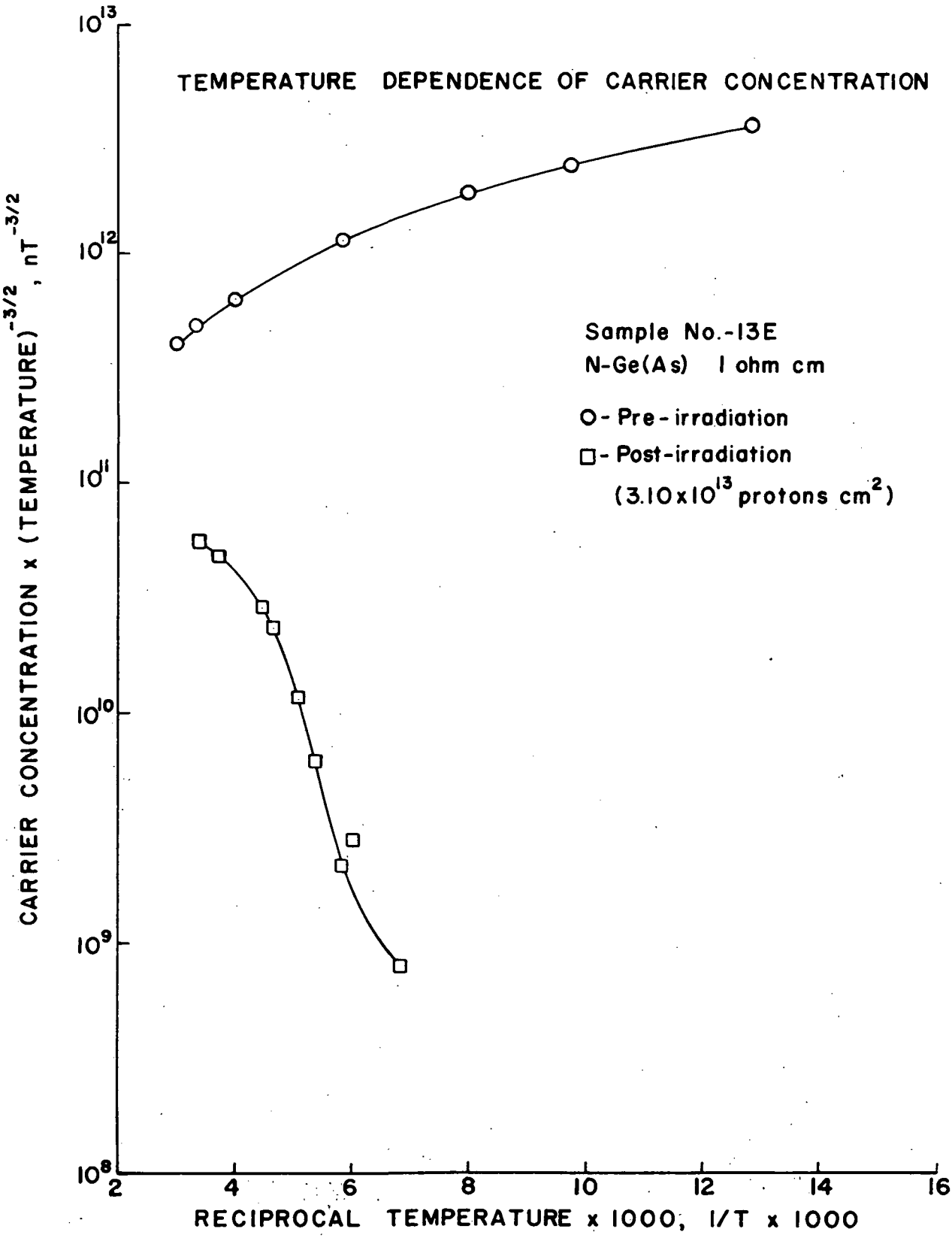
TEMPERATURE DEPENDENCE OF CARRIER CONCENTRATION
Sample No.-13E
N-Ge(As) 1 ohm cm
O- Pre-irradiation
□- Post-irradiation
(3.10x10^13 protons cm^2)
CARRIER CONCENTRATION x (TEMPERATURE)^-3/2, nT^-3/2
RECIPROCAL TEMPERATURE x 1000, 1/T x 1000
10^13
10^12
10^11
10^10
10^9
10^8
2
4
6
8
10
12
14
16

Figure 9.

INITIAL REMOVAL RATE AS A FUNCTION OF FERMI LEVEL

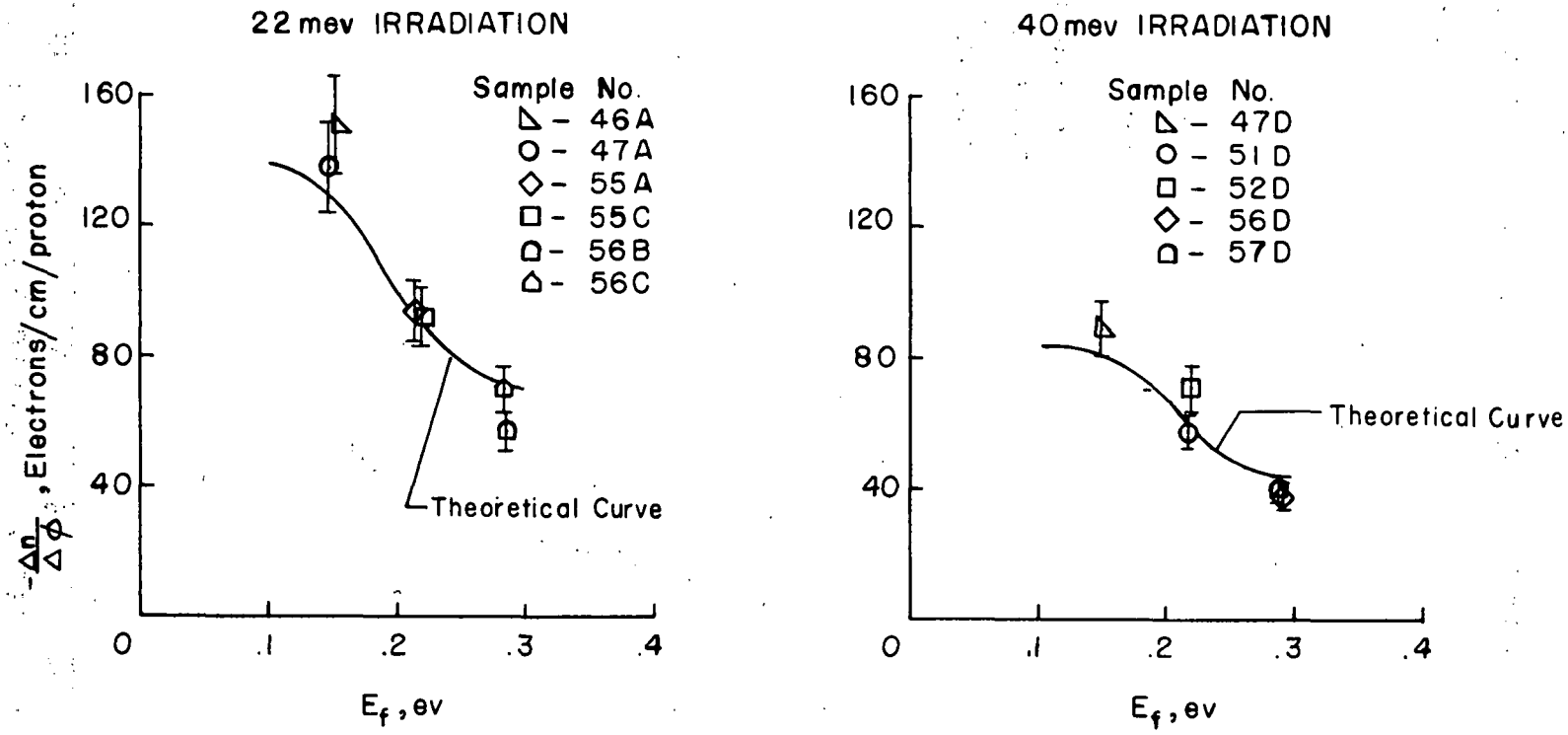

Figure 10.

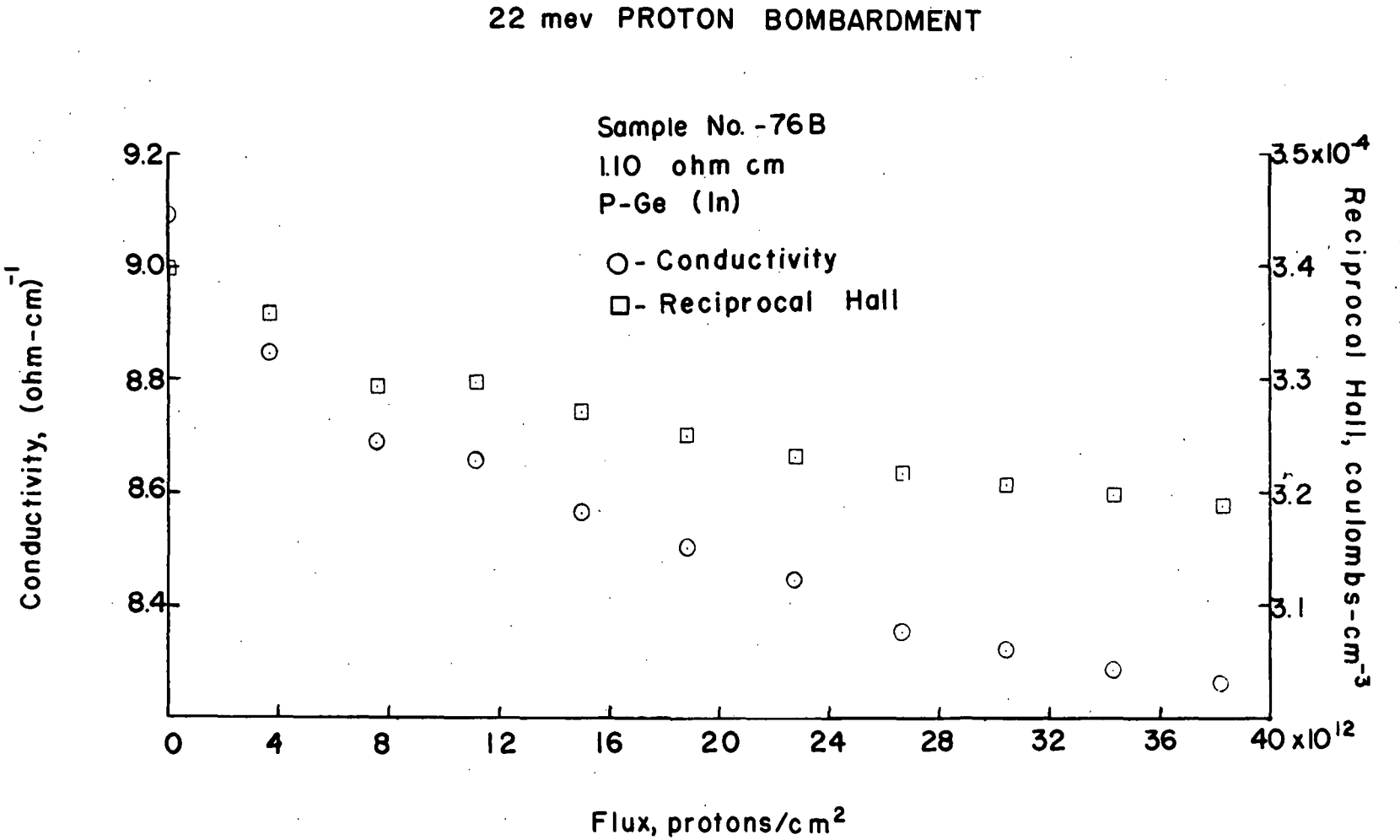
22 mev PROTON BOMBARDMENT
Sample No. -76B
1.10 ohm cm
P-Ge (In)
○ - Conductivity
□ - Reciprocal Hall
Conductivity, (ohm-cm)$^{-1}$
Reciprocal Hall, coulombs-cm^{-3}
9.2
9.0
8.8
8.6
8.4
3.5x10^{-4}
3.4
3.3
3.2
3.1
0
4
8
12
16
20
24
28
32
36
40 x10^{12}
Flux, protons/cm^2

Figure 11.

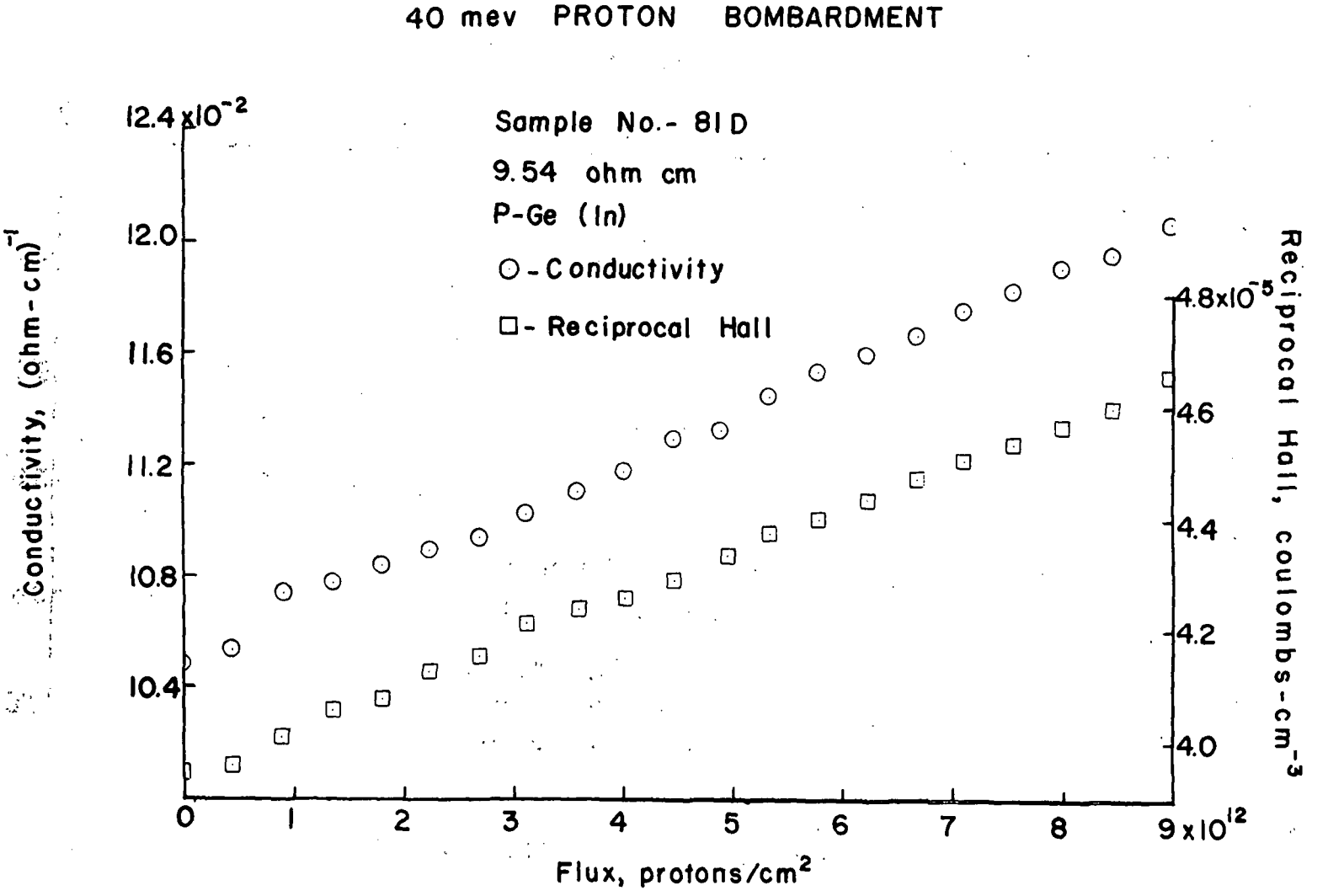
40 mev PROTON BOMBARDMENT
Sample No.- 81D
9.54 ohm cm
P-Ge (In)
⊙ - Conductivity
□ - Reciprocal Hall
Conductivity, (ohm-cm)$^{-1}$
12.4 x10^{-2}
12.0
11.6
11.2
10.8
10.4
Reciprocal Hall, coulombs-cm^{-3}
4.8x10^{-5}
4.6
4.4
4.2
4.0
0
1
2
3
4
5
6
7
8
9 x10^{12}
Flux, protons/cm^2

Figure 12.

TABLE I

INITIAL REMOVAL RATES FOR SAMPLES WITH VARYING INITIAL FERMI LEVELS

I. BOMBARDMENT WITH 22 mev PROTONS AT 299°K (n-type Ge)

CONDUCTIVITY $(ohm\text{-}cm)^{-1}$	CARRIER CONCENTRATION e/cm^3	INITIAL FERMI LEVEL ev	INITIAL REMOVAL RATE $(-dn/d\phi)_o$ (e/cm/p)	SAMPLE NUMBER
12.9	3.04×10^{16}	$E_c - 0.151$	150.3	46A
14.5	3.62×10^{16}	$E_c - 0.147$	137.3	47A
1.32	2.78×10^{15}	$E_c - 0.214$	92.9	55A
1.14	2.26×10^{15}	$E_c - 0.219$	92.0	55C
0.078	1.84×10^{14}	$E_c - 0.287$	56.8	56B
0.089	1.92×10^{14}	$E_c - 0.283$	70.2	56C

II. BOMBARDMENT WITH 40 mev PROTONS AT 296°K (n-type Ge)

CONDUCTIVITY $(ohm\text{-}cm)^{-1}$	CARRIER CONCENTRATION e/cm^3	INITIAL FERMI LEVEL ev	INITIAL REMOVAL RATE $(-dn/d\phi)_o$ (e/cm/p)	SAMPLE NUMBER
12.1	3.39×10^{16}	$E_c - 0.144$	88.3	47D
1.17	2.51×10^{15}	$E_c - 0.215$	57.0	51D
1.08	2.33×10^{15}	$E_c - 0.213$	70.8	52D
0.063	1.36×10^{14}	$E_c - 0.283$	38.0	56D
0.071	1.50×10^{14}	$E_c - 0.278$	40.4	57D

TABLE II

INITIAL REMOVAL RATES FOR SAMPLES WITH VARYING INITIAL FERMI LEVELS

I. BOMBARDMENT WITH 22 mev PROTONS AT 299°K (p - type Ge)

CONDUCTIVITY $(ohm-cm)^{-1}$	CARRIER CONCENTRATION p / cm^3	INITIAL FERMI LEVEL ev	INITIAL REMOVAL RATE $(dp/d\phi)_0$ (h/cm/p)	SAMPLE NUMBER
10.6	4.62×10^{16}	$E_v + .125$	- 25.3	71 B
8.76	3.62×10^{16}	$E_v + .132$	- 19.7	71 C
0.909	2.50×10^{15}	$E_v + .202$	- 8.0	76 B
0.946	2.67×10^{15}	$E_v + .201$	- 8.4	77 A
0.110	3.22×10^{14}	$E_v + .255$	7.3	81 B
0.126	3.50×10^{14}	$E_v + .252$	13.9	84 B

II. BOMBARDMENT WITH 40mev PROTONS AT 296°K (p - type Ge)

CONDUCTIVITY $(ohm-cm)^{-1}$	CARRIER CONCENTRATION p / cm^3	INITIAL FERMI LEVEL ev	INITIAL REMOVAL RATE $(dp/d\phi)_0$ (h/cm/p)	SAMPLE NUMBER
9.71	4.23×10^{16}	$E_v + .124$	- 21.6	71 D
11.2	5.07×10^{16}	$E_v + .120$	- 12.6	72 D
0.105	2.90×10^{14}	$E_v + .253$	5.4	81 D
0.102	2.92×10^{14}	$E_v + .253$	7.5	82 D

A METHOD FOR MEASURING THE DIFFUSION LENGTH IN SOLAR CELLS AND PRELIMINARY RESULTS

By Marvin E. Beatty* and Gerald F. Hill*
NASA Langley Research Center

ABSTRACT

Associated equipment designed for determining diffusion length in P-N junction photovoltaic devices will be described. Radiation damage data on photovoltaic devices obtained utilizing the above equipment are presented. The relative merits of diffusion length determination over the ordinary short-circuit current and power measurements for studying radiation damage are discussed. The correlation of radiation damage to devices with basic material studies is discussed with emphasis on minority carrier lifetime and defect energy level determination.

INTRODUCTION

Due to the presence of the Van Allen Radiation Belts, solar flares, and the artificial radiation belt from the nuclear bomb testing (refs. 1, 2, and 3), the effects of particulate radiation upon space vehicles have risen to one of eminent importance. The solar cell is one of the more easily damaged semiconductor devices. Since the solar cell is very important to space vehicles, it was decided that the cell should be used as the means of correlating between basic material and device studies of radiation damage in semiconductors.

The parameter chosen to observe during radiation damage to the solar cell was the diffusion length for the minority carrier of the base region of the cell. From the diffusion length the lifetime of the minority carrier can be obtained. The lifetime may be used in an appropriate experiment to determine the radiation-induced energy levels and minority carrier capture cross sections. These parameters may be used in a correlation study with similar measurements made on the same type semiconductor material using basic material study methods. It is hoped that, as a result of this correlation study, a better understanding of radiation damage phenomenon may be obtained. The end result of this type of experiment would desirably be the development of a more radiation-resistant device; therefore, the data obtained would also be beneficial in a study of radiation damage to solar cells and their improvement.

*Aerospace Technologist.

THEORY

The diffusion length is a statistical constant for a particular solar cell, and is defined as the distance to which minority carriers (electrons or holes) will move before being reduced to a factor of $1/e$ of their original value due to the recombination process. The diffusion length is a good parameter of the solar cell to observe. From an accurate measurement of the diffusion length, the lifetime may be obtained using the relation:

$$L = (D\tau)^{1/2} \tag{1}$$

where D is the diffusion coefficient in cm^2/sec. From the lifetime such quantities as the radiation-induced energy levels in the forbidden gap and minority carrier capture cross sections are determined from temperature dependent experiments (refs. 4 and 5).

The diffusion length can be determined by use of a monochromatic light source and the relation (see refs. 6, 7, and 8)

$$\frac{1}{L} = \alpha(\lambda)\left\{\frac{H[1 - R(\lambda)]}{h\nu(\lambda)Isc(\lambda)} - 1\right\} \tag{2}$$

where L is the diffusion length, α is the absorption coefficient for the particular wavelength, H is the photon flux per cm^2 incident upon the cell, $h\nu$ is the energy of the particular photons involved, and Isc is the short-circuit current obtained.

By using a 1.0-micron wavelength, whose absorption coefficient is only 110 cm^{-1}, the surface effects may be neglected and the diffusion length of the minority carrier of the base region is measured.

The diffusion length is seen to be a better parameter to observe than ordinary short-circuit current or power measurements since a change in incident light flux can be compensated for and lifetimes of minority carriers obtained.

The source of the protons used for obtaining the preliminary results was the University of Minnesota linear accelerator. The accelerator is capable of producing a time-average beam current of 10^{-8} amperes (approximately 6×10^{10} protons/sec). The cross-sectional area of the proton beam is approximately 1.25 square inches.

A schematic of the experimental setup used during irradiation is shown in figure 3. The short-circuit current from the solar cells was read with a milli-micro voltmeter. The photon flux incident upon the cells was measured with a thermopile.

DISCUSSION AND RESULTS

Good repetition was obtained with the equipment. The same measurements on the same samples were measured at various times with the results always being within ±5 percent of the initial measurement.

Eleven 1- by 2-cm solar cells were irradiated during the 40 mev test to obtain some preliminary results of the use of the equipment. Ten of the cells were silicon with efficiencies varying from 9 to 12 percent. Specimens irradiated included four 25-ohm-cm p on n, six 10-ohm-cm n on p, and one gallium arsenide solar cell.

Typical data for the diffusion length and lifetime of these cells are shown in figures 4 and 5.

The determination of low lifetimes ($\tau < 1$ microsecond) is easily obtained using this method as shown by the data. Determination of energy levels, therefore, will be possible. The data obtained also show the characteristic degradation of solar cells under radiation bombardment. Therefore, the data obtained can be used for research in solar cells, as well as a correlation study between device and basic material.

The main type of radiation damage produced in solar cell material is atomic displacements (refs. 9 and 10) in the form of Frenkel defects (vacancy interstitial pairs) which result from an atom being displaced from its normal lattice position by incident radiation. These defects cause recombination centers in the base region which results in a loss of excess minority carriers for current production. This decrease shows up as a reduction in diffusion length and lifetime of the carriers.

APPARATUS AND PROCEDURE

An apparatus was designed which would give a low level light flux of 1-micron wavelength. A tungsten photospot lamp was used as the light source. The light from this lamp was passed through a system of lenses and filters (see fig. 1) in order to reduce it to a monochromatic light source. The optical system is housed in 1/8-inch aluminum tubing to afford some protection from radiation scatter as well as collimate the light beam (see fig. 2). End plates were provided with copper coils for cooling the solar cells.

The interference filters were monopass filters with peak transmission of 36 percent.

The entire analyzer was composed of four separable parts which could be oriented to fit the desired experiment or allow maneuverability in cramped quarters.

An ion chamber was used to monitor the beam and was calibrated against a Faraday Cup by using a current integrator. The windows of the chamber were

very thin aluminized mylar which caused negligible loss to the energy of the proton beam.

REFERENCES

1. Smith, R. V., Fischer, P. C., Imhof, W. L., and Reagan, J. B.: Midas IV Proton Measurement in the Inner Van Allen Belt. (Rep.) 3-77-62-6 (Contract AF 19(604)-8028) Nuclear Physics Dept., Lockheed Missiles and Space Corporation, Feb. 1962.

2. Freden, Stanley C., and White, R. Stephen: Protons in the Earth's Magnetic Field. Phys. Rev. Letters, Vol. 3, No. 1, July 1, 1959, pp. 9-11.

3. Foelsche, Trutz: Current Estimates of Radiation Doses in Space. NASA TN D-1267, 1962.

4. Aukerman, L. W., and Reid, F. J.: Energy Levels Produced in Semiconductors by High Energy Radiation. Contract AF 33(616)-5171, Task No. 60001, Project No. 2133, Technical Memorandum No. 4, Battelle Memorial Institute, July 15, 1958.

5. Loferski, J. J., and Rappaport, P.: Radiation Damage in Ge and Si Detected by Carrier Lifetime Changes: Damage Thresholds. Phy. Rev. 111(2): pp. 432-439, July 15, 1958.

6. Cummerow, Robert L.: Photovoltaic Effect in p-n Junctions. Phys. Rev. 95(7): p. 16, July 1, 1954.

7. Oliver, J. W.: Charged Particle Radiation Damage in Semiconductors II: Minority Carrier Diffusion Analysis in Photovoltaic Devices. S.T.L. Report 8987-0001-RU-001.

8. Brooks, E. H., Cocca, U., and Seigworth, D. W.: Proton-Neutron Damage of Silicon Solar Cells. A.I.E.E. Electro-Nuclear Conference, Richland, Washington, May 1, 1963.

9. Billington, D. S., and Crawford, J. H.: Radiation Damage in Solids. Princeton University Press, 1961. a-p. 57, b-pp. 312-368.

10. Seitz, Frederick, and Koehler, J. S.: Displacement of Atoms During Irradiation. Solid State Physics, Vol. 2, Frederick Seitz and David Turnbull, eds., Academic Press, Inc. (New York), 1956, pp. 305-448.

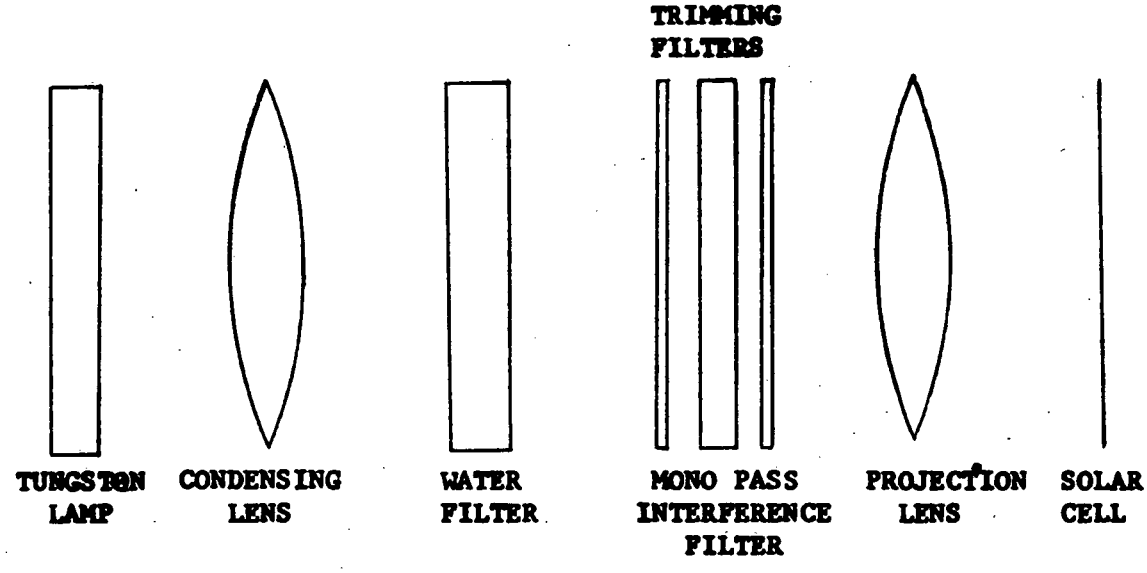

Fig. 1. Optical diagram for diffusion length analyzer.

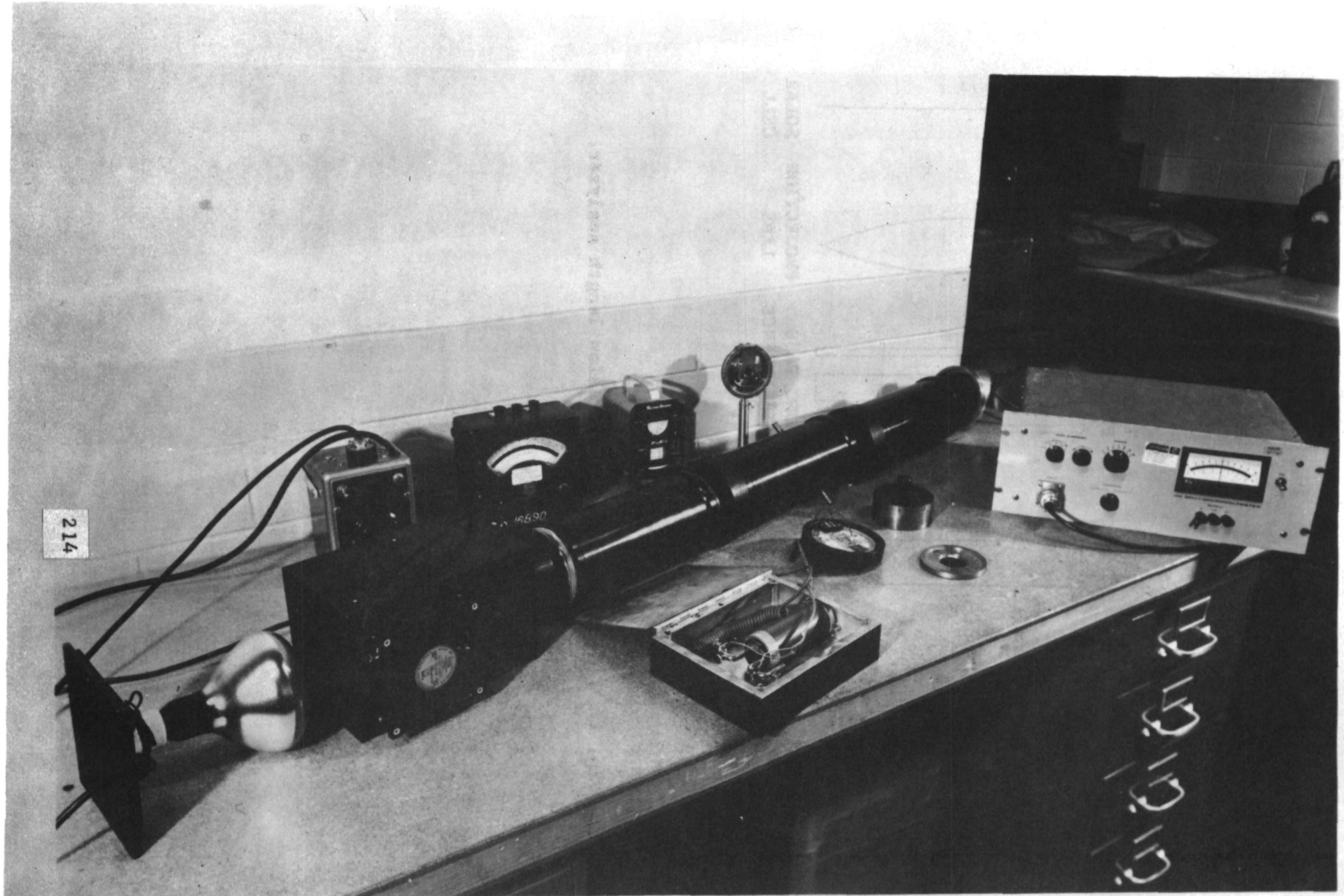

Figure 2. Diffusion length analyzer.

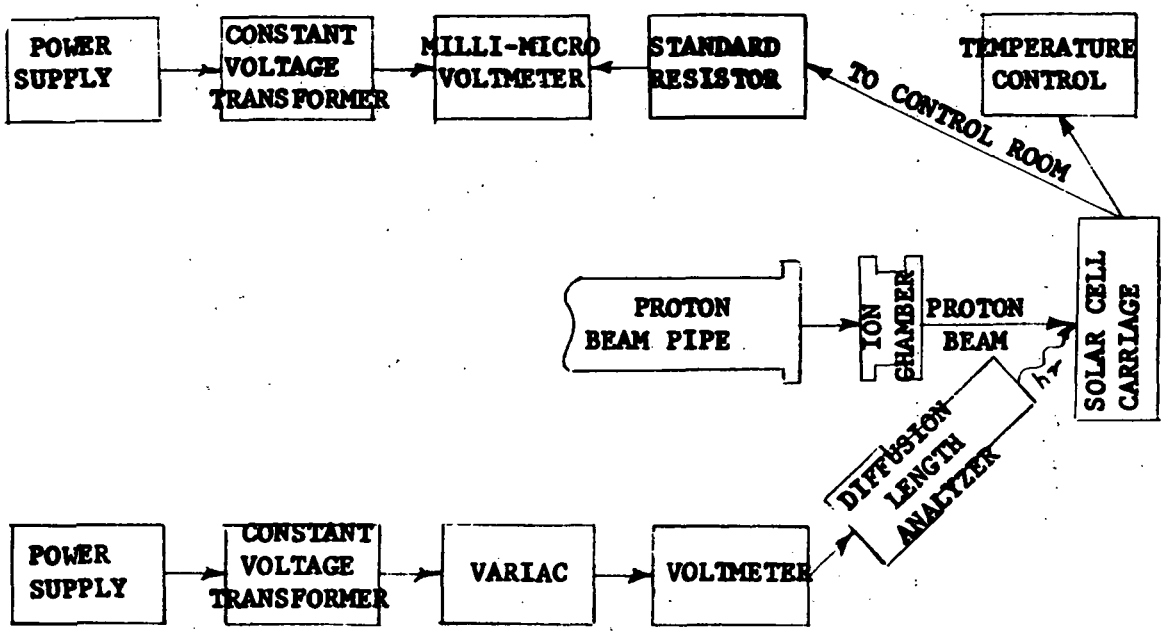

Fig. 3. Schematic diagram of readout system used in in-beam measurements.

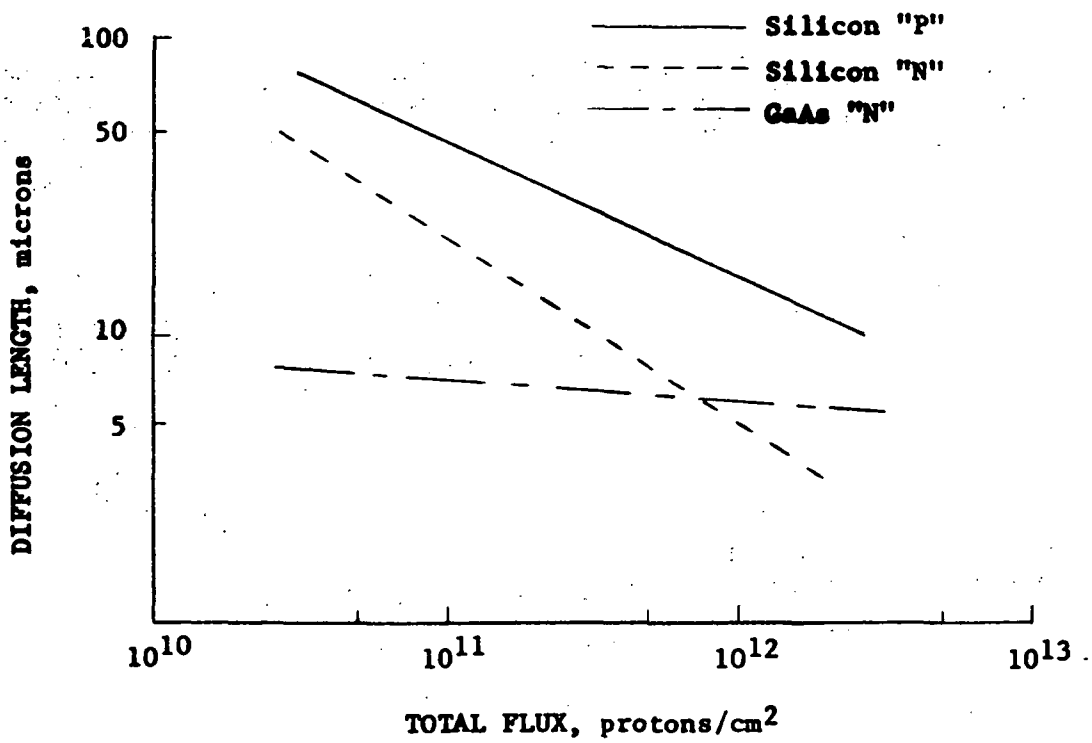

Fig. 4. Diffusion length versus total integrated flux - 40 mev protons.

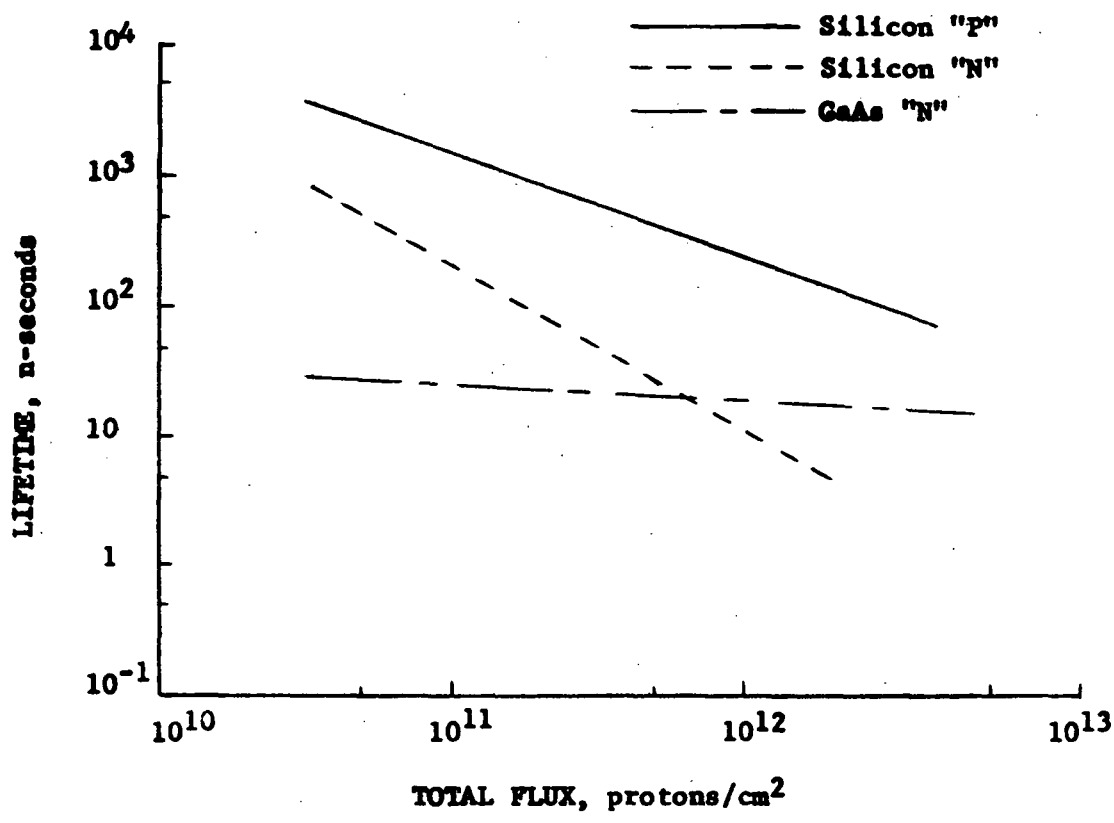

Fig. 5. Lifetime versus total integrated flux - 40 mev protons.

LOCATION OF ENERGY DEFECT LEVELS IN PROTON AND ELECTRON IRRADIATED SILICON BY MEANS OF INFRARED ABSORPTION

By Gerald F. Hill* and Marvin E. Beatty*
NASA Langley Research Center

SUMMARY

Silicon with resistivities of approximately 0.10 ohm-cm to 100 ohm-cm were irradiated with 22 Mev protons and approximately 40 Mev electrons. Preirradiation and postirradiation evaluation of the samples was made using infrared absorption from 1 micron to 25 microns at room temperature and liquid nitrogen temperature. Increased absorption was observed in the samples with resistivities of 0.10 ohm-cm, 10 ohm-cm, and 40-100 ohm-cm. The defect levels producing these absorptions have been located in the forbidden gap of the semiconductor at E_c - 0.16 ev (5.5 microns), E_c - 0.17 ev (12 microns) and E_c - 0.21 ev (1.8 microns and 3.4, 3.6 microns).

INTRODUCTION

Electrical components manufactured from semiconductor materials are subject to damage of various types when bombarded with particulate and electromagnetic radiation. Since the success of space missions frequently depends on the reliability of these components, an understanding of the damage mechanism caused by radiation will provide the information needed to minimize or eliminate these effects.

Several methods of investigating radiation damage in semiconductors have been used in the past. Energy levels produced by bombardment of silicon have been detected with the help of several methods: by plotting the rate of carrier removal versus the Fermi energy; by considering temperature dependence of the Hall coefficient; by studying mobility and lifetime; and by infrared absorption and photoconductivity (refs. 1 to 7). A vast amount of data has been obtained on irradiated silicon using the technique of infrared absorption. However, the bulk of these data has been obtained with electrons, neutrons, and deuterons. Very little, if any, data exist for proton irradiation. Since protons form a considerable part of the radiation belts and solar flares, experimental information using these particles would be particularly advantageous. The work described herein deals with the experimental investigation of silicon, a basic material used in semiconductor devices, when irradiated with protons and electrons.

---

*Aerospace Technologist.

PAGE 218 INTENTIONALLY BLANK

SYMBOLS

B	magnetic field
cm	centimeter
d	thickness
e^-	electronic charge
e	2.718
ev	electron volt
E	energy of defect level produced by irradiation
E_c	edge of conduction band
E_f	Fermi level
Eg	energy of forbidden gap
E_v	edge of valence band
f(E)	probability of occupancy for a state of energy E
g(E)	density of states function or number of states available per unit energy
h	Planck's constant $(6.625 \times 10^{-27}$ erg sec$)$
I_a	current
k	Boltzmann's constant $(1.379 \times 10^{-16}$ erg/$^oK)$
ln	natural logarithm
m	mass of electron
m_n	effective mass of electron
m_p	effective mass of hole
Mev	million electron volt
n	carrier concentration
P	momentum

p^+	concentration of holes
R_H	Hall coefficient
T	temperature
%T	percent transmission
V	voltage
β	spin degeneracy (statistical weight factor)
π	3.14
μ	micron (10^{-4} cm)

Notation:

n-type	excess electrons (doped with group V atoms)
p-type	excess holes (doped with group III atoms)

DISCUSSION OF DAMAGE THEORY

Radiation damage to solids has been analyzed theoretically in references 8 and 9. Defects in the form of atomic displacements produced primarily by charged particulate radiation give rise to electronic states or energy levels in semiconductor materials. The atomic displacements result in vacancy interstitial pairs (VI pairs). Vacancies behave as acceptors and interstitials behave as donors.

The number of energy levels introduced by radiation and their position within the forbidden gap enables one to better understand the effects of radiation on electrical components. Infrared absorption techniques permit the detection and location of these defect energy levels.

Defect levels produced by radiation cause carrier removal which shifts the position of the Fermi level. The decrease in the free carriers is the reason one observes a degradation of current when a material is irradiated. An understanding of these defect levels and their production processess will permit the development of a more radiation resistant component. It is with this in mind that the following investigation was performed.

SAMPLE PREPARATION

The silicon used in the investigation was purchased commercially in ingot form. Both float zone grown and pulled silicon were used in the investigation.

Samples were made by slicing the silicon ingot into wafers using a diamond cutoff saw. After slicing, the samples were optically polished so as to reduce the reflectance thereby increasing the transmission.

EXPERIMENTAL PROCEDURE AND METHOD OF ANALYSIS

Each sample was measured for transmission properties from 1 micron to 16 microns on an infrared spectrophotometer before irradiation. The 10 ohm-cm sample was then irradiated with 22 Mev protons to an integrated flux of 3.7×10^{13} protons/cm^2. The other samples were irradiated with 40 Mev electrons to an integrated flux of 2×10^{18} electrons/cm^2.*

After irradiation, the samples were again measured for transmission properties from 1 micron to 16 microns. The infrared absorption properties of the proton irradiated sample were made at room temperature and the electron irradiated samples were checked both at room and liquid nitrogen temperatures.

Accurate location of the Fermi level is of considerable importance when the position of the radiation induced defect level is to be determined. The position of the Fermi level can be evaluated by the method given in reference 10. This is determined by measuring the Hall coefficient which gives the carrier concentration. The Hall coefficient for the 10 ohm-cm sample used in the proton irradiation was measured in a bridge sample made from the wafer (fig. 3). The Hall coefficient was calculated from the expression

$$R_H = \left(\frac{Vd}{I_a B}\right) \times 10^8 \qquad (1)$$

The carrier concentration was determined using the result of equation (1) and the equation

$$R_H = \frac{3\pi}{8}\left(\frac{1}{e^-}\right)\left(\frac{1}{n}\right) \qquad (2)$$

For a spherical energy band in a semiconductor

$$g(E) = 4\pi\left(\frac{2m_n}{h^2}\right)^{3/2} E^{1/2} \qquad (3)$$

where $E = \frac{p^2}{2m}$ and $g(E)$ is the density of states function. Defining the function $f(E)$ as the probability of occupancy for a state of energy E we have

*Performed by Dr. John C. Corelli at Rensselaer Polytechnic Institute under grant NsG-290 sponsored by NASA.

the relationship

$$f(E) = \left[1 + \beta e^{(E-E_f)/kT}\right]^{-1} \tag{4}$$

Using equations (3) and (4) an expression for the carrier concentration of electrons can be written as

$$n = 2\left(\frac{2\pi m_n kT}{h^2}\right)^{3/2} e^{-(E_c-E_f)/kT} \tag{5}$$

Solving equation (5) for E_f an expression for the position of the Fermi level is obtained for n-type material.

$$E_f = E_c - kT \ln\left[\frac{2(2\pi m_n kT)^{3/2}}{h^3 n}\right] \tag{6}$$

and similarly for p-type material

$$E_f = kT \ln\left[\frac{2(2\pi m_p kT)^{3/2}}{h^3 p^+}\right] + E_v \tag{7}$$

RESULTS AND DISCUSSION

Figure 1 shows the preirradiation and postirradiation transmission measurements of the 10 ohm-cm sample which was irradiated with protons. Since the preirradiation transmission measurement showed a slight absorption from 6 to 7 microns, a difference in percent transmission curve was plotted (fig. 2). This shows a distinct absorption peak which occurs between 4.5μ and 7.6μ. Assuming the ionization to begin at the longer wavelength, the defect level is located at 0.16 ev below the conduction band ($E = E_c - 0.16$ ev). The probability of this defect level being occupied with electrons was found from equation (4) to be 0.736. This was using the position of the Fermi level calculated from equation (6) which was $E_f = E_c - 0.134$ ev.

Several of the electron irradiated samples exhibited distinct absorption peaks at liquid nitrogen temperature. Figure 4 shows a strong absorption peak at 1.8μ. This absorption was seen in both float zone and pulled silicon at room temperature and liquid nitrogen temperature. The defect level causing this

absorption is located at 0.21 ev below the conduction band (E_c - 0.21 ev). This level is not seen if it is populated with electrons.

Two absorption peaks were found at 3.4μ and 3.6μ (fig. 5) at liquid nitrogen temperature in a float zone grown silicon sample with a resistivity of 0.10 ohm-cm. These absorptions are caused by a defect level occupied with electrons located at E_c - 0.21 ev.

A pulled sample with a resistivity of 40 to 100 ohm-cm was checked at liquid nitrogen temperature. An absorption peak was found at 12μ (fig. 6). This level is the silicon A center found in silicon with large amounts of oxygen. The level is located at E_c - 0.17 ev. The absorption is caused by the vibration of a substitutional oxygen atom in the silicon lattice (fig. 7).

Figure 8 gives pertinent information on the samples irradiated and figure 9 shows a schematic diagram of the positions of all the defect energy levels reported.

REFERENCES

1. Fan, H. Y., and Ramdas, A. K.: Infrared Absorption and Photoconductivity in Irradiated Silicon. Jour. Appl. Phys., vol. 30, no. 8, August 1959, pp. 1127-1134.

2. Spear, W. E., McKay, J. W., Klontz, E. E., and Lark-Horovitz, K.: B.A.P.S., vol. 3, 1958, p. 141.

3. Wertheim, G. K.: Recombination Properties of Bombardment Defects in Semiconductors. Jour. Appl. Phys., vol. 30, no. 8, Aug. 1959, pp. 1166-1174.

4. Loferski, J. J., and Rappaport, P.: Electron-Bombardment Induced Recombination Centers in Germanium. Jour. Appl. Phys., vol. 30, no. 8, Aug. 1959, pp. 1181-1183.

5. Watkins, G. D., Corbett, J. W., and Walker, R. M.: Spin Resonance in Electron Irradiated Silicon. Jour. Appl. Phys., vol. 30, no. 8, Aug. 1959, pp. 1198-1203.

6. Brown, W. L., Augustyniak, W. M., and Waite, T. R.: Annealing of Radiation Defects in Semiconductors. Jour. Appl. Phys., vol. 30, no. 8, Aug. 1959, pp. 1258-1268.

7. Corbett, J. W., Watkins, G. D., Chrenko, R. M., and McDonald, R. S.: Defects in Irradiated Silicon. II. Infrared Absorption of the Si-A Center. Phys. Rev., vol. 121, no. 4, Feb. 15, 1961, pp. 1015-1022.

8. Seitz, Frederick, and Koehler, J. S.: Displacement of Atoms During Irradiation. Solid State Physics, vol. 2, Frederick Seitz and David Turnbull, eds., Academic Press, Inc. (New York), 1956, pp. 305-448.

9. Mitchell, E. W. J.: The Effects of Radiation Damage on Electronic Properties of Solids. British Jour. Appl. Phys., vol. 8, no. 5, May 1957, pp. 178-189.

10. Aukerman, L. W., and Reid, F. J.: Energy Levels Produced in Semiconductors by High-Energy Radiation. The Radiation Effects Information Center, Technical Memorandum No. 4, July 15, 1958.

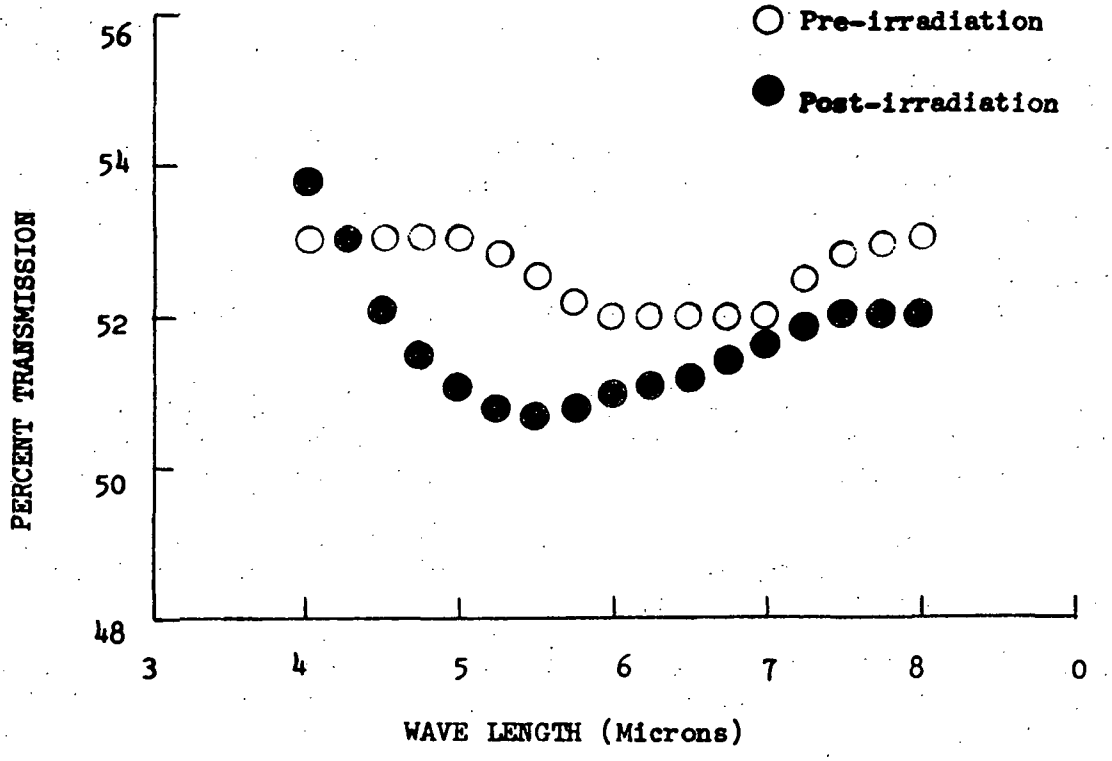

Figure 1. Transmission of 22 Mev proton irradiated n-type (phosphorous) silicon (float zone); 10 ohm-cm; flux = 3.7×10^{13} P/cm^2; thickness = 0.0356 cm; Fermi level after bombardment $E_f - E_c = 0.134$ ev at 300°K.

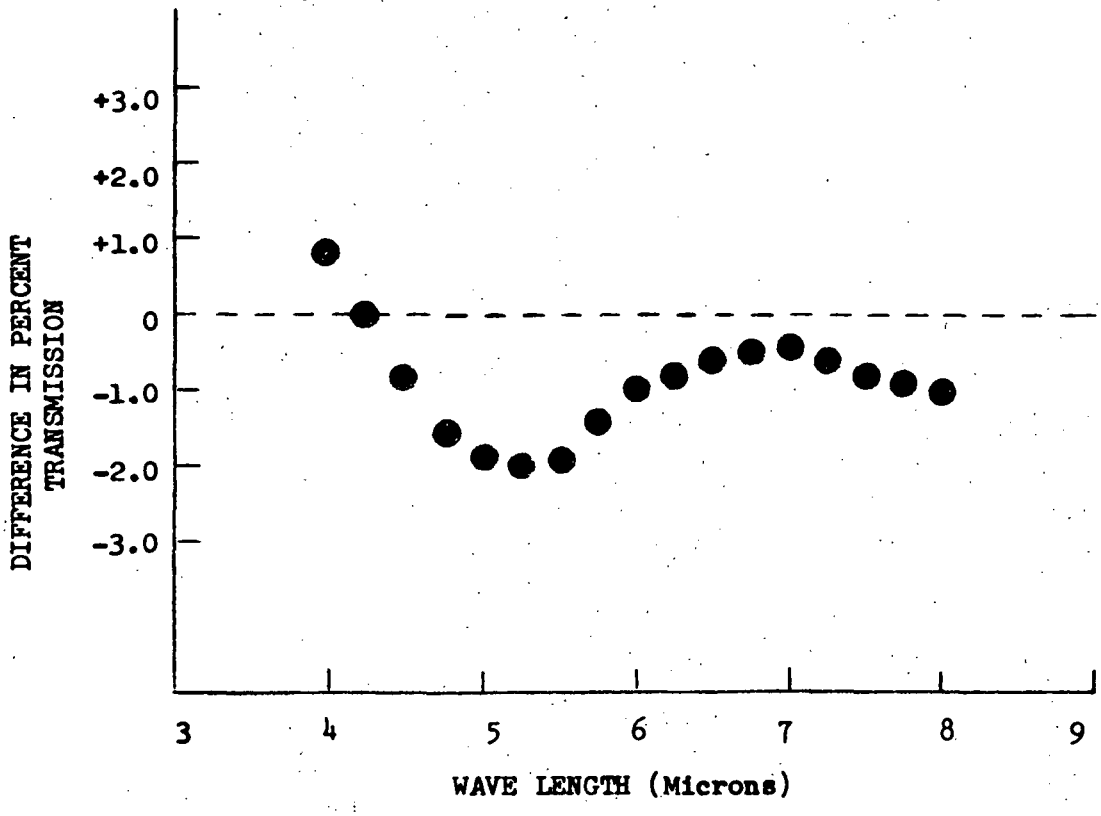

Figure 2. Difference in pre- and post-percent transmission versus wavelength for 22 mev proton irradiated n-type silicon.

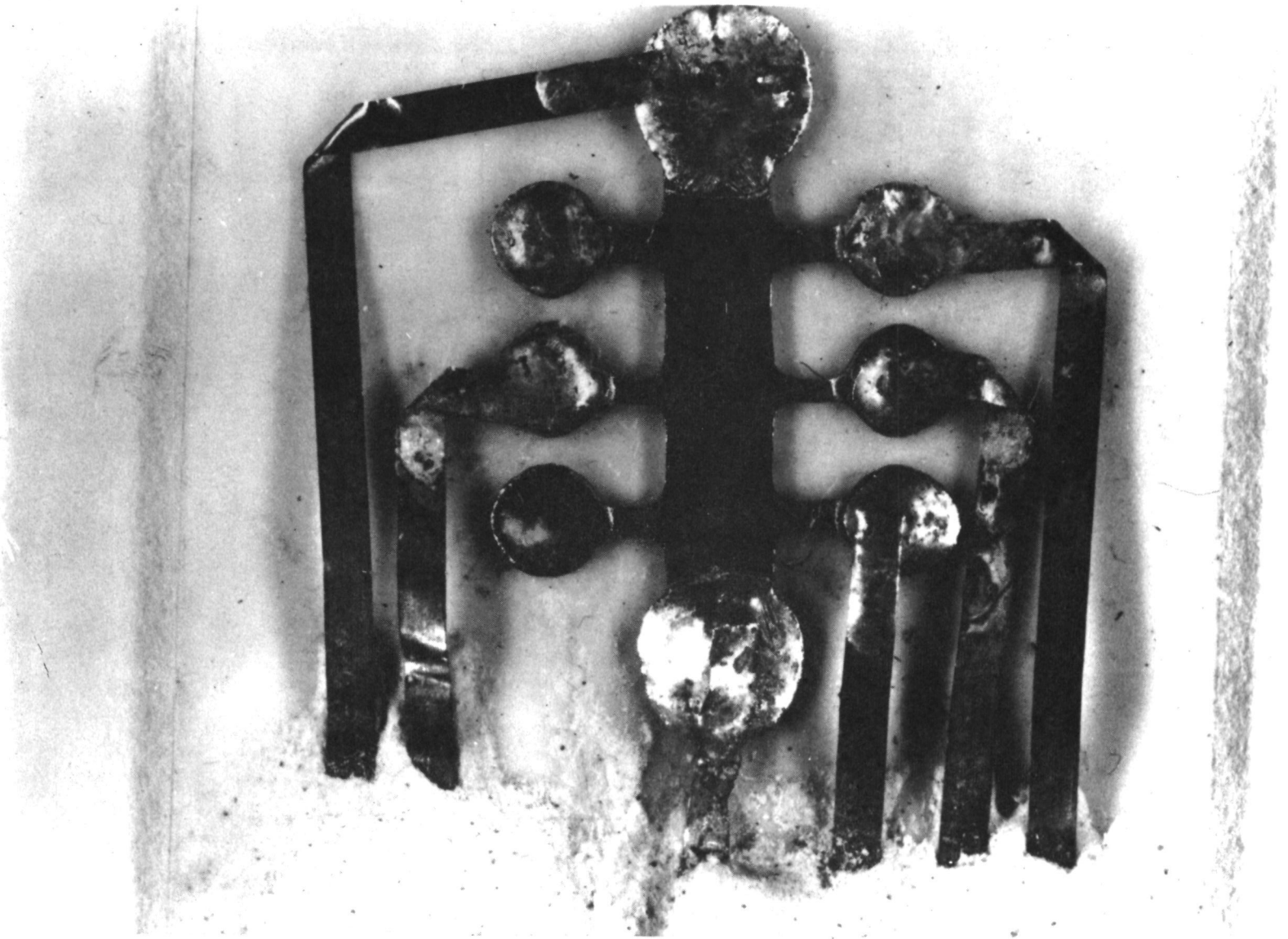

Figure 3. Bridge sample used in calculating the Hall coefficient.

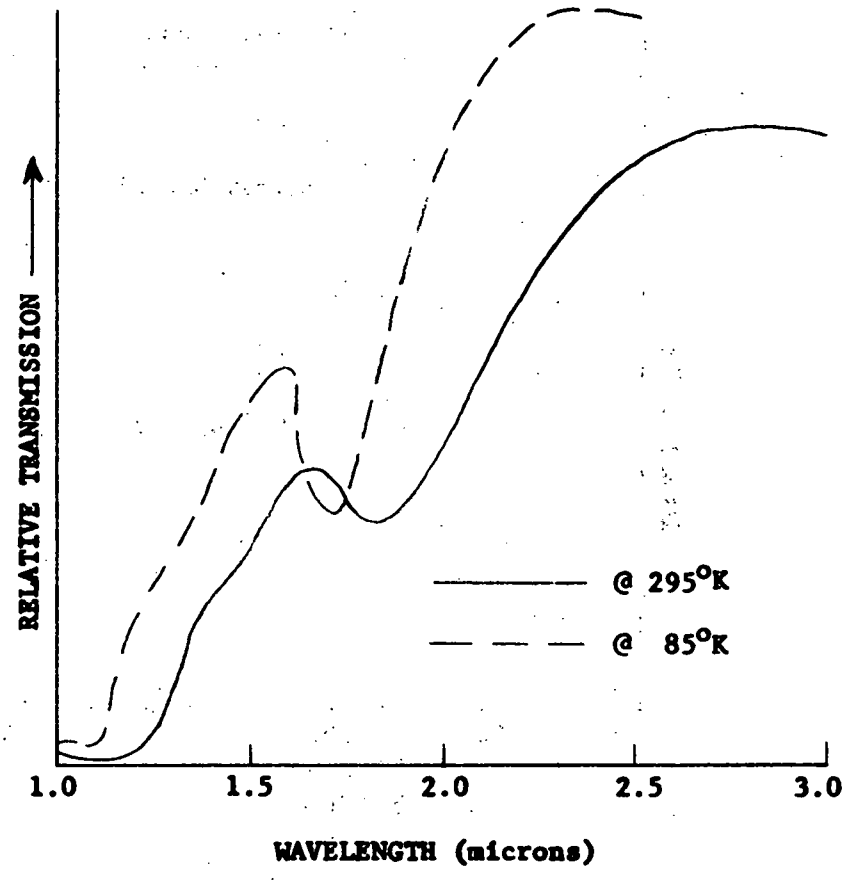

Fig. 4. Transmission of N-type silicon showing absorption peak at 1.8 microns.

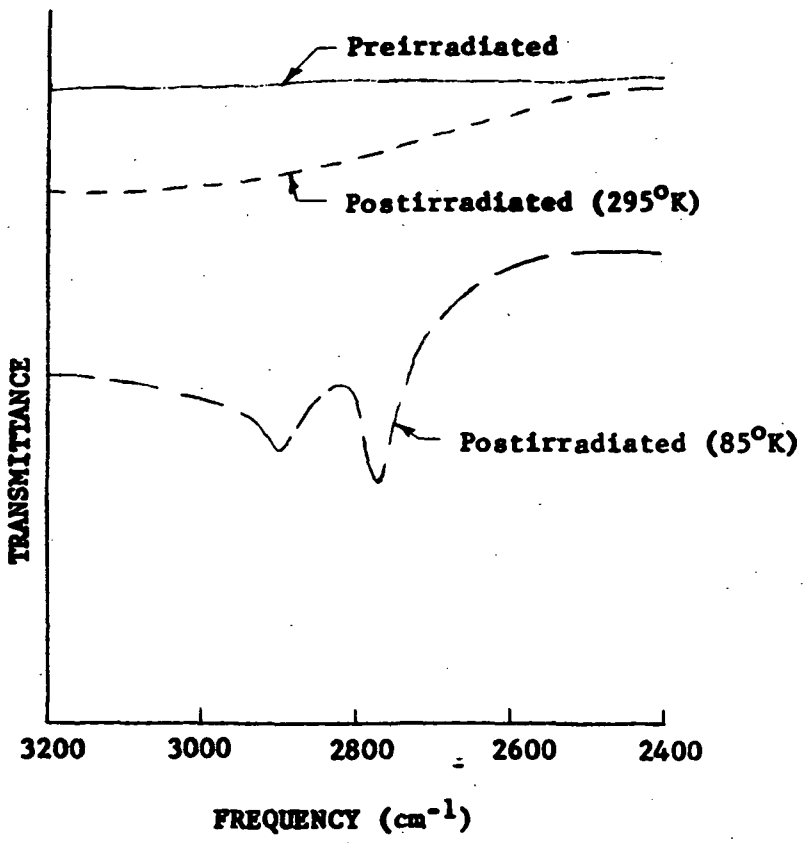

Fig. 5. Transmission of N-type silicon showing absorption peaks at 3.4 and 3.6 microns.

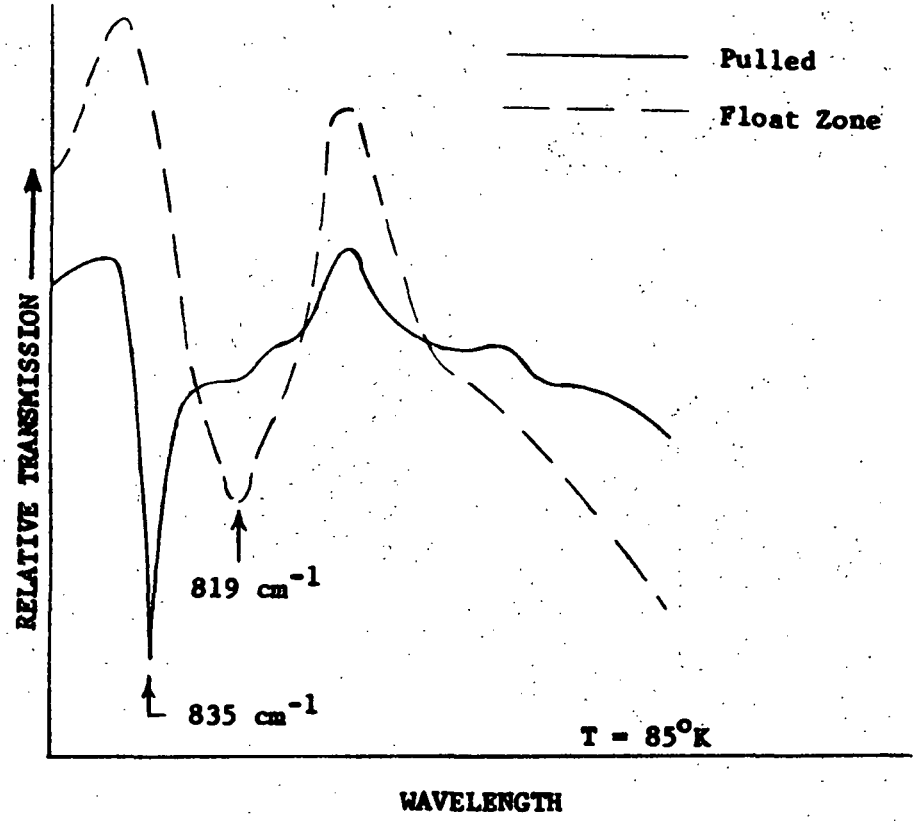

Fig. 6. Transmission of N-type silicon showing absorption peak at 835 cm^{-1} (12μ).

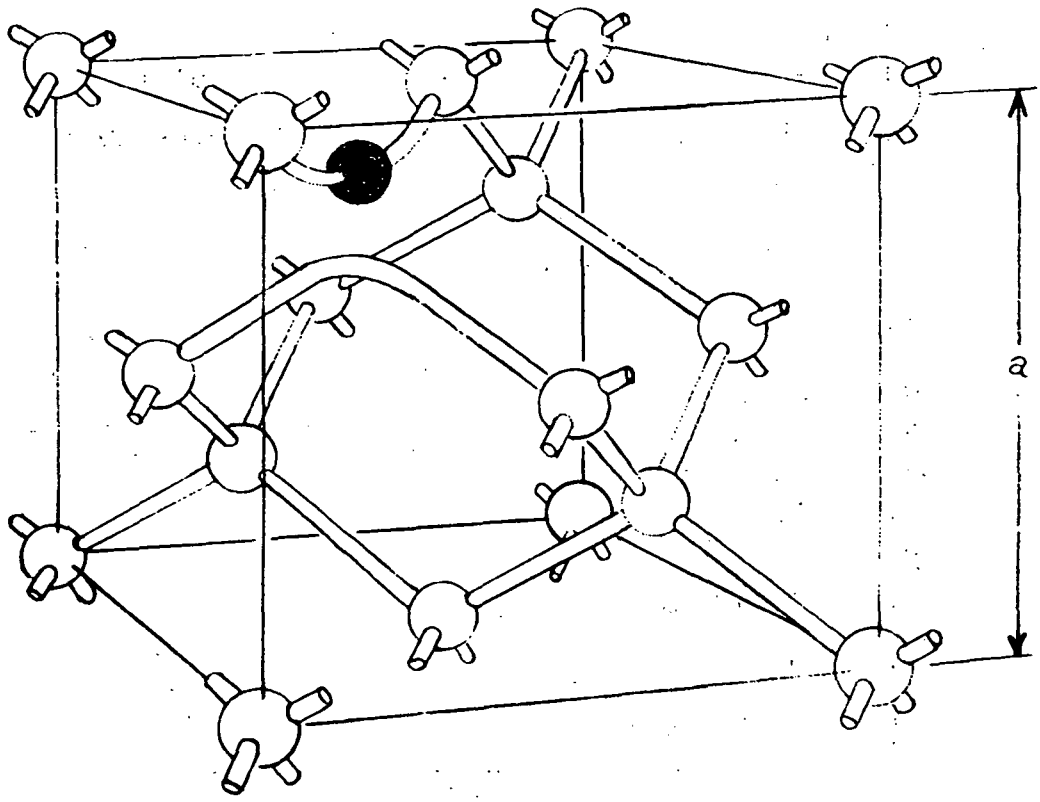

Figure 7. Silicon Unit Cell Showing Interstitial Oxygen.

Figure 8. Data For Silicon Samples Irradiated

Absorption Peak	Method Growth	Resistivity	Energy (Mev)	φt	Energy Level
1.8 μ	Pulled	40-100 Ω-cm	40	$2 \times 10^{18} e^-/cm^2$	E_c-0.21 ev
1.8 μ	Float Zone	0.10 Ω-cm			
3.4 - 3.6 μ	Float Zone	0.10 Ω-cm	40	$2 \times 10^{18} e^-/cm^2$	E_c-0.21 ev
5.5 μ	Float Zone	10.0 Ω-cm	22	3.7×10^{13} P/cm^2	E_c-0.16 ev
12 μ	Pulled	40-100 Ω-cm	40	$2 \times 10^{18} e^-/cm^2$	E_c-0.17 ev

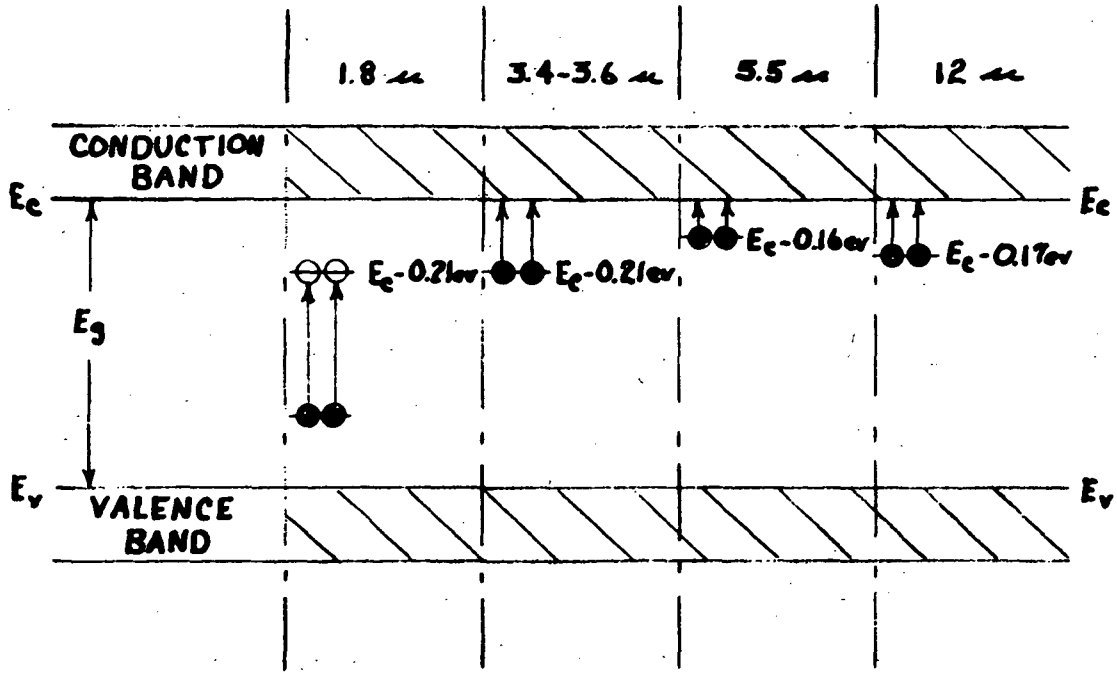

Figure 9. Schematic diagram of defect energy levels observed.

REMARKS ON DOSES OUTSIDE THE MAGNETOSPHERE, AND ON EFFECTS ESPECIALLY ON SURFACES AND PHOTOGRAPHIC FILMS

By Trutz Foelsche

NASA Langley Research Center
Langley Station, Hampton, Va.

Presented at Meeting to Discuss Charged Particle Effects
NASA, OART, March 19-20, 1964, Washington, D. C.

REMARKS ON DOSES OUTSIDE THE MAGNETOSPHERE, AND ON EFFECTS ESPECIALLY ON SURFACES AND PHOTOGRAPHIC FILMS

By Trutz Foelsche

ABSTRACT

Flare particle doses during high solar activity years of the last cycle are summarized. With respect to damage on unprotected surfaces or thin devices, an estimate of the number of low energy particles (≈1 Mev), detected during November '60 and July '61 events, for longer periods is given. The resulting number of $\approx 10^{12}$ p/cm^2 for 1 1/2 years near the earth orbit emphasizes the importance of investigating sensitive elements with particle beams of low energy and limited penetration range. Calculations of dose distributions inside a film roll behind different shielding for the lunar orbiter mission show that the tolerance level of certain fast films would be surpassed even behind 10g/cm^2 shielding during the major events of the year '59 and '60. The magnitude of effects and their dependence on particle energy are varying in wide limits for different kinds of films. With respect to the importance of photography, especially for moon and interplanetary reconnaissance missions, supplementary investigations with accelerators of effects of charged particles on different kinds of photographic films seem a research task, where additional effort is required.

INTRODUCTION

The discussions of today and yesterday dealt in great part with large doses and their effects which can occur with orbiting vehicles staying within the highly populated belts or within the magnetosphere of the earth or planets. The following remarks refer to doses and effects which we might expect outside the magnetospheres on space probes or on trips to the moon and planets.

Insofar as we know, the most intense radiation which we encounter in this more distant environment of the earth are solar flare particles. Observed are mainly protons and α of energies $E > 200$ kev, up to many Bev, in some cases, during the solar activity years. Electrons of low energy in the wake of solar events cannot be excluded e.g. electrons of ≈ 20 kev were observed outside the magnetosphere with Explorer XII after the September 28, 1961 solar event at times of a magnetic storm which indicated the arrival of a plasma cloud. The electron fluxes seem to have, however, no higher intensities and less duration than the low energy proton fluxes and would be thus less effective. Also at quiet times, as reported by J. Simpson on the basis of IMP-A experiments, electrons of $E > 150$ kev are with high probability the cause for a sharp peak of the counting rate observed within the shock layer of the solar wind in front of the magnetosphere. The main intensity of these electrons appears, of course, to be highly localized in a very thin sheet. Because of lack of more detailed data electrons are not discussed in the following.

I. Low energy flare particles and effects

The first remark, I want to make, refers to the number of low energy protons and α, which may be encountered during solar events. Their intensitives and numbers are less well known than those of flare particles of higher energy, therefore, the following estimate for longer periods is also hypothetical to a large degree. Under low energy particles are understood here protons and α of some 100 kev/nucleon to some Mev/nucleon or roughly around 1 Mev/nucleon, which may be rather effective on the surface of sensitive elements.

The high intensities and the presence for appreciable duration of the influx of such low energy particles was first detected during the Nov 12, 1960 event (See Figure 1) with rockets by Ogilvie, Bryant, and Davis (Ref 1).

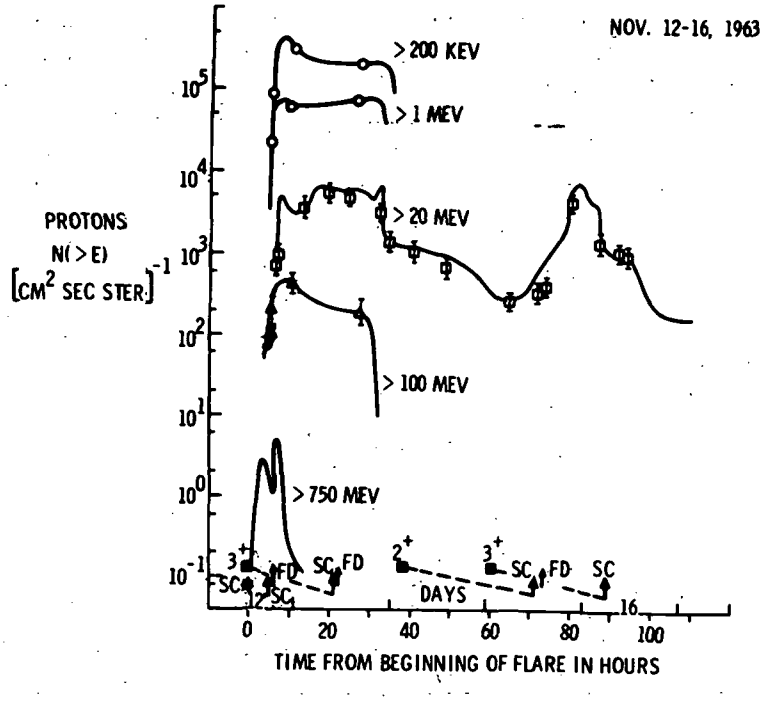

Figure 1.- Time profiles of intensities of particles above different energies during the November 12, 1960 event.

They are not detectable by ionospheric measurements with riometers or short wave scattering networks.

The maximum fluxes observed are: $E > 200$ kev of 2×10^5 p/cm^2 sec ster and $E > 1$ Mev of 6×10^4 p/cm^2 sec ster continuously for about 24 hours. Integrated over the time there are obtained

$E > 200$ Mev $\approx 3 \times 10^{11}$ p/cm^2 $\approx 10^6$ rad

$E > 1$ Mev $\approx 10^{11}$ p/cm^2 $\approx 60{,}000$ rad

Such low energy protons were again later on found in most events, as by Pieper et al. (Ref 2) with Satellite Injun I on July 12, 1961 and by Hoffman, Davis and Williamson (Ref 4) and Bryant, Cline, Desai and McDonald (Ref 5) on September 30, 1961. In the latter case the vehide was outside the magnetosphere.

For the July 12 event (See Figure 2) by integrating over time $\approx 2 \times 10^{10}$ p/cm^2 $E > 1$ Mev are obtained.

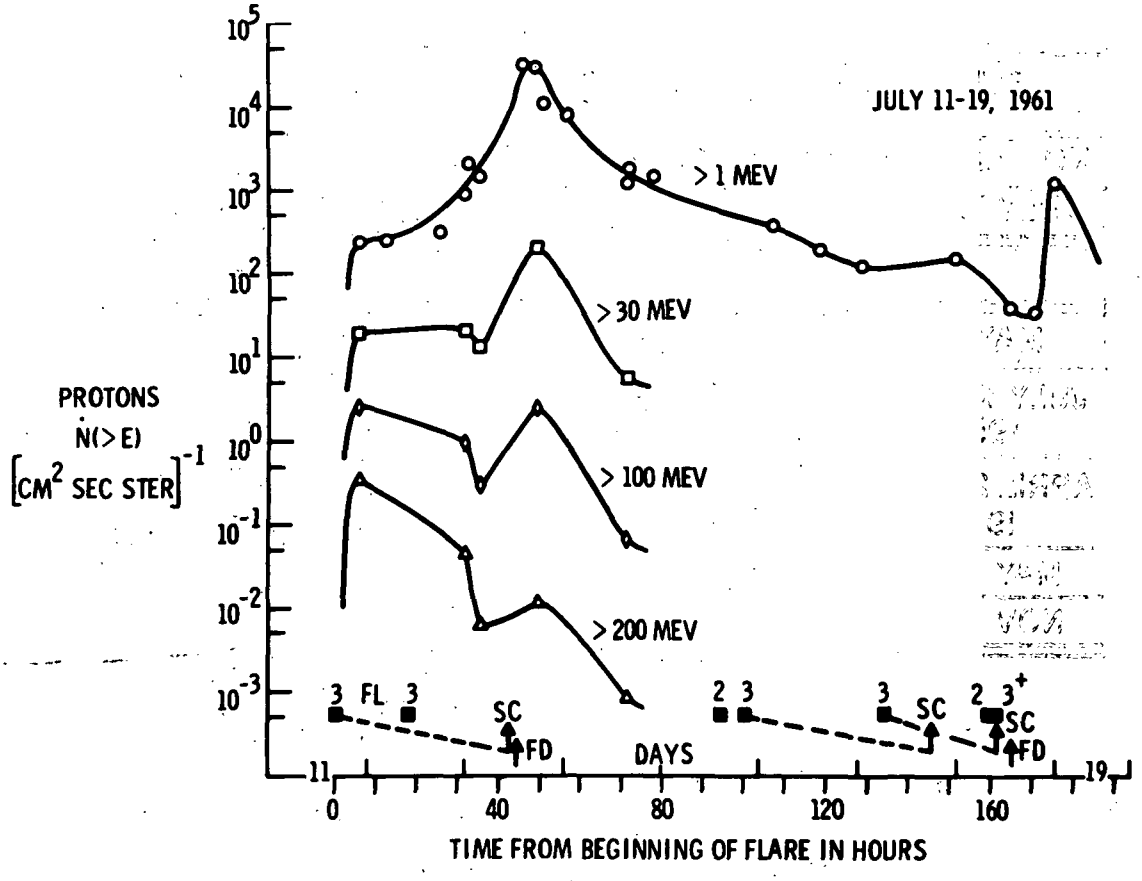

Figure 2.-Time profiles of intensities during July 11-14, 1961. (Derived from Ref. 2, Pieper et al and Ref. 3 Freier and Webber)

NASA

We assume in the following that also in the cases of July '61, November '60 and earlier the particles are not accelerated near or within the magnetosphere but are generally contained in large magnetic clouds which arrive from the sun after Type IV radio noise flare events. Type IV noise is considered as indicative that particles are accelerated on the sun during the flare. These assumptions are not proven. They serve here to obtain an estimate toward the safe side, what number of particles might be expected outside the magnetosphere for an extended period of time of high solar activity.

With these assumptions for longer periods of solar activity as the 1 1/2 year period from May 1959 to November 1960 one arrives at about

4×10^{11} to 10^{12} proton/cm^2 > 1 Mev

(or $\approx 3 \times 10^6$ rad on the surface of material from particles E > 1 Mev), according to the table Figure 3. (For details see Ref 6).

Figure 3.- Time Integrated Fluxes of Low Energy Protons E > 1 Mev During the Period May 1959 to November 1960 under the Assumptions Outlined in the Text

EVENT	db	DURATION OF MAX. PHASE	k_p	P/cm^2 >200KEV	P/cm^2 >1 MEV
NOV 12, 1960	>20	24 hr	9	2.8×10^{11}	7×10^{10}
JULY 12, 1961	≥14	≈12 hr	8+		1.8×10^{10}
		MAY 59 – NOV 60			
MAY 10	>20	36 hr	6	1.1×10^{12}	2.8×10^{11}
JULY 10, 14, 16 1959	>20	≈3×24 hr	7, >9, 9		
APRIL 28- MAY 1960	12	6-12 hr (1 OF 4 EVENTS)	9		3.6×10^{10}
MAY 6-15	12	6-12 hr	9		
NOV 12, 15	≈20	24, 10 hr	9,8	2.8×10^{11}	9×10^{10}
				1.4×10^{12}	4×10^{11}/cm^2

These are just threshold doses for permanent effects on sensitive devices as solar cells, infra-red sensors and solid state particle detectors itself, which later have to be exposed directly without protection to measure low energy particles. In Figure 4 the orders of magnitude of threshold doses for permanent effects on certain elements are recalled.

FIGURE 4 THRESHOLD DOSES FOR EFFECTS ON MATERIALS.

Material	Primarily affected by	Protons per cm^2	Dose, rad	Damage	Reference
Solar cells; Transistors:	Displacements			30% decrease in gain	(13, 14)
Ge (low frequency)		4 times 10^{11}	10^5		
Field transistors		to 8 times 10^{12}	to 2 times 10^5		
Glasses	Displacements + ionization	3 times 10^9 to 3 times 10^{14}	10^3 to 10^8	Optical transmission affected	(15, 16)
Plastics:					
Teflon	Ionization	3 times 10^{11}	10^5	Electrical (useless) mechanical	(15, 16)
Mylar, Polystyrene		to 3 times 10^{15}	to 10^9	Still usable	

In discussing effects of these low energy protons it must be realized, that the penetration depth of 1 Mev protons is only 13 μ in Aluminum and of comparable magnitude in Silicon. The effects of Figure 4 are measured with particles of higher energy, which penetrate the hole specimens. The effect may therefore be different. Although e.g. the junction layer in solar cells is only in 1 μ depth from the surface and the specific ionization of low energy protons is higher by about a factor 10, their effect may be less because the bulk of the material is not affected. Additional effort on the investigation of permanent and transient effects of low energy protons and α should therefore be warranted. The low energy particles are not only in comparable intensities permanently present within the belts, but may have according the foregoing without protection measures significant effects outside the magnetosphere especially when the spacecraft approaches the sun more closely, where a considerable

increase of their number should be expected. Also transient effects, for instance charge storage and discharges in thin dielectrica should occur even in a higher degree as with electrons of equal energy and may lead to failures.

Figure 5, (July '59) shows rough data on the intensity time profiles of the July '59 events. It is recalled that solar events occur often in groups or short succession after long silent periods, thus during those events no substantial recovery is expected. Three strong events with a main phase of 24 hours each occurred on July 10th, 14th, 16th within one week. Low fluxes were observed still after 2 weeks. The upper curves show riometer records which indicate the intensity of particles above ≈ 10 - 20 Mev energy. The lower curves are measurement in balloons in Minnesota and Fort Churchill indicate the intensities above ≈ 100 Mev in the decreasing phases of the events mainly.

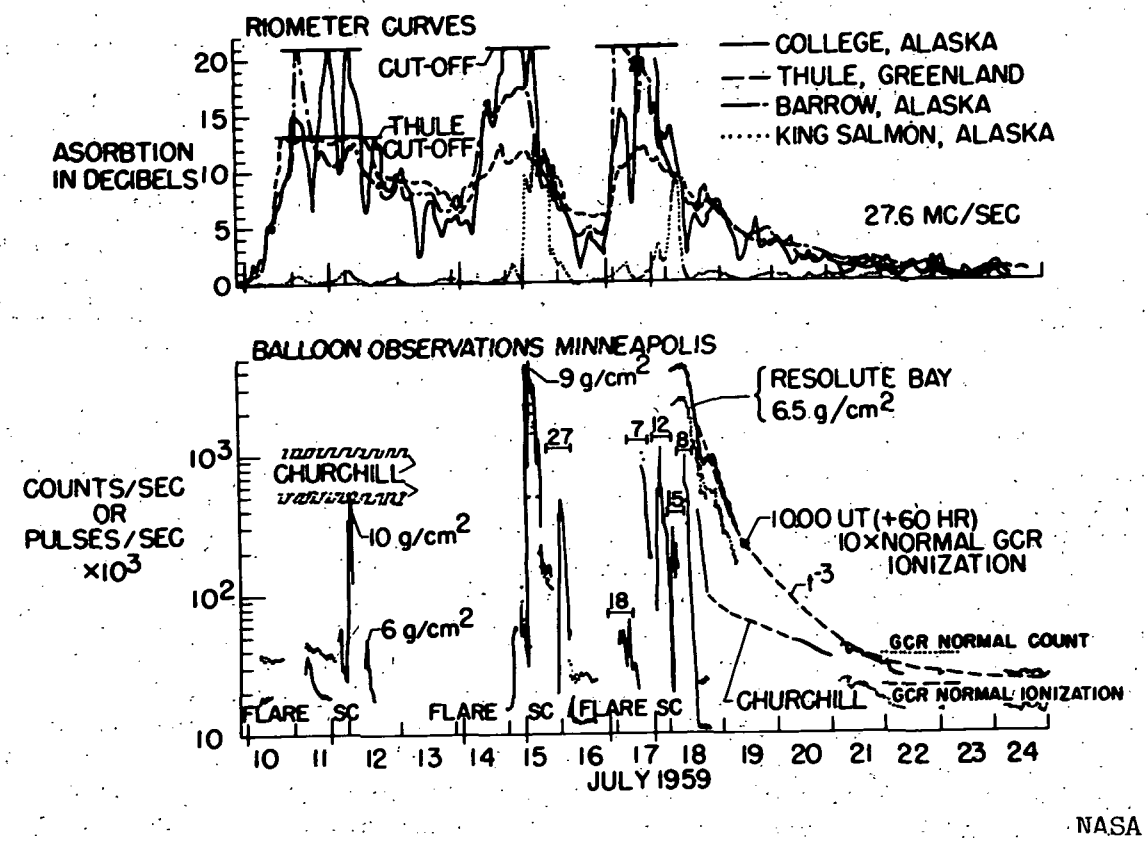

NASA

Figure 5.- Balloon measurements (see **Winckler**, J. R., et al., ref 7 and Anderson, K. A., et al., ref 8) and riometer records (see Reid, G. C., and Leinbach, H., ref 9) during the July 10th, 14th, and 16th solar events.

II. Doses inside a vehicle in outer space and their effects especially on photographic films.

The second remark refers to doses inside a vehicle or inside amounts of shielding in the order of 1/2 - 20 g/cm^2. If one increases the shielding thickness or inside thicker objects the dose falls off very fast in most events. (Figure 6).

Figure 6.-SUMMARY OF FLARE DOSES FOR THE PERIOD OF $1\frac{1}{2}$ YEARS MAY 1959 TO NOVEMBER 1960. IN THE THIRD COLUMN OF EACH SECTION SKIN DOSES ARE GIVEN, TAKING SELFSHIELDING OF MAN'S BODY INTO ACCOUNT BY A FACTOR OF 1/2. THE DOSES IN THE LAST COLUMN ARE DOSES IN THE CENTER OF A SPHERICAL BODY PHANTOM OF 15 cm RADIUS INSIDE A SPHERICAL SHIELD OF 5g/cm^2 THICKNESS

(NEGLECTING SELF-SHIELDING)

OUTER SHIELD	0.5 g/cm^2			1 g/cm^2			2 g/cm^2			6 g/cm^2			20 g/cm^2	
* DOSE, LIMITS	RAD UPPER	RAD LOWER	1/2	RAD UPPER	RAD LOWER	1/2	RAD UPPER	RAD LOWER	1/2	RAD UPPER	RAD LOWER	1/2	RAD UPPER	RAD LOWER
EVENTS:														
MAY 10, 59	≈ 3,700		≈ 1,850	≈ 1,100		≈ 550	≈ 360		≈ 180	≈ 38		≈ 19	≈ 1.1	
JULY 10, 59	≈ 1,000		≈ 500	≈ 450		≈ 225	≈ 240		≈ 120	≈ 47		≈ 23	≈ 3.8	
JULY 14, 59	2,400	1,600	1,000	1,020	780	450	458	305	190	105	70	44	8.7	5.8
JULY 16, 59	2,600	1,300	975	1,000	500	375	400	200	150	76	38	29	5.5	2.7
Σ JULY			≈ 2,475			≈ 1,050			≈ 460			≈ 96		
NOV. 12, 60	≈ 2,700		≈ 1,350	≈ 1,500		≈ 750	≈ 680		≈ 340	≈ 115		≈ 58	≈ 10.5	
NOV. 15, 60	≈ 1,300		≈ 650	≈ 750		≈ 375	≈ 300		≈ 150	≈ 57		≈ 29	≈ 5	
Σ DOSES	13,700	11,600	≈ 6,325	5,820	5,080	≈ 2,725	2,438	2,085	≈ 1,130	438	365	≈ 202	34.6	28.9

*The doses are derived from measurements within the earth magnetosphere, which was disturbed and may have modulated the intensities during part of the time of the events. In free space the doses might have been higher than the upper limits given in the table.

The table Figure 6 shows the doses behind distant spherical shields of different thicknesses for the largest events or event groups observed so far - except for the February '56 event - which occurred in 1 1/2 years from May '59 - November '60. The much more energetic and therefore penetrant February '56 event is not included and is discussed later on. As shown before, the doses on the surface are in the order of 10^5 to 10^6 rad for one extreme event; this is however only on the very surface. With 1/2 g/cm^2 distant shield the dose is already decreased to some 1000 rad. Behind 2 g/cm^2 such event groups as in July '59 and November '60 would

produce in 1 week on the surface of objects which are largely shielded from one side about 500 rad, behind $6 g/cm^2$ about 100-200 rad. (These values are taken from the third column in Figure 6, where self shielding from a solid angle 2 is roughly taken into account by a factor 1/2).

Although these doses are small they are except for their biological significance of major importance for such sensitive devices as e.g. photoemulsions or ordinary photographic films, which are an important tool in some space missions. This is especially true for instrumented probes, when the vehicle itself grants generally only shielding in the order of $1 g/cm^2$ or less from a large solid angle. One has to calculate in such a case carefully, what doses behind different amounts of shielding would occur, if photography is an integral or main part of a mission during solar activity years. In the next figure as example the dose distributions within a film roll in a lunar reconnaissance vehicle with $2 g/cm^2$ distant wall, are given (Figure 7).

Figure 7.- Upper limits of doses on the surface and in the center of a film sphere surrounded by additional shields for the largest solar event groups of the Sunspot cycle 1954-1964.

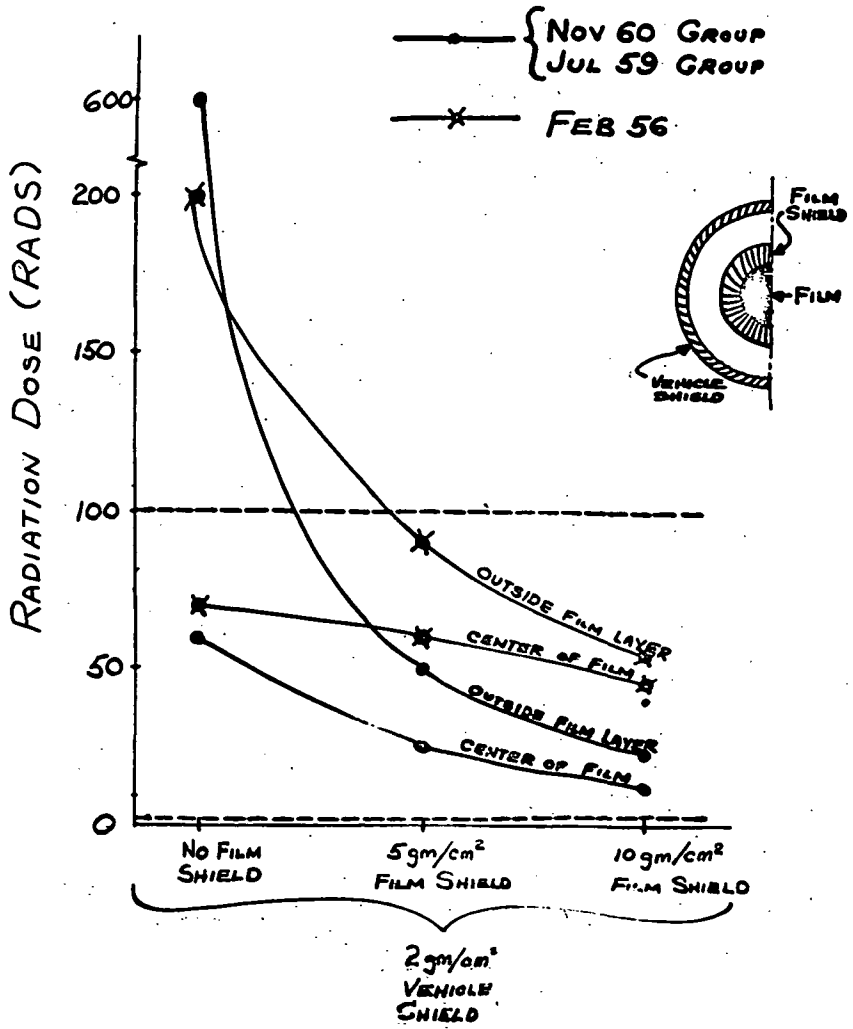

Estimated are the doses in the surface of the film package and in the center assuming spherical geometry if surrounded by a close fitting additional spherical shield of 0 - 10g/cm^2. This is done for the largest event groups of the last cycle. The doses are upper limits, based on upper limits of number spectra as used in Table Figure 6 (Ref 6) which are considered as trustworthy to a factor 1/2. The event groups of both July '59 and November '60 give about the same dose distribution. February '56 was obviously a far more penetrant event, which occurred of course only one time with such high intensity during the last cycle.

To cite some numbers; at 10g/cm^2 shield the dose in the center is still in between 10 and 40 rad for one of these events or event groups. The horizontal lines in the picture are the tolerance levels of different films for 1 Mev x-radiation. One sees that the tolerance level of the fast film of 3r is surpassed even at 10g/cm^2 additional shielding-assuming that the effects of equal doses of x- and proton radiations are the same - also if one uses lower limits of doses. The slow film may favorably have about 5g/cm^2 additional shielding if its tolerance level of 100 r shall not be surpassed. The effect of 1 Mev x-radiation and the tolerance levels on a fast and a slow film are shown in Figure 8.

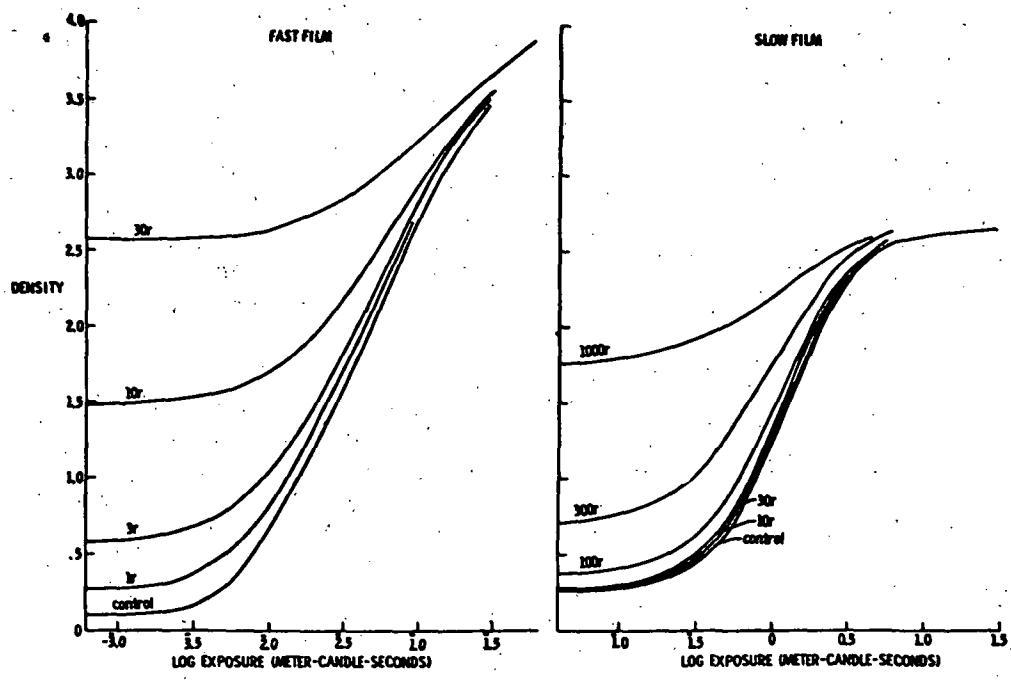

Figure 8.- Film density curves after preirradiation with 1 Mev x-radiation.

The curves show density, i.e. the logarithm of the ratio of transmission before and after exposure, as function of light exposure taken after pre-irradiation with different amounts of 1 Mev x-radiation.

Considering the fast film (left) 3 r would already substantially degrade the slope in the lower part of the density curve. For the slow film 100 r would be tolerable without jeopardizing the mission. The tolerance levels are valid for energetic γ- irradiation or $\approx$ 1 Mev x-radiation. It remains the question if 3 rad or 100 rad of proton particle radiation have the same effect on the considered films than 3 r or 100 r of energetic x-radiation. This is apparently not in general the case. Certain slow and fast commerical films respond different to γ-radiation than to proton radiation. In certain fast films the density is nearly independent of the energy of the protons or their specific ionization and approximately only dependent on the number flux of the protons i.e. protons /cm^2 which penetrate the film. The dose distribution in the film roll shown before would therefore not correspond to the density distribution. The fast film would be more black in the center relative to the surface, than indicated by the dose distribution, since the number of particles falls off with depth more slowly than the dose. In contrast to this, for certain slow films there exist indication of a near dose proportionality of the density. This behavior is shown (Ref. 8) with a parallel beam of particles of equal energy penetrating through film packs. In a parallel beam the number of penetrating particles is approximately constant for each cross section. The dose is proportional to the specific ionization, which increases strongly toward the end of the beam. If the density is dose proportional (NTV-film, slow) the film within different positions of the parallel beam shows the Bragg peak. This is not the case for the faster film (Translite), which shows constant density along the beam indicating a saturation condition. The low specific ionization of the high energetic particle seems to suffice already to render the large grains developable or to saturate the grains. The higher specific ionization near the end of the beam is useless for saturated grains.

Because of the variety of responses, supplementary investigations on light response and degradation in resolution after preirradiation with particles of different energy appear warranted and are intended especially on those films, which might be used in moon and planetary exploration, and in Astronomy, Astro-physics and Cosmic ray physics in space.

REFERENCES

1. Ogilvie, K. W., Bryant, D. A., and Davis, L. R.: Rocket Observations of Solar Protons During the November 12, 1960 Event. Goddard Space Flight Center. See also Jour. Geophys. Res. 67, no. 3, Mar. 1962, pp. 929-937.

2. Pieper, G. F., Zmuda, A. J., Bostrom, C.O., and O'Brien, B. J.: Solar Protons and Magnetic Storms in July 1961. Jour. Geophys. Res.,, vol. 67, no. 13, Dec. 1962, pp. 4959-4981.

3. Freier, P. S., and Webber, W. R.: Exponential Rigidity Spectrums for Solar-Flare Cosmic Rays. Jour. Geophys. Res., vol. 68, no. 6, Mar. 15, 1963, pp. 1605-1629.

4. Hoffman, R. A., Davis, L. R., and Williamson, J. M.: Protons of 0.1 to 5 Mev and Electrons of 20 kev at 12 Earth Radii During Sudden Commencement on September 30, 1961. Jour. Geophys. Res., vol. 67, no. 13, Dec. 1962, pp. 5001-5005.

5. Bryant, D. A., Cline, T. L., Desai, U. D., and McDonald, F. B.: Jour. Geophys. Res., vol. 67, December 1963, pp. 4983-5000.

6. Foelsche, T.: (a) Spectral Intensity Variations with Time in Specific Solar Flare Events and Radiation Doses. Paper presented at ASTM Meeting, June 24-28, 1963, Atlantic City, New Jersey. (b) Radiation Doses in Interplanetary Flight. Paper presented at Ninth Annual American Astronautical Society Meeting of the Interplanetary Missions Conference, Los Angeles, Calif., Jan 15-17, 1963.

7. Winckler, J. R., Bhavsar, P. D., and Peterson, L.: The Time Variations of Solar Cosmic Rays During July 1959 at Minneapolis. University of Minnesota, TR-CR-31, Oct. 1960.

8. Anderson, K. A., and Enemark, D. C.: Observations of Solar Cosmic Rays Near the North Magnetic Pole. Jour. Geophys. Res., vol. 65, no. 9, Sept. 1960, pp. 2657-2671.

9. Reid, G. C., and Leinbach, Harold: Morphology and Interpretation of the Great Polar Cap Absorption Events of May and July, 1959. Report Geophysical Institute, University of Alaska, College Alaska, 1 April, 1960.

10. Tochilin, E., Shuway, B. W., and Kohler, G. D.: Response of Photographic Emulsions to Charged Particles and Neutrons. Radiation Research 4, (1956), pp. 467-482.

CHARGED PARTICLE RADIATION EFFECTS MEETING

List of Attendees

NAME	CENTER
John E. Duberg	Langley Research Center
Bernard E. Cunningham	Ames Research Center
Raymond M. Hansen	Langley Research Center
Bernard G. Achhammer	NASA Headquarters
Raymond L. Gause	Marshall Space Flight Center
J. W. Keller	NASA Headquarters
J. W. Freeman	NASA Headquarters
Robert Janda	Goddard Space Flight Center
Jacob Trombka	NASA Headquarters
F. G. Casal	NASA Headquarters
H. W. Talkin	NASA Headquarters
P. T. Maxwell	NASA Headquarters
R. L. Haley	NASA Headquarters
George F. Pezdirtz	Langley Research Center
Gilbert A. Haynes	Langley Research Center
George D. Sands	Langley Research Center
Walter E. Ellis	Langley Research Center
Floyd R. Bryant	Langley Research Center
William E. Price	Goddard Space Flight Center
Trutz Foelsche	Langley Research Center
R. D. Shelton	Marshall Space Flight Center
J. W. Blue	Lewis Research Center
H. H. Grimes	Lewis Research Center
H. E. Wannemacher	Goddard Space Flight Center
P. H. Fang	Goddard Space Flight Center
V. Danchenko	Goddard Space Flight Center
M. M. Sokoloski	Goddard Space Flight Center
F. G. Cunningham	Goddard Space Flight Center
R. L. Van Allen	Goddard Space Flight Center
F. Gordon	Goddard Space Flight Center
William R. Cherry	Goddard Space Flight Center
Herbert D. Hendricks	Langley Research Center
Harry H. Heyson	Langley Research Center
Conrad P. Mook	NASA Headquarters
Newell D. Sanders	Lewis Research Center
George F. Pieper	Goddard Space Flight Center
Lawrence Kobren	Goddard Space Flight Center
William C. Hulten	Langley Research Center
John L. Patterson	Langley Research Center
R. C. Waddel	Goddard Space Flight Center
Ralph R. Nash	NASA Headquarters
B. R. Baker	Manned Spacecraft Center
Marjorie Townsend	Goddard Space Flight Center

PAGE 248 INTENTIONALLY BLANK

NAME	CENTER
J. Mandelkorn	Lewis Research Center
G. Eubanks	Goddard Space Flight Center
W. M. Redler	NASA Headquarters
Wm. D. Green	NASA Headquarters
E. O. Pearson	NASA Headquarters
P. A. Cerreta	NASA Headquarters
M. T. Charak	NASA Headquarters
Leo Fox	NASA Headquarters
E. T. Kruszewski	Langley Research Center
L. F. Vosteen	Langley Research Center
J. C. Boyle	Goddard Space Flight Center
E. Rind	Langley Research Center
C. Gross	Langley Research Center
T. P. Tsacoumis	NASA Headquarters
M. Schach	Goddard Space Flight Center
M. E. Beatty	Langley Research Center
G. F. Hill	Langley Research Center
Armand A. Lakner	NASA Headquarters
R. A. Breckenridge	Langley Research Center
Harry Harrison	NASA Headquarters
Arthur Reetz	NASA Headquarters

GPO 878-374